SUPERCONDUCTIVITY IN BINARY EUTECTIC ALLOYS.

A thesis submitted in partial requirement for the
degree of Doctor of Philosophy at the University of Warwick.

J.E. Goodfellow,
School of Engineering Science,
University of Warwick,
May 1969.

Declaration

This thesis is my own original work except where otherwise stated. No part of it has previously been presented to any other institution.

Acknowledgements

Abstract.

A brief description of the fundamentals of superconductivity is followed by a description of the preparation and microstructures of the alloys concerned in this work. The experimental apparatus used for the superconducting measurements is described.

The effect of the presence of a precipitate on several super-conducting parameters has been investigated by making magnetisation, critical current and resistance transition measurements on ten eutectic alloys and many of their component solid solutions in isolation. All the eutectics after suitable heat treatment were, with one exception, type II superconductors. The presence of a precipitate, whether superconducting or normal, was found to cause flux pinning which varied in some cases according to the precipitate orientation with respect to the external magnetic field. The pinning effects can be eliminated by consideration of very thin specimens.

The properties of a eutectic alloy were found to be not necessarily the sum of the properties of the conjugate solid solutions in isolation; a proximity effect occurs in three eutectic systems examined, i.e. a phase that on its own would be normal is superconducting in the presence of another superconducting phase.

In the absence of precipitates, the magnetic hysteresis is thought to be due to surface currents. It is suggested that the so-called 'major loop' of a superconductor is a measure of the relative effects of surface currents and bulk currents. The effect of edges on the magnetisation behaviour has been examined by considering slit and unslit hollow cylinders and hollow ellipsoids. Surface conditions were also examined. Roughening the surface was found to decrease specimen magnetisation (particularly in the region of H_{c1}) and

also to reduce the critical transport current in the mixed state and the surface sheath current above H_{c2}. Plating with Cu and Cd reduces sheath currents above H_{c2} but plating with ferromagnetics Ni and Fe actually increases them for the case of field not parallel to the specimen surface.

The model of St.James and DeGennes' surface sheath above H_{c2} is endorsed and the mechanism confirmed as the same for type I and type II superconductors. The suggestion is made that the sheath may also exist below H_{c2} to account for the initial part of the resistance transition curve. The presence of a precipitate increases the current carrying capacity of the sheath and may also increase H_N, the field at which the specimen becomes completely normal. A model of internal surface superconductivity is proposed to account for these results.

Finally, applications of the results of this work are discussed and future lines of research suggested.

Corrections suggested during the oral examination
are inserted in the text in black ink.

1. Introduction

Since its discovery[1] in 1911 by the Dutch Physicist Kamerlingh Onnes, the phenomenon of superconductivity has aroused much interest among scientists who have attempted to utilize the property of lossless current flow.

Early attempts were frustrated[2] by the discovery that only a limiting current can be passed along a superconductor before it is driven normal and this limiting current decreases to zero in the presence of an applied magnetic field. Enthusiasm consequently waned.

The first magnet to be successfully wound from a superconductor was made by Ynetma[3] in 1955 who used cold worked niobium wire to produce a field of 7 KOe. This precipitated renewed efforts to discover superconductors which were capable of carrying high currents in an intense field and attention was primarily focused on the refractory alloys of niobium. The result is that nowadays superconducting solenoids capable of producing fields exceeding 100 KOe are commercially available.

Despite the masses of data accummulated on the subject a relatively small amount exists in which the metallurgical condition of the material is accurately defined. In this research the effects of the presence of a second phase on the superconducting properties of an alloy are examined and the metallurgical conditions are well established by considering eutectic alloys.

Before discussing the research, the general properties of super-conductors and the theories of superconductivity are briefly described. For a more complete description the reader is referred to the literature[4].

2. General Properties of Superconductors

In 1914 Onnes[5] discovered that superconductivity is destroyed by the application of an external magnetic field (the critical field, H_c) the magnitude of which depends on the temperature approximately as

$$H_c = H_o \left[1 - \left(\frac{T}{T_c} \right)^2 \right] \qquad \text{_____ (2.1)}$$

where H_o is the critical field at 0°K and T_c is the superconducting critical temperature. He also found that when a current is passed along a super-conductor it is driven normal when a certain critical current is reached. Silsbee[6] suggested that it is the field associated with the current that destroys superconductivity and this is confirmed by applying the equation known as the 'Silsbee Relationship' :

$$I_c = 5r \ H_c \qquad \text{_____ (2.2)}$$

where I_c is in amps., r is the radius of the wire in cm. and H_c is the critical field in oersted.

Another important effect was noticed by Meissner and Ochsenfeld[7] in 1933. If a long, thin superconductor is cooled from above T_c in a longitudinal magnetic field less than H_c, the field is excluded from the inside of the specimen at the transition temperature.

This so-called Meissner effect cannot be deduced merely from the premise that a superconductor has zero resistivity as can be seen from the following argument:

According to classical theory,

$$E = \rho \ J \qquad \text{_____ (2.3)}$$

where ρ is the resistivity, J is the current density resulting from the application of an electric field E.

If ρ is zero and J finite, then E = 0.

$$\therefore \quad \text{curl } \bar{\bar{E}} = 0 \qquad \text{_____ (2.4)}$$

and therefore, from Maxwell's equation:

$$\frac{d\bar{\bar{B}}}{dt} = c \text{ curl } \bar{\bar{E}} = 0 \tag{2.5}$$

where $\bar{B}$ is the magnetic induction inside the specimen.

Equation (2.5) means the flux cannot change on cooling and in particular it cannot change on cooling through the transition temperature. Since this is in direct contradiction to the Meissner effect, this must be an independent property of a superconductor.

This vanishing of the magnetic induction in the interior of a super-conductor was attributed to circulating surface currents whose associated magnetic field was equal and opposite to the external field. A super conductor behaves as a perfect diamagnetic below H_c, i.e. in a field $\bar{\bar{H}}$:

$$\bar{B} = \bar{H} + 4\pi \bar{M} = 0 \tag{2.6}$$

where $\bar{M}$ is the magnetisation per unit volume.

It is now recognised that there are two kinds of superconductors, type I and type II, characterised (when no demagnetising effects are present) by the reversible curves shown in fig. 1.

In fact, the induction does not change discontinously to zero at the surface. The field penetrates a very small amount, the penetration depth, λ. This is the depth in which the surface currents flow.

3. Phenomenological Macroscopic Theories

The reversibility of the Meissner effect indicated that thermo-dynamics may be applied to the normal - superconducting transition. The theories of London, Pippard and Ginzburg-Landau introduce respectively the concepts of penetration depth, coherence length and spacial variation of the density of superconducting electrons.
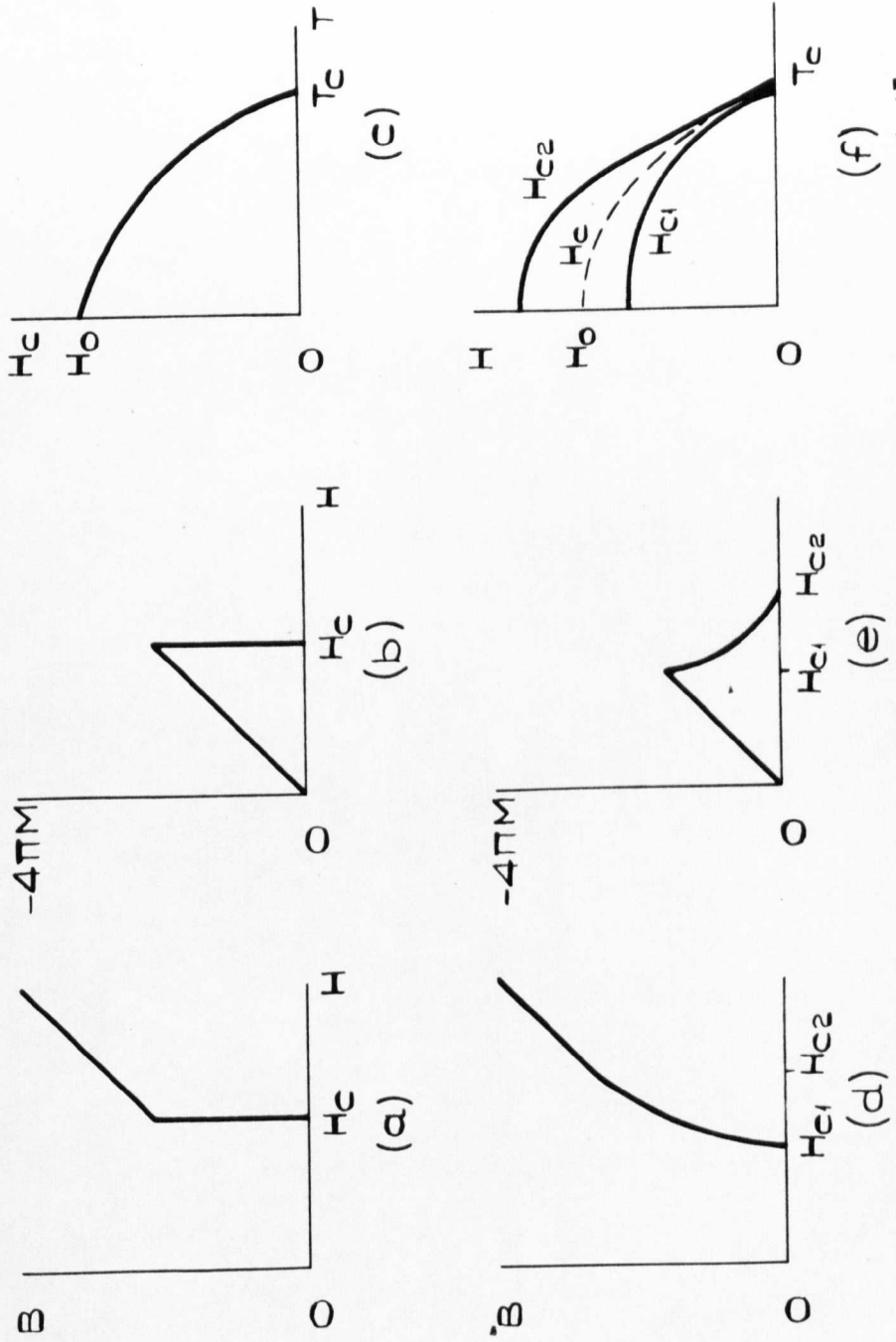
FIG. 1. MAGNETIC BEHAVIOUR OF TYPE I [CURVES (a), (b) & (c)] & TYPE II [CURVES (d), (e) & (f)] SUPERCONDUCTORS.

3.1. Thermodynamics of the normal to superconducting transition

The Gibbs free energy of a superconductor G_s is raised by the application of a field, H:-

$$G_s(H) = G_s(o) - \int_0^H M dH \qquad \text{(3.1.1)}$$

Integrating w.r.t. H, (and incorporating (2.6))

$$G_s(H) = G_s(o) + \frac{H^2}{8\pi} \qquad \text{(3.1.2)}$$

When $H = H_c$, the superconducting and normal states are in equilibrium:

$$G_n(H_c) = G_s(H_c) \qquad \text{(3.1.3)}$$

In the normal state the susceptibility is negligible

$$\therefore \quad G_n(H_c) = G_n(o) \qquad \text{(3.1.4)}$$

$$\therefore \quad G_n(o) - G_s(o) = \frac{H_c^2}{8\pi} \qquad \text{(3.1.5)}$$

The entropy, S, is given by:

$$S = -\left(\frac{\partial G}{\partial T}\right)_{P,H} \qquad \text{(3.1.6)}$$

$\therefore$ differentiation of (3.1.5) yields:-

$$S_n(o) - S_s(o) = -\frac{H_c}{4\pi} \cdot \frac{dH_c}{dT} \qquad \text{(3.1.7)}$$

As $\frac{dH_c}{dT}$ is found always to be negative, the entropy

of the superconducting state is less than that of the normal state. Thus the superconductor below H_c is in a more ordered 'condensed state'.

3.2. London's Theory

Consider a perfect conductor with a current density J flowing as a consequence of the application of an applied electric field E.

$$\bar{J} = ne\bar{v} \qquad \text{(3.2.1)}$$

where n is the number of electrons and v is their velocity

$$e\bar{E} = m\dot{\bar{v}} \qquad \text{_____(3.2.2)}$$

$$\therefore \quad \bar{E} = \frac{4\pi\lambda_L^2}{c^2}.\dot{\bar{J}} \qquad \text{_____(3.2.3)}$$

where $\lambda_L^2 = \dfrac{mc^2}{4\pi ne^2}$ _____(3.2.4)

Maxwell's equation is:-

$$\text{curl } \bar{E} = -\frac{\dot{\bar{H}}}{c} \qquad \text{_____(3.2.5)}$$

Combining (3.2.5) with the curl of (3.2.3) :-

$$\left(\frac{4\pi\lambda_L^2}{c}\right) \text{ curl } \dot{\bar{J}} = \dot{\bar{H}} \qquad \text{_____(3.2.6)}$$

From Maxwell:

$$\text{curl } \bar{H} = \frac{4\pi\bar{J}}{c} \qquad \text{_____(3.2.7)}$$

Combining the differential of (3.2.7) with (3.2.6) gives:-

$$\text{curl curl } \dot{\bar{H}} = \frac{\dot{\bar{H}}}{\lambda_L^2} \qquad \text{_____(3.2.8)}$$

Since div $\bar{H}$ = 0, div $\dot{\bar{H}}$ = 0.

$\therefore$ (3.2.8) becomes

$$\nabla^2\dot{\bar{H}} = \frac{\dot{\bar{H}}}{\lambda_L^2} \qquad \text{_____(3.2.9)}$$

This means that $\dot{\bar{H}}$ disappears exponentially inside the surface of a macroscopic perfect conductor.

Integration of (3.2.9) w.r.t. time yields:-

$$\nabla^2(\bar{H} - \bar{H}_o) = \frac{(\bar{H} - \bar{H}_o)}{\lambda_L^2} \qquad \text{_____(3.2.10)}$$

where H_o is the (arbitrary) field inside the body when it lost its resistance.

But the Meissner effect showed that H_O must be zero inside the specimen, so (3.2.10) does not satisfy the conditions in a superconductor.

F.& H.London[8] considered the electrons in a superconductor to be either normal or superconducting with the number of superconducting electrons given by an order parameter $W = 1 - x$, where x is the fraction of normal electrons. Zero resistance occurs because below T_c the superelectrons short out the normal ones. They modified the above mathematics to account for the Meissner effect by suggesting that:-

$$\left(\frac{4\pi\lambda_L^2}{c} \right) \quad \text{curl } \bar{\bar{J}} = -\bar{\bar{H}} \qquad\qquad (3.2.11)$$

and substituting n_s for n in (3.2.4) where n_s is the number of superconducting electrons.

Combining (3.2.7) with (3.2.11) yields

$$\nabla^2 \bar{\bar{H}} = \frac{\bar{\bar{H}}}{\lambda_L^2} \qquad\qquad (3.2.12)$$

F.London[9] indicated that (3.2.11) can only be derived from quantum theory if it is assumed that the wave function is 'rigid' in the presence of a field. This corresponds to a constant order parameter with respect to field.

The physcial significance of (3.2.12) is that the field H decays exponentially inside a superconductor. λ_L is known as the penetration depth and is of the order of 5×10^{-6} cm. for pure metals. It is the depth at which the field has decayed to $\frac{1}{e}$ of its value at the surface.

Although a macroscopic specimen is essentially diamagnetic, a thin specimen of size the order of λ_L is not. Since the energy change per unit volume must be the same for both macroscopic and microscopic superconductors when they are driven normal by a magnetic field, the small specimen must stay superconducting up to a higher value of field.

Equation (3.1.2) shows that the energy of a superconductor is raised in the presence of a magnetic field. Its energy would be lowered if it split up into alternate superconducting and normal layers such that the thickness of the superconducting layers was of the order of λ_L and the thickness of the normal layers so small that their contribution to the local energy was negligible.

The Meissner effect will therefore only occur if a positive interphase boundary energy exists. In order to split up, a slab of thickness d must have $\dfrac{d}{\lambda}$ such layers, i.e.

$$\sigma_{ns} \geqslant \frac{\lambda}{2} \cdot \frac{H_c^2}{8\pi}$$

where σ_{ns} is the interphase surface energy.

For the Meissner effect not to occur this surface energy must be negative.

Several experimental results, however, were outside the concepts of the London theory, e.g.:

(i) λ_L decreases with In concentration in Sn - In alloys,

(ii) λ_L is field dependent in Sn - In alloys.

This prompted Pippard[10] to introduce the concept of coherence length.

3.3. Pippard's Non-Local Theory

The vector potential $\bar{A}$ is defined by the relationship

$$\bar{H} = \text{curl } \bar{A} \qquad \qquad (3.3.1)$$

(3.3.1) and (3.2.11) combine to relate the current density at a point R, $\bar{J}(R)$ to the vector potential at that point, $\bar{A}(R)$

$$\bar{J}(R) = \frac{c}{4\pi\lambda_L^2} \cdot \bar{A}(R) \qquad \qquad (3.3.2)$$

Pippard assumed that the wave function which describes the distribution

of the superconducting electrons extends over a distance $\xi \approx 10^{-4}$ cm, the 'coherence length'. This means that the current density at a point is not proportional to the vector potential at that point as given by (3.3.2) but is of the form of an integral of $\bar{A}$ over a distance ξ surrounding the point.

If $\bar{A}(R)$ is the vector potential at a point R then Pippard proposed the relationship:

$$\bar{J}(R) = -\frac{3ne^2}{4\pi\xi_o mc} \int \frac{\bar{R}\left[\bar{R}.\bar{A}(R)\right]}{R^4} \exp\left(\frac{-R}{\xi}\right) d\tau \underline{\hspace{1cm}}(3.3.3)$$

This equation is called the Pippard non-local relation.

The coherence length, ξ , is related to the mean free path, L, by the equation:

$$\frac{1}{\xi} = \frac{1}{\xi_o} + \frac{1}{\alpha L} \underline{\hspace{3cm}}(3.3.4)$$

where ξ_o is the coherence length of the pure metal and α is a constant of the order of unity.

The penetration depth for an infinitely thick specimen may be defined independently of the mode of decay of the field by:-

$$\lambda = \frac{1}{H_o} \int_0^\infty H(x)\, dx \underline{\hspace{3cm}}(3.3.5)$$

where H_o is the applied field and x is the distance inside the specimen.

The penetration depth as defined in (3.3.5) can be determined from (3.3.3.) explicitly in two limiting cases:-

$$\lambda = \lambda_L \left(\frac{\xi_o}{\xi}\right)^{\frac{1}{2}} \qquad \text{for } \xi \ll \lambda \quad \text{("London limit")} \underline{\hspace{1cm}}(3.3.6)$$

$$\lambda_o = \left[\frac{\sqrt{3}}{2\pi}\xi\lambda_L^2\right]^{\frac{1}{3}} \qquad \text{for } \xi \gg \lambda \quad \text{("Pippard limit")} \underline{\hspace{1cm}}(3.3.7)$$

In fact, whenever small or impure superconductors are being considered, λ is taken as:

$$\lambda = \lambda_b \sqrt{\frac{\xi_o}{\xi}}$$
(3.3.8)

where λ_b = the empirically determined penetration depth for a bulk sample.

ξ is associated with the 'configurational surface energy' of a super-conducting -normal boundary. As the field penetrates the superconducting region, the free energy of this region is increased. This increase in configurational surface energy must be balanced against the decrease in magnetic energy for the field penetration to obtain the total surface energy, i.e.

Configurational surface energy + magnetic energy = total surface energy
(increases as field penetrates)   (decreases as field penetrates)

If $\xi \gg \lambda$ the total surface energy is positive.

If $\xi \ll \lambda$ the total surface energy is negative.

This allows a distinction to be made between two types of superconductor:-

Type I with $\xi \gg \lambda$, i.e. a total positive surface energy showing
a complete Meissner effect.

Type II with $\xi \ll \lambda$, i.e. a total negative surface energy showing
an incomplete Meissner effect.

All pure superconducting elements are type I with the exception of niobium. With alloying the mean free path decreases and ξ becomes $\ll \lambda$ and they become type II.

3.4. The G.L.A.G. Theory

This theory is so called in deference to its contributors, Ginzburg, Landau, Abrikosov and Gor'kov.

Ginzburg and Landau[11] assumed that the density of superconducting electrons at a point, $n_s(r)$, in a magnetic field varies spatially and they introduced an order parameter which they assumed behaves like a true wave function

$$\psi(r)\psi^*(r) = |\psi|^2 = n_s(r) \qquad \text{(3.4.1)}$$

In zero field the free energy/unit volume of a superconductor may be written

$$G_s(o) = G_n(o) + \alpha|\psi|^2 + \frac{\beta}{2}|\psi|^4 \qquad \text{(3.4.2)}$$

where α and β are functions of temperature and when $T \approx T_c$ have the form:

$$\alpha(T) = (T_c - T) \cdot \left(\frac{\partial \alpha}{\partial T}\right)_{T=T_c} \qquad \text{(3.4.3)}$$

$$\beta(T) = \beta T_c \cong \beta_c \qquad \text{(3.4.4)}$$

In an applied field the free energy must have an extra term added to allow for the gradient in ψ, since ψ is not rigid in the presence of an applied magnetic field.

Ginzburg and Landau assumed a form of this extra energy term and then minimised the total free energy with respect to ψ^* and $\overline{A}$ to obtain the famous pair of coupled non-linear Ginzburg-Landau equations:

$$\frac{1}{2m}\left(-i\hbar\nabla - \frac{e^*\overline{A}}{c}\right)^2\psi + \frac{\partial G_s(o)}{\partial \psi^*} = 0 \qquad \text{(3.4.5)}$$

$$\nabla^2\overline{A} = \frac{2\pi i e^* \hbar}{mc}\left[\psi^*\overline{\nabla}\psi - \psi\nabla\psi^*\right] + \frac{4\pi e^{*2}}{mc^2}|\psi|^2\overline{A} \qquad \text{(3.4.6)}$$

where e^* is the charge on the current carriers.

They introduce two parameters:

$$\delta^2 = \frac{mc^2\beta}{4\pi e^{*2}|\alpha|} \qquad \text{(3.4.7)}$$

and

$$k^2 = \left(\frac{\beta}{2\pi}\right)\left(\frac{mc}{e^*\hbar}\right)^2 = \left[\frac{2e^{*2}}{\hbar^2 c^2}\right]H_c^2\delta^4 \qquad \text{(3.4.8)}^*$$

where H_c is the thermodynamic critical field

$$H_c^2 = \frac{4\pi\alpha^2}{\beta} \qquad \text{(3.4.9)}$$

* k is the Greek 'kappa'

When H≈0, ψ remains practically constant

$$\therefore \qquad \psi \approx \psi_0 \text{ and } \nabla \psi = 0$$

(3.4.6) then reduces to:

$$\nabla^2 \bar{A} = \frac{4\pi e^{*2}}{mc^2} \left| \psi_0 \right|^2 \bar{A}$$

$$\therefore \quad \nabla^2 \bar{A} = \frac{\bar{A}}{\delta^2} \underline{\hspace{3cm}} (3.4.10)$$

This is the same as London's Equation (3.2.12) and $\lambda_L = \delta$ for this weak field case.

The significance of k is manifested when they calculate the surface energy. They found that for $k < \frac{1}{\sqrt{2}}$, σ_{ns} is positive, and as seen in section (3.3) this results in a type I superconductor. When $k > \frac{1}{\sqrt{2}}$, σ_{ns} is negative and a type II superconductor results.

Abrikosov[12] assumed that the splitting up of type II superconductors so as to allow the field to penetrate would occur at a field H_{cl} in the form of singly quantised lines of flux variously called flux threads, flux lines, flux filaments, fluxoids or vortex lines (since a supercurrent vortex is responsible for the presence of the flux).

At H_{cl} flux threads are nucleated at the surface and move into the superconductor due to their mutual replusion to form a homogeneous array as shown in fig.2.

These flux lines carry persistent currents circulating as shown along their whole lengths as current walls. Inside these walls and coupled to them is a magnetic field containing the single quantum of flux. They may terminate only at a surface or form closed loops.
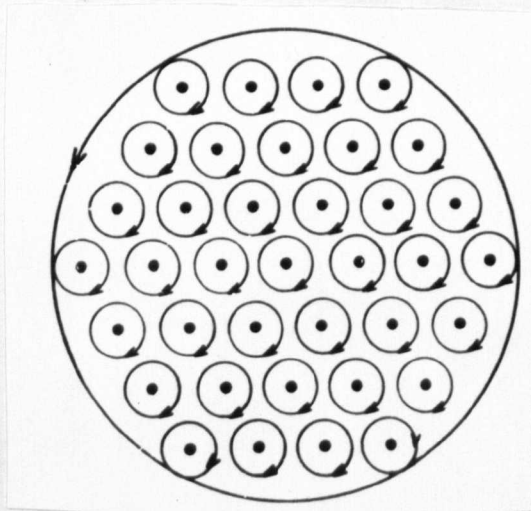
Fig.2. (Livingston & Schadler[4])

On the basis of this model Abrikosov calculated the value of H_{c1} to be

$$\frac{H_{c1}}{H_c} = \left(\frac{H_c}{H_{c2}}\right) \text{Ln} \left(\frac{H_{c2}}{\sqrt{2} \ k}\right) \qquad \qquad \text{(3.4.11)}$$

where H_{c2} is the maximum field for which the Ginzburg-Landau equations have a finite solution for an infinitely thick superconductor of $k > \frac{1}{\sqrt{2}}$

$$H_{c2} = \sqrt{2} \ k \ H_c \qquad \qquad \text{(3.4.12)}$$

The field range H_{c1} to H_{c2} (when a type II superconductor goes normal) when fluxoids are present is known as the 'mixed state'.

Goodman[13] calculated H_{c1} for a laminar model using the London Equations and he obtained

$$\left(\frac{H_{c1}}{H_c}\right)^2 = \frac{H_c}{H_{c2}} \qquad \qquad \text{(3.14.13)}$$

For large values of $\frac{H_{c2}}{H_c}$, i.e. large k, it can be seen from (3.4.12) and

(3.4.13) that H_{c1} (laminar) $>$ H_{c1} (filaments).

This means that the filament structure of Abrikosov is the most stable since for any field H between H_{c1} (filament) and H_{c1} (laminar)

G (filament) $<$ G (Meissner effect)

and G (laminar) $>$ G (Meissner effect)

Abrikosov's original calculation of the magnetisation curve for a type II superconductor assumed the fluxoid array in the mixed state to have the form of a square lattice. In fact, theoretical work by Matricon[14] has shown that a triangular lattice has the lowest energy and recent experimental work by Essman and Träuble[15] has confirmed this.

Gor'kov[16] showed that the Ginzburg-Landau equations follow from the B.C.S.[17] microscopic theory for $T \approx T_c$ for both pure metals and alloys if e^* in the expression for k is substituted by 2e. The physical meaning of this is that electron pairs are responsible for superconductivity.

He showed that k for a pure metal is given by:

$$k_o = \frac{.96 \, \lambda_L(o)}{\xi_o} \qquad\qquad (3.4.14)$$

where $\lambda_L(o)$ is the London penetration depth at $T \approx 0$.

The dependence of ξ, λ and k on the mean free path, L, in the normal state was calculated by Gor'kov and Caroli et al[18] for $T \approx T_c$ and

$$\lambda(T) = 0.64 \lambda_L(o) \left(\frac{\cdot \xi}{L}\right)^{\frac{1}{2}} \left[\frac{T_c}{T_c - T}\right]^{\frac{1}{2}} \qquad\qquad (3.4.15)$$

$$\xi(T) = 0.85 \left(\xi_o L\right)^{\frac{1}{2}} \left[\frac{T_c}{T_c - T}\right]^{\frac{1}{2}} \qquad\qquad (3.4.16$$

$$k = 0.75 \frac{\lambda_L(o)}{L} \qquad\qquad (3.4.17)$$

Goodman showed that Gor'kov's[16] calculations may be written, within a few per cent as

$$k = 0.96 \lambda_L(o) \left[\frac{1}{\xi_o} + \frac{1}{1.32} .L \right] \qquad \text{(34.18)}$$

for all values of L, and

$$k = k_o + 7.5 \times 10^{-3} \gamma^{\frac{1}{2}} \rho \qquad \text{(34.19)}$$

where γ is the electronic specific heat in erg cm^{-3} $^oK^{-2}$ and ρ is the residual resistivity in Ω-cm.

3.5 The St.James and DeGennes surface sheath

Abrikosov's calculation of H_{c2} from the Ginzburg-Landau equations assumed an infinitely large body. St.James and DeGennes[19] pointed out that the highest value of $|\psi|^2 \neq 0$ for the boundary conditions of a superconductor bounded by an insulating surface, when the field is directed parallel to the surface, is:

$$H_{c3} = 1.695 \ H_{c2} \qquad \text{(3.5.1)}$$

for $k > 0.419$

Superconductivity occurs between H_{c2} and H_{c3} in a surface sheath of thickness of the order of ξ . H_{c3} tends to H_{c2} as the angle between the applied field and the specimen is increased to 90°.

Tinkham[20] proposed the following formula which fits some experimental data for H_{c3} as a function of θ, the angle between the field and the surface.

$$\left[\frac{H_{c3}(\theta)}{H_{c3}(o)} \right]^2 \cos^2\theta + \left[\frac{H_{c3}(\theta)}{H_{c2}} \right] \sin\theta = 1 \qquad \text{(3.5.2)}$$

The existence of H_{c3} has been amply demonstrated experimentally[21].

Equilibrium behaviour of superconductors may conveniently be represented on a k-H diagram, fig. 3.
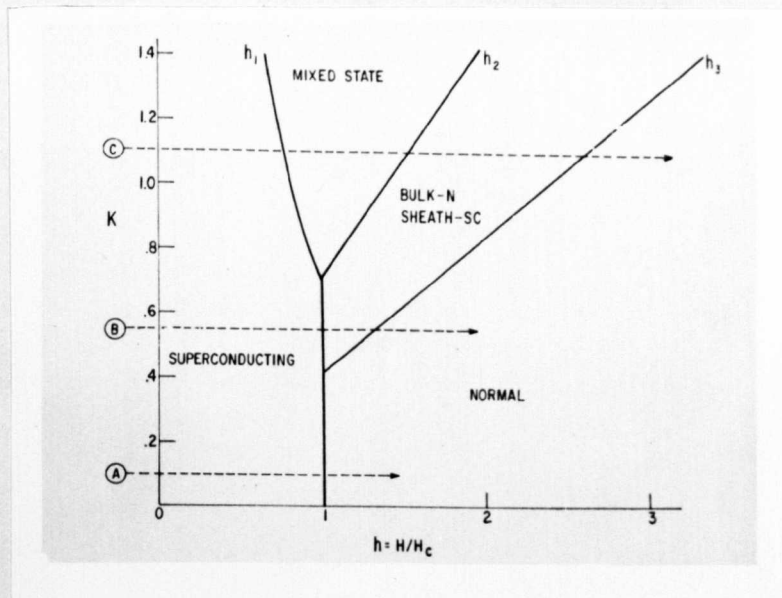
Fig.3 (Livingston & Schadler[4])

Superconductor A with $k \leqslant 0.419$ has one transition only, at H_c, thus behaving as a classic 'soft' type I superconductor.

B, with $.419 < k < .707$ is still type I except that after the transition of the bulk at H_c a surface sheath remains.

C, with $k > .707$ is type II and goes through three transitions. At H_{c1} it enters the mixed state, at H_{c2} the bulk goes normal leaving a sheath which persists up to H_{c3}.

4. Irreversible Behaviour

The GLAG theory has considered reversible behaviour and a uniform distribution of fluxoids in the mixed state. This means that a type II superconductor may only carry a lossless current up to a value

$$I_c = 5rH_{c1} \hspace{4cm} (4.1)$$

in a wire of radius rcm., and this will be carried on the surface.

At higher currents, the annular fluxoids formed contract inwards to reduce their line tension and this flux motion causes a voltage to appear. In the presence of an external field the critical current will, of course, be less; the resultant field must be inserted in (4.1) to find I_c. No size dependence of the magnetisation curve is predicted by any theory thus far.

In practice non-reversible magnetisation curves are obtained with a specimen size dependence. These superconductors are known as type III or 'hard' superconductors.

4.1. Flux Gradients and Flux Creep.

Maxwell's equation, curl $\bar{H} = \dfrac{4\pi\bar{J}}{c}$, means that a flux gradient is necessary to support a current in a conductor. A type I (and a type II below H_{c1}) superconductor excludes all field except within the penetration depth, and so the current can only flow within this region.

In the mixed state of a type II superconductor, the field gradient may only result from a gradient in the density of the Abrikosov flux lines. Anderson[22] suggested that flux lines could be pinned at low energy positions by defects, such as dislocations and precipitates, and a flux gradient produced. This gradient is equivalent to an internal macroscopic surface transport current greater than I_c given by (4.1), or an internal macroscopic induced current in the case of magnetisation measurements.

Flux lines in such a gradient experience a Lorentz force tending to drive them further into the specimen; this is resisted by the pinning effect of the defects (see fig. 4).
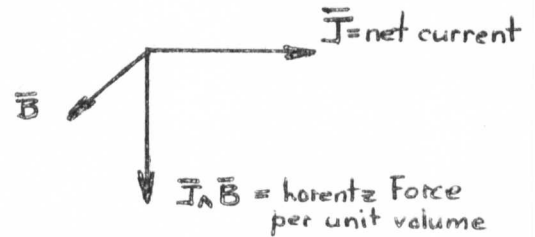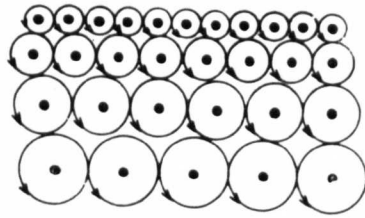
Fig 4 (Livingston and Schadler[4])

Despite the fact that it is energetically unfavourable to have a microscopic variation in the local flux line density, Anderson[23] suggested that the arrangement can be irregular only on a scale greater than the penetration depth δ.

This is the idea behind the 'flux bundle' concept. Though an individual flux line can be pinned, that line itself cannot overcome the pinning barrier because it would become out of equilibrium with the local density nearby. A whole bundle of flux lines of radius of $\sim \delta$ must move. These bundles can slide past one another easily.

The pinning can be overcome by thermal activation at all temperatures greater than $T = 0^{\circ}k$. Anderson[23] calculated that a particular barrier allows lines through at a rate

$$R = W_o e^{-\frac{E_b}{kT}} \hspace{3cm} (4.1.1)$$

where E_b is the magnitude of the pinning free energy barrier and W_o is the vibrational frequency of a bundle, $\sim 10^5 - 10^{10} \sec^{-1}$. *k is Boltzman's constant - not to be confused with kappa*

This 'flux creep' is dissipative, and if the thermal energy produced is not conducted away, 'flux avalanches' or 'flux jumps' occur resulting in a sudden loss of a large fraction of the magnetisation. Such flux jumps are erratic and are a function of the rate of field change (or rate of impressed current change).

Friedel et al[24] calculated the magnetic driving force per unit length

on a flux line by considering a two-dimensional array of flux lines as a compressible fluid. They found the force, in the case of a slab, to be

$$F_m = - \frac{\phi_o}{4\pi} \cdot \frac{d\overline{H}(\overline{B})}{dx} \quad\quad\quad (4.1.2)$$

where x is the distance normal to the slab surface,

        H(B) is the external field which would be in equilibrium

        with the internal field (induction B)

and ϕ_o is the unit quantum of magnetic flux

Campbell[25] considered the more general case of curved flux lines and he concluded:

$$F_m = - \frac{\phi_o}{4\pi} \; \text{curl } \overline{H}(\overline{B}) \quad\quad\quad (4.1.3)$$

At zero temperature the flux lines cannot become unpinned until the magnetic driving force overcomes the pinning force. When these forces are equal, a 'critical flux gradient' exists given by:

$$\left(\frac{\partial B}{\partial x}\right)_c = \frac{4\pi \mu}{\phi_o} \cdot F_L \quad\quad\quad (4.1.4)$$

where μ is the derivative $\frac{d\overline{B}}{d\overline{H}(\overline{B})}$ of the ideal reversible $\overline{B} \vee \overline{H}$ curve, and F_L is the pinning force per unit length on a flux line.

The viewpoint of a critical flux gradient offers a method of quantitatively calculating magnetisation curves from a knowledge of $J_c(B)$. The 'critical current' for a given field is related to the critical flux gradient by Maxwell's equation. In the case of a slab with the field directed parallel to a face:

$$\left(\frac{dB_z}{dx}\right)_c = \frac{4\pi J(y)_c}{10} \qu\quad\quad\quad (4.1.5)$$

where B_z is in oesteds and J_y in amps/cm^2.

Considering only two dimensions:

$$- 4\pi M = H_e - \frac{1}{x} \cdot \int_o^x B(x) \, dx \qu\quad\quad\quad (4.1.6)$$

where H_e is the applied external field.

Hence, if $\left(\dfrac{d\bar{B}}{dx}\right)_c$ is known as a function of $\bar{B}$,

$$\int_0^x \left(\frac{d\bar{B}}{dx}\right)_c dx = \bar{B}(x) \qquad\qquad (4.1.7)$$

$\bar{B}(x)$ can thus be substituted into (4.1.6) and the magnetisation curve plotted.

4.2. The Critical State

A superconductor is said to be in the 'critical state' when the local current is everywhere equal to the critical current corresponding to the local field or is zero. In order to solve equation (4.1.6) B must be expressed as a function of position. To facilite this calculation Bean[26] made the following assumptions:

(i)   The rate of flux creep is slow compared with the time taken to perform any experiment.

(ii) J_c is constant, i.e. not a function of B.

(iii) At the surface $B=H_e$ where H_e is the external field[27]. In fact a better assumption is $B=B_{eq}$, the internal field in equilibrium with H_e in a defect-free material obtainable from the ideal BvH curve.

The macroscopic internal field and current distribution may now be plotted across the section of a sample as in fig.5 for the case of a slab.

Consider H_e to be raised to fields above H_{c1}. As H_e is increased, flux penetrates a 'macroscopic penetration depth', Δ, (see fig.5(i)a), by equation (4.1.5).-

$$\frac{B_{eq}}{\Delta} = \frac{4\pi J_c}{10}$$

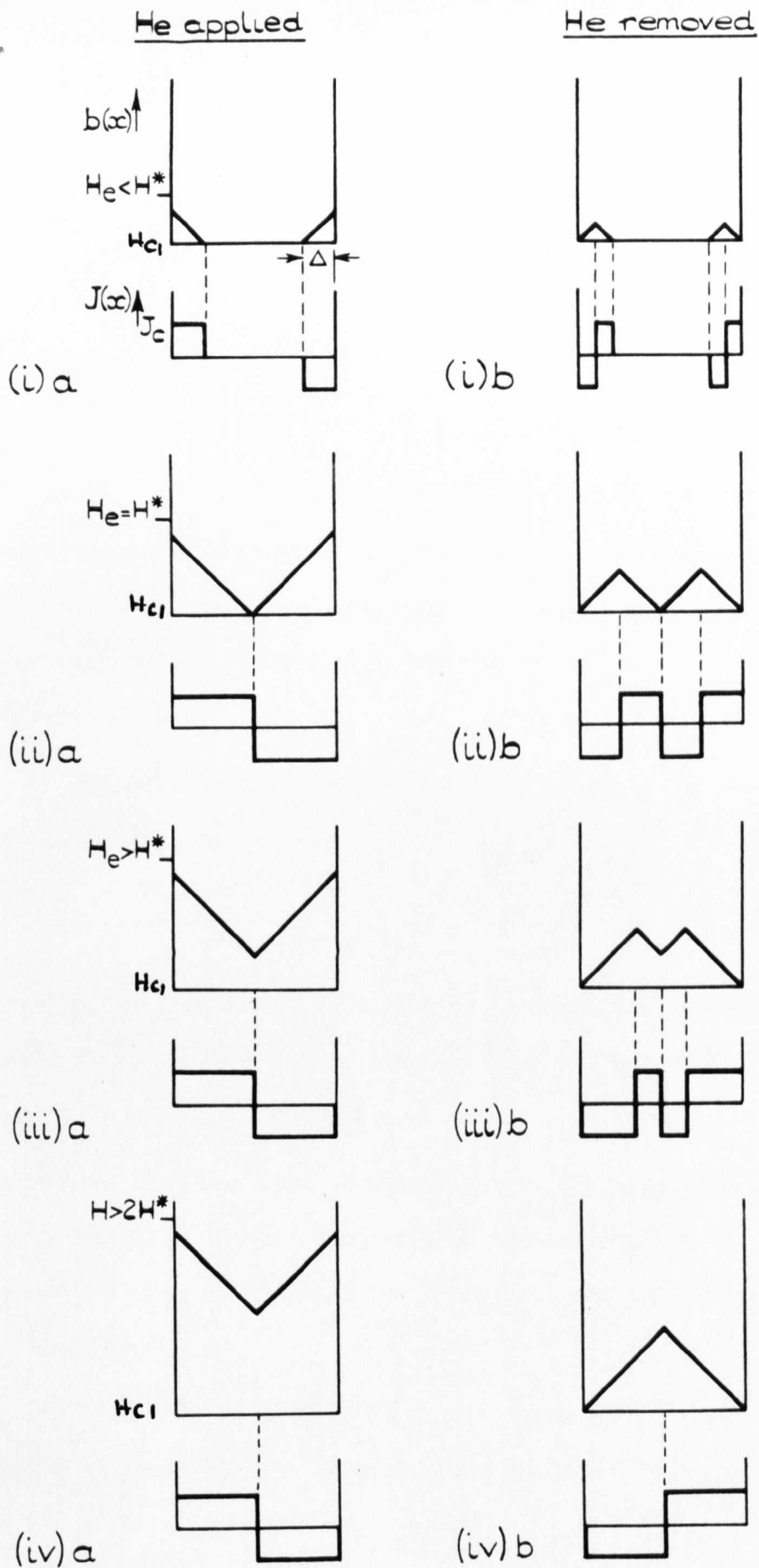or: $$\Delta = \frac{10\,B_{eq}}{4\pi J_c} \qquad\qquad (4.2.1)$$

FIG.5. INTERNAL CURRENT & MAGNETIC FIELD
DISTRIBUTIONS IN A SUPERCONDUCTING
SLAB WHEN AN EXTERNAL MAGNETIC
FIELD IS APPLIED & THEN REMOVED.

If both J_c and δ, the specimen thickness, are small enough, a field H^* is reached when critical currents, J_c, flow throughout the specimen before H_{c2}, i.e. the specimen is in the critical state (see fig.5(ii)a). Further increase in field only results in the upward displacement of the field profile (fig.5(iii)a). Any change in H_e is assumed to cause the induced currents to change from the surface.

This model can be seen from fig.5(i)-(iv)b, to predict flux trapping for all $H_e > H_{c1}$. Maximum trapped flux occurs when $H_e \geqslant 2H^*$.

Fig.6 illustrates the internal field and current distributions for a transport current in zero applied field. If a transport current is impressed such that J_c exists in a depth Δ and then removed, some flux will remain trapped.

H^* is defined in fig. 5 as the field for which $\Delta = \dfrac{\delta}{2}$, so from equation (4.2.1):

$$H^* = \frac{\pi \delta J_c}{5} \qquad\qquad (4.2.2)$$

Clearly, the value of H^* determines the resultant magnetisation curve; hysteresis increases with increasing H^*. Thus for a constant J_c, hysteresis increases with specimen thickness.

This model does not lead to a decrease in hysteresis as H_{c2} is approached and J_c is in fact dependent on the internal field. The form of J_c is expected to be sensitive to the type, size and distribution of any defects present.

Campbell et al[27] argue that for a weak pinning force and where the number of flux lines is much less than the number of pinning centres, the pinning force per unit volume may reasonably be expected to be independent of B and Bean's assumption J_c = constant will apply.
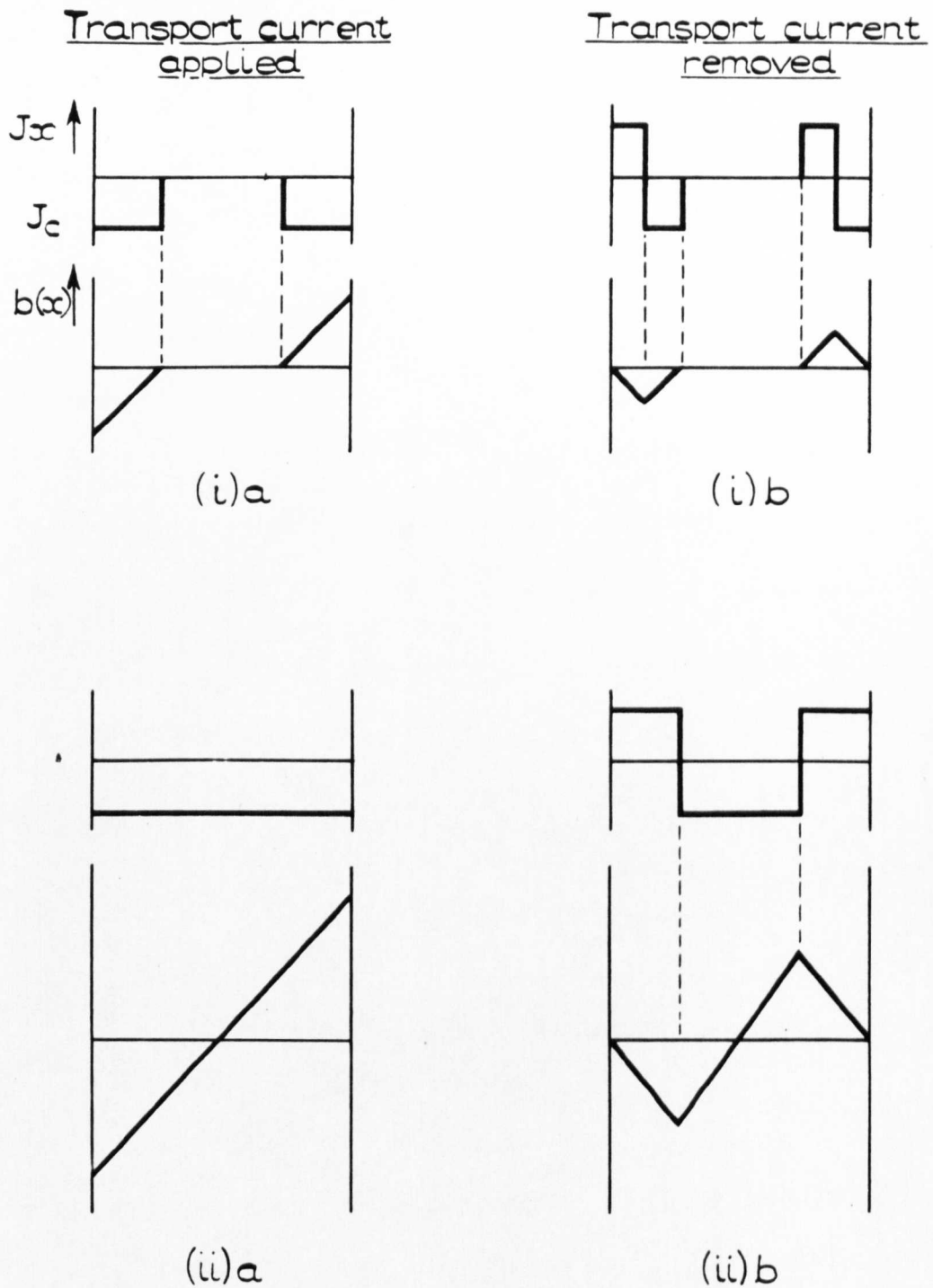
FIG. 6. INTERNAL CURRENT & MAGNETIC FIELD
DISTRIBUTIONS IN A SUPERCONDUCTING
SLAB WHEN A TRANSPORT CURRENT IS
APPLIED & THEN REMOVED IN ZERO
EXTERNAL FIELD.

As B increases, the number of lines at a pinning centre increases and if the pinning force of a centre is assumed to remain constant, the driving force it can withhold decreases. Campbell[27] by setting the pinning force per unit volume, $F_p \propto \frac{1}{B}$ found

$$\frac{dB}{dx} = \frac{constant}{2B} \qquad\qquad (4.2.3)$$

$$\text{i.e. } J_c = \frac{constant}{B} \qquad\qquad (4.2.4)$$

This gave a reasonable fit to Evetts[28] results on Pb-Bi eutectic.

Kim et al[29] found empirically that the relationship

$$J_c = \frac{constant}{(H + B_o)} \qquad\qquad (4.2.5)$$

(where B_o is a constant approximately equal to the thermodynamic critical field) held for several samples of Nb - 25%Zr alloy and a Nb_3Sn specimen.

Fietz et al[30] considered that a better fit for Nb - 25%Zr was

$$J_c = \frac{a_o}{b_o} \exp\left(\frac{-B}{b_o}\right) + c_o \qquad\qquad (4.2.6)$$

where a_o b_o and c_o are constants.

A recent result of Campbell et al[59] is that the relation

$$J_c = \frac{33S_v \, M_{(rev)}}{B^{1/2}} \qquad\qquad (4.2.7)$$

held for a range of microstructures in a Pb-Bi eutectic alloy. (S_v is the surface area of normal phase per unit volume and $M_{(rev)}$ is the magnetisation at B obtained from the ideal Abrikosov curve).

5. Objectives of this research

In order to carry a large current in the presence of a substantial external magnetic field, extended defects must be introduced into the matrix of a type II superconductor. However, much work remains to be done to show this relationship between microstructure and superconducting properties.

The object of this research is to consider the effect of one such defect, a precipitate, and see how its nature, morphology and distribution affect the superconducting properties of binary eutectic alloys. These alloys have been chosen for this investigation for the following reasons:-

(i) Precipitation from a supersaturated solid solution suffers from the disadvantage that, as ageing proceeds, the morphology and distribution of the precipitate and the chemical nature of both the precipitate and matrix are continually changing. Consequently, any effects observed will be due to a complex of variables.

(ii) On the other hand, these two-phase alloys consist of conjugate solutions, the equilibrium chemical composition of which is uniquely determined by temperature. The distribution (and sometimes the morphology) of the discontinuous phase is determined by the cooling conditions. Heat treatment of suitable alloys, therefore, allows a quantitative determination of morphology and distribution of the precipitate and a precise knowledge of the chemical composition of both phases.

(iii) A larger volume fraction of the second phase can be obtained in the matrix than by precipitation from a supersaturated solid solution.

No examination of bulk properties can be considered complete unless the effect of surface condition is also known. It is therefore intended to examine surface effects on the superconducting behaviour at the same time.

The superconducting parameters to be investigated are specimen magnetisation, critical current carrying capacity in a field and super-conductivity in the surface sheath.

Finally, with the information obtained, some relevant conclusions are expected to be drawn concerning current ideas on the superconducting processes involved.

6. Preparation of Specimens

6.1. Casting of alloys

All metals used were supplied by Johnson, Matthey Limited, to their spectrographically pure specifications. Either 25 or 50 gm. ingots were weighed out and sealed in cleaned pyrex or silica moulds under a vacuum of approximately 10^{-4} torr at constriction (i). Diagrams of the moulds used are shown in fig.7.

After heating to about $10^{\circ}C$ above the melting temperature of the higher melting point constituent, the alloy was thoroughly mixed by shaking and poured through constriction (ii) and sealed off.

The ingots were removed by breaking the mould and machined to shape on a Metals Research Servomet spark machine. Subsequent heat treatment was carried out in a Metals Research two inch diameter tube furnace under a vacuum of 10^{-4} - 10^{-6} torr.

6.2 Heat-treatment procedure

(a) Solid solutions

Those alloys that are equilibrium solid solutions at room temperature were homogenised within a few degrees of the melting range for a fortnight while still in the mould, then quenched and finally removed from the mould. After machining they were annealed just below the melting range for a few hours to remove any possible work damage.*

Solid solutions that are supersaturated at room temperature and which would precipitate out a second phase were homogenised in the solid solution

*no subsequent analysis. Possible change in composition during vacuum anneal not known.

1.0 cm

Constriction (i)

Constriction (ii)

4 cm

3 cm

(b)

MOULD FOR SLAB INGOT

12 cm

0.5 cm

(a)
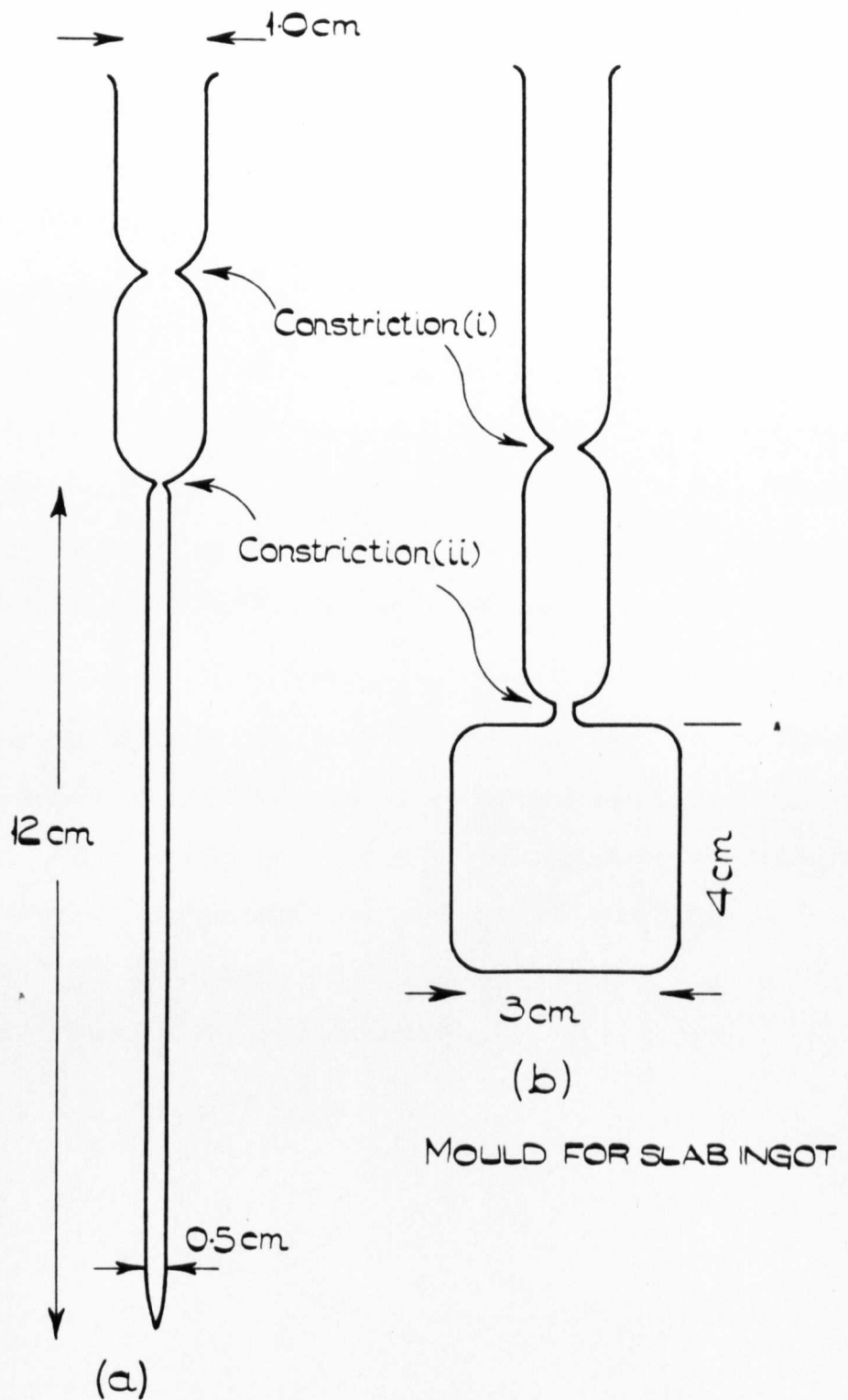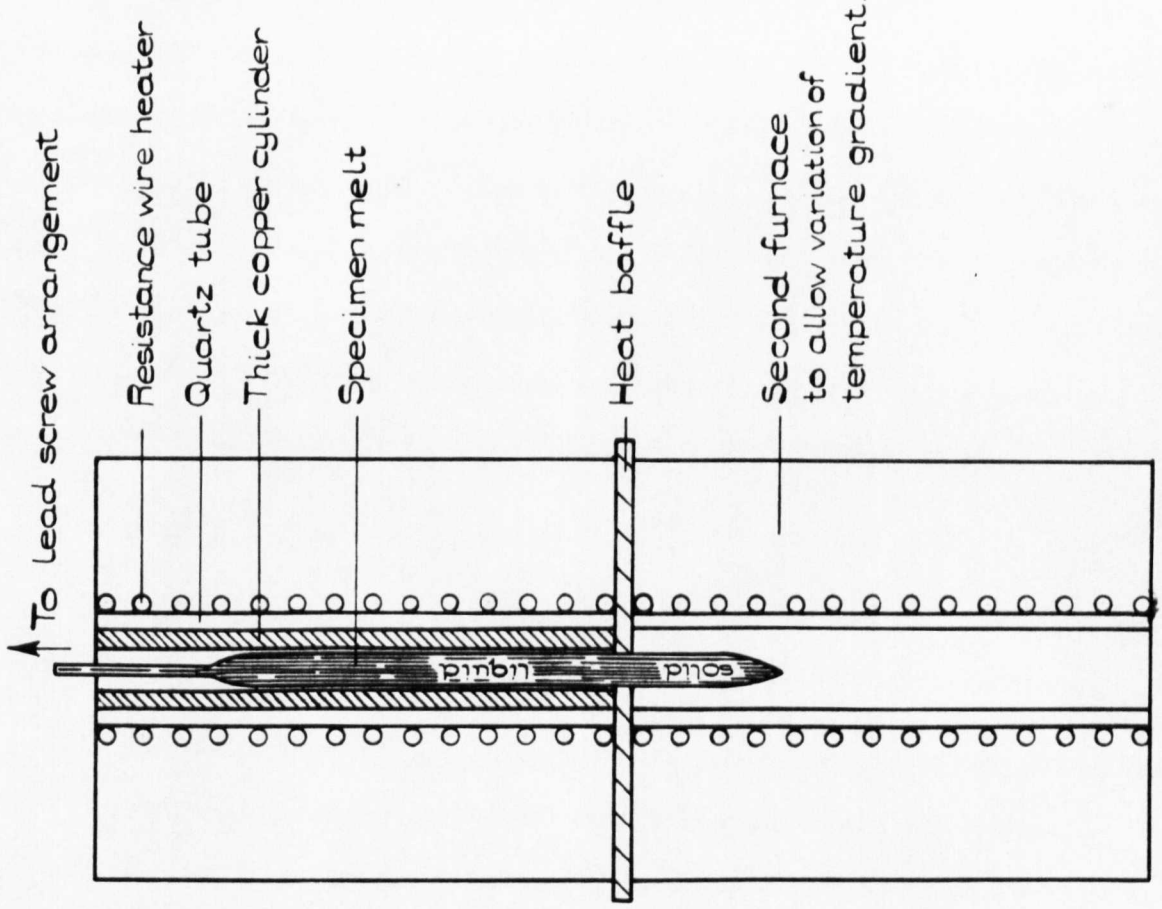
MOULD FOR ROD-SHAPED INGOT

FIG. 7.

phase field for a fortnight, quenched in liquid nitrogen, removed from the mould and shaped. Since the time required to perform the spark machining allowed precipitation to occur, their previous heat treatment was repeated in the vacuum furnace from whence they were quenched into liquid nitrogen in which they were stored until required in labelled capsules.
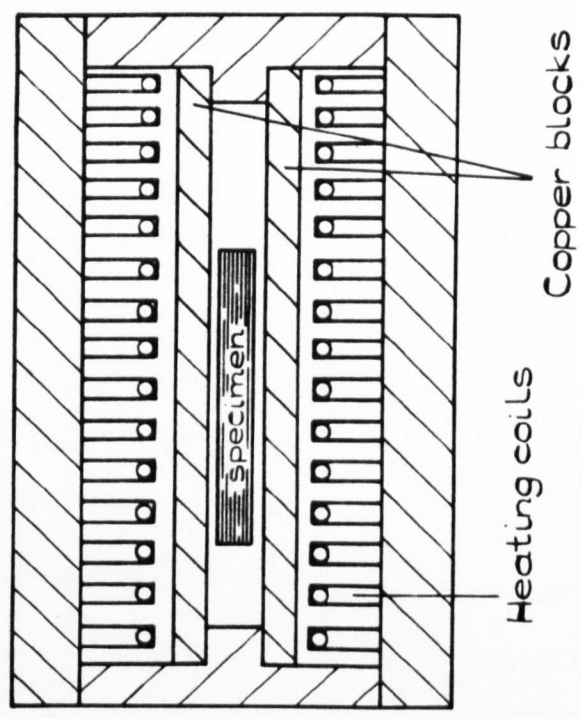
(b)   Eutectic alloys

When an as-cast structure was required, the mould was cooled in air and the ingot removed, machined to shape, usually chemically polished, and heat-treated in the vacuum furnace at a temperature designed to give the desired chemical composition of the two conjugate phases. From this temperature they were quenched into liquid nitrogen and stored at the low temperature.

Specimens to be uni-directionally frozen were sealed off at constriction (ii) and after attaching a pyrex or silica rod they were lowered through the furnace arrangement of fig.8 by means of a variable speed motor and lead-screw system. After removal from the mould, the ingots were optically examined to confirm the required structure prior to shaping (a procedure also undertaken for the as-cast alloys). They were then heat treated as previously described for the as-cast samples.

To lead screw arrangement

Resistance wire heater

Quartz tube

Thick copper cylinder

Specimen melt

Heat baffle

Second furnace to allow variation of temperature gradient.

liquid   solid

(a) FURNACE CYLINDRICAL SPECIMENS
     VERTICAL SECTION

Copper blocks

Specimen

Heating coils

(b) FURNACE FOR SLAB SPECIMENS
     UNDERSIDE SECTION

FIG. 8.

7. Solidification of binary eutectic alloys

7.1. Freezing of typical alloys in the system

Fig.9 illustrates a typical eutectic equilibrium phase diagram. It has two characteristic features:

(i) complete miscibility of metals A and B in the liquid state and incomplete miscibility in the solid state;

(ii) the freezing point of both metals is depressed by addition of the other.

The eutectic reaction occurs when the eutectic alloy, distinguished by having the lowest melting point, is cooled through the eutectic temperature, T_E. At this point the system has zero degrees of freedom according to the phase rule and is known as invariant. Consequently, the temperature must remain fixed until one of the phases disappears and the system becomes univariant. This occurs by the liquid depositing the two solid solutions α and β in constant proportion so there are no changes in the composition of the phases until solidification is complete. The solid deposited is in the form of an intimate mixture of the phases α and β, the relative proportions of which are given by the lever rule:-

$$\frac{\text{amount of } \alpha}{\text{amount of } \beta} = \frac{QR}{PQ}$$

Further decrease in temperature results in the two conjugate solid solutions α and β altering in composition along PT and RS respectively.

If the cooling rate is rapid, there is not enough time for diffusion of A and B atoms to occur over appreciable distances and there is a departure from equilibrium. The eutectic alloy does not solidify at the eutectic temperature but several degrees below it (it 'undercools'). The mixture of α and β phases is now much finer.
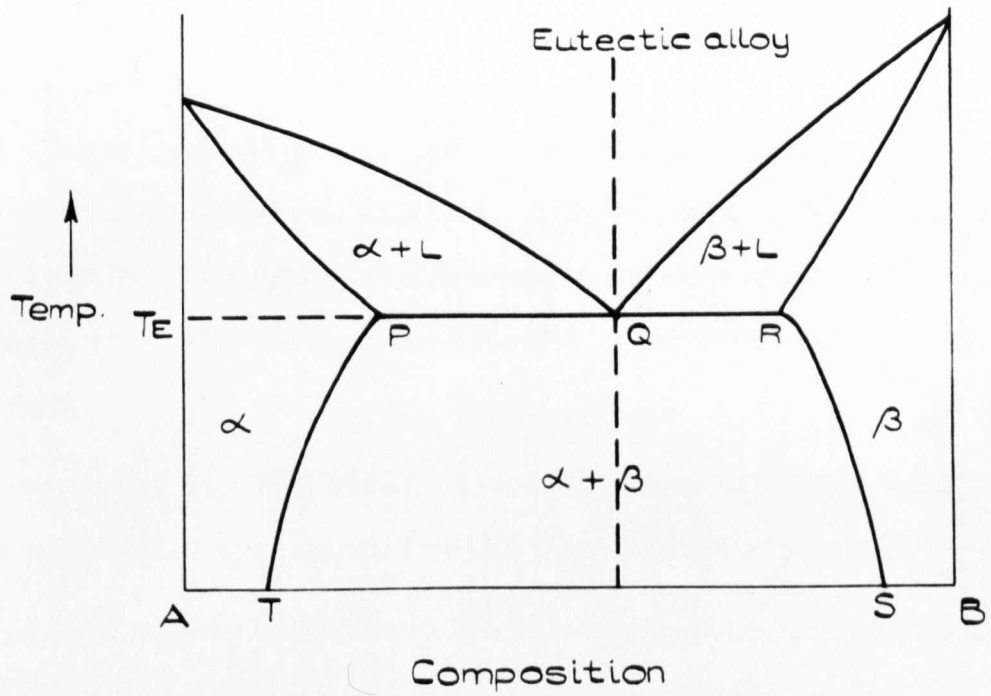
FIG. 9. A TYPICAL EUTECTIC DIAGRAM

It may be that under these non-equilibrium conditions the undercooling of the two phases is different so the resultant structure would show primary crystals of either α or β in a matrix of eutectic i.e. the eutectic point would have shifted.

An alloy having composition between T and P and in the temperature range above the solubility line TP and below the solidus during cooling consists of one phase only, α solid solution. Under equilibrium conditions, β phase is precipitated from solution when the solvus line TP is reached. If this alloy is rapidly cooled from this phase region (e.g. by quenching into water) to a temperature where the diffusion of B atoms required for the precipitation of β phase cannot occur or is very slow, the α-phase is retained as a meta-stable supersaturated solid solution at the lower temperature.

Elevation of the temperature allows diffusion and precipitation may proceed (the higher the temperature the more rapid the rate).

Alloys of composition between P and Q and Q and R solidify with primary crystals of α and β respectively in a matrix of eutectic.

7.2. Microstructure of eutectic alloys

The microstructure of an as-cast binary eutectic alloy consists of one phase distributed in a continuum of the other. The distributed or minor phase may be present as rods, laminae, discs, spheroids, needles or more complicated shapes. Consequently, a two dimensional section may give a wrong impression of the morphology of the structure. Particles seen in section may or may not be locally connected to one another.

Many classifications of microstructures exist, none of which is universally accepted. Chadwick[31] classified eutectics as 'continuous', 'discontinuous' and 'spiral' (only two of the latter are known and they will

not be considered further). 'Continuous' here means both phases must be continuous in the growth direction, 'discontinuous' means that only one is (the matrix always will be of course). Lamina and rod-like eutectics satisfy the requirement to be classified as continuous.

Lamellar eutectics are the most common in metals and it is generally accepted [32,33,34] that this growth arrangement is the preferred one because certain orientation relationships are of lower energy than others and these are most completely attained in a laminar structure.

Unidirectional freezing of a pure lamellar eutectic results in a striking redistribution of the laminae i.e. they extend in an edgewise manner in a direction parallel to the direction of heat flow (see for example, micrograph 12 section 8.). This occurs because a molten eutectic alloy freezes at a definite temperature like a pure metal and if it is positioned in a stable temperature gradient such that part of the ingot is above the melting point, a planar solid-liquid interface results. If an ingot is lowered through such a temperature gradient as in the apparatus of fig.8 at a suitable rate (1-10 cm/hr), enough time is allowed for diffusion to take place which allows preferential precipitation to occur. An actual temperature gradient(obtained by lowering a thermocouple through the furnaces) is shown in fig.10.

The resulting ingot consists of many grains within which the laminae are equi-spaced and parallel. Laminae in different grains are not parallel to each other, however, but are randomly orientated about the growth axis. As directional solidification proceeds some grains grow at the expense of others so that their number decreases along the length of the ingot. The spacing, λ, of laminae within a grain is determined by the growth rate, R, and is found experimentally and theoretically to be

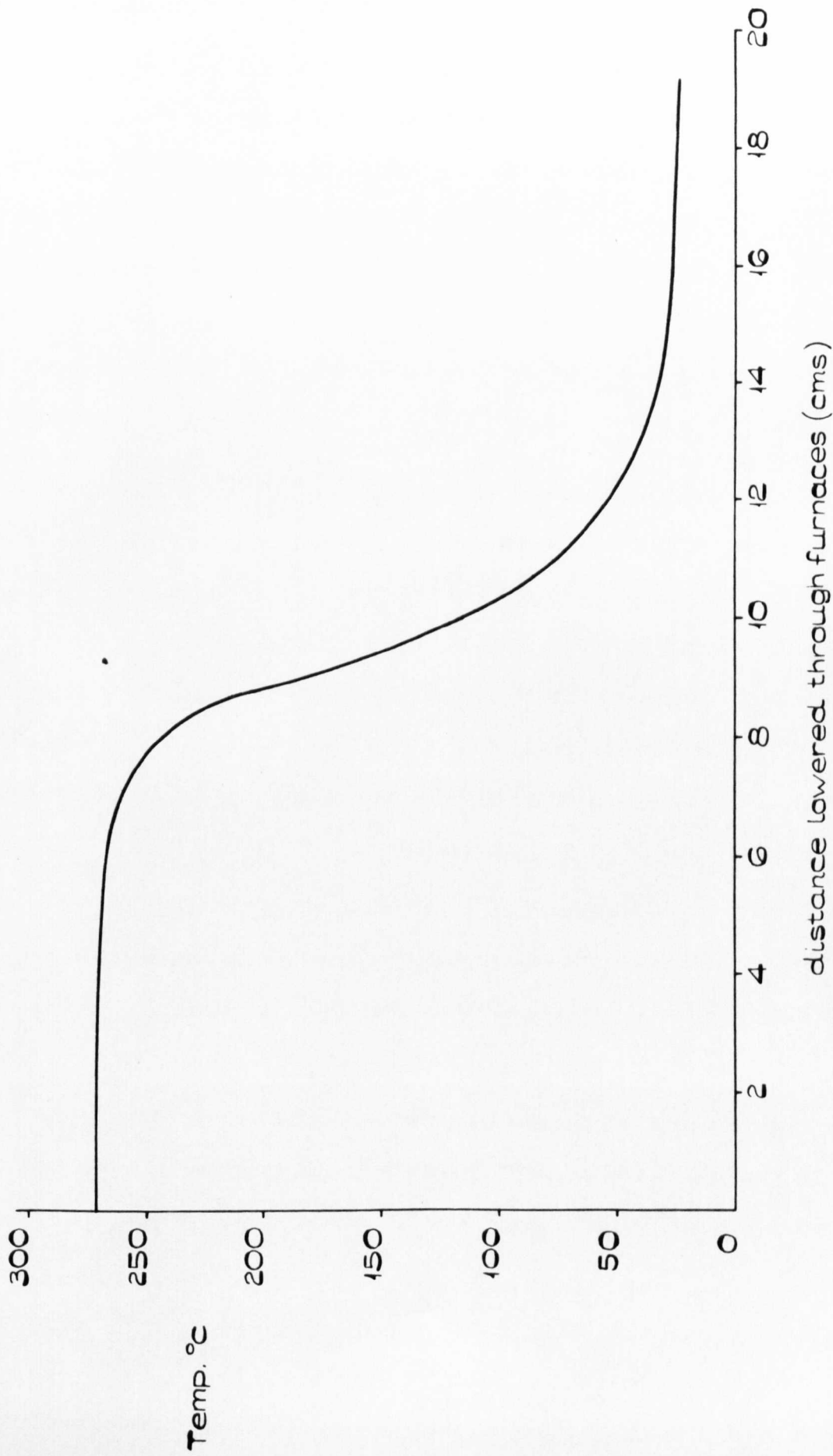$$\lambda = \frac{A}{R^{\frac{1}{2}}} \quad [31,35.]$$

FIG. 10. TYPICAL TEMPERATURE GRADIENT OBTAINED WITH FURNACE ARRANGEMENT OF FIG. 8.

where A is a constant for a given system which depends on the diffusion characteristics.

Very slow rates of growth sometimes result in the laminae fragmenting into a 'degenerate' structure (see micrograph 6). The reason for this is not fully understood but it is thought that if the orientation relationships between the phases are not the characteristic equilibrium orientations, then the structure may decrease its total energy by changing to the degenerate mode. In this state the total area of boundary may be greater but the product of boundary area times the interphase boundary energy is less than before.

Weart and Mack[36] showed that a eutectic may have three definite structural features, i.e. i) the grain structure of the matrix, ii) the 'colony' structure and iii) the eutectic mixture structure, each being contained by its predecessor. They observed that the laminae in a lead-tin eutectic occurred in colonies or regimes within a grain of matrix and that these colonies could be associated with a cellular solid-liquid interface. A colony boundary is distinguished mainly because of a change in particle shape.

The cellular structure is believed to be caused by a constitutional supercooling ahead of the solid-liquid interface by impurity rejection from the melt. Any protusion into this supercooled region will be maintained, thus resulting in a cellular interface.[37].

Some lamellar eutectics transform to a rod-like eutectic when impurity is present. An impurity may have one of three effects according to Chadwick[38] who considered the shape of the ternary phase diagram resulting from the impurity addition.

(i)   If the partition coefficients of the impurity in both phases

are equal i.e. $k_\alpha = k_\beta$, laminae will be stable for a planar
or cellular interface since long range supercooling is
involved.

(ii)   When $k_\alpha \neq k_\beta$ the laminae may form rods because short range
supercooling is involved.

(iii)   If $k_\alpha = k_\beta$ at low impurity concentrations but $k_\alpha \neq k_\beta$ at
high impurity contents then a colony structure occurs
with rods at the colony boundaries only.

Hunt and Chilton[33], however, showed that rods could be formed when
grains of some pure laminar eutectic alloys are made to grow such that the
growth direction is not contained in the plane of the laminae, thereby
proving that the solid-liquid interface curvature can have an effect.

Hellawell and co-workers[39,40,41] have directionally frozen several
eutectics and they agree with Hunt and Chilton that there can be no
modification of the laminar structure without a curved interface. Both
groups agree that the transformation is most likely to occur in a system with
a high volume ratio of the two phases.

8.   Microstructures of specimens examined

Photomicrographs obtained for the various alloy systems measured are
shown in this section. The phase diagrams have also been included to
clarify the text. They are taken from Hanson[42].

8.1.   In-Bi system.
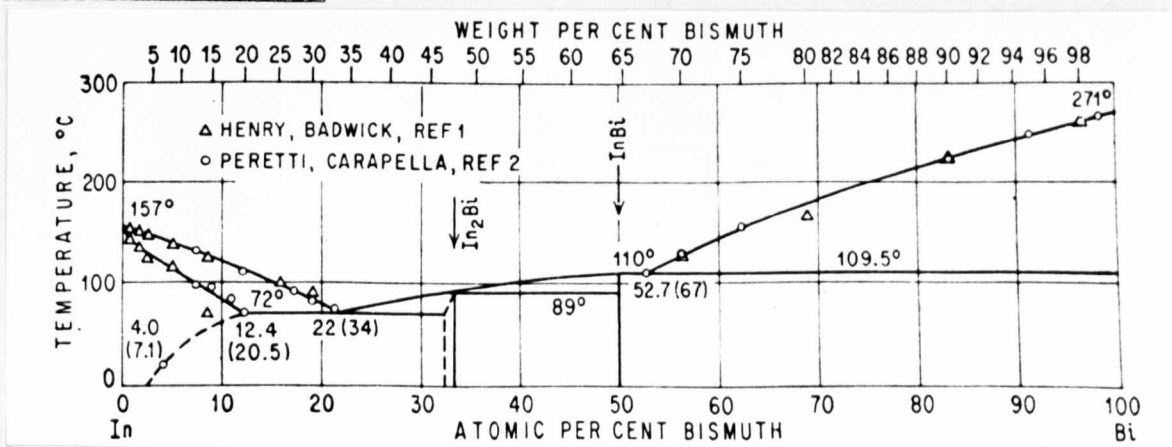
Two eutectics exist in this system but only the one occurring at 34 wt.% Bi is superconducting at 4.2°k. After heat treatment at 60°C the alloy consists of laminae of In_2Bi in a matrix of In + 12% Bi solid solution. No lamina to rod transformation occurred on addition of impurities (Sn, Sb,Cd).

The polished specimens were etched in hydrochloric acid, picric acid and alcohol which caused the In-rich phase to appear dark under the microscope and the In_2Bi phase white. The phases were identified by adding excess Bi to a sample of the eutectic alloy and observing the colour of the primary crystals formed. This technique was used for identification of phases in other systems where necessary.

8.2   Bi-Tl system.
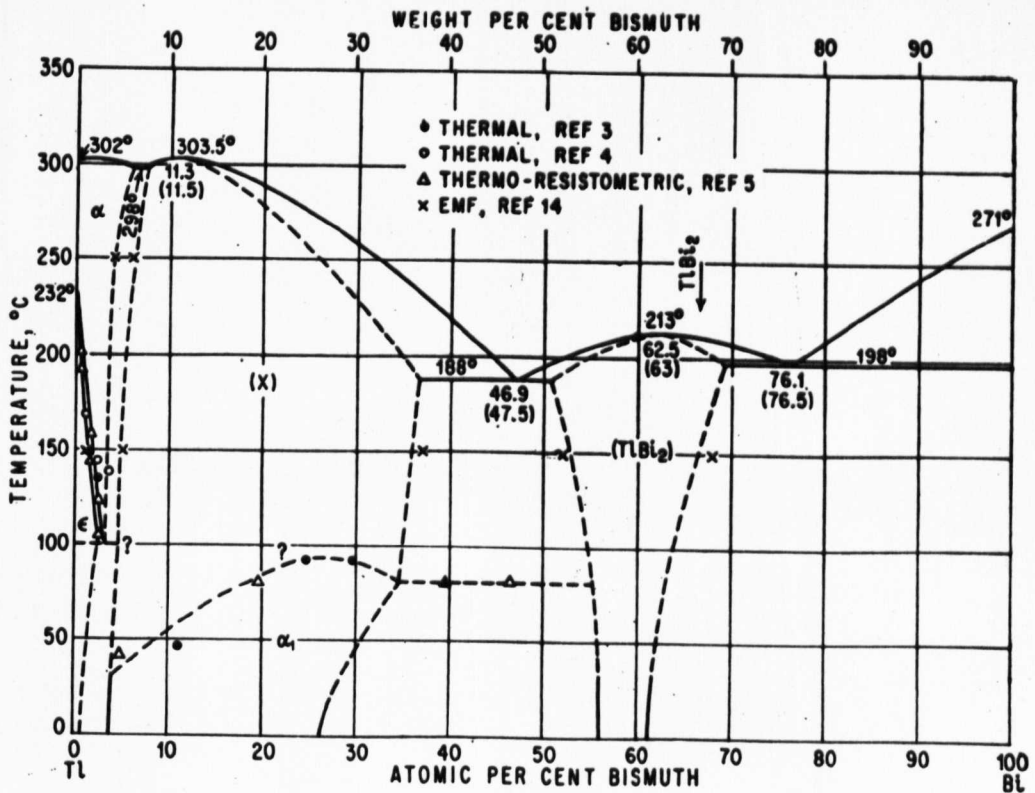
Two eutectics were examined.

  (i) Alloy at 47.5 wt.% Bi.

       The Tl Bi$_2$ solid solution forms the matrix and etched with

       2% nital appears light with X-solid solution showing as

       dark laminae. An obscure transformation occurs in the

   X phase at about 80°C.

  (ii) Alloy at 76.5 wt.% Bi.

       Again the Tl Bi$_2$ solid solution forms the matrix but in

       this case appears dark when etched with nital. The light

       etching Bi particles are dispersed in a 'chinese script'

   or 'herring-bone' formation.

8.3   Cd-Pb system
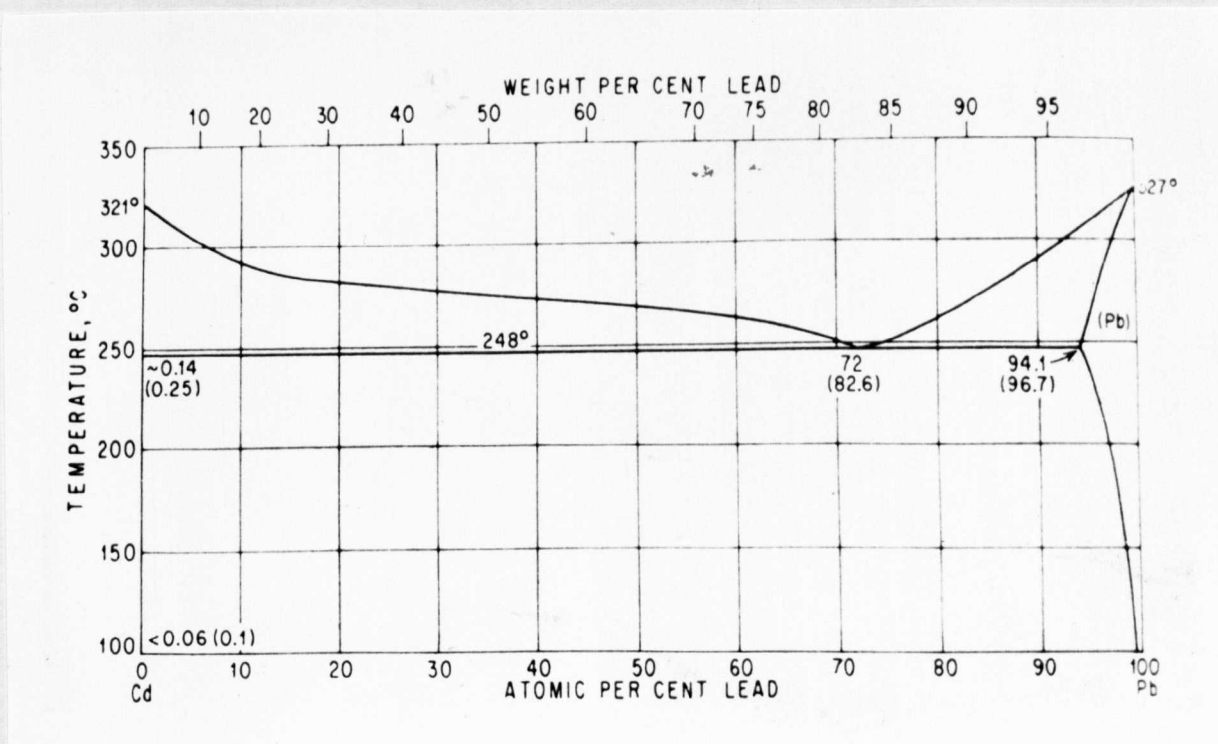
When pure materials are used this eutectic consists of laminae of

almost pure Cd in a matrix of Pb-rich phase. When .1% Sb is added the

Cd laminae are transformed to rods. Etched with a mixture of 4 parts

glacial acetic acid and about one part hydrogen peroxide (100 vols.) the

Cd appears dark.

8.4.   Hg - Tl system
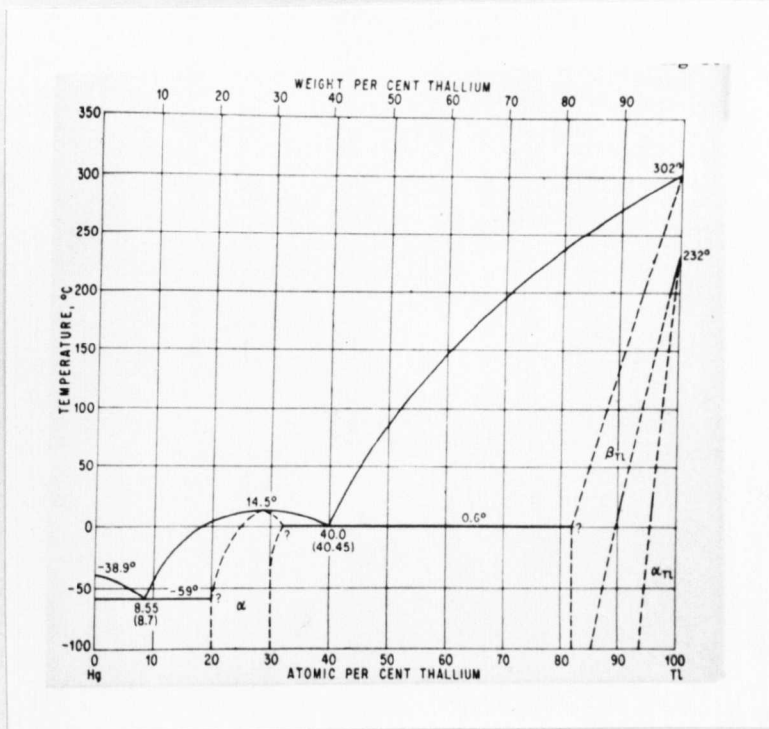
The eutectic at 40.45 wt.% Tl was examined. No microscopic examination was possible with this alloy because it is liquid at room temperature but the phase diagram indicates that it consists of a matrix of α - solid solution.

8.5.   Mg - Pb system
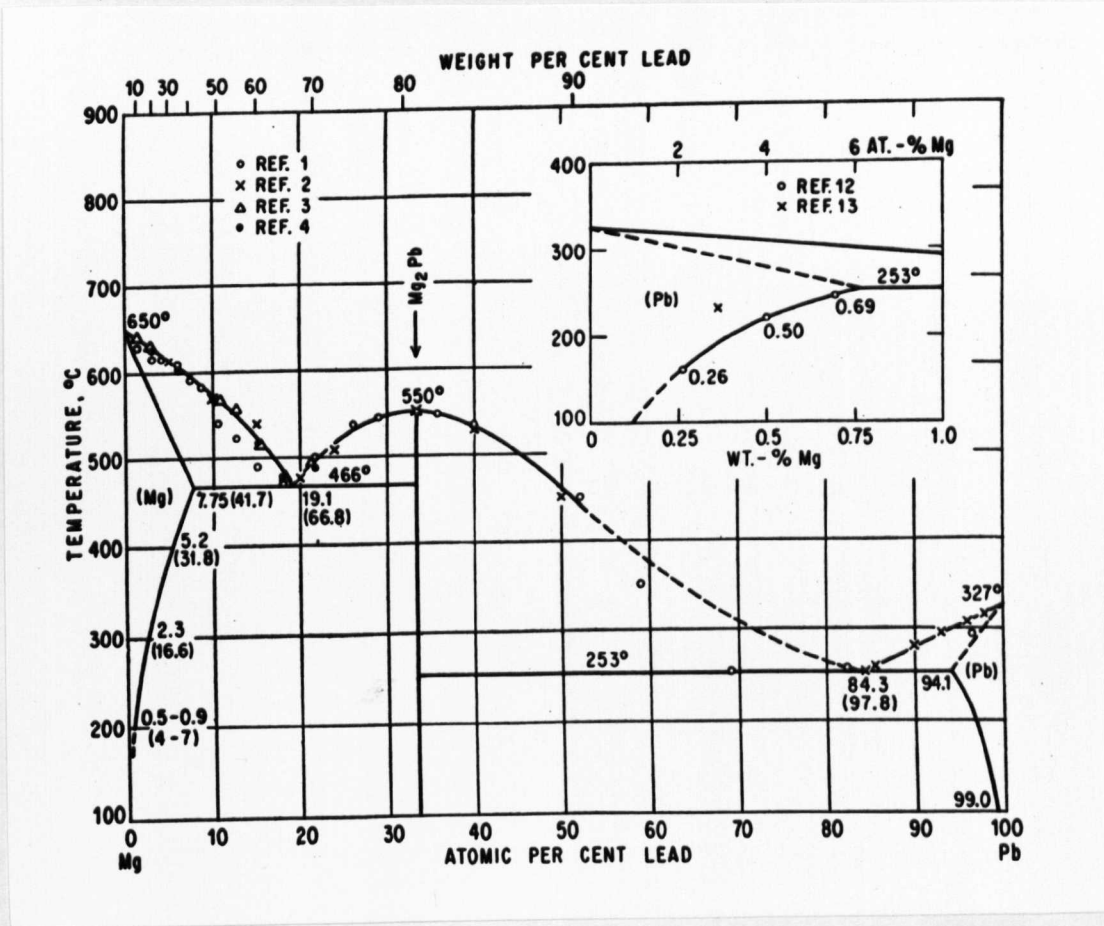
The eutectic alloy at 97.8 wt.% Pb was examined. It consists of a Pb-rich matrix with particles of Mg$_2$Pb dispersed discontinuously throughout and appearing dark when etched with 4 parts acetic acid and 1 part hydrogen peroxide (100 vols.)

8.6.   Pb - Sb system
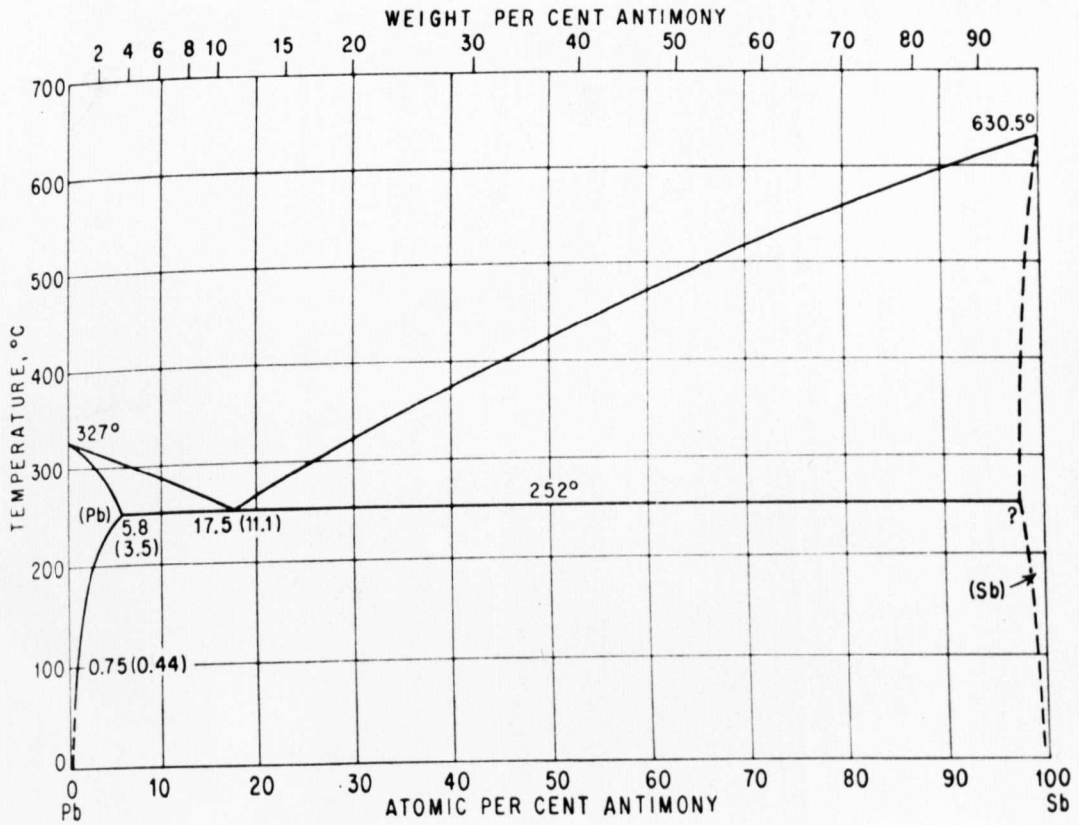
This eutectic alloy consists of acicular randomly dispersed particles of Sb-rich phase in a groundmass of Pb-rich phase. When etched in nital (2%) the Sb-rich phase appears white.

## 8.7.   Pb - Sn system
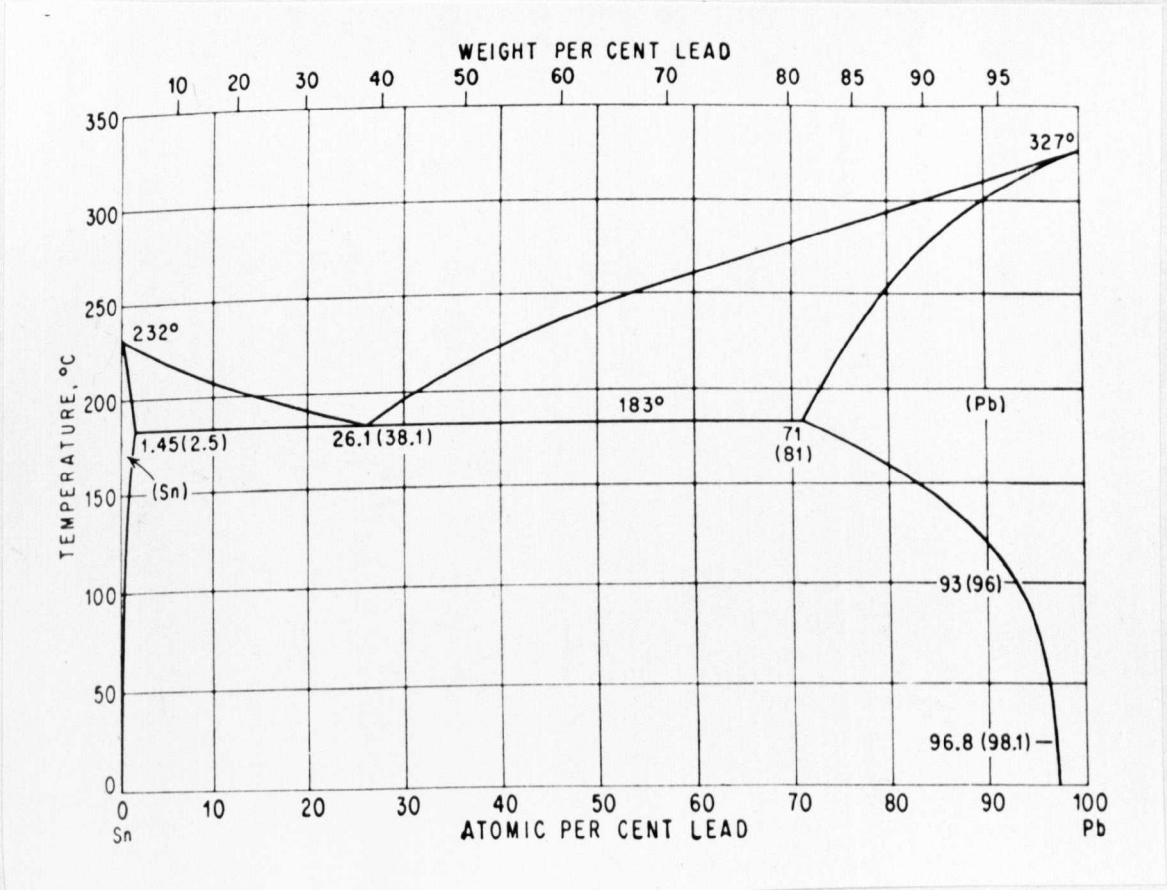
When heat treated at $118^{\circ}C$ this eutectic alloy consists of laminae of Pb + 6% wt.Sn in a matrix of nearly pure Sn. The laminae appear dark when etched with 2% nital. No lamina to rod transformation occurred when impurities were added.

8.8. Pb - Zn system
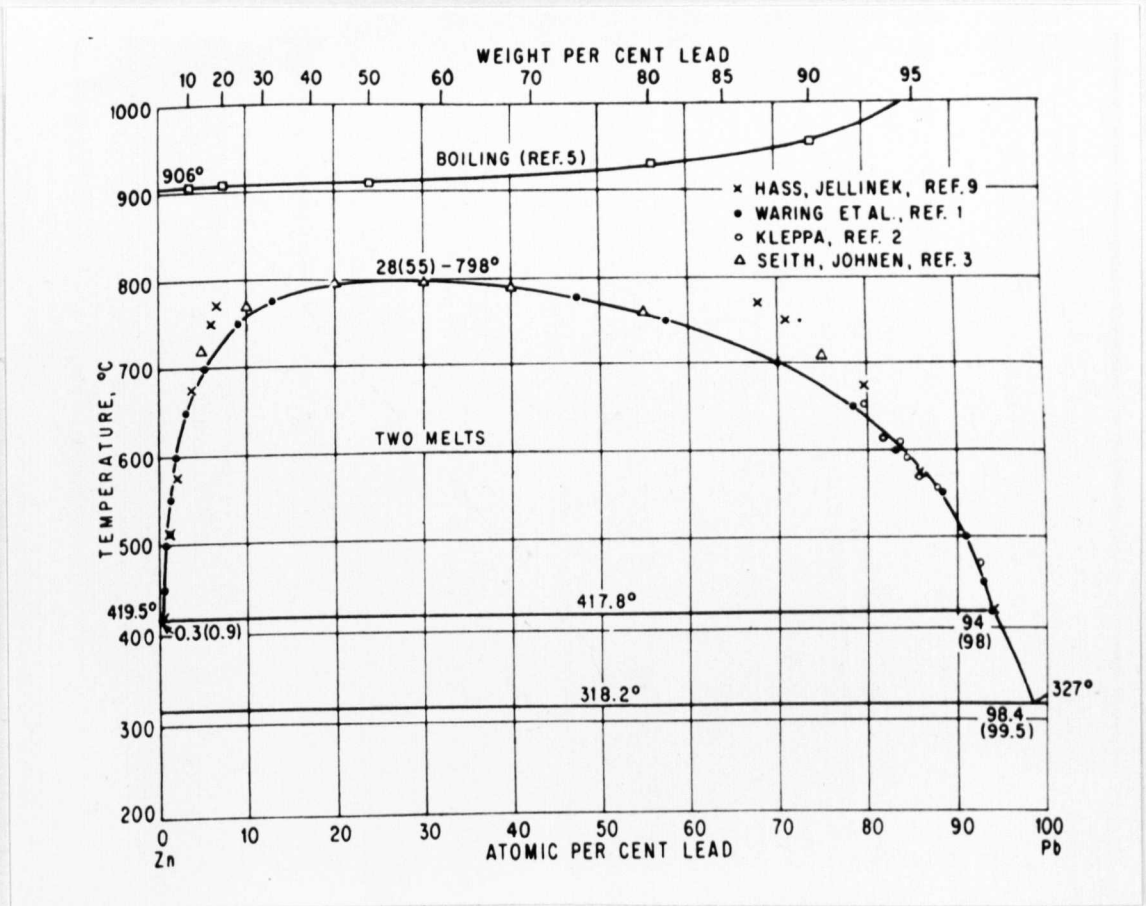
The Pb-Zn eutectic consists of almost pure Pb with Zn particles
distributed discontinuously throughout.

8.9.   Sb - Tl system
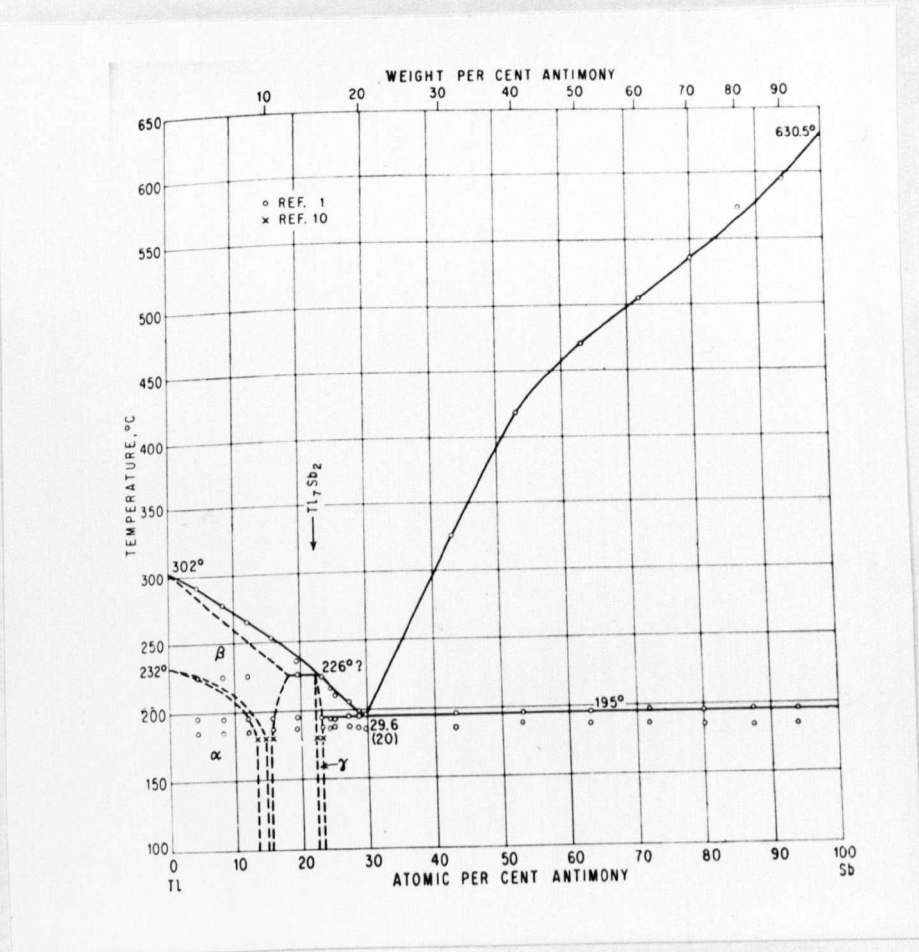
Acicular needles of nearly pure Sb reside in a matrix of Tl_7Sb_2 in this eutectic. The Tl_7Sb_2 appears dark when etched with 2% nital and the Sb white.

8.10. Photomicrographs.
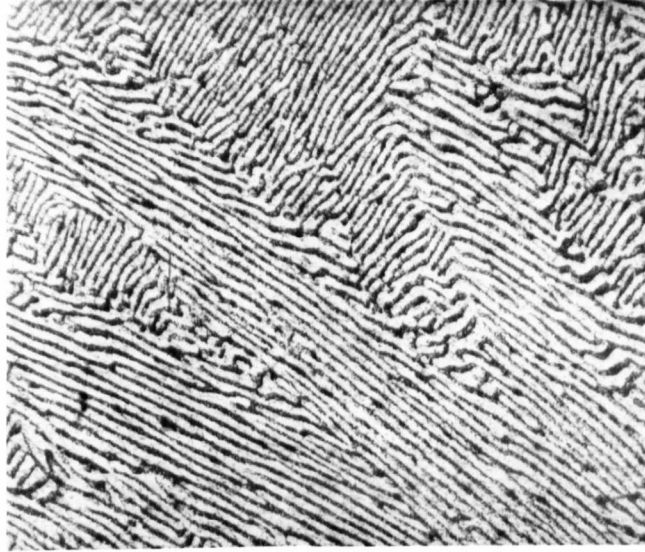
1. In-Bi eutectic as cast. White laminae of In_2Bi are dispersed in a matrix of In-rich solid solution. Mag. x 140.
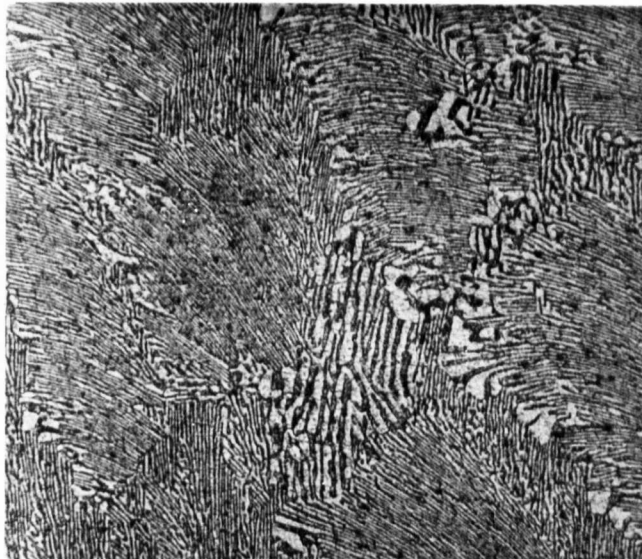
2. In-Bi eutectic. Transverse section of slab directionally frozen at 4.6 cm/hr. Mag. x 130.
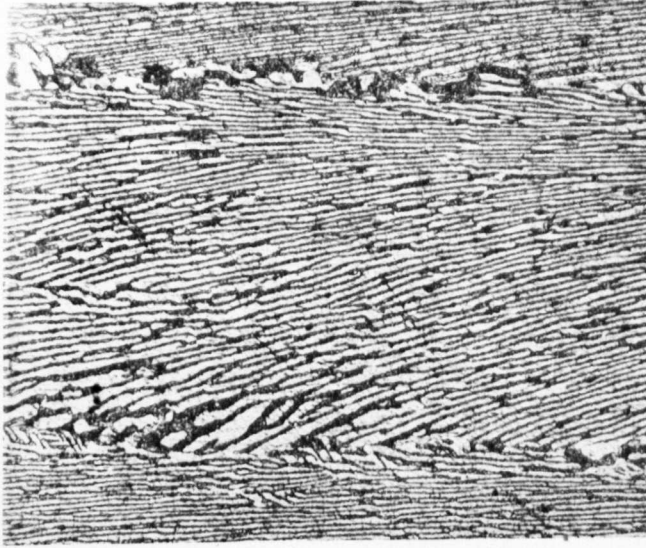
3. In-Bi eutectic. Longitudinal section of 2. Mag. x 145.
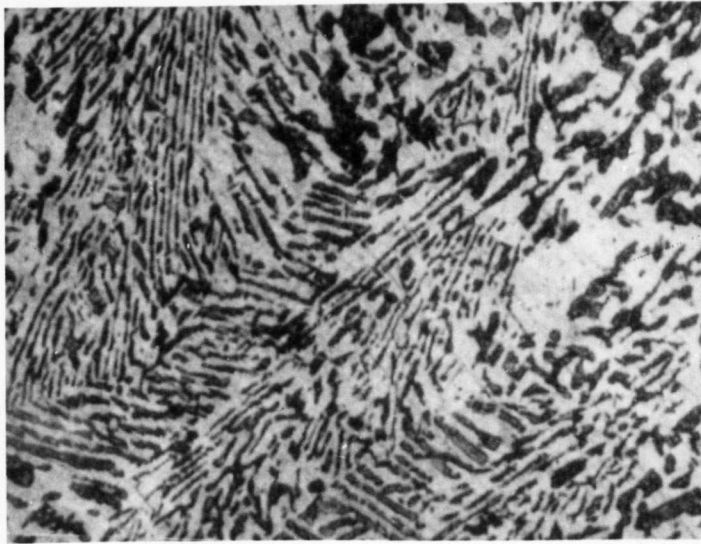
4. Bi-Tl eutectic (47.5 wt.% Bi) as-cast. The light etching $TlBi_2$ matrix contains dark laminae of X solid solution. Mag. x 225.
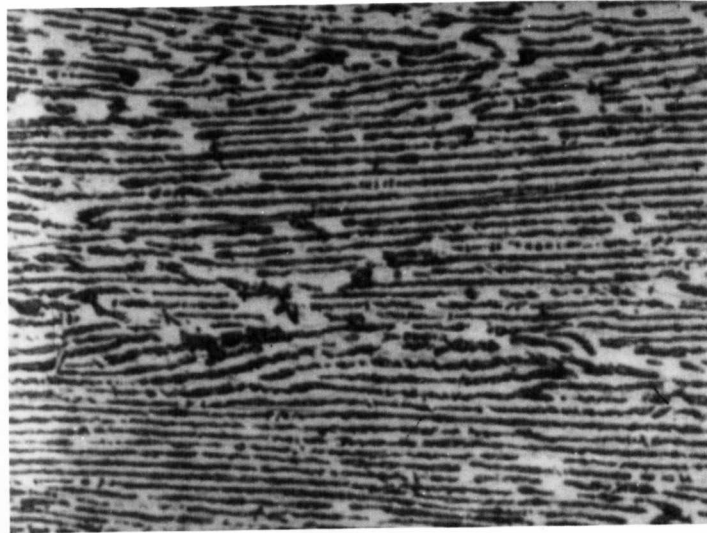
5.   Bi-Tl eutectic (47.5 wt.% Bi) directionally frozen at 4.6 cm/hr.
Longitudinal section.   Mag. x 225.
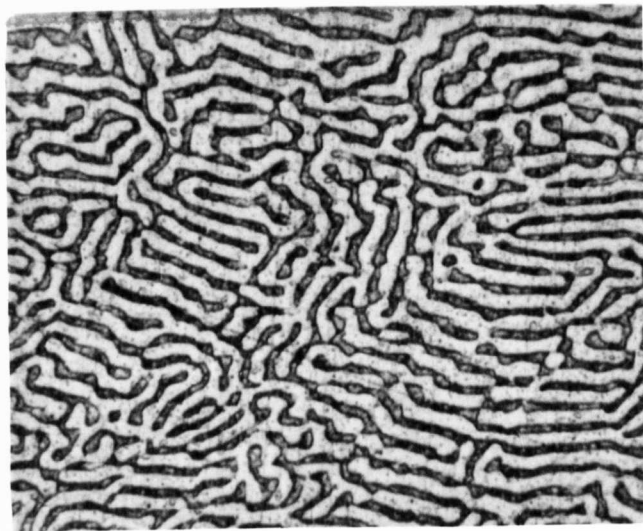
6.   Region of degenerate laminar structure contained in 5.   Mag. x 455.
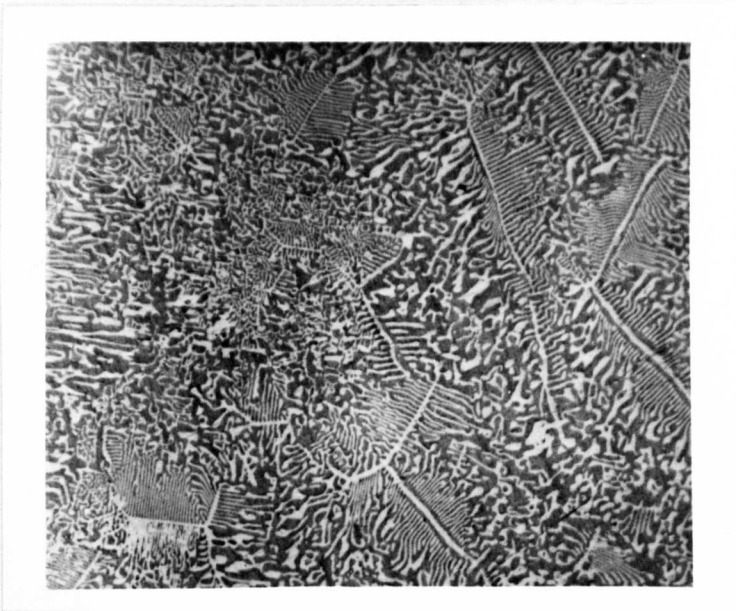
7. Bi-Tl eutectic (76.5 wt.% Bi). The dark matrix of TlBi$_2$ contains Bi particles distributed in a 'herringbone' or 'chinese script' manner. Mag. x 140.

8. As above. Mag. x 500.
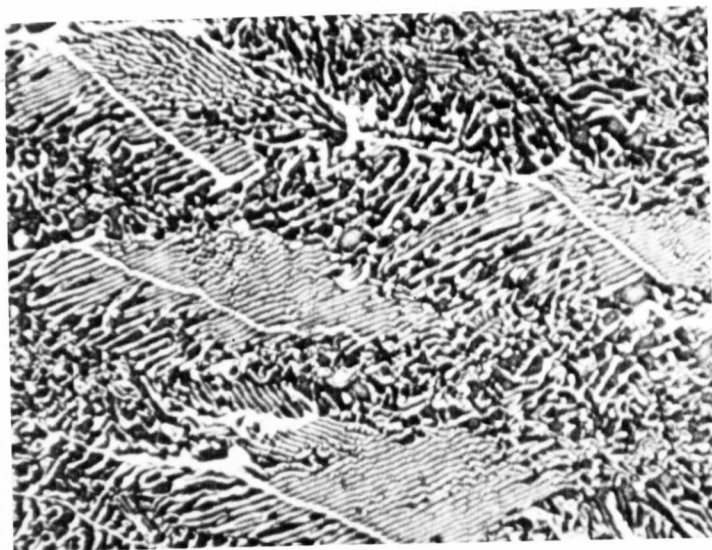
9.   Bi-Tl eutectic (76.5 wt.% Bi) directionally frozen at 3.8 cm/hr.
Longitudinal section.   Mag. x 135.
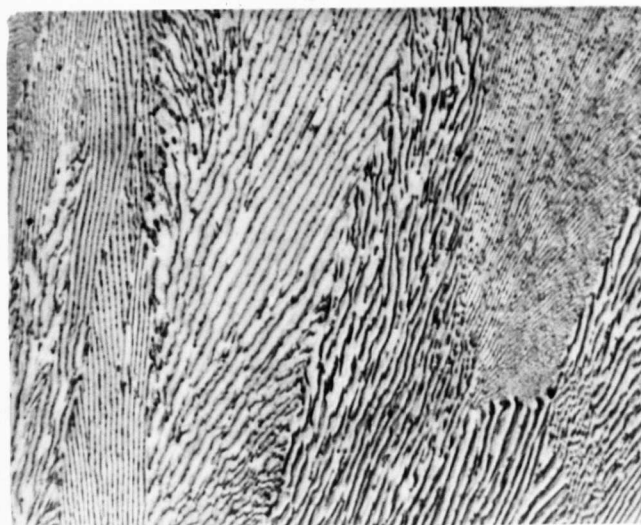
10.   Pb-Cd eutectic as-cast. Columnar grains of Pb-rich phase with
dark Cd-rich laminae. Mag. x 225.
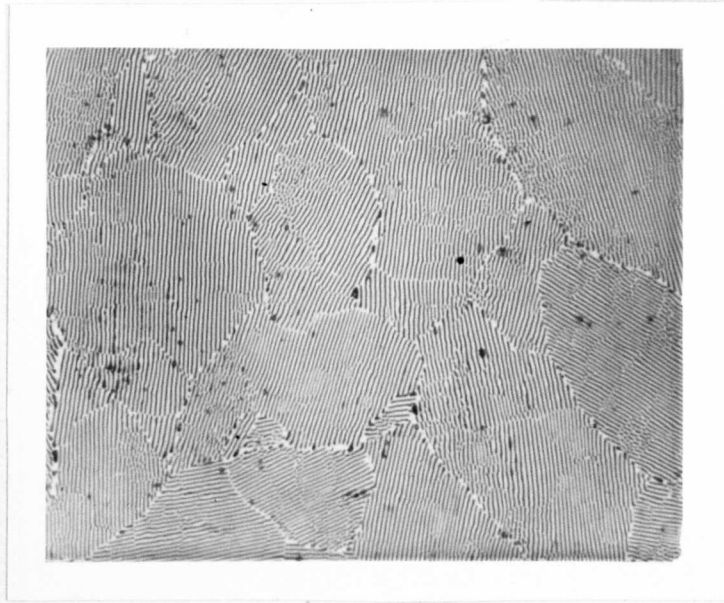
11.   Pb-Cd eutectic, directionally frozen. Section transverse to
       direction of growth. Mag. x 290.
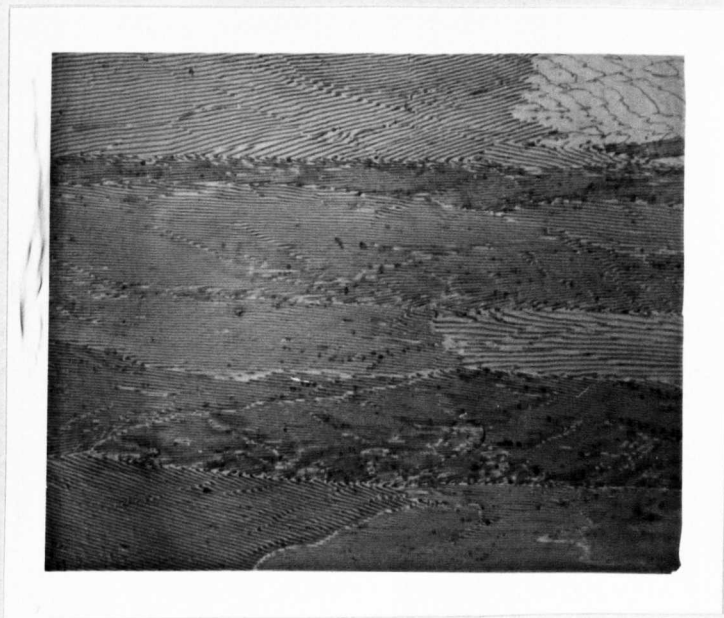
12.   Pb-Cd eutectic directionally frozen at 4.6 cm/hr. Section
       parallel to heat flow. Mag. x 215.
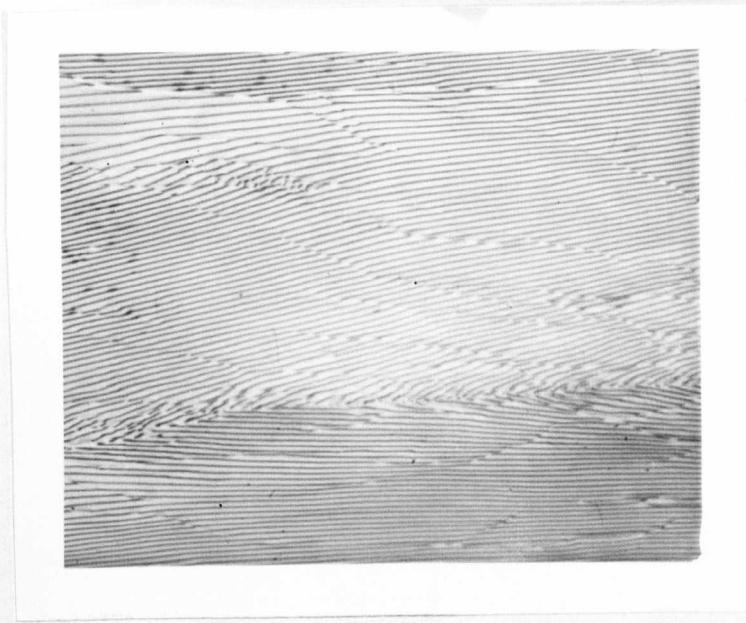
13.   Same as (12).   Mag. x 285
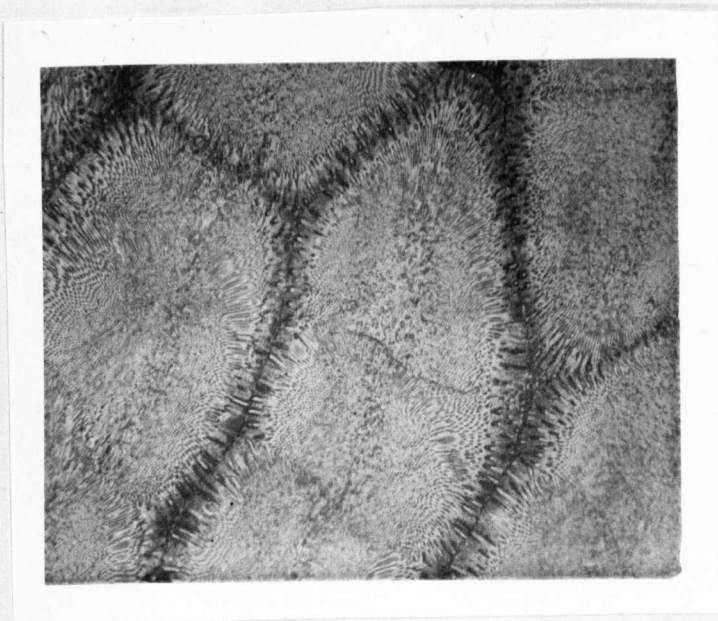
14.   As-cast columnar grains of Pb-Cd eutectic containing .1% Sb.

Mag. x 290.
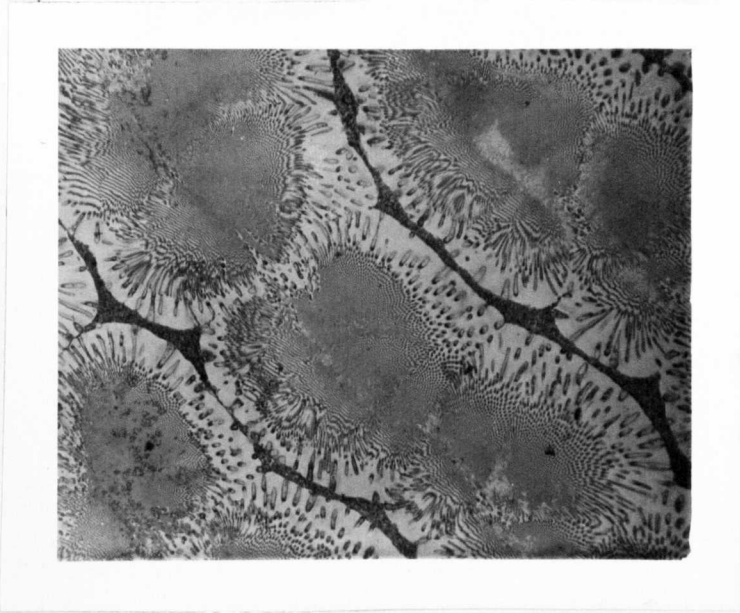
15. Pb-Cd eutectic with .1% Sb. Directionally frozen at 4.6 cm/hr.
     Section transverse to direction of growth.   Mag. x 225.
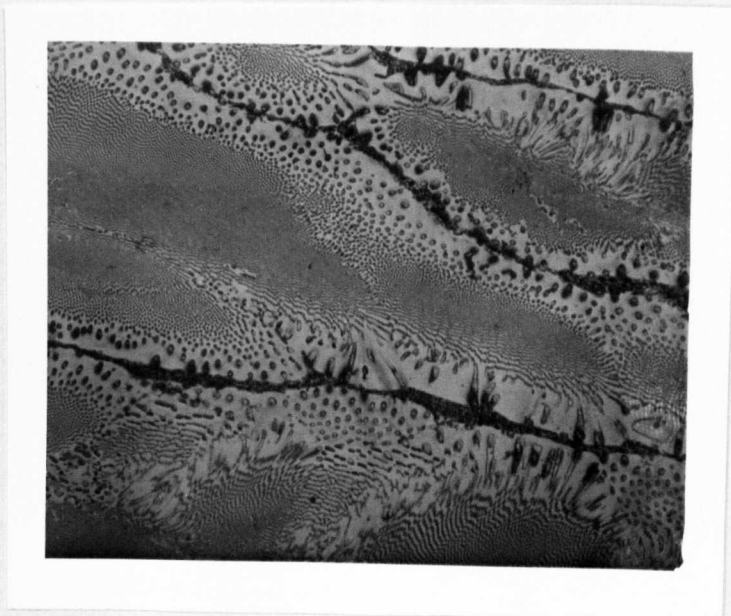
16. As above. Section parallel to growth direction.   Mag. x 225.
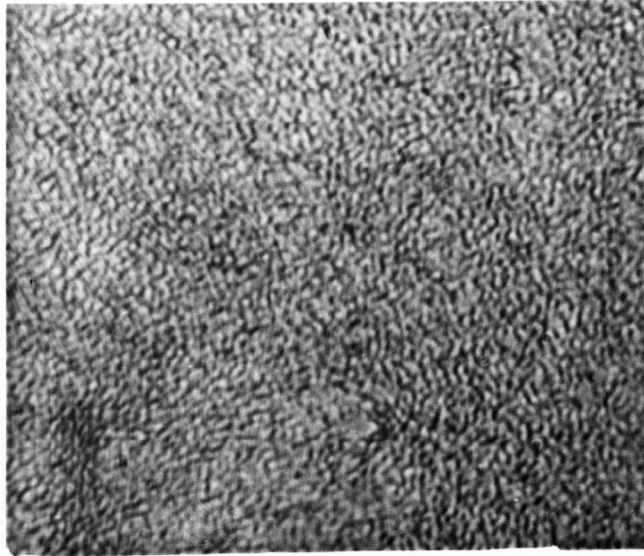
17.   Pb-Mg eutectic, as-cast. The dark particles are Mg_2Pb dispersed in a Pb-rich matrix.   Mag. x 1160.
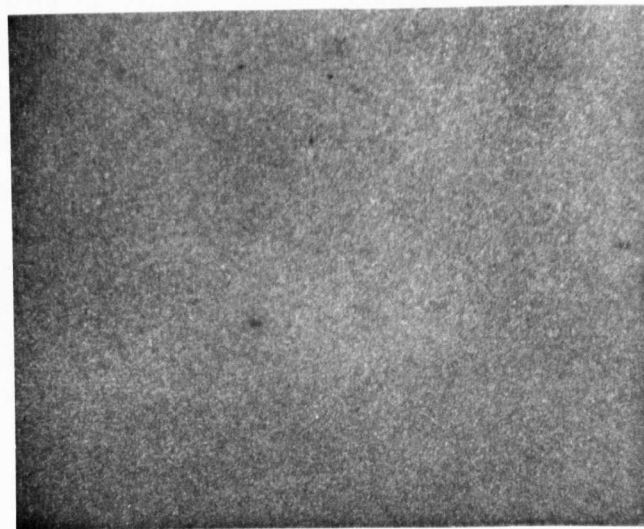
18.   Pb + .5%Mg. Quenched from 250°C and aged 20 hrs. at room temperature. Finely dispersed Mg_2Pb has precipitated.   Mag. x 300.
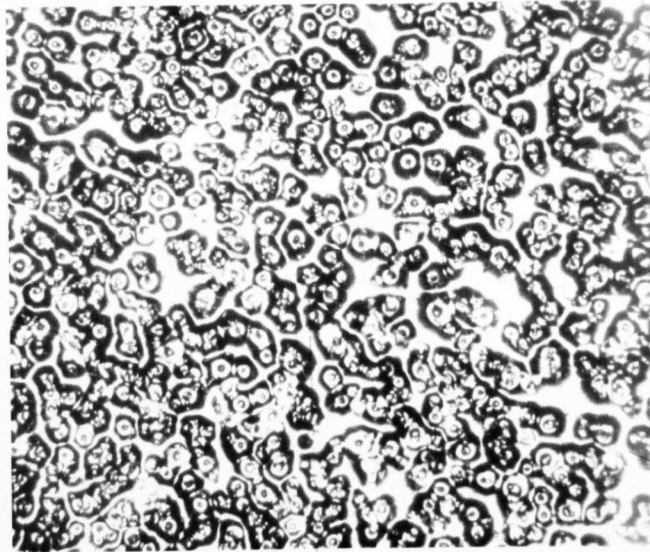
19.   Pb + .5%Mg. Quenched from 250°C and aged 3 weeks at room
temperature. More Mg$_2$Pb has precipitated and the finely
dispersed particles have coalesced.   Mag. x 75.
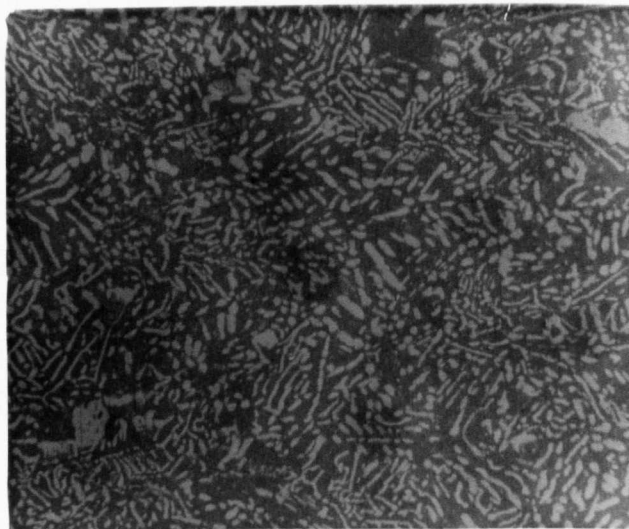
20.   Pb-Sb eutectic, as-cast. Light acicular particles of Sb are
dispersed in a dark Pb-rich matrix.   Mag. x 400.
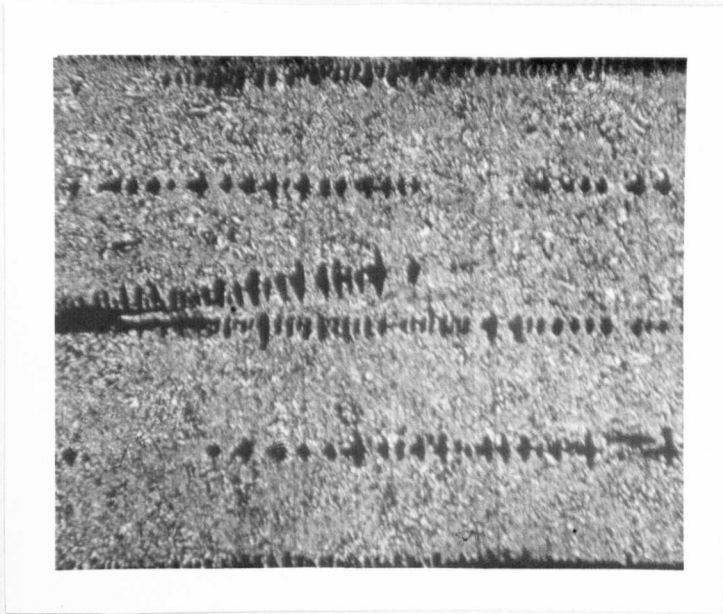
21. Pb-Sb eutectic directionally frozen. Gravity segregation of the
     liquids has occurred and the dendrites of the Pb-rich primary solid
     solution can be seen which are orientated approximately in the growth
     direction.   Mag. x 95.
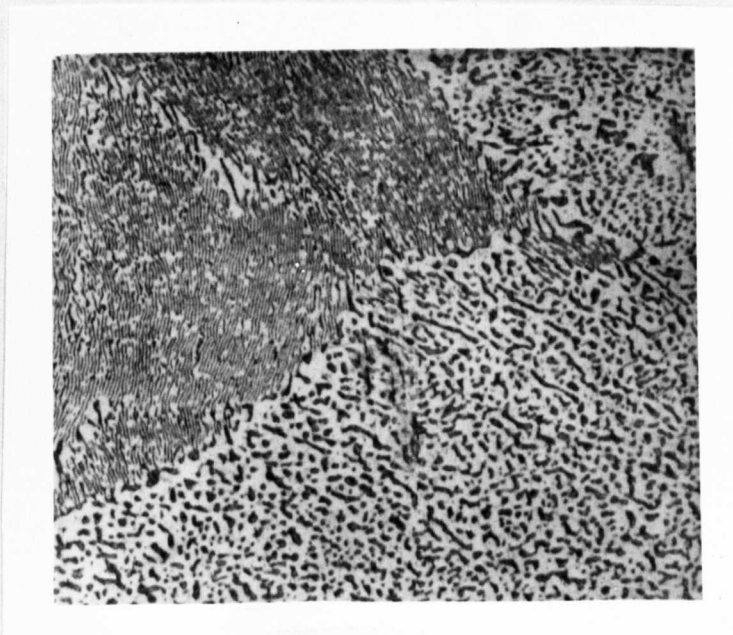
22. Pb-Sn eutectic, as cast. The dark Pb-rich phase exists as laminae
     and broken laminae in the Sn-rich matrix.   Mag. x 270.
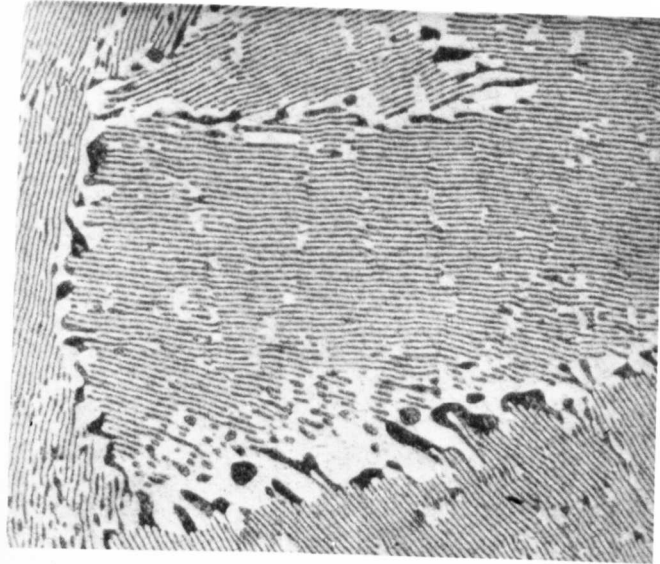
23.   Pb-Sn eutectic directionally frozen. Section perpendicular to growth direction. Mag. x 400.
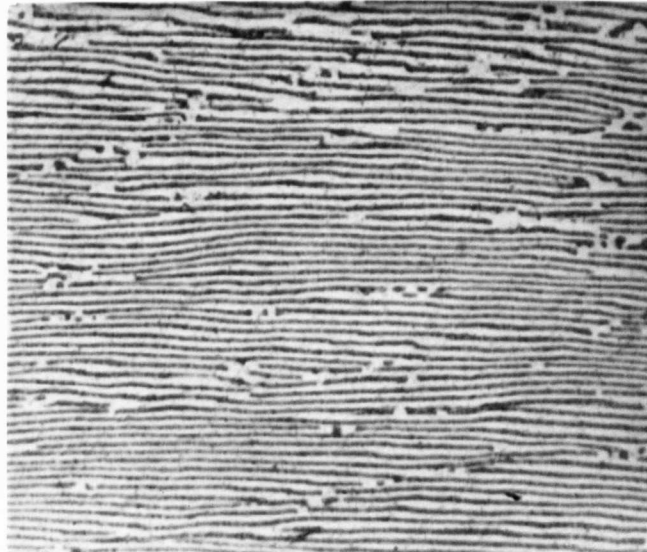
24.   Pb-Sn eutectic directionally frozen. Section parallel to direction of growth. Mag. x 160.
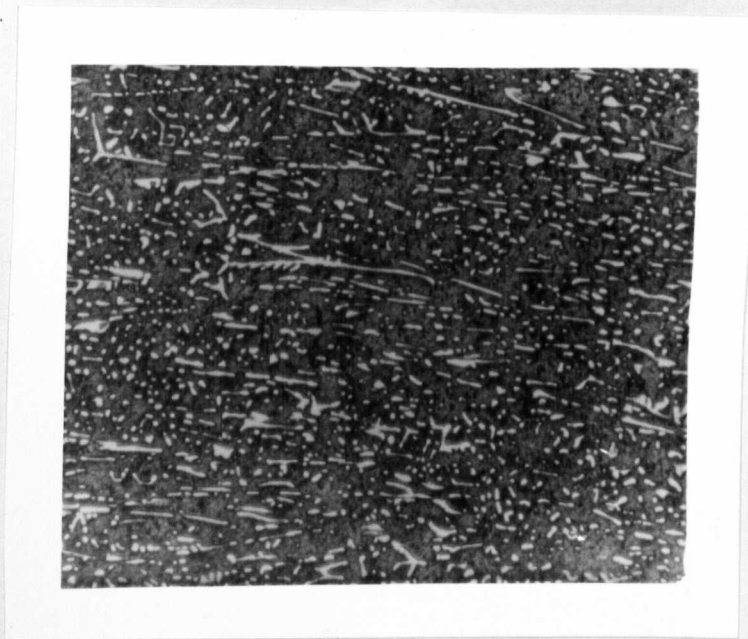
25. Sb-Tl eutectic directionally grown at 4.6 cm/hr. longitudinal section.
The dark matrix of Tl_7Sb_2 contains acicular particles of nearly pure Sb.

Mag. x 300.

26. As above. Transverse section. Mag. x 300.

8.11.   Some remarks on the microstructures.

Chadwick's[31] classification of eutectic microstructures into 'continuous' or 'discontinuous' clearly is not complete; a graduation of the degree of continuity seems to exist. Pb-Sb eutectic exhibits the same discontinuous microstructure when directionally frozen as when 'as-cast'. When this particular eutectic is directionally frozen, however, gravity segregation occurs which causes the lower portion of the ingot to become richer in Pb so that it freezes as a hypoeutectic alloy containing primary lead crystals. These are elongated and their longitudinal axis lie within a few degrees of the growth direction.

Both Sb-Tl and Bi-Tl (76.5% wt.Bi) could be referred to as 'semi-continuous'. The Sb particles in the Sb-Tl eutectic show a tendency to grow in the direction of heat flow but not to any extent (see micrographs 25 and 26). The Bi particles in the Bi-Tl (76.5% wt. Bi) eutectic are partly distributed in fern-like skeletons, the laminated branches of which tend to be oriented parallel to the growth direction. This eutectic could be called 'semi-laminar'. (see micrographs 7-9).

Even in the laminar eutectics the laminae are not perfectly parallel sheets within any one grain. Kraft and Albright[32] first pointed out that faulted regions occur in the lamellar arrangement when viewed transverse to the growth direction. These faulted regions resemble the arrangement of atomic planes in the region of an edge discolation. In fact, micro-graphs 12 and 13 show that in Pb-Cd eutectic the laminae eventually reach a similar mismatch surface in a longitudinal direction. An extra lamina usually seems to lie on the side of the fault solidifying last, but some faults contain no extra plane.

Pb-Sn eutectic is similar in the transverse section, but in the

longitudinal direction the laminae terminate randomly, i.e. a definite
boundary of mismatch does not seem to occur.

All the directionally frozen laminar eutectics showed a slight cellular
structure indicating the presence of impurities. These impurities may have
been present in the 'as received' material or they may have been introduced
during the sample preparation (this seems unlikely, however, in view of
the care taken).

The non-laminar eutectics do not show a cellular structure even in
the presence of appreciable (.1%) amounts of deliberately added impurity.

The Cd rods in in the Pb-Cd eutectic containing .1% Sb are not
continuous along the specimen axis for long. This is presumably due to
the cellular interface the Sb imposes on the system. The cell walls appear
to be full of Cd. Superconductivity measurements presented later suggest
that this is not the case, however.

9. Experimental Apparatus for Superconducting Measurements

9.1. Specimen Magnetisation.

All measurements were made at $4.2^{\circ}K$, the boiling point of liquid
helium at atmospheric pressure, (except where otherwise stated) on a
modified Foner vibrating sample magnetometer [68] having a resolution of
about two gauss [43]. A block diagram of the apparatus is shown in fig.11.
The specimen was vibrated sinusoidally between two closely matched pick-up
coils, connected in series opposition. These pick-up coils were wound from
5,000 turns of 50 s.w.g. enamelled copper wire. To avoid demagnetising
effects the samples were cylindrical (4mm. diameter and 30mm. long with
the ends rounded to approximate an ellipsoid).

The sample vibrator was driven by a Servomex Waveform Generator
L.F. 141 via a Pye-Ling 5VA Power Amplifier. The magnetic field was
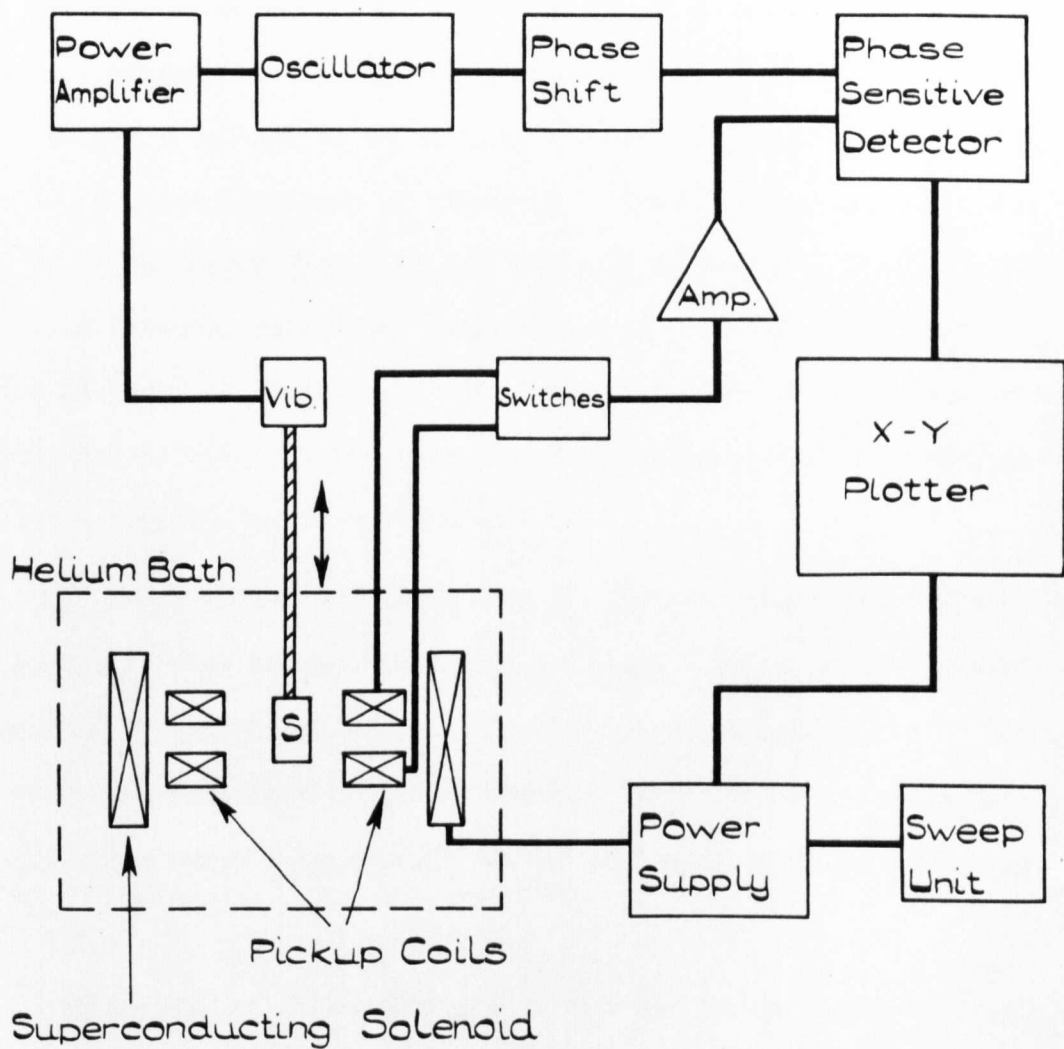
FIG. 11. BLOCK DIAGRAM OF THE VIBRATING SAMPLE
MAGNETOMETER.

provided by an Oxford Instrument superconducting solenoid with a 3 cm. bore capable of delivering up to 30 koesteds and driven by an Oxford Instrument power supply. The axis of the specimen, the coils and the solenoid were colinear (see fig.12).

When the specimen in the superconducting state was vibrated (at a typical frequency of 70 c/s) the change in flux linkages in the pick-up coils caused a voltage to be induced proportional to the specimen magnetisation for a given amplitude of vibration. This voltage was amplified by a Dawe Valve Voltmeter Type 614C and fed into a Brookdeal Electonics Phase Sensitive Detector Unit which was referenced from the Variable Phase Unit of the Servomex oscillator and its output displayed on the vertical axis of a Moseley Model 7000H X-Y recorder. A voltage proportional to the applied field was applied to the horizontal axis.

The sample holder was adjustable so that the sample could be positioned symmetrically with respect to the pick-up coils, this position being determined by switching the coils in series and adjusting for minimum signal. Any deviation from this critical position produced anomolies in the magnetisation curve - especially in the region of small magnetisation near H_{c2}.

A sweep rate of about one oersted per second was used throughout; this value being slow enough to cause negligible sweep rate effects, (Seebold[44] has shown that the equilibrium magnetisation lags behind the field by an amount that depends on the sweep rate).

For all the curves the assumption was made that the specimen was perfectly diamagnetic at small fields so that the magnetisation could be calibrated by setting the output from the phase sensitive detector equal to the applied field at a low value of field.

Direction of vibration

Heating coil

Sample

Superconducting solenoid

Tufnol sample holder

Perspex former

Pickup Coils
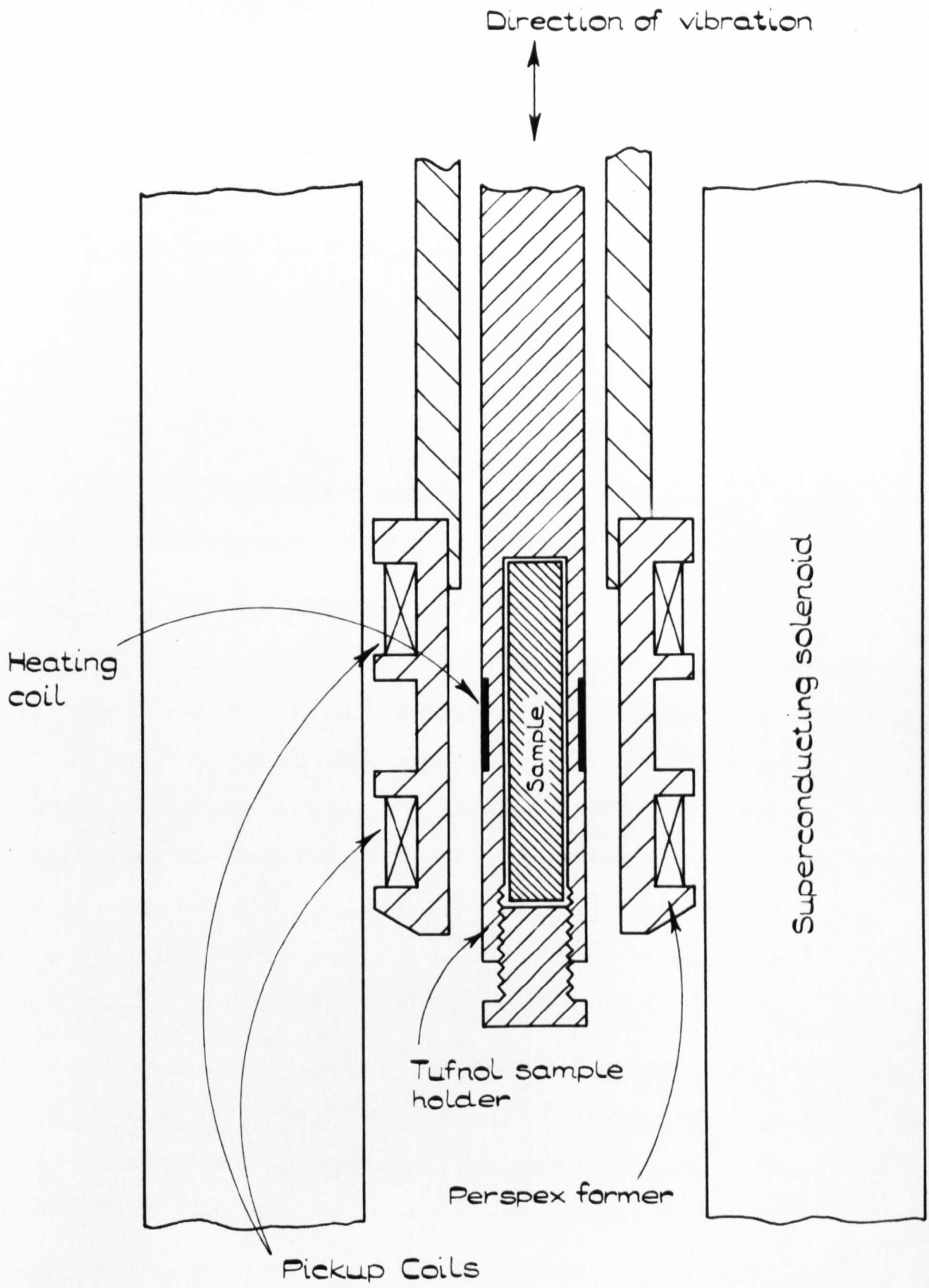
FIG. 12. DETAILS OF VIBRATION MAGNETOMETER

H_{c2} was taken to be that value of field at which no further superconductivity could be detected. Although a St.James and DeGennes sheath exists above H_{c2} to a field $H_{c3} = 1.69 H_{c2}$, its thickness is only of the order of the coherence length. This volume of specimen being shielded represents a magnetisation smaller than the apparatus sensitivity. The volume fraction still superconducting above H_{c2} is $\dfrac{2\xi}{r}$ where r is the radius of the specimen.

If $\xi \approx 10^{-5}$ cm and $r \approx .5$ cm.,

$$\frac{2\xi}{r} \approx 5 \times 10^{-5}$$

The maximum value of $-4\pi M$ of the alloys is about 1000 gauss and so the sheath would represent a magnetisation about 0.05 gauss.

9.2. Critical Current Measurements.

These measurements were taken in a tailed dewar assembly, suspended between the pole-pieces of a Mullard 9" electromagnet, type EE 1036 which was controlled by a Mullard Sweep Unit type EE 4044. The field was measured by means of a probe search coil, the pick-up signal of which was supplied to a Newport Magnetometer type J and thence to the Mosely X-Y recorder. This signal was also displayed on a Solartron digital voltmeter, both to facilitate the zeroing of the magnetometer and to enable any drift occurring during an experiment to be immediately compensated. A block diagram of the apparatus is shown in fig.13.

The range multiplier of a Keithley 148 Nanovoltmeter enabled the arbitrarily small voltage which defined the critical current to be amplified to ~ 1 volt. This voltage was then arranged to open a relay in the base current line of the bank of power transistors in the current supply.

During an experiment the current was increased manually at constant field and the voltage developed across a standard resistor was displayed on the X-Y recorder.

Current Supply

Standard Resistor

Current Switch

Nano-voltmeter

X-Y Recorder

Magnet Power Supply

Specimen

Sweep Unit

Magnetometer

Digital Voltmeter

Magnet pole pieces
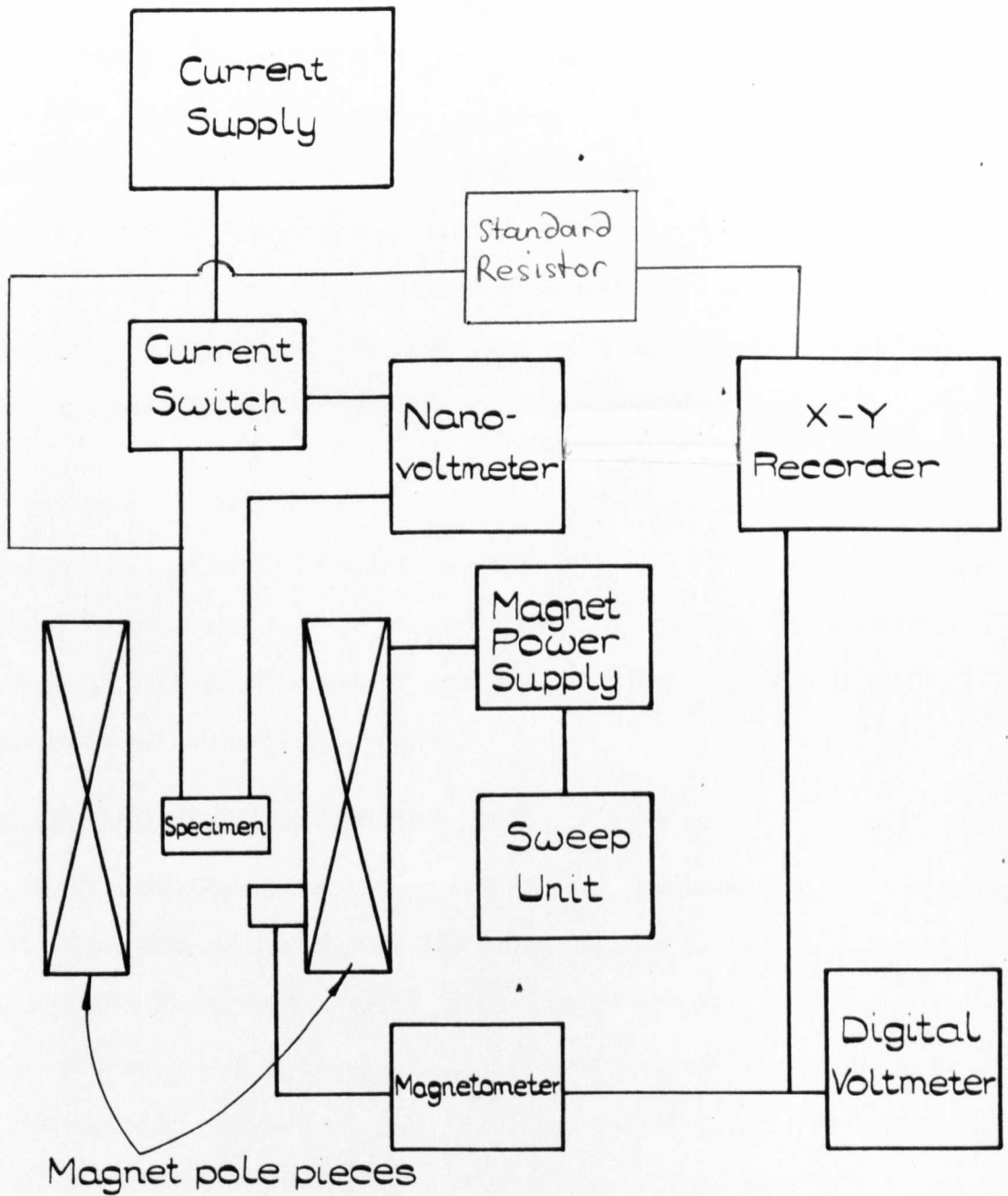
BLOCK DIAGRAM OF APPARATUS FOR MEASUREMENT
OF CRITICAL CURRENT IN A MAGNETIC FIELD
FIG. 13.

To ensure a uniform current distribution and make certain that the superconducting-normal transition did not occur at the specimen current contacts, the specimens were machined into dumb-bell shape, the reduced portion being 1 mm. in diameter and 10 mm. long. Fine copper voltage leads were joined to the sample with silver paint (see fig.14). These contacts were found to give reproducible results that were similar to those obtained with pressure or welded contacts. The voltage leads were positioned about 7 mm. apart and soldered (with indium-tin) to a coaxial copper lead within the helium cyrostat. All connections outside were pressure copper to copper contacts to reduce thermal noise.

Provided the current was not increased too rapidly, the critical currents measured were reproducible to within about four per cent. The critical current was usually defined to be that current which generated a microvolt across the specimen, and except at high fields, it was independent of the detection level.

9.3. Resistance Transitions in a magnetic field

These measurements were made on the same specimens used in determining the critical current and in the same dewar assembly. A block diagram of the apparatus is shown in fig.15. In addition several slab-shaped specimens were measured and in this case pressure contacts were used for the voltage lead connections (see fig.16). Use of these slab specimens enabled the effect of precipitate orientation with respect to the current and external magnetic field directions to be investigated on the same specimen without demagnetising effects affecting the results.

A small transport current was passed through the specimen and the resulting voltage, developed as the external magnetic field was increased, was amplified by the nanovoltmeter. A plot of voltage against field was

Current lead   Voltage lead

Tufnol probe

8 B.A. screws

Copper blocks
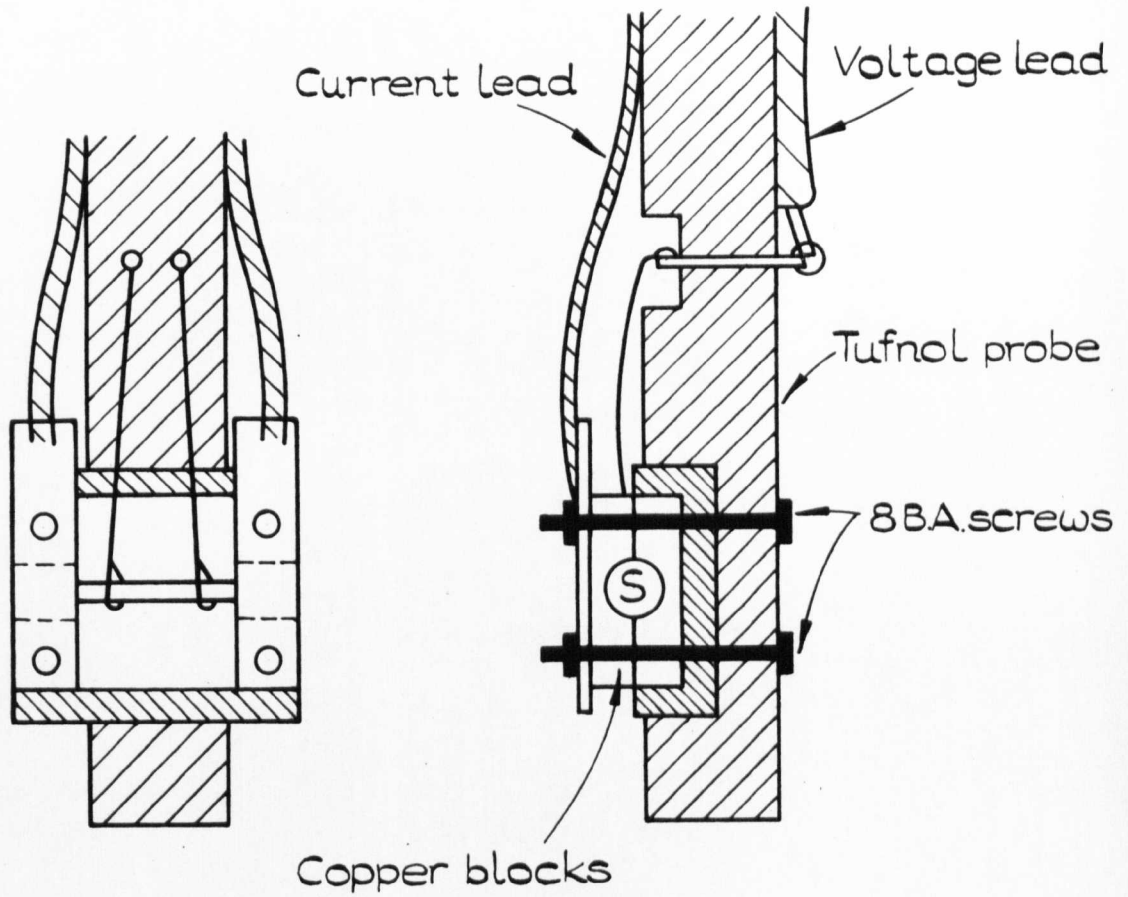
PROBE USED FOR RESISTANCE TRANSITION

& CRITICAL CURRENT MEASUREMENTS OF WIRES.

FIG. 14.
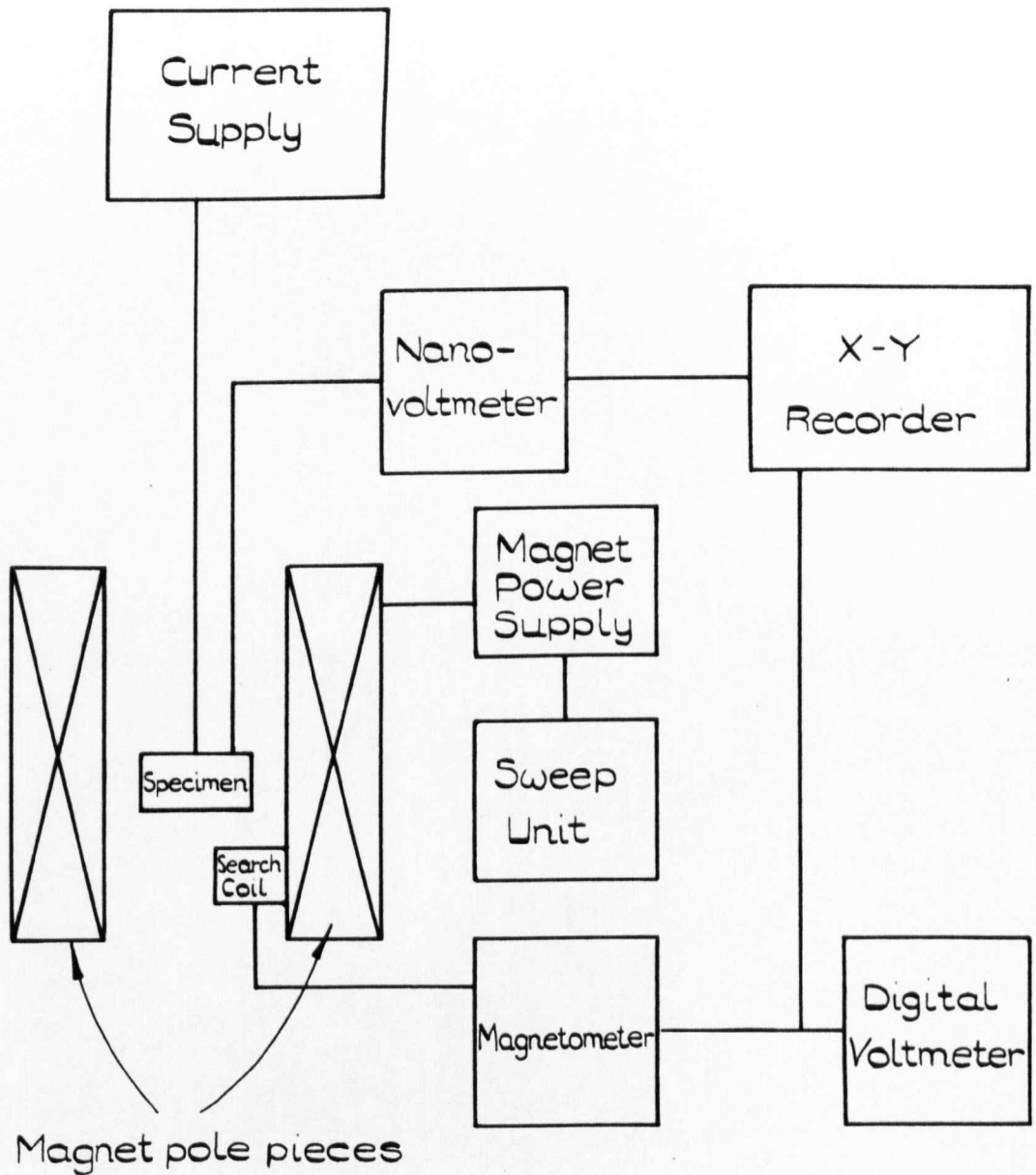
BLOCK DIAGRAM OF APPARATUS FOR MEASUREMENT OF
RESISTANCE TRANSITION IN A MAGNETIC FIELD.
FIG. 15.

Current
leads

Spring
voltage
Lead.

Copper
current
connections

Specimen
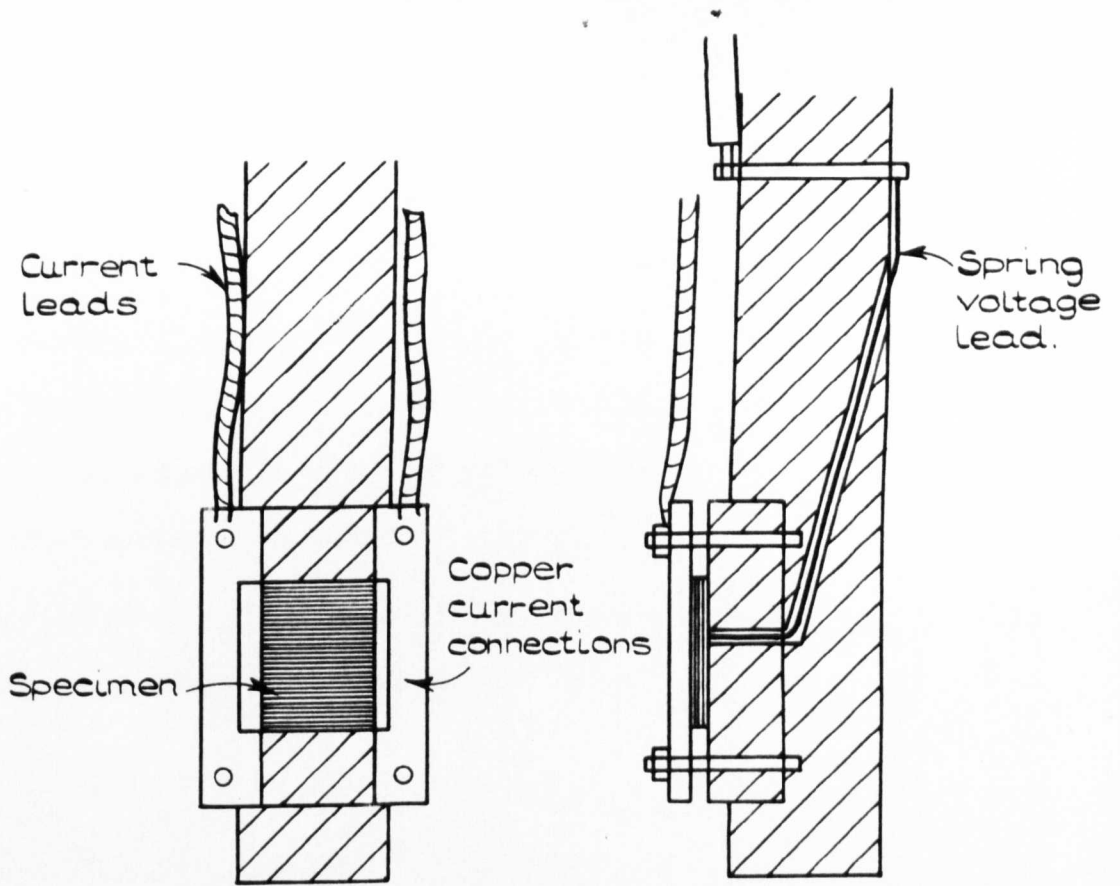
(a) Slab positioned perpendicular to the magnetic field
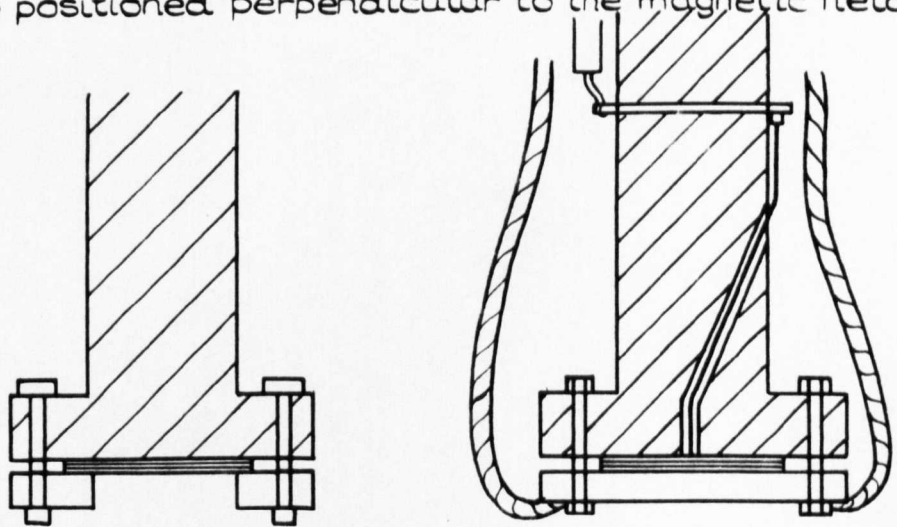
(b) Slab positioned parallel to the magnetic field

Fig. 16. Probes used for resistance transitions
of slab samples.

obtained on the X-Y recorder. The field was swept at a constant rate of about one oersted per second - this was slow enough to enable the voltage induced in the voltage leads to be conveniently 'backed off' on the nanovoltmeter.

The dumb-bell specimens were aligned parallel to the field by setting them up in the position of minimum resistance at a given field. The slab specimens were aligned by making the tufnol sample holder parallel to the field with the aid of a Hall probe.

The curves were reproducible to better than 1% and were practically identical in increasing and decreasing fields.

10.   Magnetisation Measurements.

10.1.   Introduction

Magnetisation curves of hysteretic type II superconductors are still not completely understood. Many experiments have been performed which demonstrate an increase in hysteresis of elemental and single phase alloys after cold work and a subsequent reduction after annealing. Much work has also been done on alloys which precipitate a second phase from solution on ageing. The resultant hysteresis is associated with the presence of the precipitate. The workers have usually explained their results in terms of flux pinning and the critical state. Defects or precipitates introduced into the superconducting matrix impede (or 'pin') the motion inwards of flux lines. This causes the internal magnetic field to be less than the equilibrium value in increasing external field and greater than the equilibrium value in decreasing field.

Several mechanisms have been postulated to explain how defects may pin flux lines. Webb[45] explained the interaction of a flux line and a defect in terms of the interaction of their respective strain fields. The strain field of the flux line arises because the elastic constants are different in the superconducting and normal phases.

Another hypothesis introduces the concept of flux line energy. The Ginzburg-Landau parameter, k, is inversely proportional to the mean free path and the flux line energy is roughly inversely proportional to k. This means that local regions of lower electronic mean free path cause the flux line energy in that region to be lowered. Since their line energy will be lowered, these regions will be positions of preferential location for the flux lines. Essentially they will be pinned locally.

The same arugment is true in the region of a surface. The electronic mean free path is lower and so surfaces (internal and external) will also be favourable pinning sites for flux lines. An extra force to that required to move a flux line through the superconductor is required to overcome the tendency of the flux line to reside in these low energy positions or 'energy wells'. This force will be necessary when the flux is both entering and leaving the sample and will cause hysteresis.

A given defect will have a greater relative effect on the local value of the mean free path if the material has a long mean free path (low k) than if it has a short mean free path (high k). This means that the same defect causes stronger pinning in a low k matrix than one of high k.[46, 47]

The nature, size and distribution of these defects is important. Optimum pinning at a point occurs when the defect is of the same order of size as the coherence length ξ. Livingston[48] has shown that defects which cause effective pinning in a type II matrix do not pin the more diffuse, superconducting - normal state boundaries of the intermediate state of a type I superconductor. Another study by the same author[46] showed that for a given volume fraction of roughly spherical precipitates of Sn in a Pb-Sn matrix, hysteresis decreased as the particle diameter increased from 0.2μ to about 2μ. Inclusions as large as 100μ caused no observable hysteresis at all. Sutton and Baker[49] suggested that peak pinning for a given distribution of precipitate occurs when the flux line spacing is equal to the distance between precipitates of a suitable size for pinning.

On the other hand, experiments have been performed illustrating the important role of the surface in causing hysteresis. The existence of surface currents in the mixed state has been theoretically predicted by several authors.[50-54] Barnes and Fink[55] plated specimens of Pb-Tl solid

solution alloys with normal metals and substantially reduced the hysteresis which they attributed in part, to a defect stabilized current near the surface and possibily, to the presence of the St.James and DeGennes surface sheath existing below H_{c2}. Schweitzer and Bertman[56] drew attention to the presence of the 'major' loop of a magnetisation curve as being the locus of an infinite number of reversible paths of diamagnetic slope. In a later paper[57] they argue that these surface currents do not originate from surface pinning forces or a steep field gradient in a thin outer shell but from a uniform component of internal field. Linford,[43] using an A.C. technique, has measured large surface currents in the mixed state of several superconductors. Bean and Livingstone[58] considered the interaction of a flux thread with a plane surface and suggested that in addition to the repulsive force from the external field, a flux thread feels an attractive force from its image of opposite sign outside the surface. The image thread is postulated to maintain the necessary boundary condition of zero current normal to the surface. Its presence results in delayed flux entry. Campbell et al[59] extended the idea to explain bulk pinning at the boundaries of large internal precipitates. Hart and Swartz[71] have postulated a surface 'flux spot' pinning mechanism. Field intersecting a spot of surface changes into a flux thread inside the superconductor and, at the surface, the current vortex of the thread can be considered as resulting from a magnetic dipole moment $\bar{\mu}$. The potential energy of a magnetic dipole moment is $-\bar{\mu} \cdot H$ and so any spacial variation of this energy will result in positions of preferential repose where the energy is lowest. Surface roughness causes such a spacial variation and $-\bar{\mu} \cdot \bar{H}$ will be lowered locally at points where the field is perpendicular to the surface. This model leads to an increase in hysteresis in the mixed state if nucleation of flux spots is not a dominant mechanism. This

is the case for slab specimens; flux lines can enter easily from the edges even in parallel field, unhindered by any surface barrier.

Multiple connected superconductors (e.g. a hollow cylinder) will trap flux as a consequence of their topology. This, together with the fact that a type I superconductor with a thickness of the order of the penetration depth, λ, has an enhanced critical field, promoted Mendelssohn[60] to propose his 'sponge model' for high field superconductivity. Although it was originally submitted to explain the 'hard' behaviour of alloys, he has since suggested that this sponge idea may be a structure dependent complication which may affect both type I and type II superconductors.

10.2. Results.

In the following sections (10.2.1 - 10.2.16) ten eutectics are examined with the following objectives:-

   (i)   to discover how each phase present behaves in isolation and compare it to the behaviour when they are together as conjugate solutions in a eutectic alloy;

  (ii)   to investigate the effects of precipitate nature, size, shape and orientation with respect to the applied field on the hysteresis;

(iii)   to isolate specimen surface effects from bulk effects.

10.2.1. Hg-Tl system.

The Hg-Tl system is of particular interest because it is liquid at room temperature at all compositions up to more than 40 atomic percent thallium. This composition range includes the α-phase solid solution and the eutectic alloy in which the α-phase is the major constituent. Because of their low melting points, these alloys can easily be introduced

into glass tubing of varying internal surface roughness and the magnetisation of the encapsulated specimen measured. This enables the effect of bulk precipitates and surface roughness to be isolated. Furthermore, this avoids the necessity for specimen shaping processes which change the nature of the surface being investigated.

In the measurements shown in fig.17 the same sample of α-solid solution was successfully inserted into moulds of different surface finish; thus the only variable involved was surface contour. The eutectic alloy was measured in the smooth mould so that no surface geometry differences occurred between it and the specimen of α-solid solution.

Precision bore glass tubing, 2 mm. diameter, was used to make the moulds with the following surface finishes:

(a)   smooth (i.e. as received);

(b)   medium (ground with 6μ diamond paste);

(c)   rough (ground with coarse abrasive paste).

The grinding operation was performed by coating a close fitting steel mandrel with the grinding medium and rotating it in the tube by means of an electric drill. Before grinding the tube was sealed and rounded at one end with the result that the end was not affected by the grinding process. When the alloy inside was frozen, its other end was convex and the specimen approached the shape of a perfect ellipsoid. Since in no case were the extreme ends of the specimen affected, the results observed were not due to end effects.

From fig.18 it can be seen that the α-phase is a type II superconductor with $H_{c2} = 1125$ Oe. H_{c2} of the eutectic had the same value. Roughening the surface of the α-phase decreased the mixed state induction (mainly near H_{c1}) by up to 18 percent and decreased the field of first flux

Fig. 17. Hg-Tl α-SOLID SOLUTION

I Hg-Tl EUTECTIC

II Hg-Tl ∝-PHASE ALLOY
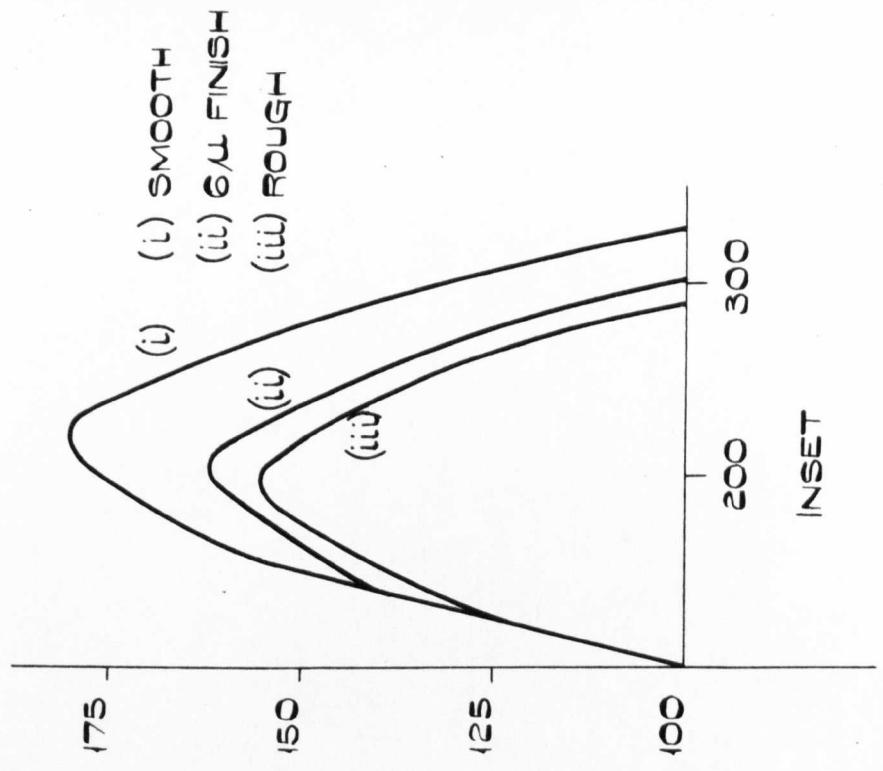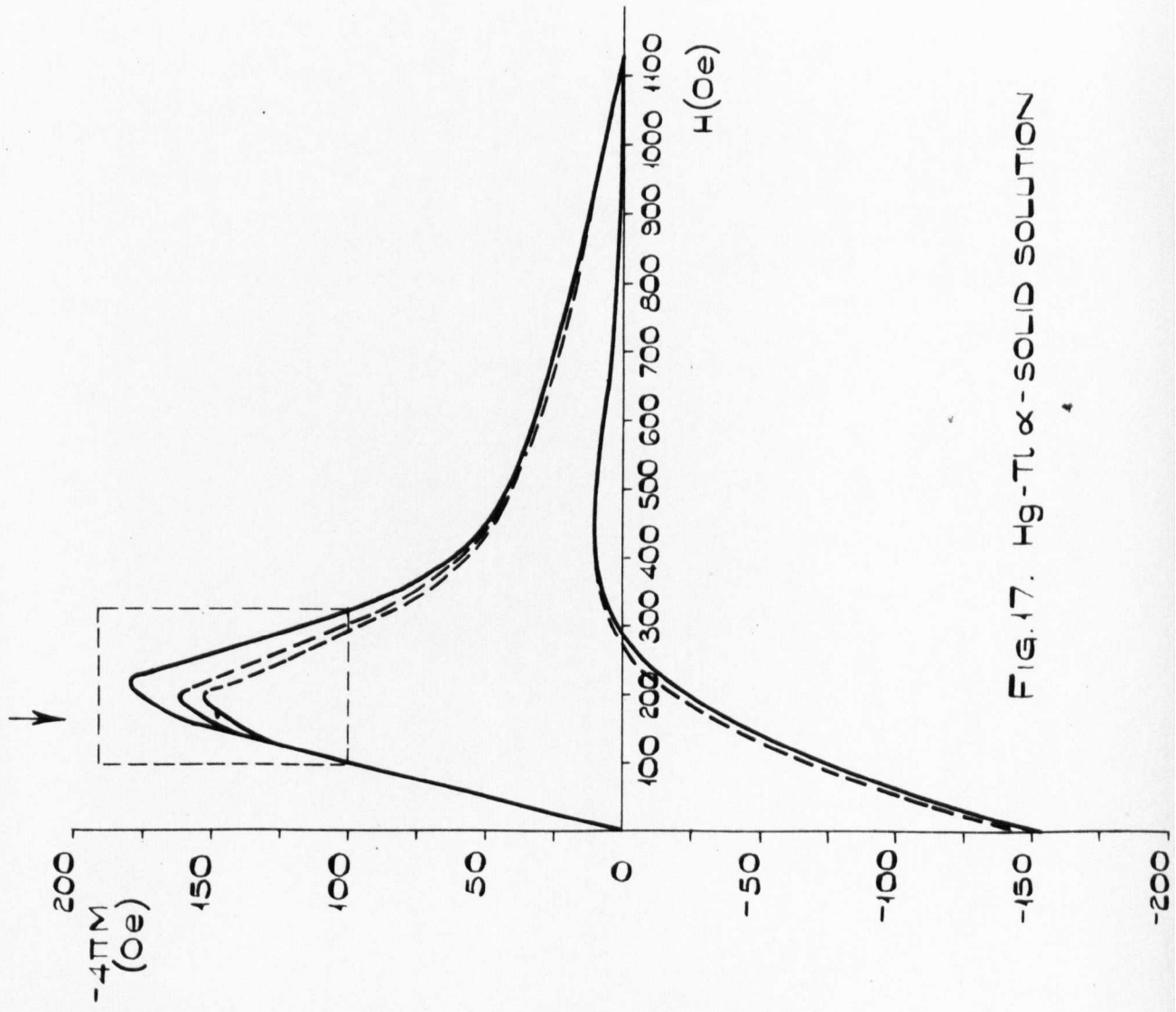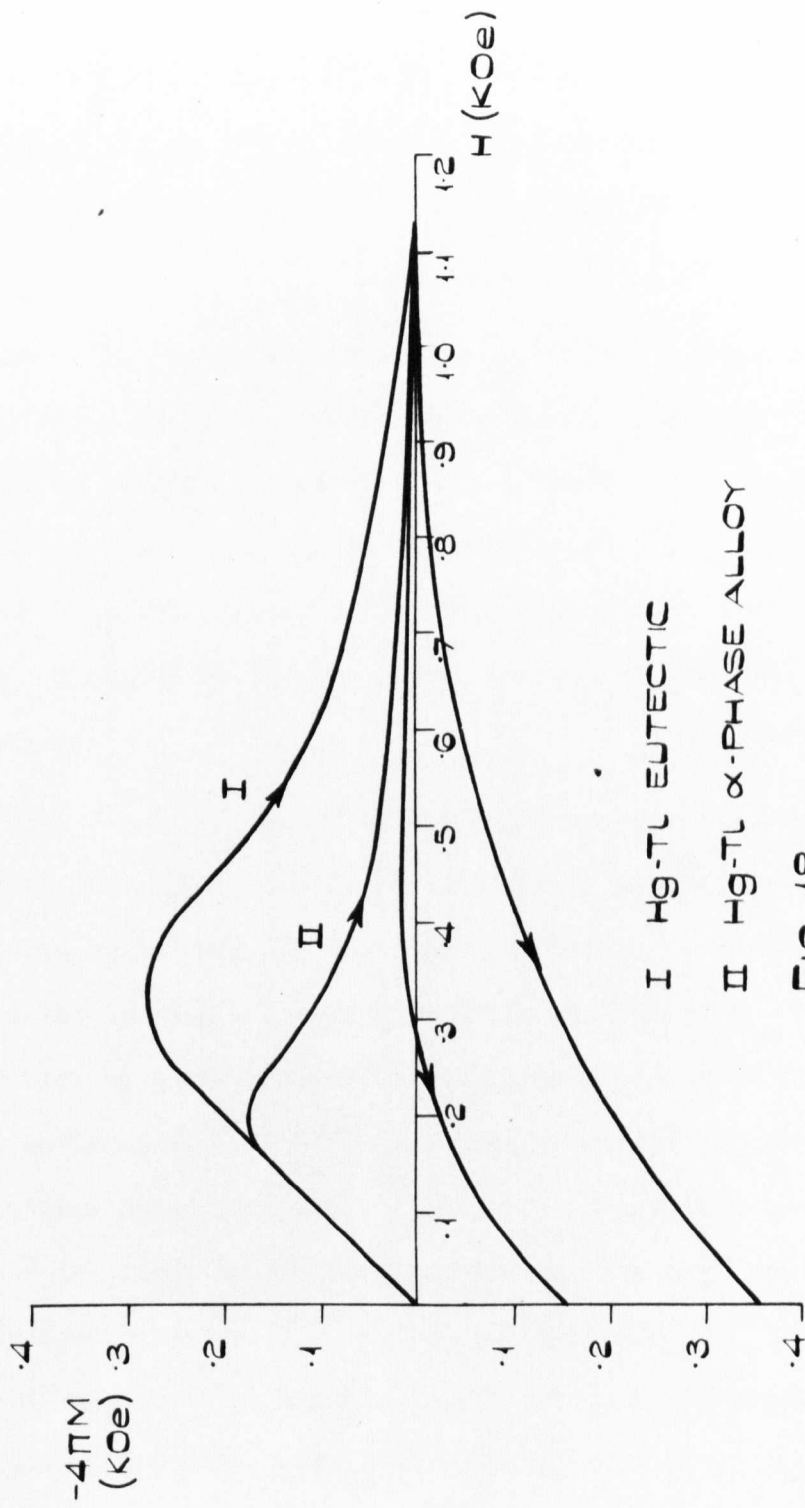
FIG. 18.

penetration, H_p, from 160 Oe (smooth mould) to 120 Oe (rough). Zero field trapped flux was not significantly affected. Hysteresis in the eutectic alloy was much greater. Trapped flux was 350 Oe and H_p was 260 Oe.

10.2.2.   Discussion of results of Hg-Tl system.

Identical values of H_{c2} for both the eutectic and the α-phase show that the superconductivity of the eutectic is due to the presence of the α-phase.

Earlier flux penetration occurring after the surface has been roughened indicates that a rough surface facilitates fluxoid nucleation. This result is consistent with the work of Bean and Livingston,[58] Joseph and Tomasch,[62] who worked on thick films, and DeBois and DeSorbo[63] all of whom observed earlier flux penetration when the surface was roughened and explained their results in terms of the Bean and Livingston surface barrier.

No other value for H_{c1} of this alloy is reported in the literature and so it is not certain whether flux entry is delayed beyond H_{c1} or not in the smooth mould case for the solid solution. Certainly roughening would cause early flux entry if fluxoid nucleation at H_{c1} was difficult because surface asperites would go prematurely into the mixed state due to demagnetising effects. Whether or not the fluxoids so formed could penetrate into the bulk is debateable, since they would be ideally situated to be pinned by the Hart and Swartz flux spot mechanism. They could only move into the bulk and thus allow $H_p < H_{c1}$ if the force of their mutual repulsion is greater than the flux spot pinning force. The size and geometry of the asperities would affect this. Probably, in this case, the value of H_p for the roughened specimen is nearest to the actual value of H_{c1} and the flux entry is delayed because of a surface barrier

to nucleation. This is possibly the image force.

If the St.James and DeGennes sheath was contributing significantly to the hysteresis one might expect roughening the surface to decrease it by removing some surface parallel to the field. However, hysteresis near H_{c2} is negligibly affected by surface contour and this is the region one might expect the sheath to have its greatest influence.[64] It may be argued that roughening increases the total surface area and hence may actually increase the sheath by increasing the area of surface parallel to the field. However, later resistance transition results presented show this not to be the case

Clearly the presence of the β-Tl precipitate is responsible for the high value of H_p of the eutectic and the greater hysteresis, including zero field trapped flux. H_p is most certainly higher because of the pinning of flux lines near the surface by the second phase. If the depth of field penetration is small in this region, no measurable deviation from the initial diamagnetic line will be detected. There is no reason why pinning should not also occur as flux penetrates further into the bulk. An increase of field was observed to cause the eutectic to be more hysteretic than the solid solution at all fields.

Since no metallographic examination was possible on this alloy, the morphology of the second phase could not be determined and so no conclusions could be made about the mechanism of the flux pinning that is associated with it.

10.2.3.   Pb-Cd system.

The solid solubility curve of Cd in Pb is so steep that it is difficult to decide how much Cd gets dissolved by Pb at the heat treating temperature (118°C) hence whether the eutectic is type I or type II.[48]

In order to find this out, several alloys were cast containing up to .8% wt. Cd. They were then heated to 250°C for fourteen days to obtain a homogeneous solid solution and quenched into liquid nitrogen. Fig.19 shows how H_{c2} (and H_c for type I alloys) changes with Cd content. The eutectic had the same value of H_{c2} as the alloy containing .5% wt. Cd.

In this system the Cd-rich laminae of the eutectic alloy undergo a lamina to rod transformation on introducing a small amount of Sb. The magnetisation curves for as-cast and directionally frozen laminae and rods are identical and nearly completely hysteretic and are shown in fig.20.

In order to eliminate the effect of flux gradients, thin specimens of the laminar and rod-like eutectics were made by coating a thin layer onto a brass rod and slitting the coatings longitudinally to make them singly connected. The magnetisation curve as a function of specimen thickness is illustrated in fig.21. The results were similar for both laminae and rods.

When the large specimens (3 mm. diameter) were left to age at room temperature the matrix became depleted with Cd and H_{c2} decreased, but the hysteresis remained complete even when the matrix had become type I. This was true for both laminar and rod eutectics, (see fig.22).

10.2.4.   Discussion of results of Pb-Cd system.

The massive size of the Cd laminae (of the order of a micron thick) excludes any possibility of a whole lamina interacting with the fluxoid cores. It must be concluded that the interaction is at the surface of the precipitates, perhaps by an image force mechanism, as suggested by Campbell et al[59] or simply because the mean free path is decreased in the region of a surface, or both.
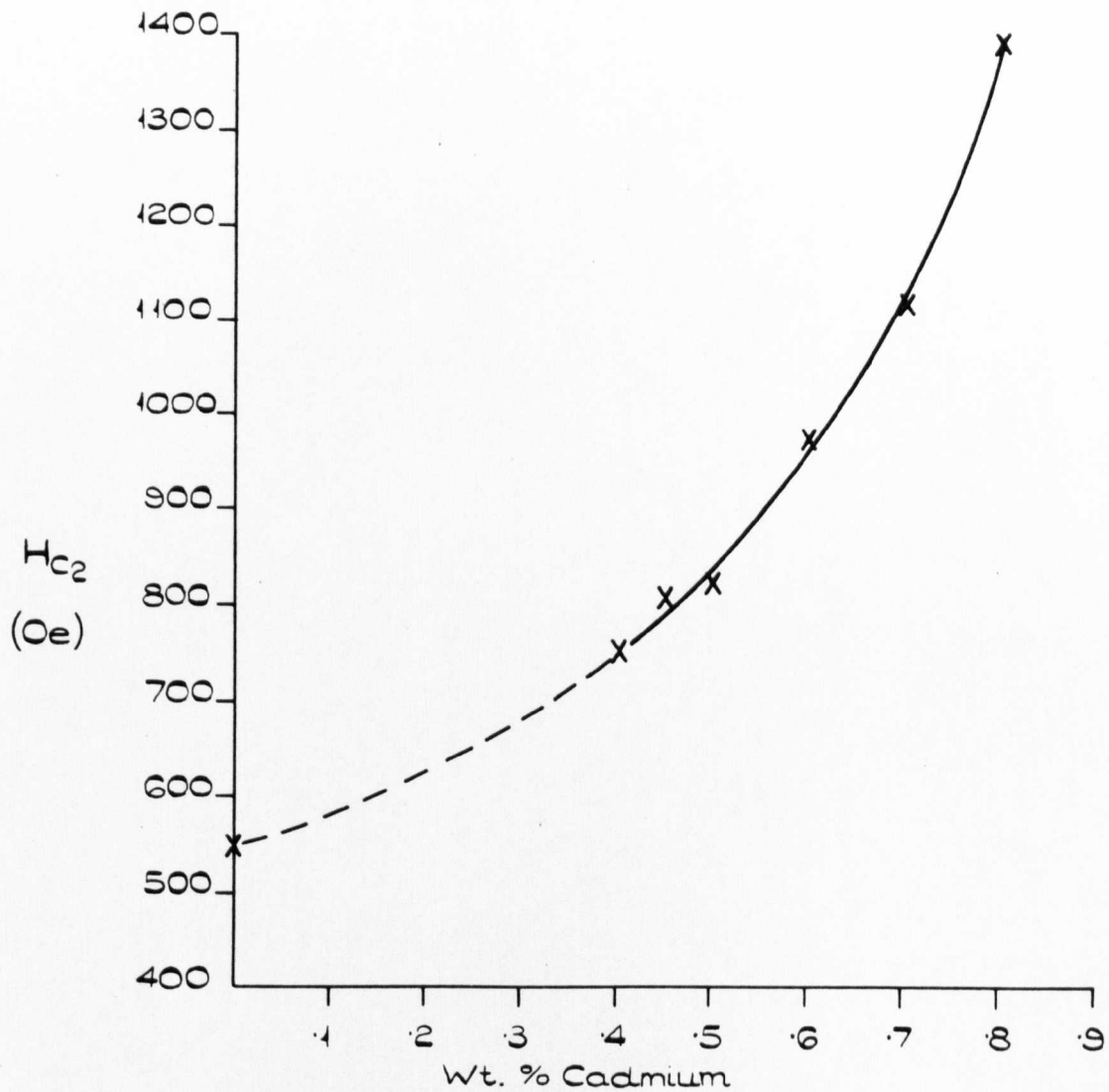
FIG. 19. DETERMINATION OF THE AMOUNT OF Cd IN THE Pb-Cd EUTECTIC WHEN HEAT TREATED AT 118°C.
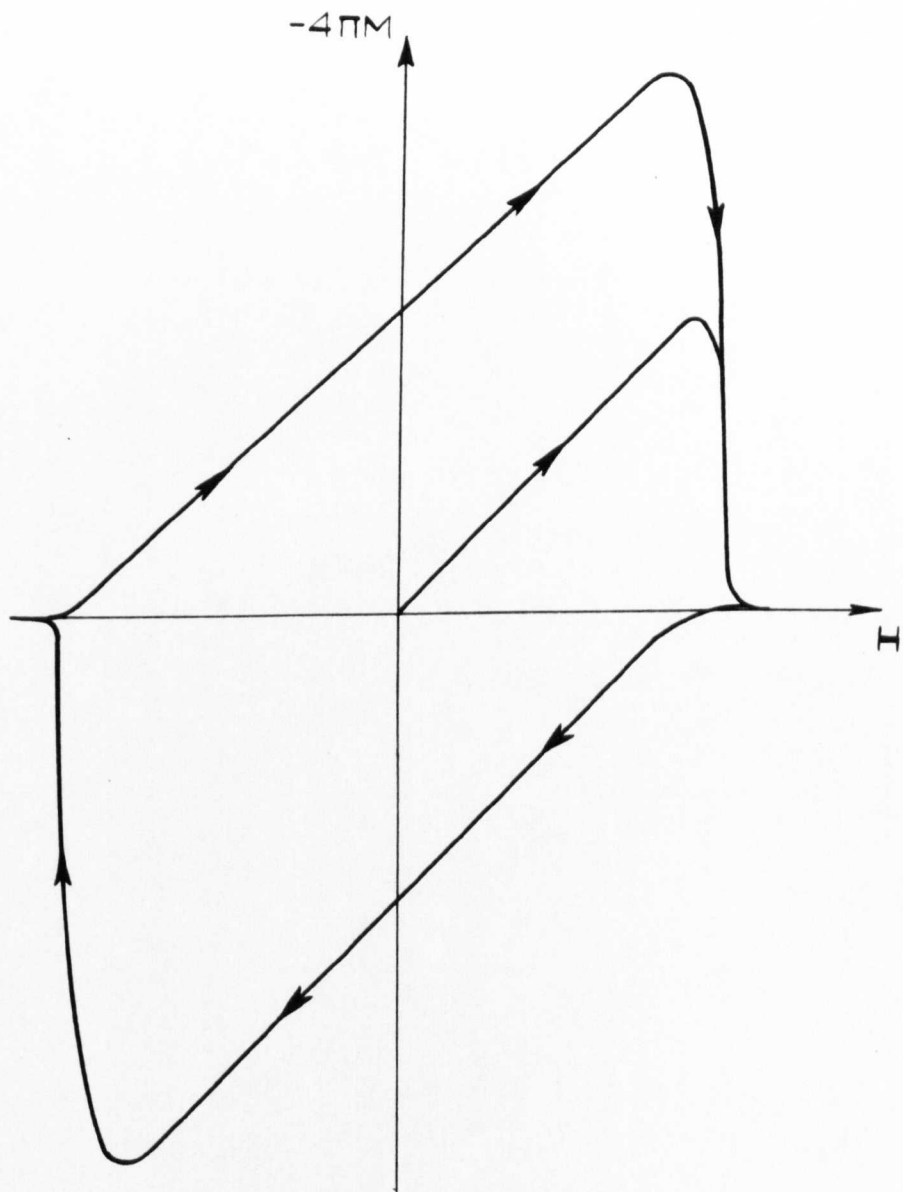
FIG.20. MAGNETISATION CURVE FOR Pb·Cd EUTECTIC ALLOY - ALMOST COMPLETELY HYSTERETIC.

Pb-Cd EUTECTIC HOLLOW
CYLINDERS SLIT

I   0.004 cm THICK

II 0.024 cm THICK

III 0.104 cm THICK

FIG. 21.

Pb - Cd EUTECTIC

A - AS QUENCHED FROM 118°C - MATRIX TYPE II.

B - AGED 9 MONTHS AT ROOM TEMPERATURE - MATRIX TYPE I.
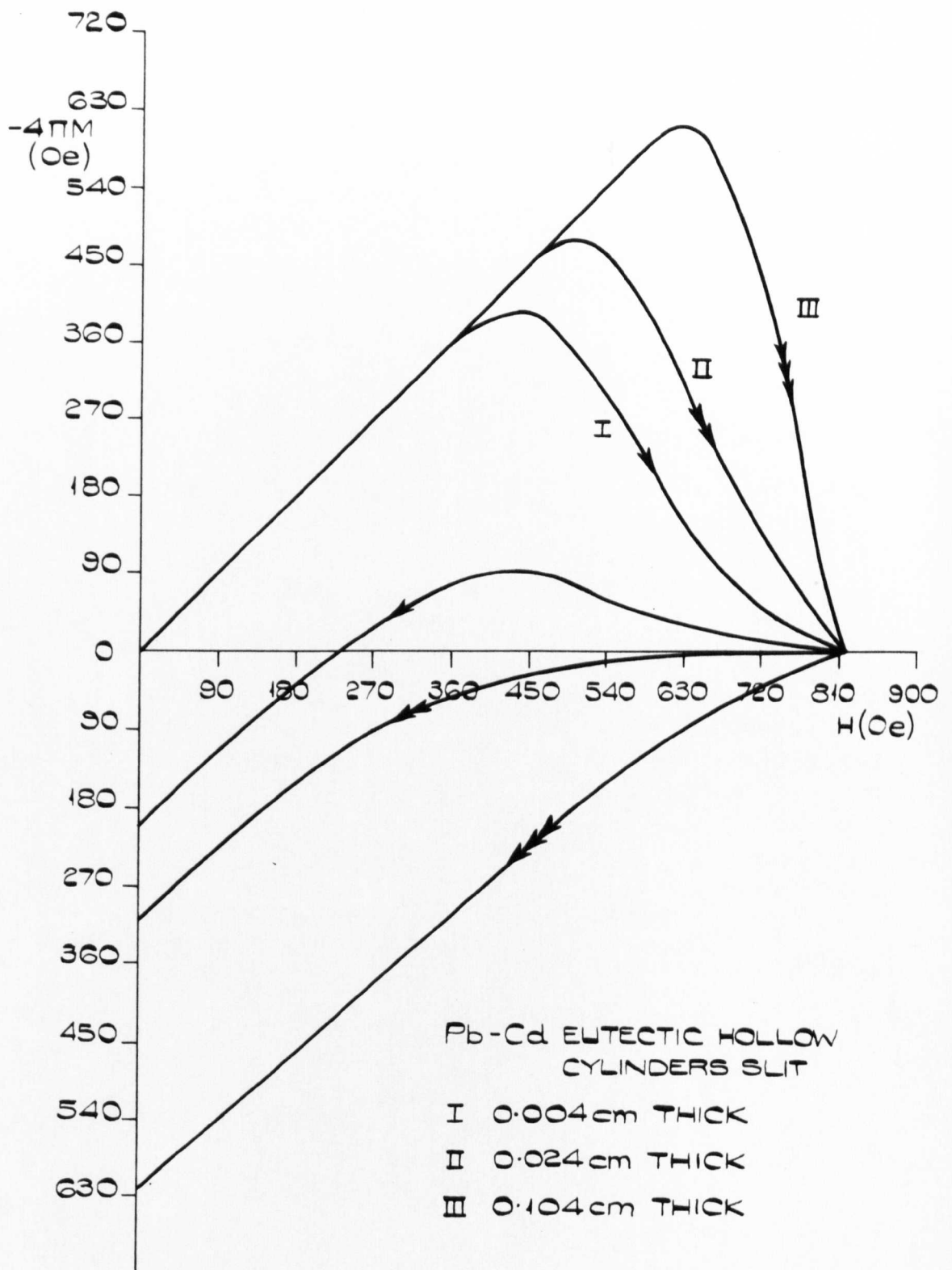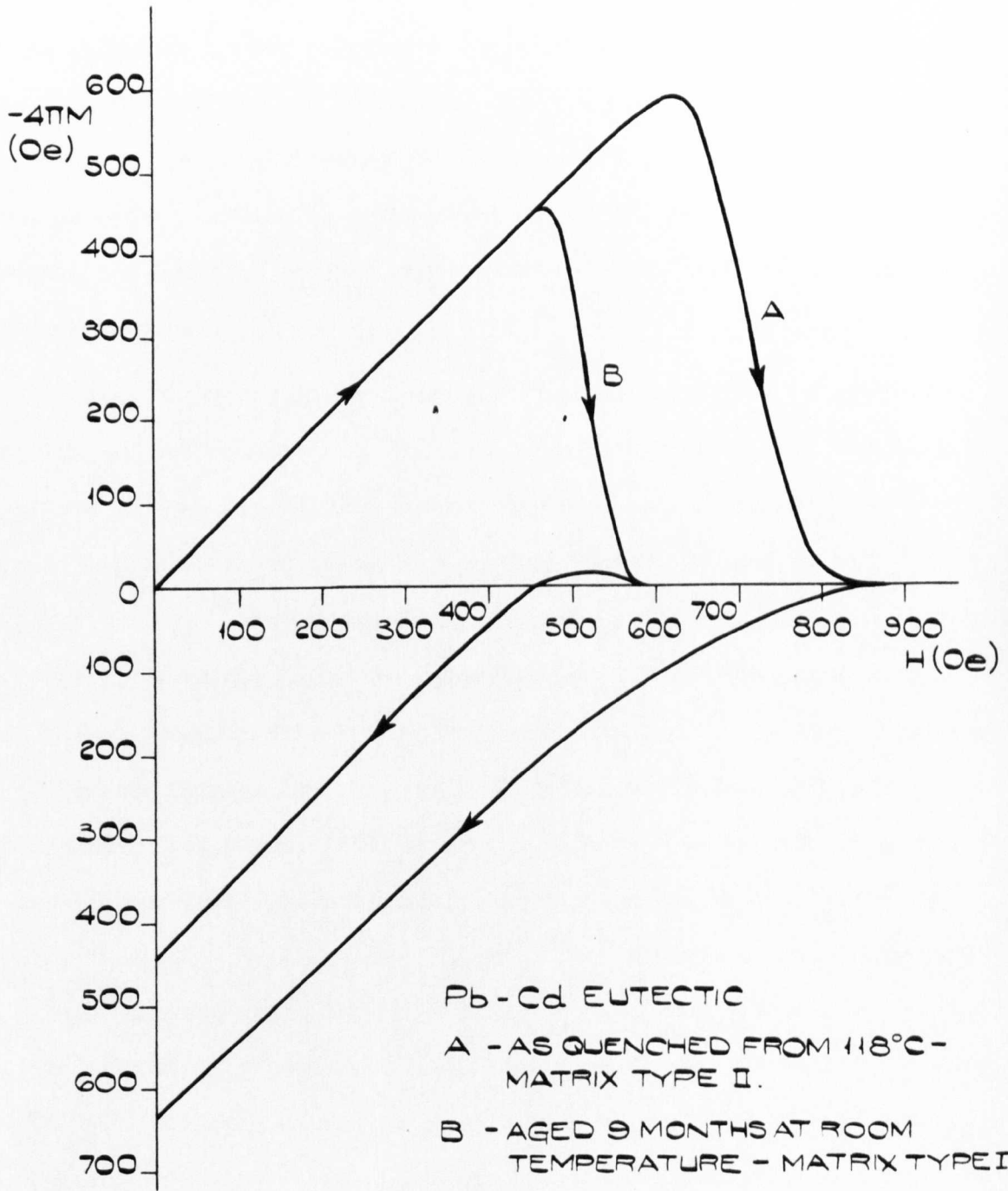
FIG. 22.

The complete flux trapping shown in fig. 20 is a consequence of the size effect on the magnetisation curve. Complete trapping occurs in a thin surface layer and H_{c2} is reached long before $2H^*$ of the Bean model. The surface layer is so thin that when flux penetrates it the total change in the induction is not measurable. This is confirmed by results on the thin, longitudinally slit cylinders. The very thin specimen shows similar behaviour to the ideal, defect-free solid solution since no appreciable gradient exists across its cross-section. As the thickness is increased, however, the specimen becomes very thick relative to $2H^*$ and complete hysteresis occurs.

A significant result is that the magnetisation curves of similarly thin laminar and rod-like eutectics are the same despite the rods having twice the surface area of the laminae and a different orientation relationship with the lattice. Kramer and Rhodes,[65] Levy et al,[66] and Evetts et al [67] have suggested that the surface area of a given volume of precipitate is the important parameter in deciding the extent of hysteresis. Clearly this cannot be the sole arbiter for several reasons. It is easy to imagine that an evenly dispersed incoherent precipitate much smaller than ξ would not impede fluxoids but at the same time have a higher surface area than a distribution of larger particles capable of pinning fluxoids. It also seems unlikely that an incoherent precipitate dispersed as cubes would trap less flux than the same volume dispersed as spheres of similar volume. It would be most surprising too if the degree of coherence with the matrix of a particular precipitate did not affect the pinning strength. The elastic strain associated with a coherent precipitate would lower the mean free path over a much larger volume than would an incoherent precipitate.

The results confirm these speculations for the case when the trapping

is most likely at the surface of the precipitate. It seems that as long as
sufficient surface area is presented to an approaching flux line it will be
trapped by an amount independent of the shape of the rest of the precipitate
which is not participating in the pinning process.

The ageing of the thick (3 mm diameter) specimens of eutectic is
essentially the sequel to Livingston's[48] experiment with a more dilute
Pb-Cd alloy (1.53 wt.% Cd). He observed that as ageing of the super-
saturated solid solution proceeded, Cd was precipitated, thus depleting
the Pb-rich matrix in Cd and hence lowering its H_{c2}. At the same time
hysteresis increased due to the increase in size and number of pins.
Finally, the hysteresis fell drastically when the matrix was so denuded in
Cd that it became a type I superconductor. The Cd particles which interacted
so well with the flux lines of the mixed state were too small to impede the
broader boundaries of the intermediate state.

In this experiment, even though the matrix has changed from type II
to type I, the defects are still large enough to restrict the movement of
the intermediate state boundaries and cause complete flux trapping.

10.2.5.   Pb-Sn system.

In the eutectic alloy the precipitate of Pb-rich solid solution is
superconducting at 4.2^{o}k but the Sn-rich matrix in isolation is not.
However, a proximity effect exists (see section 11.2.9.) and the matrix
is also superconducting despite the fact that the distance between Pb
laminae is some ten times greater than the coherence length of the Pb-rich
laminae.

Magnetisation curves for as-cast and directionally frozen eutectic
alloys, heat-treated at 118°C are given in fig.23. The directionally-grown
specimen displays slightly more hysteresis, especially near H_{c2}.
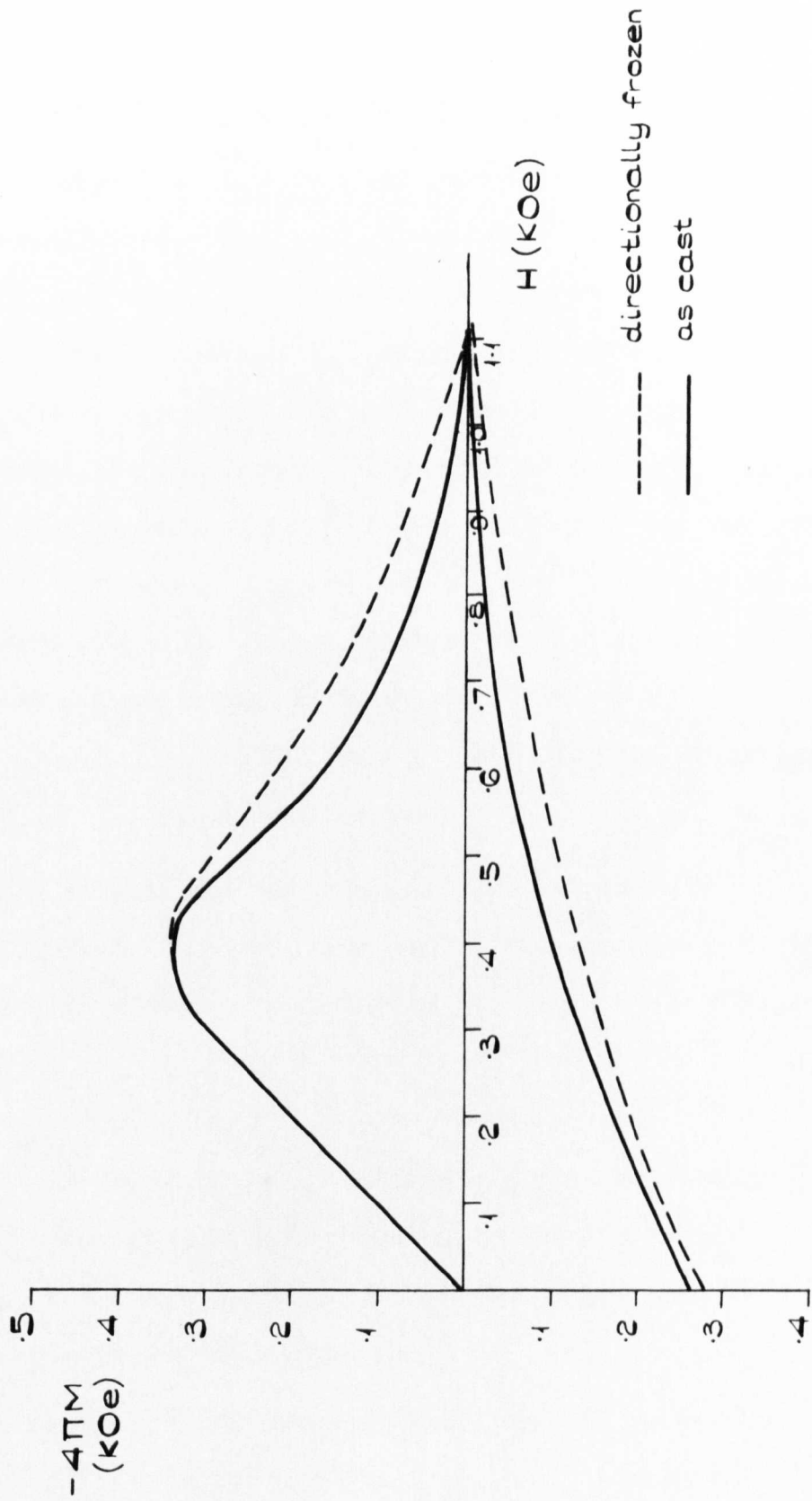
Fig. 23. Pb-Sn EUTECTIC HEAT TREATED AT 118°C.

Fig.24 shows the magnetisation curve for a thin, longitudinally slit, hollow cylinder (coated on brass) of eutectic, similarly heat treated.

10.2.6.   Discussion of results of Pb-Sn system.

This eutectic is an example of an alloy whose superconductivity is entirely due to the presence of a superconducting precipitate. Even so, these precipitates trap flux - presumably at their surface, perhaps because of differential thermal contraction. In this case, however, the flux pinning is not occurring wholly in a thin surface shell, as is the case in thick Pb-Cd eutectic specimens. The field gradient is smaller since magnetisation falls gradually to zero at 1110 Oe from a value of H_p of about 400 Oe. Flux pinning must therefore occur throughout the bulk. Surface pinning is appreciable, however, since flux entry appears to occur very much earlier when the effects of flux gradients are removed by having a very thin sample (see fig.24). This early penetration may also be due in part to 'weak spots' in the thin specimen allowing premature penetration .

If it is assumed that the pinning of the flux lines is due to local regions of lowered flux line energy causing them to resist movement through the matrix, then a reasonable assumption is [69] that the pinning force F_p is given by

$$F_p = \Delta \epsilon . \delta$$

where $\Delta \epsilon$ is the amount that the flux line energy is lowered and δ is the length over which it is pinned. Clearly, the pinning force will be greater the longer the distance over which a flux line is pinned. This argument holds whatever the mechanism of pinning .

Since the directionally-frozen specimen has its interfacial boundaries parallel to the axes of the flux lines, they are probably able to pin them over greater distances than randomly orientated precipitates, and so the
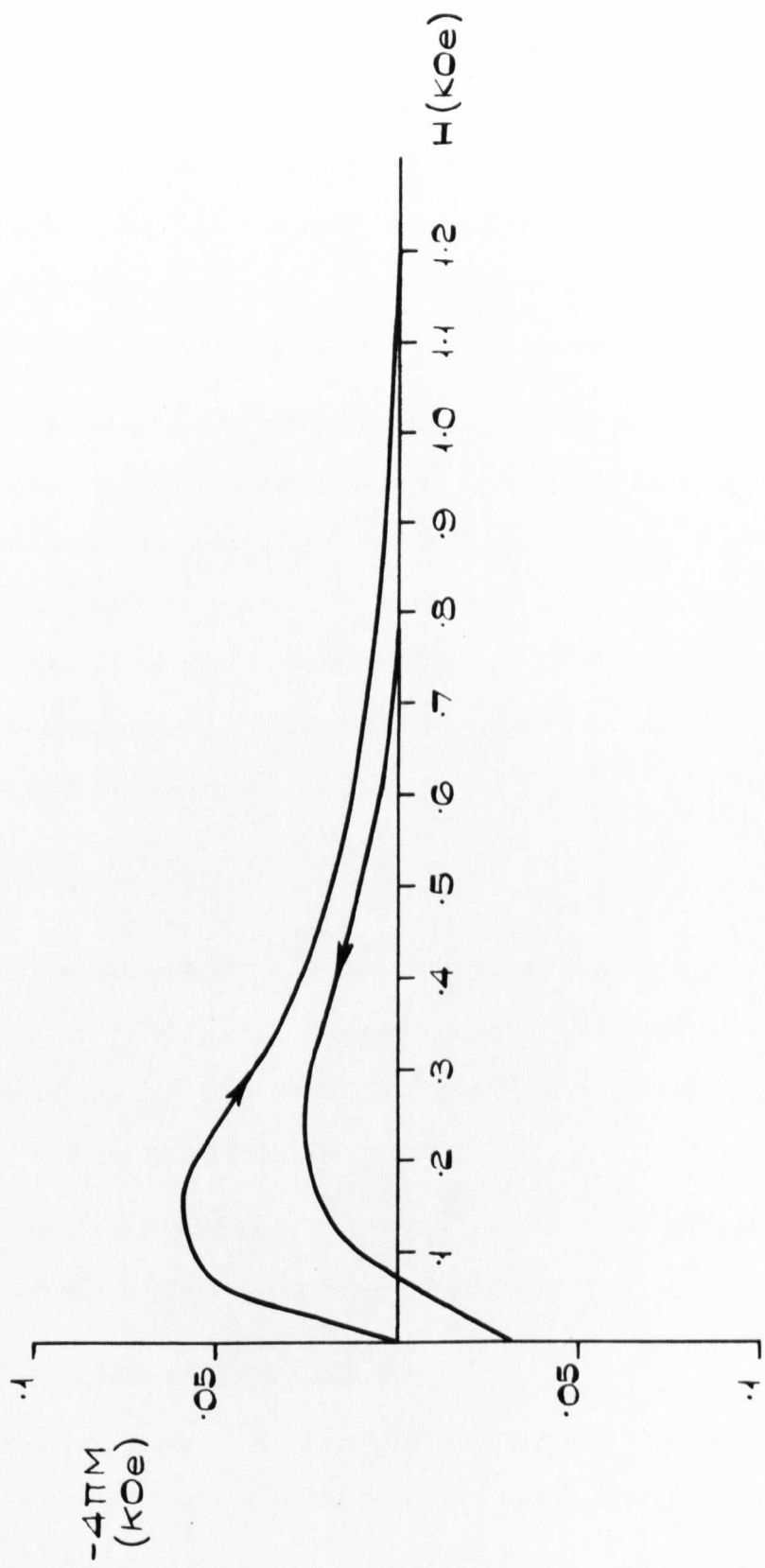
FIG. 24. Pb-Sn LONGITUDINALLY SLIT HOLLOW CYLINDER, THICKNESS 4·6×10^{-3}cm HEAT TREATED AT 118°C.

total pinning force per flux line is increased. This would lead to an increase in hysteresis as seen in fig.25. The amount by which the hysteresis increases will be governed by fluxoid mobility and the pinning force per unit length of the precipate surface. Near H_{c2} where the fluxoid lattice is most rigid, restricting the movement of any one fluxoid would have a maximum effect on its neighbours. A maximum effect would also be expected in this region because there are more neighbours anyway .

Evetts[69] has previously observed that a directionally-frozen specimen of Pb-Bi eutectic exhibits greater hysteresis than an as-cast specimen. This eutectic is not laminar like Pb-Sn but has a structure similar to Sb-Tl (see micrographs 18 - 19). He also noted a tendency for flux jumping to increase. This does not occur in Pb-Sn. Other eutectics to be mentioned also show this increase in hysteresis when directionally frozen in a direction parallel to the specimen axis.

10.2.7.   In-Bi system.

After heat treatment at 60°C the eutectic alloy consists of a matrix of In+12.1 wt.% Bi in which are laminae of In_2Bi solid solution. The magnetisation curves for each phase in isolation, together with that of the eutectic, are shown in fig. 25.

Fig.26 compares the magnetisation curves for directionally-frozen and as-cast eutectics after similar heat treatments at 60°C.

10.2.8.   Discussion of In-Bi system.

An interesting feature of the eutectic alloy is that the precipitate In_2Bi, which is undoubtedly the cause of its hysteresis, transforms from the superconducting to the normal phase at 428 Oe. Despite this, the eutectic magnetisation curve displays no increase in hysteresis at this

A   In$_2$ Bi SOLID SOLUTION

B   In +12:1% Bi SUPERSATURATED
    SOLID SOL'T'N.

C   In-Bi EUTECTIC HEAT TREATED
    AT 60°C.

FIG. 25.

In-Bi EUTECTIC HEAT TREATED AT 60°C

——— As cast

----- Directionally frozen
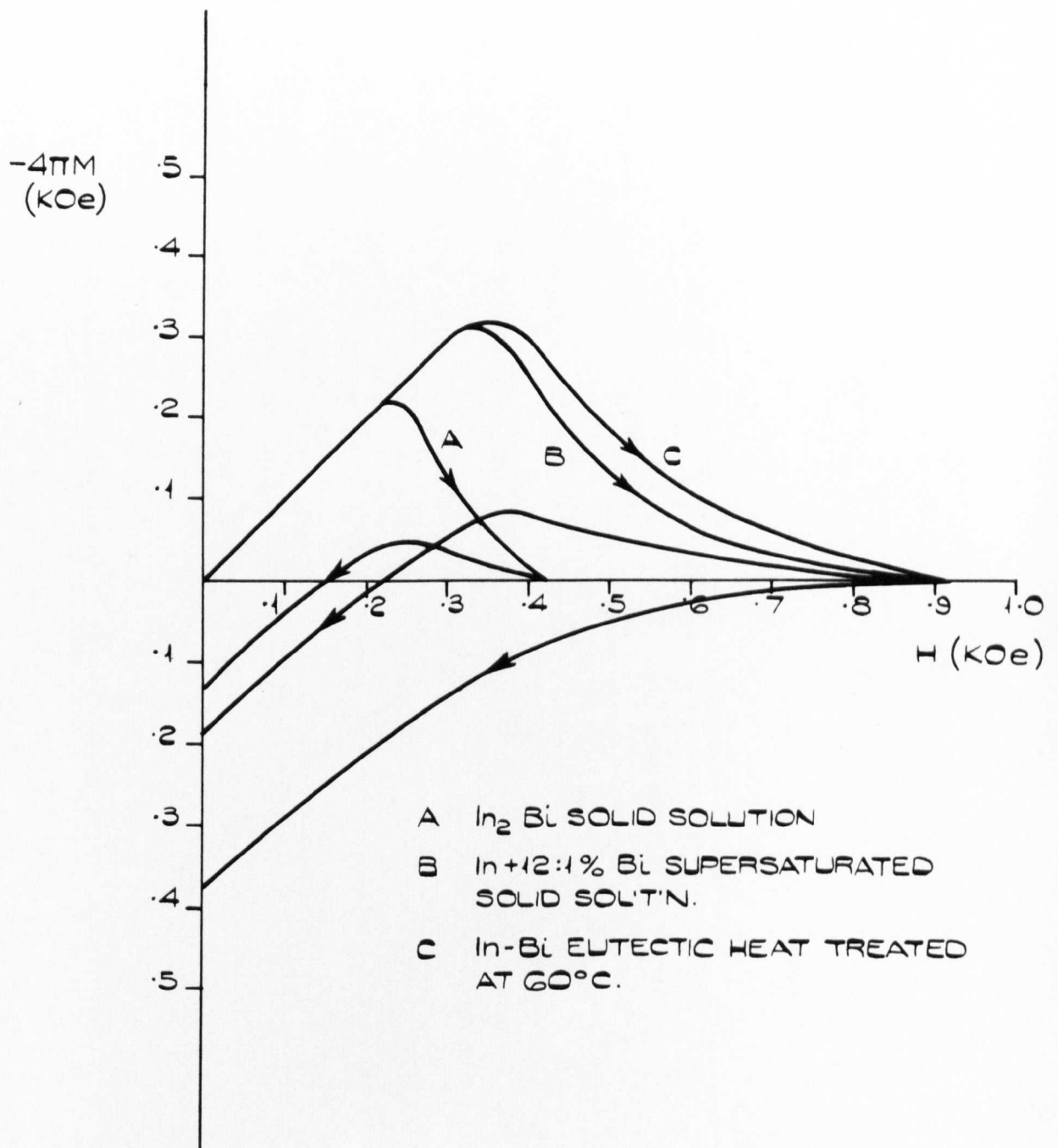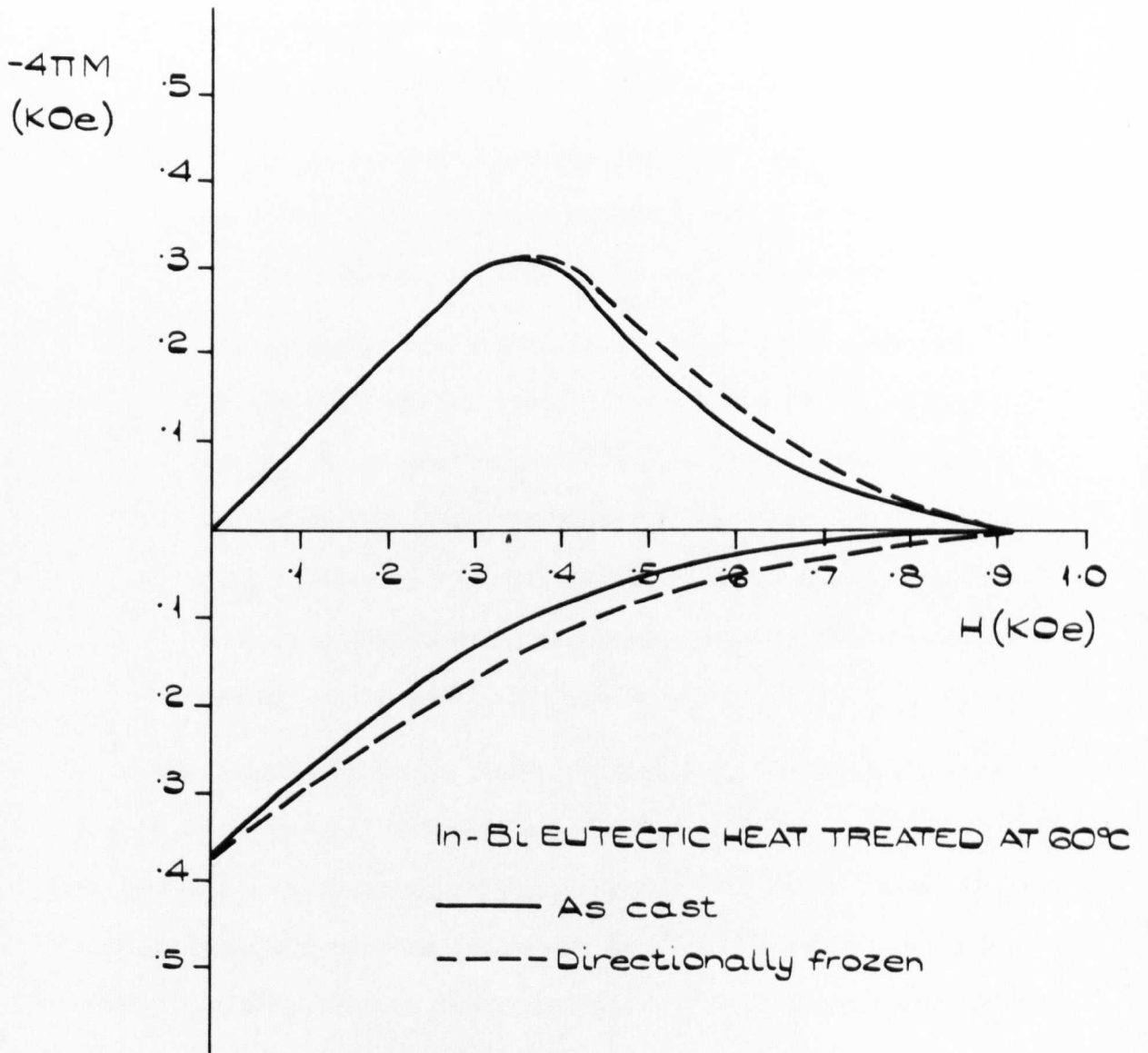
FIG. 26.

point, even though when normal, the In_2Bi should be more effective in pinning flux lines[70].

There are three possible explanations why a peak is not observed in the magnetisation curve at this point:

(i)   the precipitate is just as effective a barrier to flux line motion when superconducting as when normal;

(ii)   the In_2Bi remains superconducting up to H_{c2} of the eutectic by a proximity effect. This is possible despite the thickness of the laminae, as observed in the Pb-Sn system;

(iii)   the existence of flux gradients cause the precipitate in the bulk not to 'see' the true value of the external field. Precipitates at the top of the gradients will go normal but where the field is less than 428 Oe the In_2Bi will stay superconducting. As the flux penetrates, the precipitates will go normal gradually and a smooth magnetisation curve will result.

Explanation(iii) can be tested by measuring the magnetisation curve of a very thin specimen in which no appreciable gradient can exist. This has been done and the result is shown in fig.27. The curve is almost reversible, and field penetration occurs before it does in the solid solution, probably because flux penetrates the cylinder prematurely at certain positions along its length. No peak is observed in the region of 430 Oe despite the fact that all the In_2Bi precipitate must now be 'seeing' the external field. Discounting (i) as unlikely, it must be concluded that the precipitate is superconducting beyond its normal value of H_{c2} because of the proximity of the matrix, its flux pinning strength remaining the same.
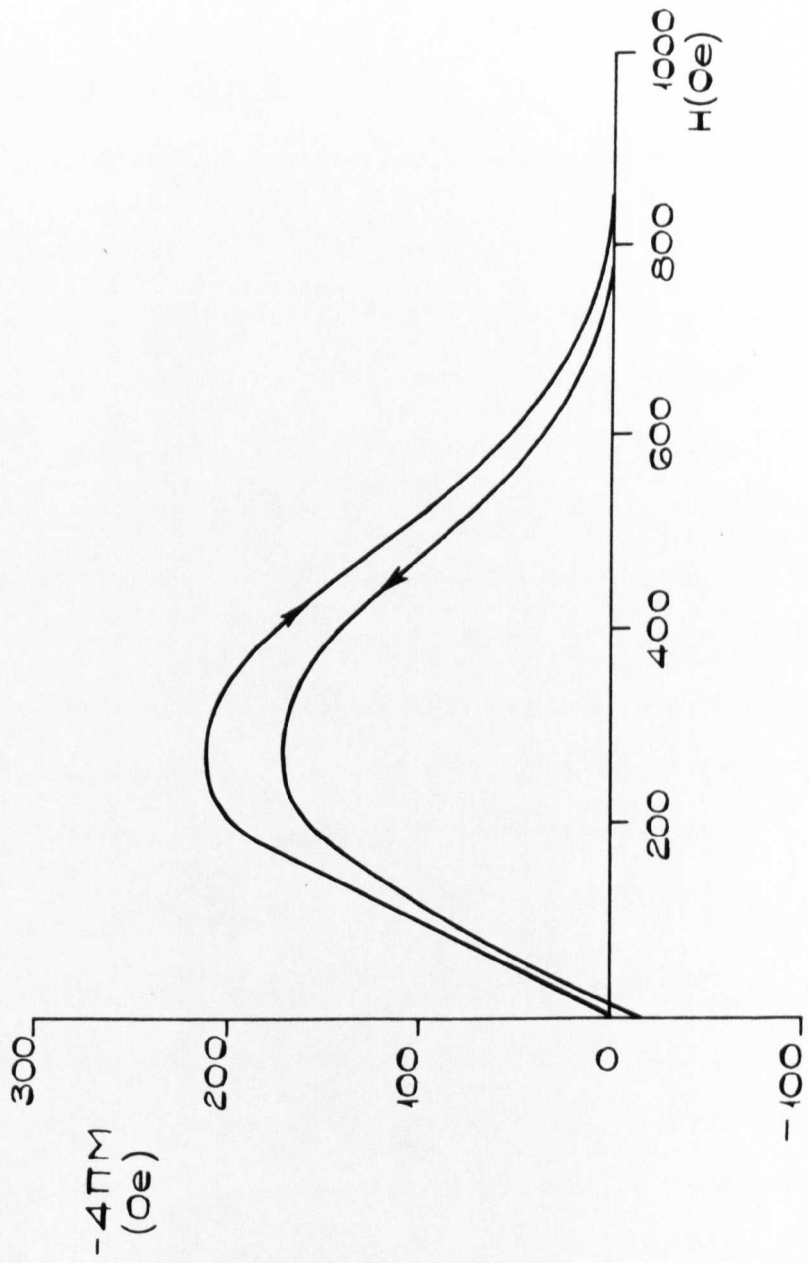
FIG. 27. In-Bi EUTECTIC LONGITUDINALLY SLIT, THIN HOLLOW CYLINDER.

The directionally-frozen eutectic behaves similarly to the Pb-Sn
specimen; it is slightly more hysteretic than the as-cast sample, probably
for the same reason: the pinning surfaces now lie along the axes of the
flux lines and are able to pin them over greater lengths. Measurements
of critcial currents give further credence to this suggestion (see
section 11.3).

10.2.9.   Pb-Zn system.

The magnetisation curve for the eutectic alloy is given in fig.28.

10.2.10.   Discussion of Pb-Zn system.

Since the solubility of Zn in Pb at the eutectic temperature is so
small, it is not surprising that the magnetisation curve is almost the
same as that of pure Pb, i.e. type I. The field at which superconductivity
completely disappears and the field at which it is nucleated in decreasing
field do not coincide and their separation appears to be a function of
sweep rate.[44]   However, H_c, their mid-point, remains constant. The Zn
precipitate causes no hysteresis suggesting that the magnetisation loop
is entirely due to surface currents since, as the external magnetic
pressure is removed, the induction approaches zero.

10.2.11.   Pb-Mg system.

All precipitation studies from a supersaturated solid solution are
limited, as mentioned previously, by the continuously changing chemical
composition of the matrix and the precipitate. At the Pb-rich end of
this system, however, excess magnesium is rejected from the Pb-rich solid
solution as an intermetallic compound, Mg_2Pb. Consequently, the precipitate
remains constitutionally unchanged throughout the precipitation process.

Pb + ·5 wt.% Mg solid solution was prepared by quenching from $250^{\circ}C$
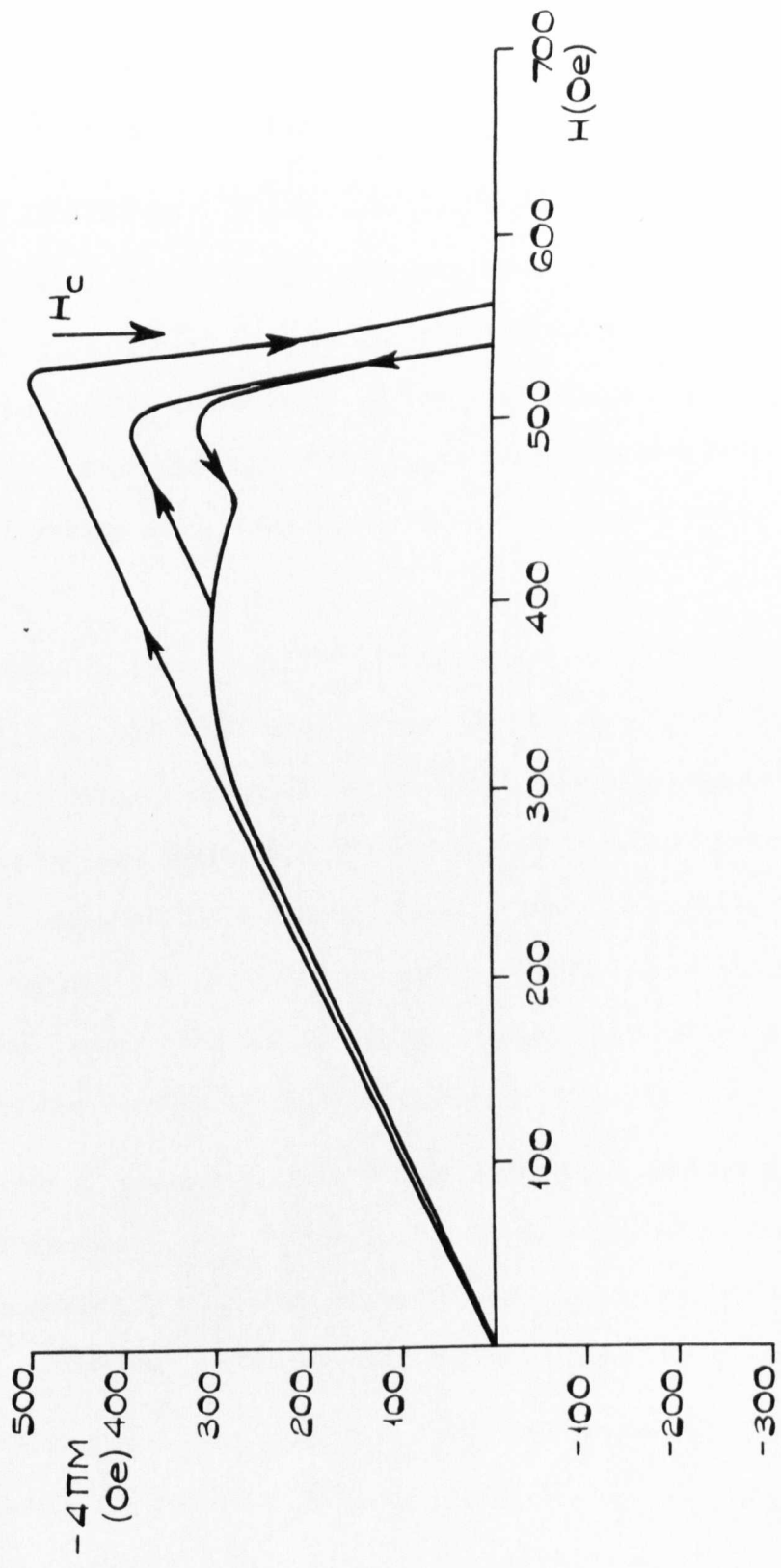
Fig. 28. Pb-Zn EUTECTIC HEAT TREATED @ 87°C.

and was then aged at room temperature. Fig. 29 shows how the distribution of a normal second phase affects the hysteresis.

The eutectic alloy has similar properties to that in the Pb-Cd system i.e. complete flux trapping occurs in a thin surface shell.

10.2.12. Discussion of results of Pb-Mg system.

This experiment is similar to that of Livingston's on Pb-Sn alloys mentioned in section (10.1.). As Mg_2Pb is precipitated, the matrix is denuded in Mg and so H_{c2} decreases. At the same time H_{c1} increases. This, together with flux line pinning of the Mg_2Pb near the specimen surface results in an increase of H_p, the field at which flux penetrates significantly.

Precipitation in this system is continuous, i.e. it occurs homo-geneously throughout the structure. After 20 hours ageing at room temperature the particles of Mg_2Pb are so small that they cannot be resolved optically (see micrograph 18) and so are probably able to interact with the normal cores of the fluxoids, pinning them and causing hysteresis. After 21 days ageing, the particles are massive (700μ) (see micrograph 19) and are now much larger than the coherence length. Flux pinning must be occurring at the surface of these particles.

If the ratio of trapped flux to H_{c2} is taken as a measure of hysteresis and is plotted against H_{c2} as in fig.30 the curve is smooth and suggests no obvious discontinuity where the mechanism of pinning has changed. It is reasonable, therefore, to assume that the transition is gradual.

These results invoke the question of why some large defects, e.g. the cellular lattice of Sn-depleted Pb-Sn in Livingston's[46] experiment (cell diameter 100μ), do not pin fluxoids while other like Mg_2Pb in this

Fig. 29. Pb + 5% Mg QUENCHED FROM 250°C AND AGED AT ROOM TEMP.
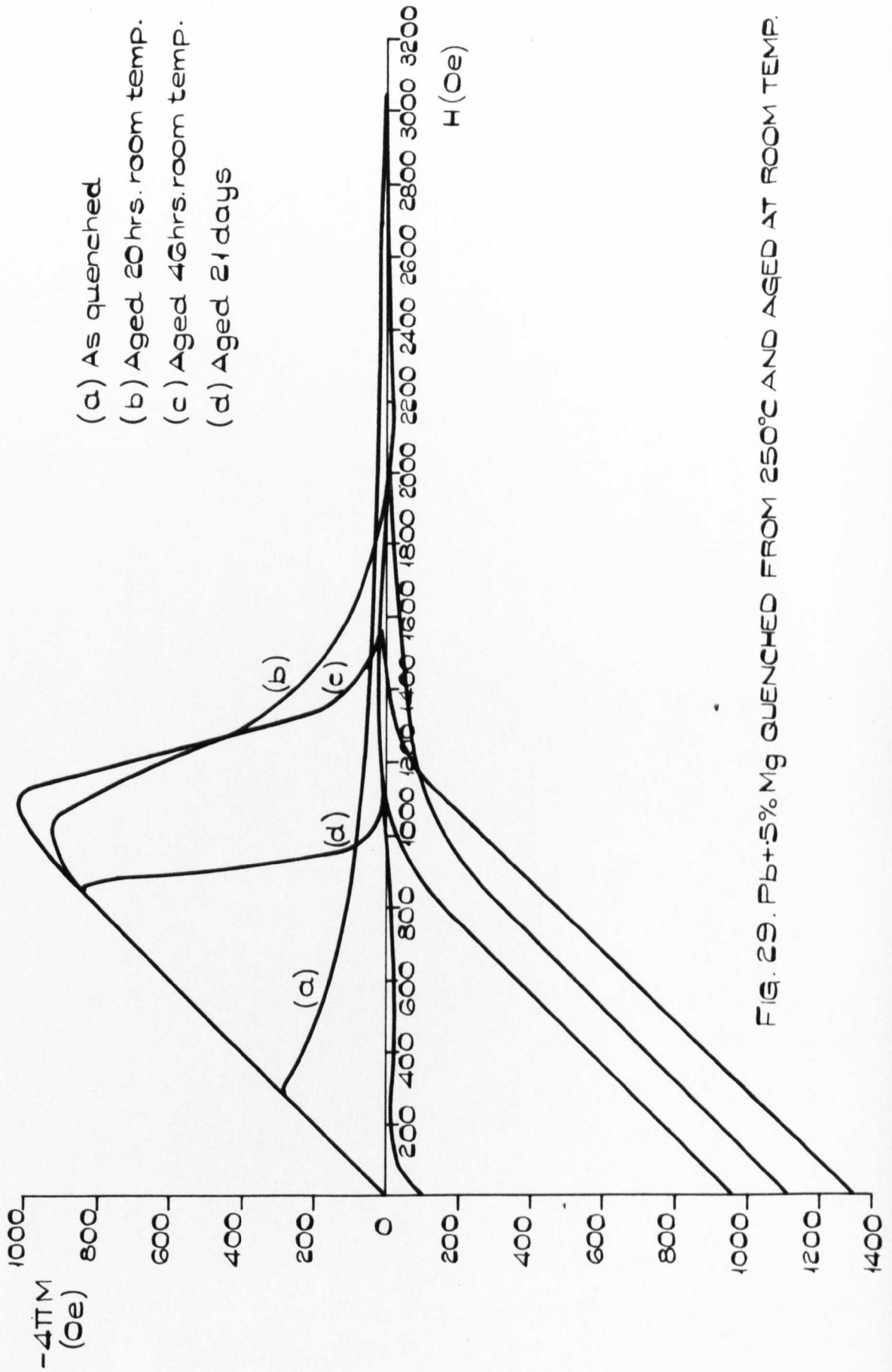
(a) As quenched
(b) Aged 20 hrs. room temp.
(c) Aged 46 hrs. room temp.
(d) Aged 21 days
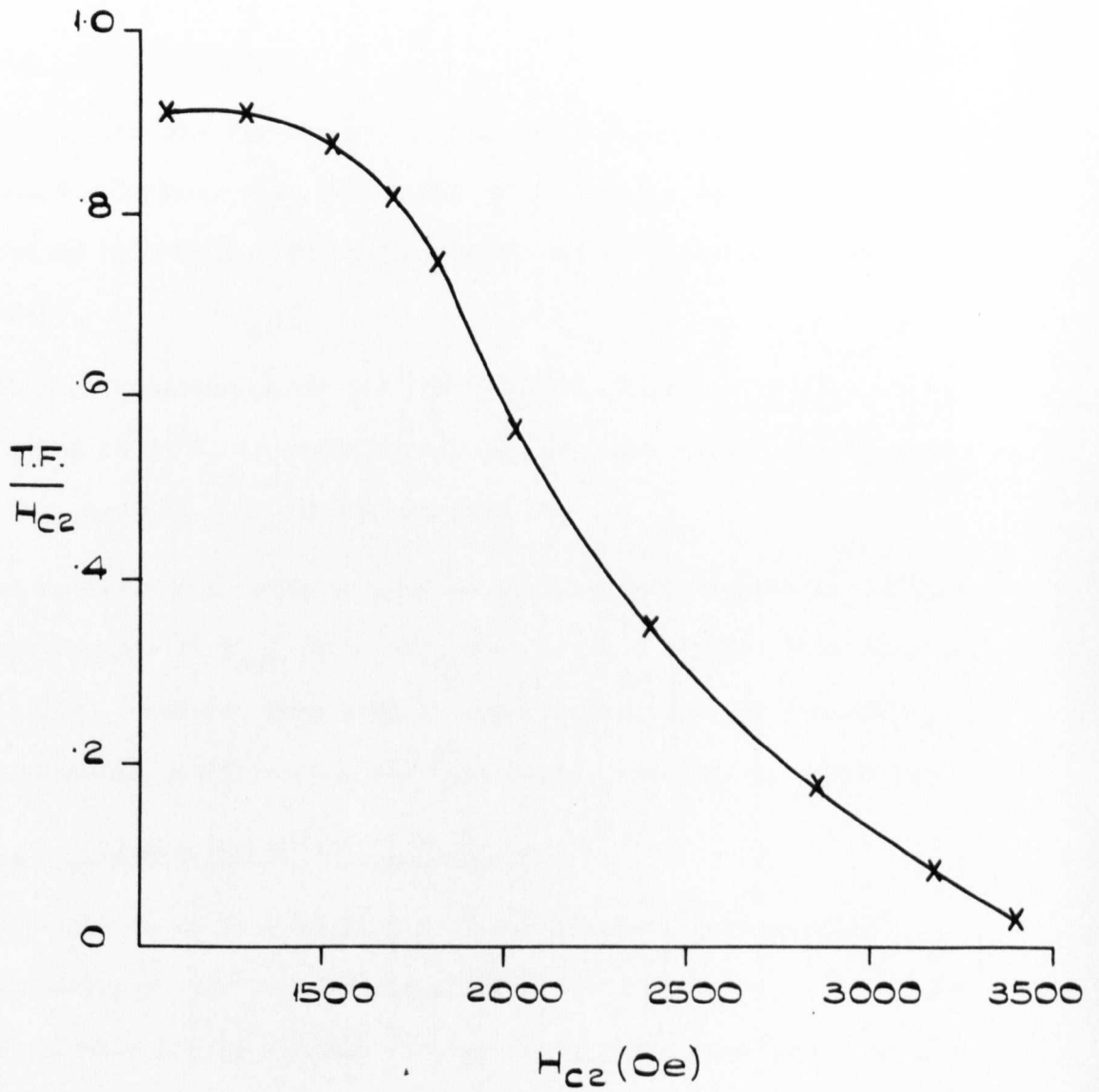
FIG. 30. PLOT OF HYSTERESIS AGAINST H_{C_2} FOR Pb + ·5% Mg
SOLID SOLUTION AGED AT ROOM TEMPERATURE.

experiment, do pin them. This is even more difficult to understand when the alloys are similar as in this case and in Livingston's work. A possible explanation is that the duplex cellular structure in Livingston's alloys does not go normal as he supposed. This is not unlikely in view of the fact that the Pb-Sn eutectic does exhibit a proximity effect.

10.2.12.   Bi-Tl system.

This system has two eutectics, each with essentially the same matrix of Bi_2Tl solid solution, the composition of this solid solution being slightly different in each case. The major difference between each eutectic is the precipitate.

The magnetisation curve for the eutectic occurring at 76.5 wt.% Bi, heat-treated at $91^{\circ}C$, is shown in fig.31, together with a specimen of its matrix in isolation. H_{c2} occurs at 2040 Oe.

The eutectic occurring at 47.5 wt.% Bi is more reversible and has a much higher value of H_{c2}, (6395 Oe), when given a similar heat treatment (see fig.32). However, when aged at room temperature for four days, H_{c2} of this eutectic decreases and the hysteresis increases as shown in fig.33.

10.2.13.   Discussion of the Bi-Tl system.

The eutectic at 76.5 wt.% Bi is type II and clearly owes its superconductivity to the presence of its matrix of Bi_2Tl. The hysteresis is most probably due to fluxoid pinning occurring at the surfaces of the Bi precipitate, since these are much larger than the coherence length. The directionally-frozen specimen traps slightly more flux, presumably because the branches of the 'herring bone' parts of the precipitate are more favourably orientated for pinning in this case, i.e. they lie more nearly parallel to the field.

The hysteresis present in the solid solution of Bi_2Tl is probably due

-4πM (Oe)

H(Oe)
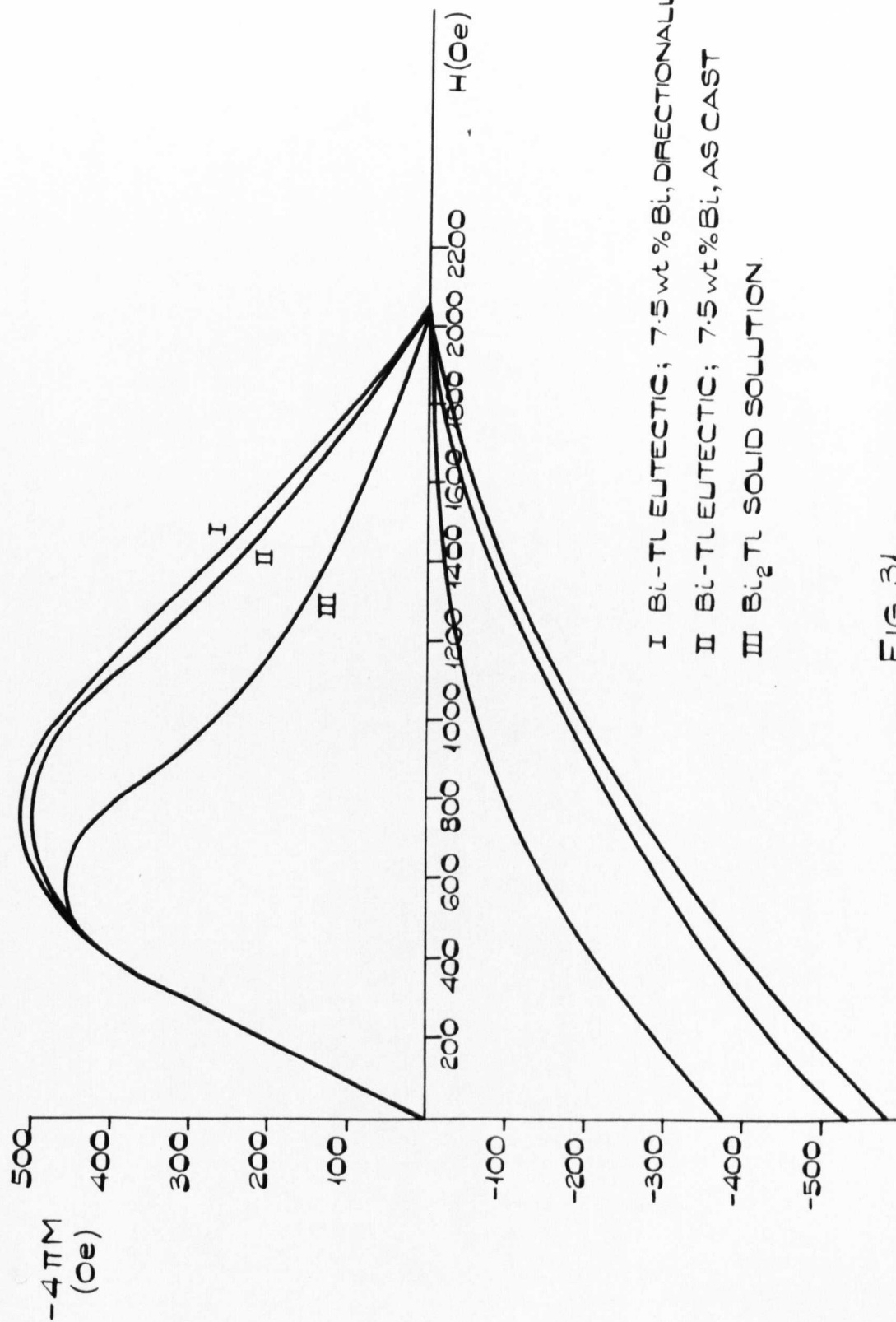
I Bi-Tl EUTECTIC; 7·5wt% Bi, DIRECTIONALLY FROZEN

II Bi-Tl EUTECTIC; 7·5wt%Bi, AS CAST

III Bi₂Tl SOLID SOLUTION.

FIG. 31.
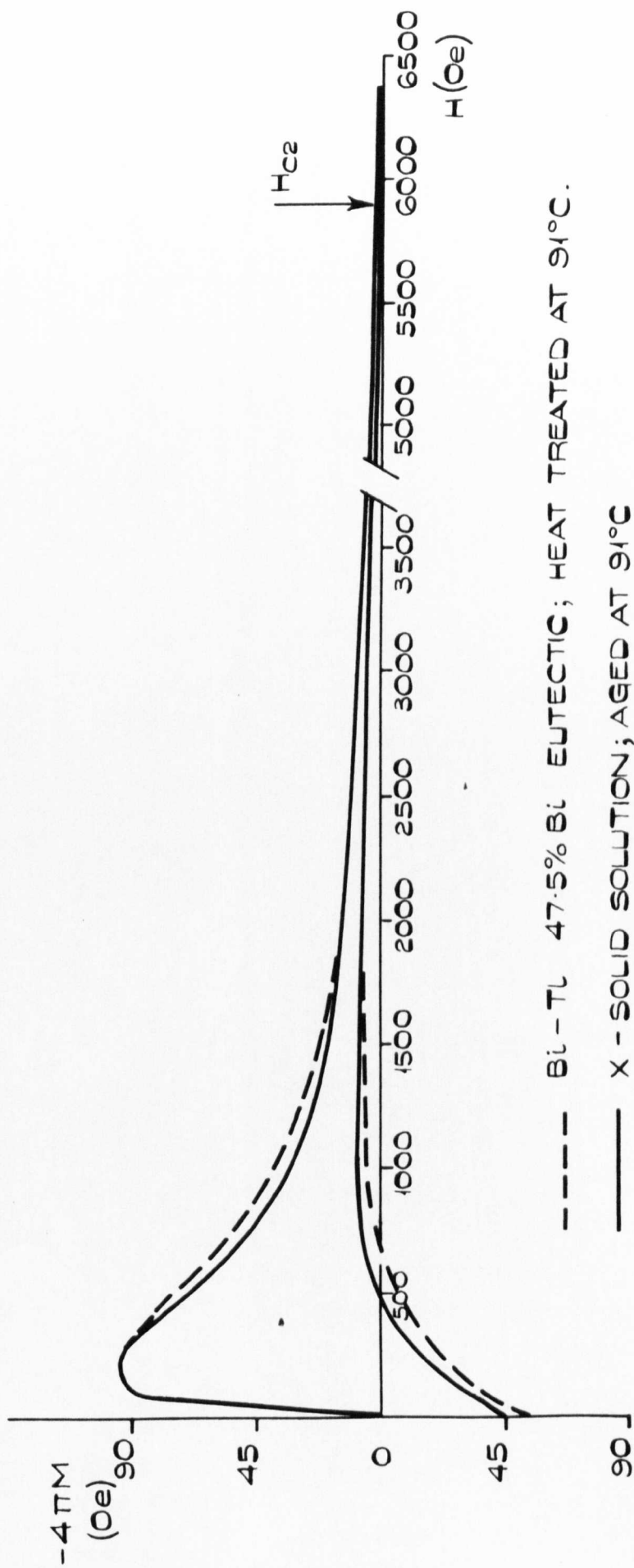
FIG. 32.

--- Bi-Tl 47.5% Bi EUTECTIC; HEAT TREATED AT 91°C.

X - SOLID SOLUTION; AGED AT 91°C
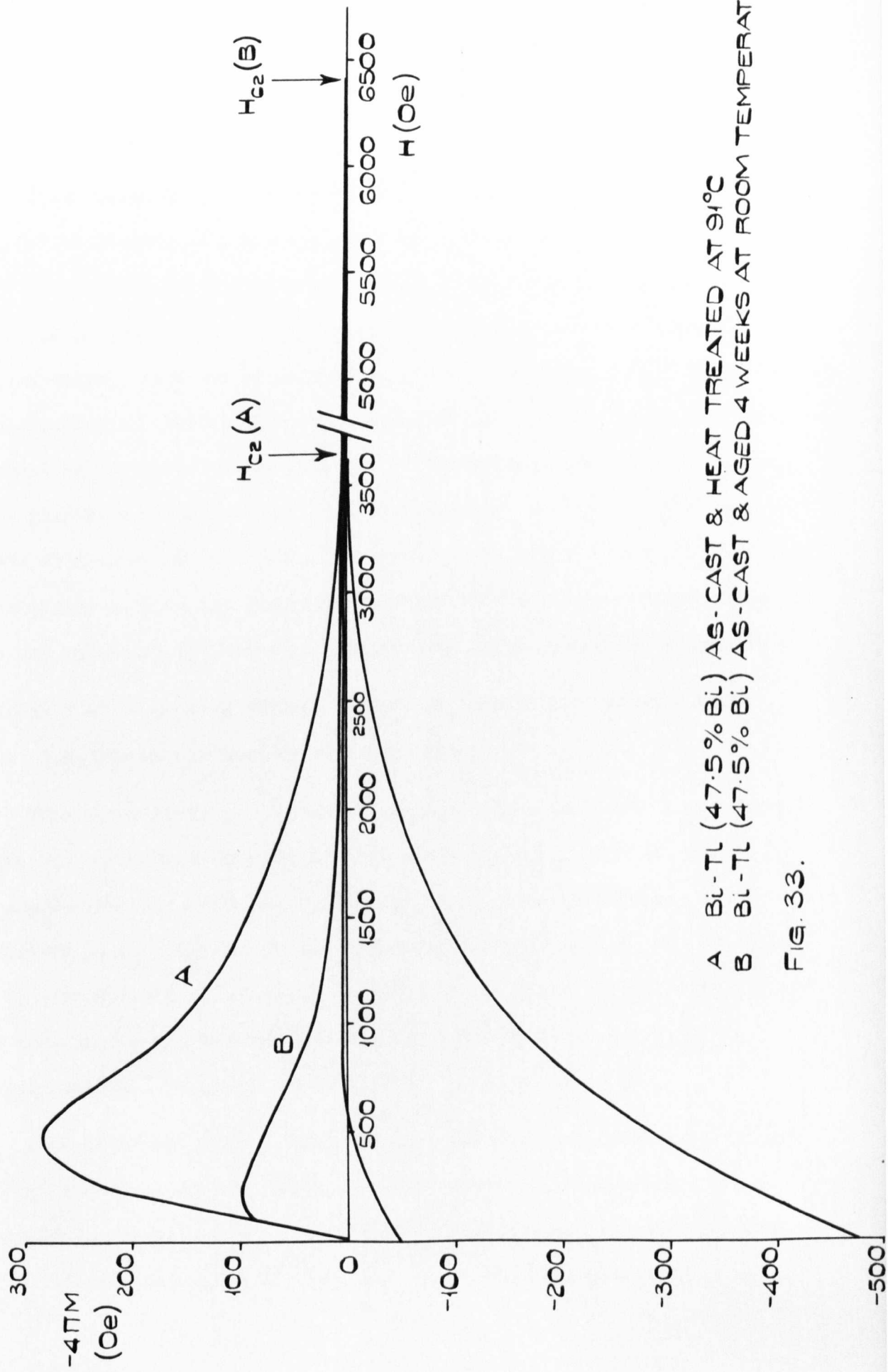
A   Bi-Tl (47.5% Bi) AS-CAST & HEAT TREATED AT 91°C
B   Bi-Tl (47.5% Bi) AS-CAST & AGED 4 WEEKS AT ROOM TEMPERATURE.

Fig. 33.

to the relatively poor surface finish of this alloy. A suitable chemical etchant could not be found to remove the effects of the tarnishing which occurred in the atmosphere.

Superconductivity in the eutectic at 76.5 wt.% Bi persists up to H_{c2} of the X-solid solution and no discontinuity is seen in the region of 2000 Oe when the matrix,which is present in the largest quantity, should have become normal. It is reasonable to assume that if the matrix did become normal, then the magnetisation of the sample would fall rapidly at this field strength. That it does not indicates that the matrix is still super-conducting by virtue of the presence of the superconducting precipitate. This proximity effect is confirmed by resistance transition data presented later which show that a transport current may be carried beyond H_{c2} of the precipitate without any resistance being detected. Since the precipitates are not connected and are separated by more than a coherence length, the current must be passing through surface regions of the matrix without loss, i.e. the matrix must be superconducting.

This eutectic is in a sense the opposite to that in the In-Bi system where the superconducting precipitate has a lower H_{c2} than its matrix but is superconducting above this field due to a proximity effect. This behaviour is also similar to that observed in Pb-Sn except that the matrix in this case would be normal in isolation because its upper critical field had been surpassed, whereas in Pb-Sn the critical temperature of the Sn-rich matrix is exceeded at 4.2°K.

A directionally-grown sample of the eutectic, similarly heat treated, did not show much more hysteresis. This is not surprising since this eutectic is reversible anyway. Clearly the matrix-precipitate interface has little effect either in the field range where the matrix would be

superconducting in its own right or where it would otherwise be normal were it not for the presence of the precipitate. The orientation of this precipitate is thus of little consequence as far as fluxoid pinning is concerned. This point is considered further in section (11.3.).

The results of fig.33 are evidently due to the transformation of the X-solid solution to α_1 solid solution on aging at room temperature. This new phase has a lower critical field and the presence of the new interfaces now affects the hysteresis considerably. This new mixture still appears to exhibit a proximity effect.

10.2.14. Pb-Sb system.

This eutectic consists of normal Sb particles in a low k Pb-rich matrix and the magnetisation curve is similar to that of Pb-Cd eutectic (fig.20) with H_{c2} = 682 Oe, when heat-treated at 118°C. Directional freezing does not change the precipitate orientation (see micrographs 20, 21).

10.2.15. Sb-Tl system.

This system contains a eutectic of virtually pure Sb particles in a matrix of Sb_2Tl_7. Fig.34 shows that the eutectic is a type II superconductor due to the matrix of Sb_2Tl_7 which has an upper critical field of 544 Oe after heat treatment at 91°C. The composition range of Sb_2Tl_7 is small, so ageing after heat treatment had little effect.

The magnetisation curve for a directionally grown specimen was the same.

10.2.16. Discussion of Sb-Tl system.

Superconductivity in this alloy is undoubtedly due to the Sb_2Tl_7 matrix and the hysteresis is presumably due to fluxoid pinning at the surface of the Sb particles.

Despite the directionally frozen specimen having the particles of Sb
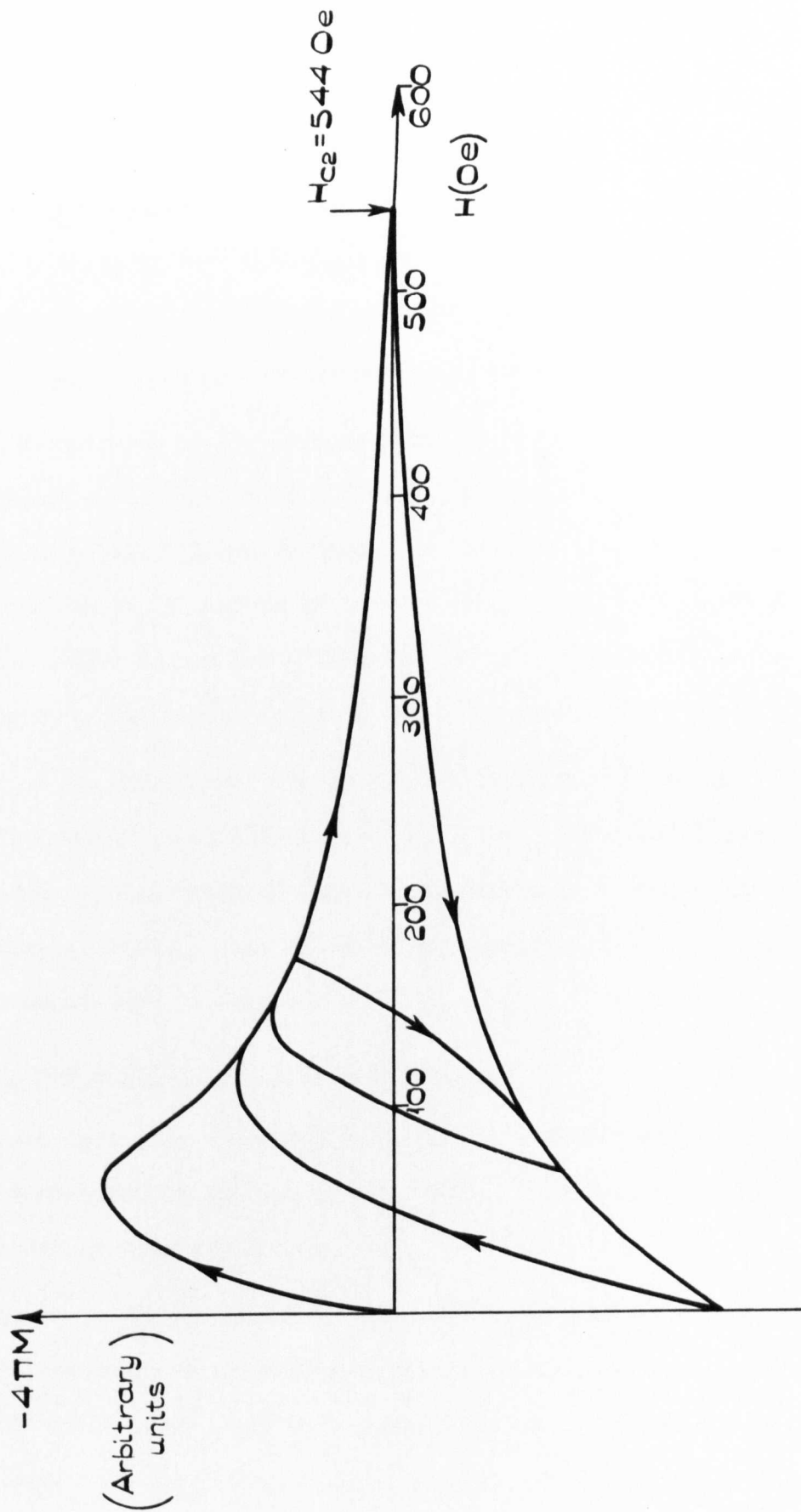
Fig. 34. Sb-Tl EUTECTIC AGED AT 91°C

tending to be orientated with their longest axis parallel to the growth
direction (see micrograph 25) no more hysteresis was present. The severe
irregularity of the particle surfaces is most probably the cause of this
lack of increased pinning. The surface parallel to the incoming fluxoids
is negligibly affected by the precipitate orientation. Why an apparently
similar precipitate of Bi particles in Pb-Bi does cause an increase in
hysteresis[69] when similarly orientated is not clear.

These results may be compared to those of the previous section. In
the low k Pb-Sb eutectic, the Sb particles had a much more drastic effect on
the resistance to fluxoid penetration. In the case of Sb-Tl, however,
the high k of the Sb_2Tl_7 matrix means that the presence of a surface has
only a small effect on the local value of the mean free path because it
is small anyway. Hence the low energy 'pinning well' is not so 'deep'.

A feature of this alloy is that the low field portion of the
magnetisation curve is not a straight line. Flux penetrates almost from
zero field (an applied field of only 20 Oe results in a measurable
amount of trapped flux). This is probably related to the fact that the
transition temperature is only 5.2°K.

10.2.16.   The significance of the major loop.

The presence of the so-called 'major loop' of a magnetisation curve
was first pointed out by Schweitzer and Bertman[56] and their terminology
is used throughout this discussion.

The 'initial' magnetisation curve is the curve described when the
measurements are taken on a 'virgin' specimen containing no trapped
flux, from H = 0 to H > H_{c2} and back again to H = 0. Hysteresis exists nearly
always and some zero field trapped flux remains. When the field is again
increased from this position, a curve, different from the initial

magnetisation curve, is described. However, the return paths are the same, as shown in fig.35. This curve is called the 'major loop'.

Once on the major loop at any point a field reversal results in the magnetisation changing along a diamagnetic path to the other side of the loop. Any suitable cyclic field change results in a 'minor' loop being described. No present theory of the magnetisation curve predicts these diamagnetic paths; indeed Schweitzer and Bertman[56] and Fink and Barnes[55] suggest that they indicate a surface current contribution to the magnetisation. They believe that these currents decrease until $-4\pi M = 0$ and then reverse when the field direction is reversed. In fact, the 'diamagnetics' are not completely straight with a slope of $-\frac{1}{4\pi}$; they deviate from this path to values of lower magnetisation as they approach the opposite side of the major loop. This is presumably because the currents are not uniform along the length of the sample and in parts they are not great enough to prevent some flux movement to or from the bulk.

If defect stabilized, surface currents j_m were the sole cause of magnetisation, then there would be no size dependence of the magnetisation curve, as is observed, nor any flux gradients within a specimen. Clearly, more than one mechanism is prevailing and a complete explanation must include the major loop. During the course of this work several observations have been made which support this hypothesis and suggest that the area of the major loop is merely a measure of the relative contributions of surface currents and other mechanisms.

Schweitzer and Bertman[56] noticed that the loop starts with zero area (in an ideal type II), increases to a maximum as hysteresis increases and then decreases to zero again at maximum flux trapping. This can be explained as follows:
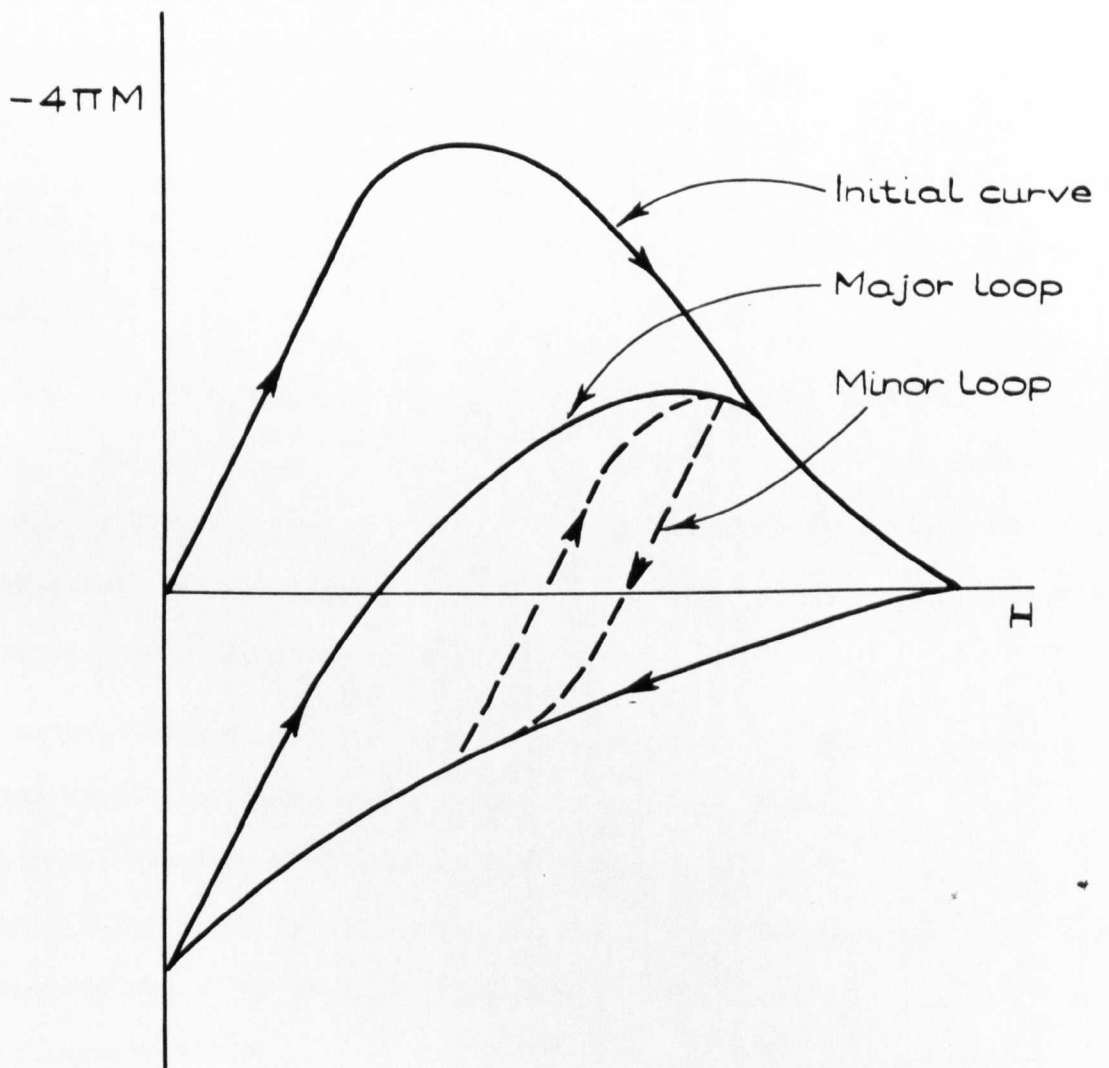
FIG. 35.

(i)   Initially, hysteresis is due to defect stabilised surface currents as suggested by Barnes and Fink.[55]

(ii)   As flux pinning effects become significant, the area of the curve decreases because the surface currents have a less significant effect.

Several experimental observations support this model. The area of the loop can be made larger for a fairly reversible sample if it is in the form of a doubly connected hollow cylinder. Then the screening currents which arise in decreasing field because of the flux in the hole add to j_m and cause a larger loop. If the sample is slit to make it singly connected the area decreases when these extra screening currents are removed (see fig.36).

The surface currents are defect stabilised because they increase with specimen thickness initially, as for example, in the thin Pb-Cd eutectic specimens shown in fig.21. The currents are thus associated with a macroscopic surface layer. Even so, the area of the loop is significantly decreased by plating with Ni (fig.37).

As the thickness of the Pb-Cd eutectic is increased, however, pinning becomes more significant and the area of the loop decreases to zero. When this extreme case is reached the pinning is so great that the depth of field penetration is very small and the specimen appears to be perfectly diamagnetic almost up to H_{c2} and is similar to a completely irreversible type I superconductor.

An important complication to any results is the effect of the specimen edges. In fig.36 the slightly earlier field penetration and decreased hysteresis in increasing field for the slit specimen is most probably because flux penetration is facilitated at the cut edges. The effect of
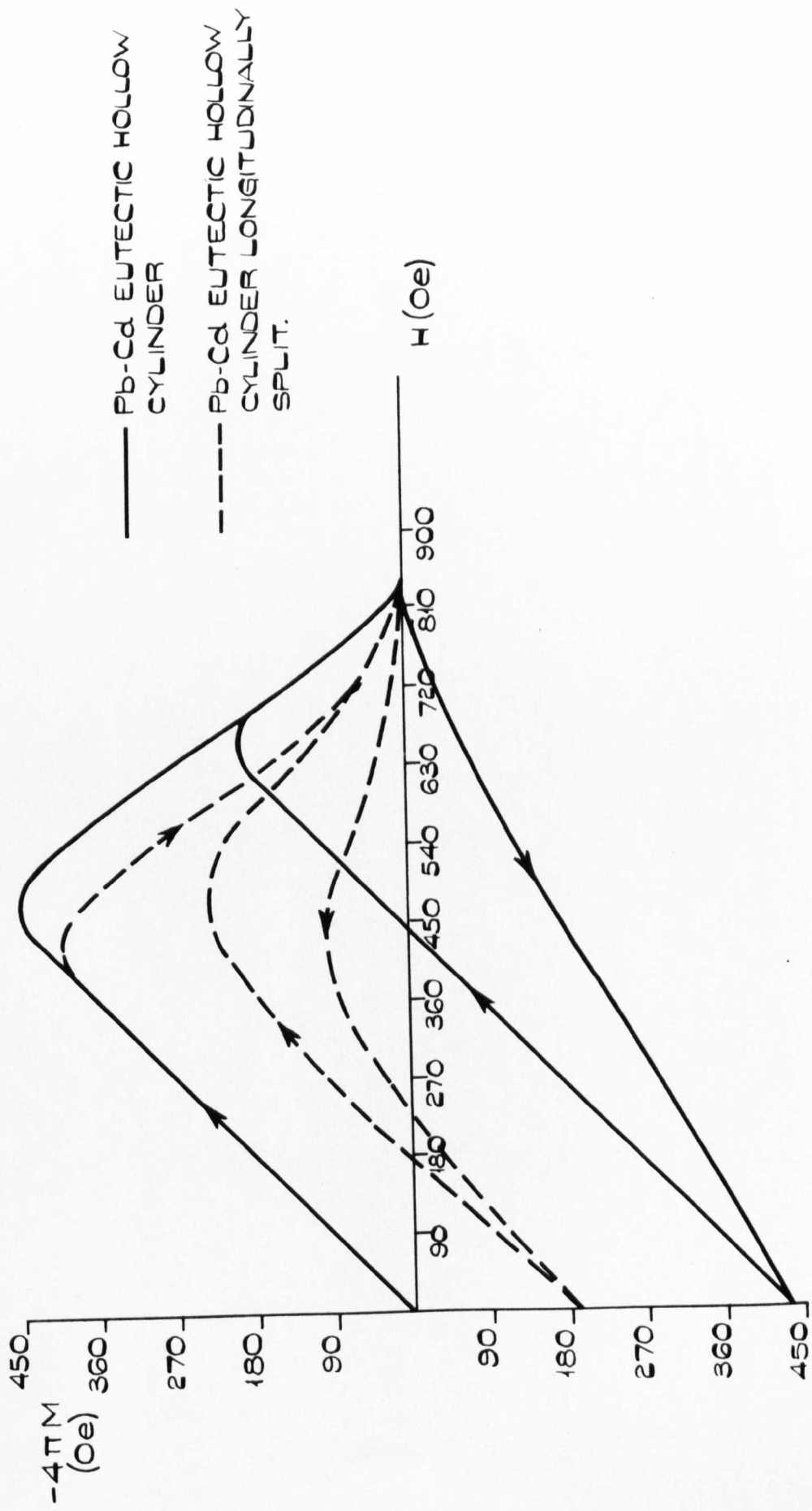
FIG. 36.
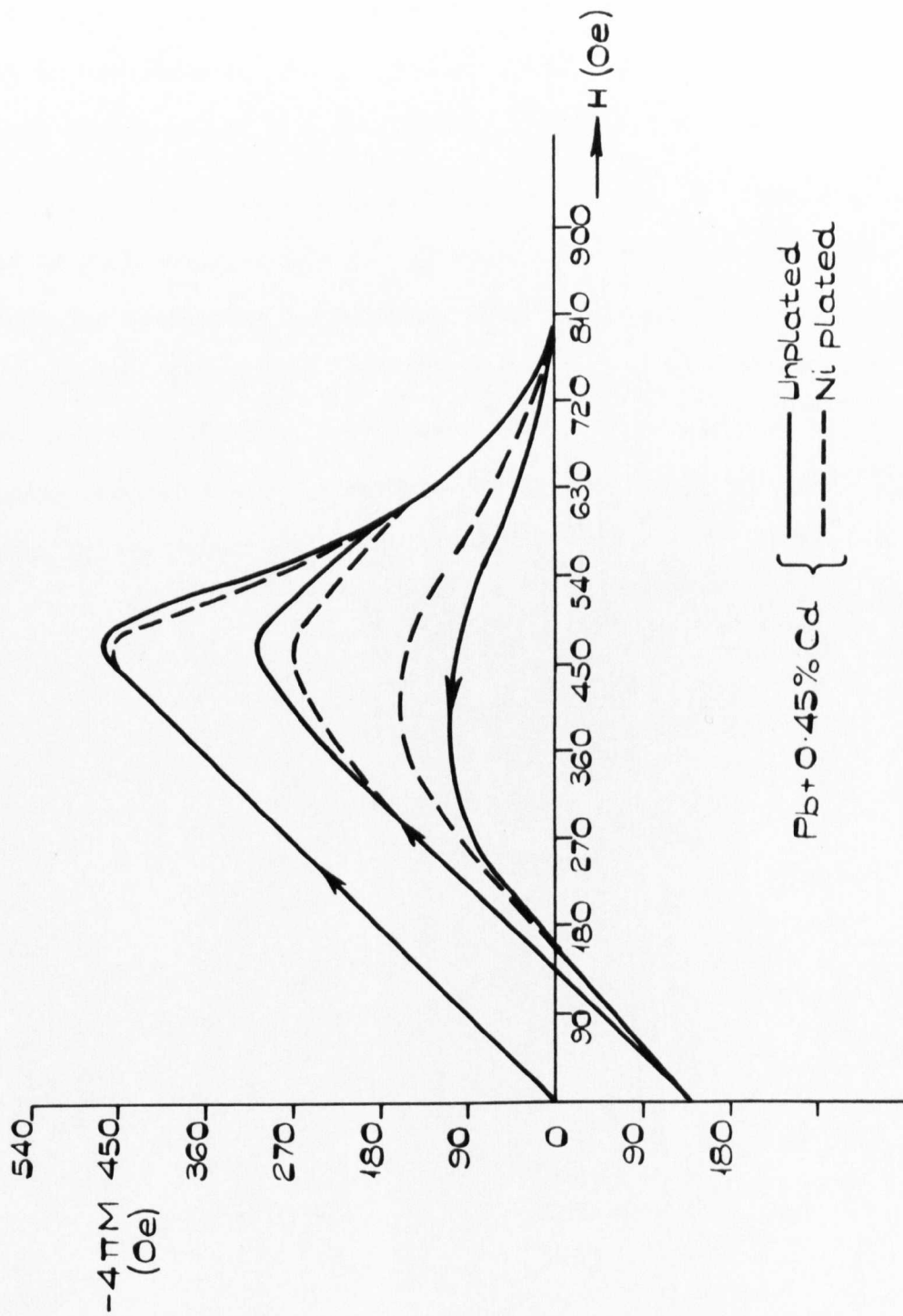
FIG. 37.

the ends on a Pb-Sn eutectic hollow ellipsoid are clearly shown in fig.38.
The edges allow flux to penetrate rapidly at a field of 60 Oe during the
initial field increase. A second field cycle results in a major loop
greater in area than the initial magnetisation curve. A minor loop cycle
results in the magnetisation increasing still further in increasing field.
All field cycles follow the same path in decreasing field.

When this hollow ellipsoid's ends were removed the magnetisation curve
changed to that shown in fig.39. Without the edges flux penetration does
not cause the hysteresis to decrease until 150 Oe and even then the rate
is much slower. The return path of the major loop is much lower and the
trapped flux much greater in this case of course because the specimen is
now doubly connected and additional screening currents are now present to
trap flux in the centre of the cylinder.
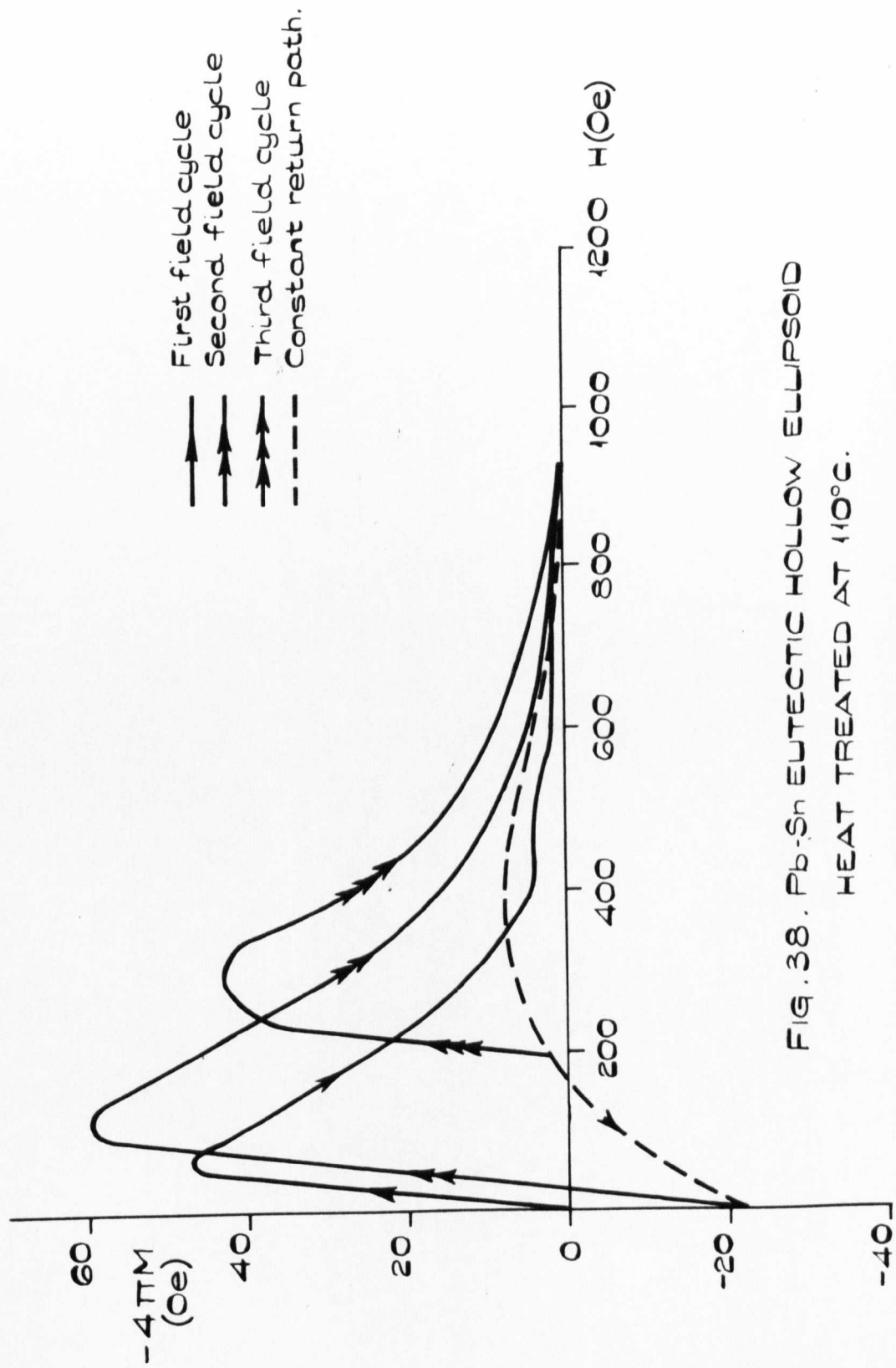
FIG. 38. Pb-Sn EUTECTIC HOLLOW ELLIPSOID
HEAT TREATED AT 110°C.
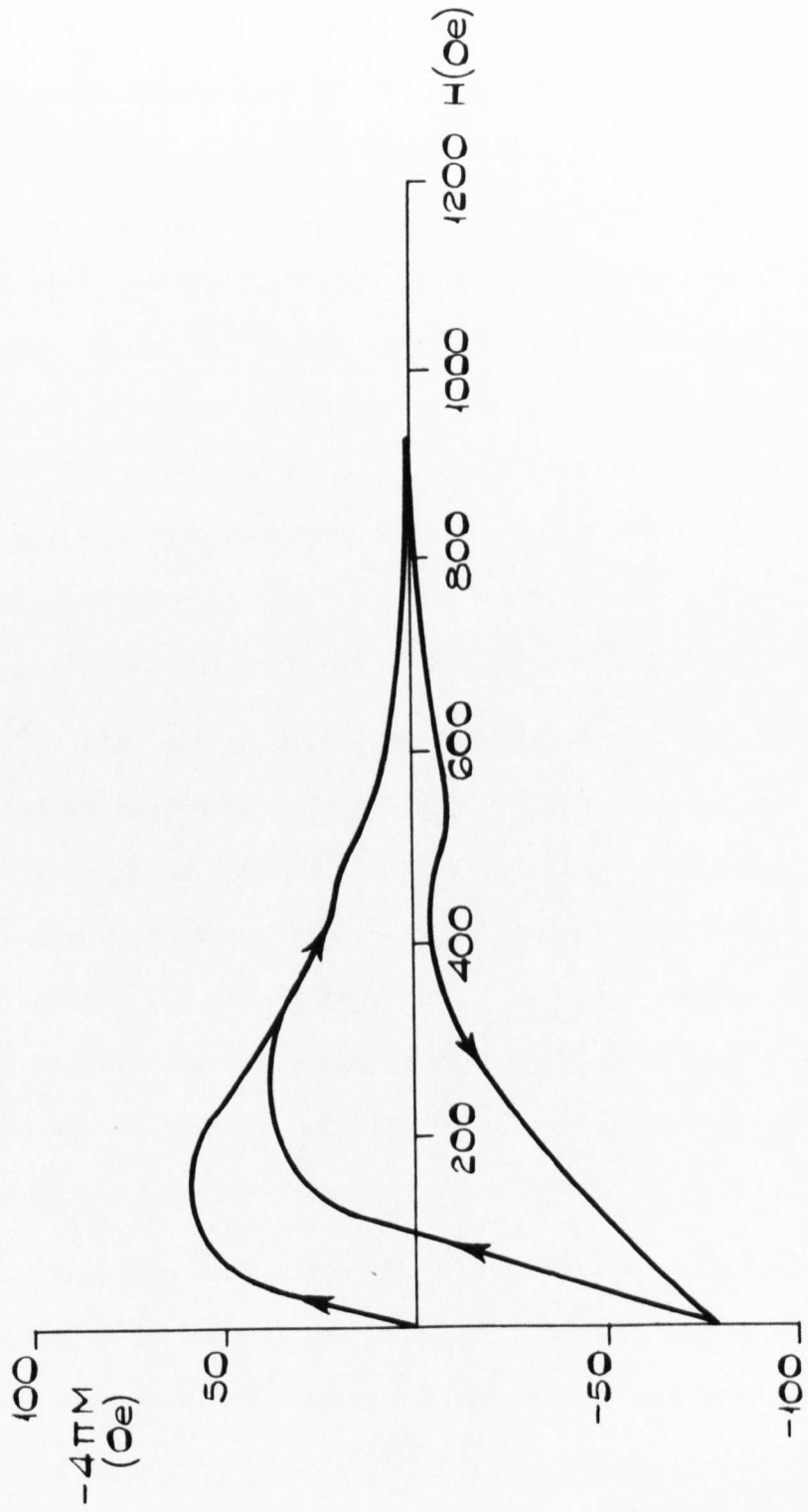
FIG. 39. Pb-Sn EUTECTIC HOLLOW CYLINDER HEAT TREATED AT 110°C.

11.   Critical Current Measurements.

11.1.   Introduction

An ideal reversible, type II superconductor cannot carry a resistanceless current in the mixed state. This can be seen by considering a slab lying in a field parallel to the plane of the slab. The self field of a surface transport current flowing perpendicular to the applied field will enhance the field at one side of the slab and reduce it at the other. (A bulk transport current is not possible since this requires a flux gradient). Since the sample is ideal, there is only one unique induction for each value of the surface field in the mixed state. Therefore, a state in which the induction is uniform (as it must be in an ideal specimen) and yet the field at each surface is different, is not an allowed state of the superconductor. No lossless transport current in the surface is possible, therefore, unless a non-equilibrium state exists at the surface.

Park,[52,54] Fink and Barnes[53] and Swartz and Hart[71] postulate such a state and predict that a resistanceless transport current can indeed flow in the surface of an ideal type II superconductor in the mixed state. The surface flux-spot pinning concept of Swartz and Hart has already been discussed and applies for fields at oblique incidence to the surface. The other theories concern the variation of the Ginzburg-Landau order parameter in the vicinity of the surface and have only been worked out for the case when H is parallel to the surface.

In a non-ideal type II superconductor, of course, internal field gradients can exist and bulk currents can be carried. In addition, surface currents of the type mentioned above and the defect stabilised surface currents suggested by Fink and Barnes[55] may also flow.

The internal flux distribution required to allow internal transport

currents is not so simple as in magnetisation experiments where the
distribution in a longitudinal applied field is straightforward. In the
case of a superconducting wire, carrying a current in zero applied field,
the fluxoids are presumed to penetrate in the form of annuli (similar in
topology to smoke rings) and the resultant gradient is equivalent to a
macroscopic internal transport current.

When the driving force (essentially the macroscopic Lorentz force)
overcomes the pinning force the fluxoids will move inwards down the gradient.
Locally in the superconductor $\frac{dB}{dt}$ will not be zero because of this movement
and by Maxwell's equation,

$$\text{Curl } \overline{E} = \frac{d\overline{B}}{dt} \neq 0$$

This rotary electric field generates small eddy currents which pass
through the normal cores of the flux threads and cause a voltage to be
observed.

The transport current which provides this driving force which is
large enough to overcome the pinning force is the critical transport
current. In this work this current is assumed to be reached when a value
of 10^{-6} volts is detected across the specimen, unless otherwise stated.

When an external field is applied, the fluxoid distribution becomes
more complicated. Consider a slab in an applied field parallel to the
surface and perpendicular to an impressed transport current (fig 40).
The applied field will be parallel to the self-field of the transport
current but will act in opposite directions on each side of the slab.
(The induced currents will therefore add to or oppose the transport current).
For transport currents less than critical, the field and current distribution
across the slab will depend on the sequence in which the applied field and
transport current are applied. The maximum critical transport current is
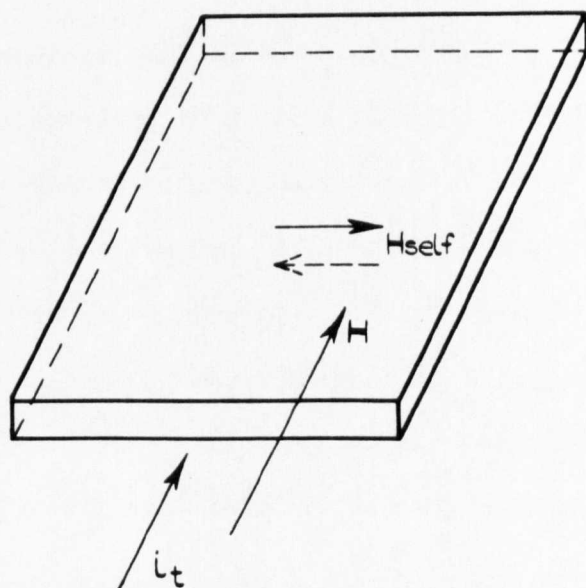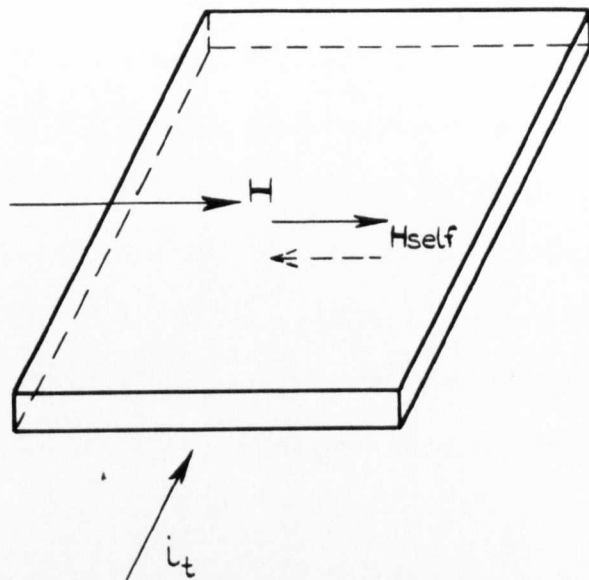
Fig. 40. Slab specimen carrying a transport current i_t which generates a magnetic field Hself in an applied magnetic field H.

reached when the internal macroscopic current is unidirectional transport current.[72]

On the other hand, if the field is applied parallel to the transport current, the induced currents and the transport currents are perpendicular to each other and a resultant current will be set up. In this case the path is a helix whose pitch will vary with the magnitudes of the transport and induced currents. The resulting fluxoid distribution is complicated and the critical state model does not seem to offer an explanation. Since the fluxoids must have the sense of the resultant field their direction will also be helical. Bergeron[73] has suggested such a configuration, with the net current everywhere parallel to the net field and so free of the Lorentz force.

Critical current measurements thus allow the interaction between precipitates and variable fluxoid distributions to be investigated.

11.2. Results.

The effect of the surface must again be separated from the bulk effects. In this case a specimen of Pb +.5% Cd solid solution was roughened on the spark machine, re-homogenised in vacuum at 250°C for four hours and quenched in liquid nitrogen. This heat treatment also removed any cold-work caused by the machining process. The curves for roughened and smooth specimens are shown in fig. 41. The roughened sample has a lower critical current for both values of θ, the incident angle of the applied field. The curves are clearly sensitive to this angle of orientation.

The low k eutectics of Pb-Cd, Pb-Sb and Pb-Sn show a behaviour only slightly dependent on θ, as can be seen from fig. 42. Roughening the surface did not significantly alter these curves.
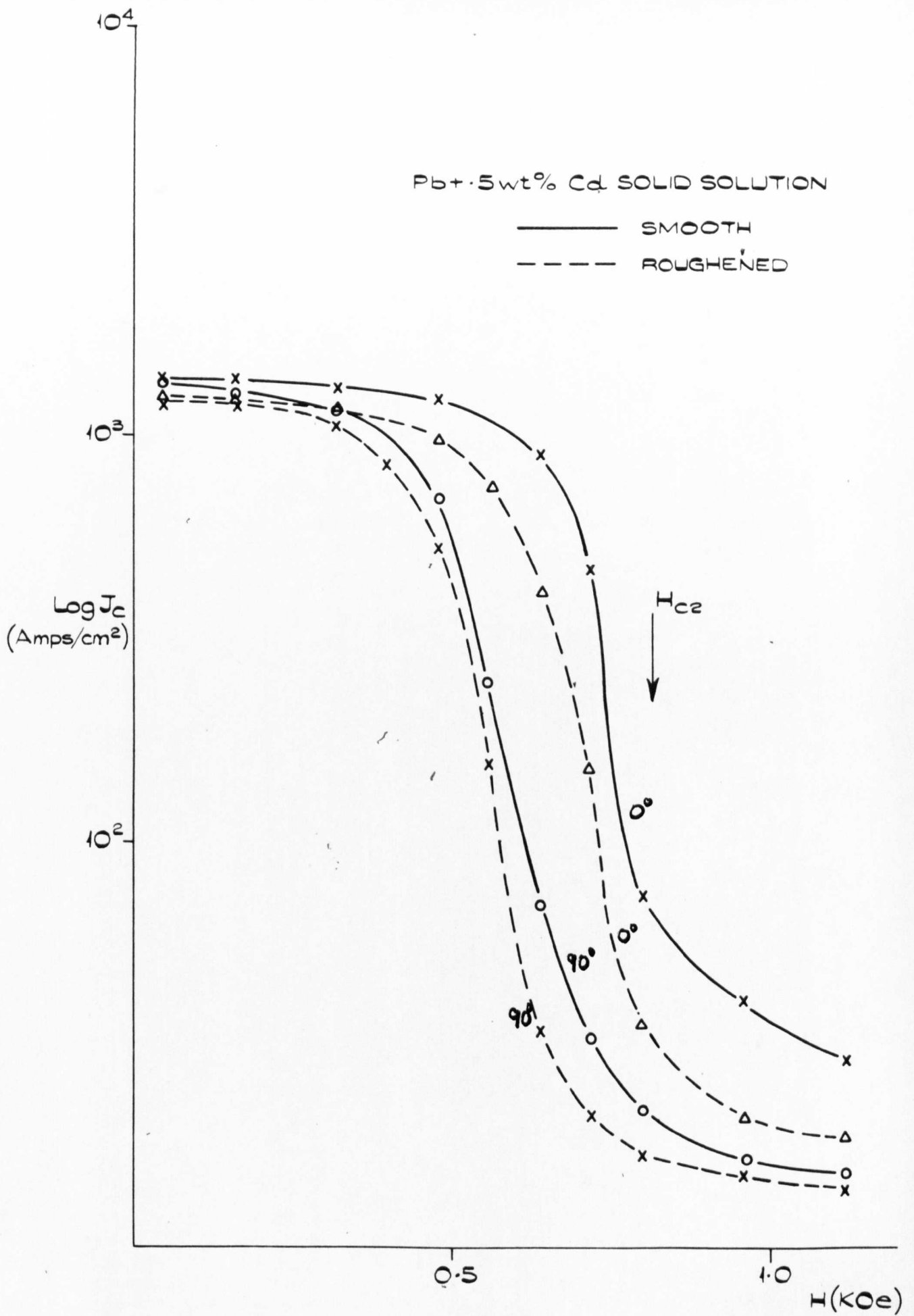
FIG. 41

Critical current of eutectic alloys.

Pb-Cd (-△——△——△- 0°
          -⊙——⊙——⊙- 90°
Pb-Sn (-□——□——□- 0°
          -⊙——⊙——⊙- 90°
Pb-Sb (-×——×——×- 0°
          -⊙——⊙——⊙- 90°

10^4

10^3

Log J_c
(Amp/cm^2)

10^2

10

0·5   1·0   1·5   2·0   H(KOe)
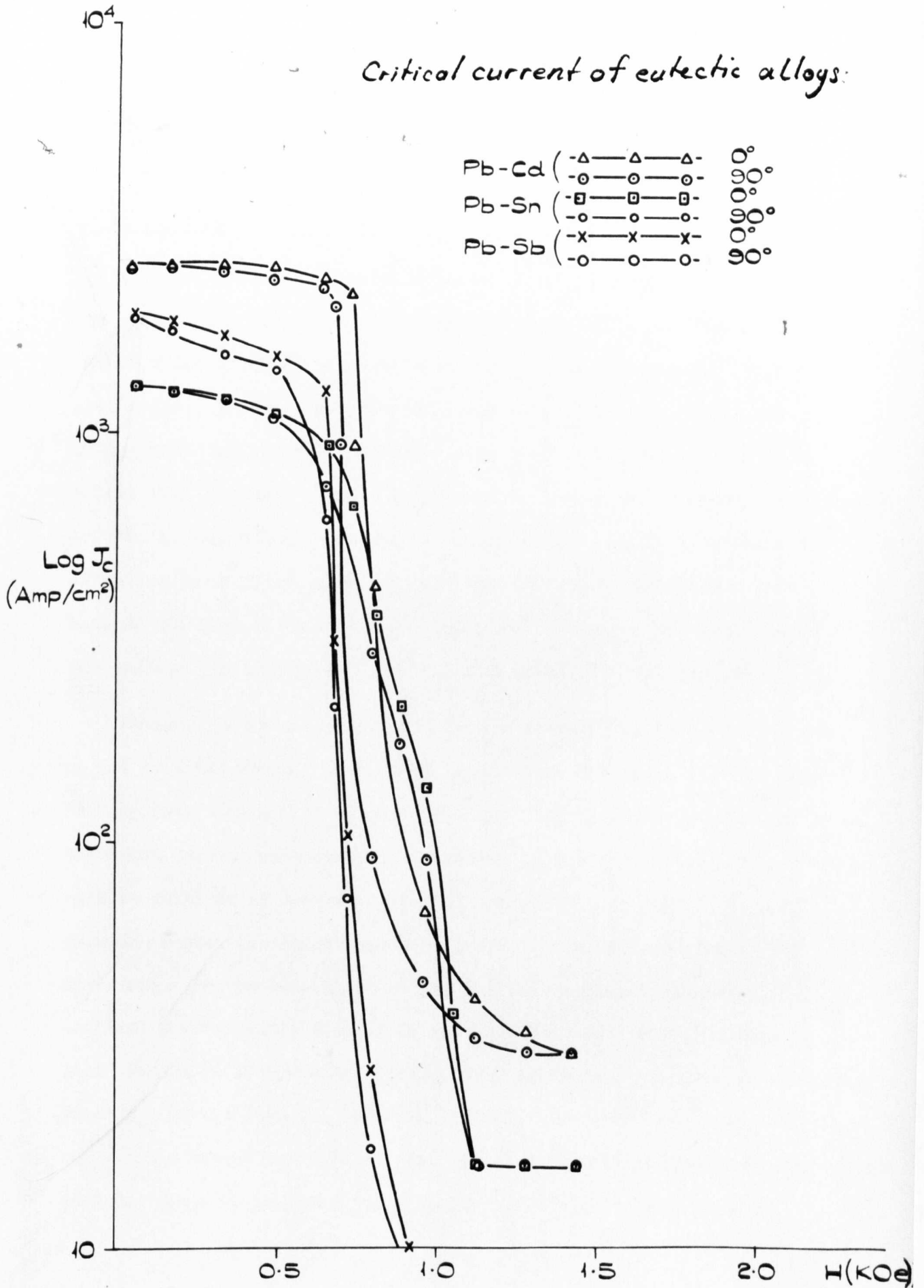
FIG. 42.

The higher k eutectics, Tl + 47.5% Bi, Tl + 76.5% Bi, Sb-Tl and In-Bi are much more sensitive to Θ (figs. 43-46). However, only In-Bi showed any significant dependence on the orientation of the precipitate and none showed any significant effect on roughening.

11.3.   Discussion of results.

Pb +.5% Cd solid solution approaches an ideal type II superconductor and so the bulk component of the current must be small. The much lower value of the critical current for $\Theta = 90^{\circ}$ is most probably due to two mechanisms. Firstly, the demagnetising effect of the specimen shape means that fluxoids will penetrate much earlier in transverse field. This effect will decrease as H_{c2} is approached. Secondly, the slight resistance offered by any defects present to the invading fluxoids will be more effective in restricting penetration in the longitudinal field case because the Lorentz force (whose magnitude depends on the angle between the macroscopic current and the internal field) is much reduced.

Roughening the surface decreases the current for both orientations of the external field. This is in qualitative agreement with the magnet-isation data obtained in section 10.2.1. on Hg-Tl solid solution and with transport current measurements of Lowell[74] below H_{c2} but at variance with results obtained by Swartz and Hart[71] and Joiner and Kuhr.[75] Lowell considered that two mechanisms were operating in his experiment: an improvement in the smoothness of the surface tending to increase the critical current while removal of the roughened and severely damaged layer tended to decrease it. Indeed this latter effect is seen to dominate above H_{c2} in his results. However, in this experiment on Pb +.5% Cd, any surface damage is annealed out. Local variation in chemical composition that may occur by preferential dissolution on electro-polishing or

BI-TL EUTECTIC (47.5% BI)

As cast
- x : 0°
- ▫ : 90°

Directionally frozen
- △ : 0°
- ● : 90°

X - Solid solution
- △ : 0°
- ⊙ : 90°

H_{c2}

Log J_c
Amps/cm²
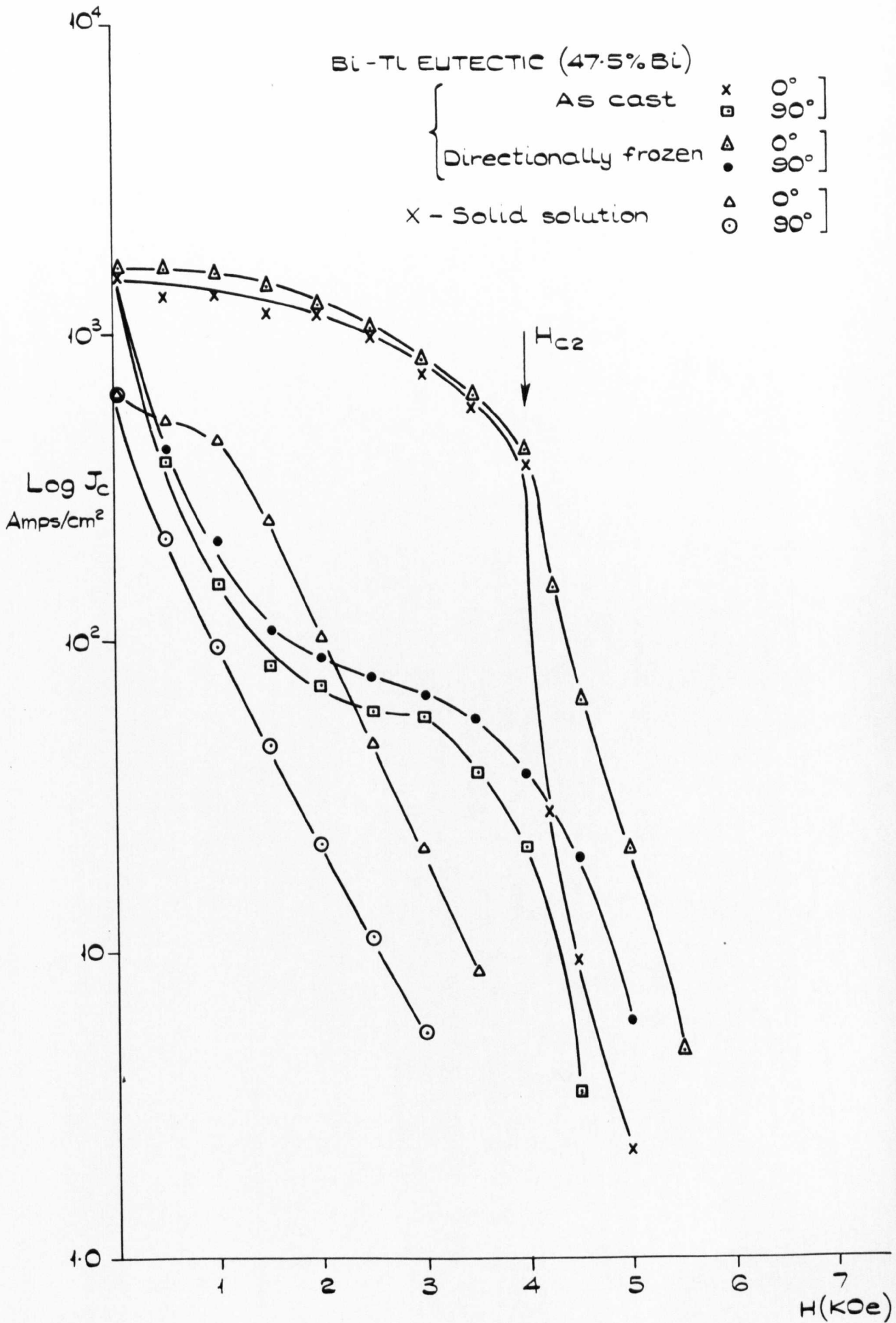
FIG. 43.
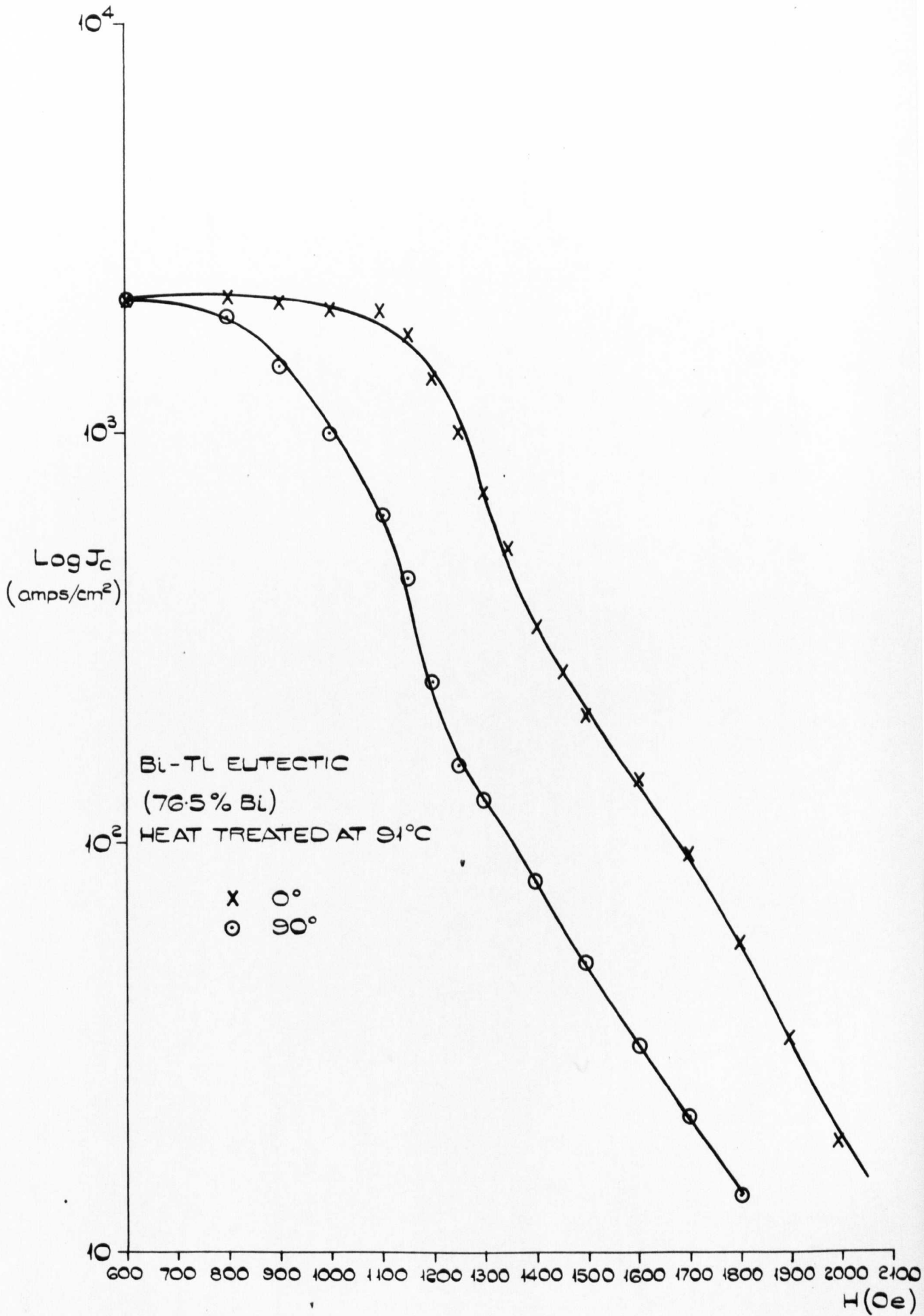
FIG. 44
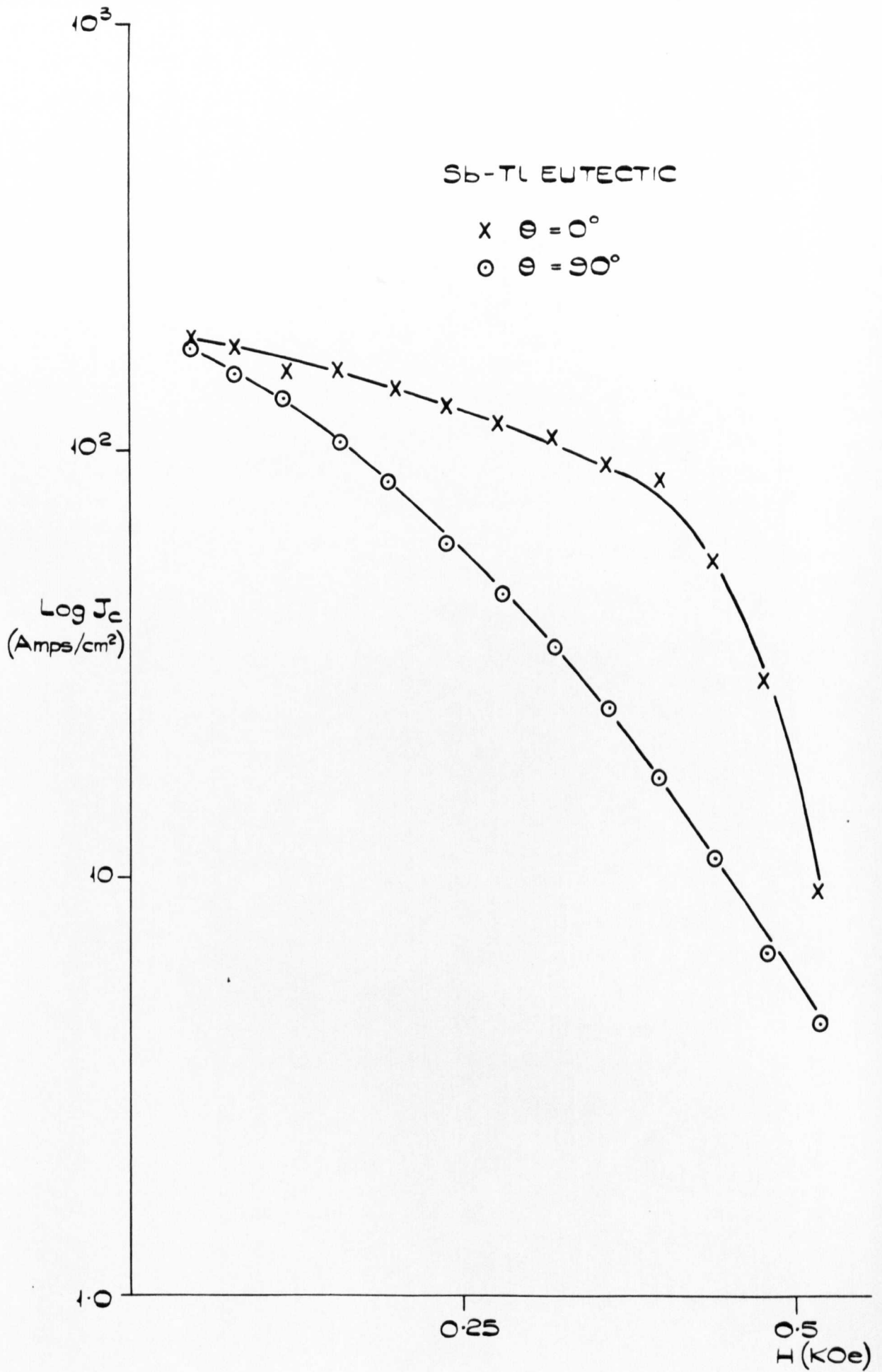
FIG. 45.
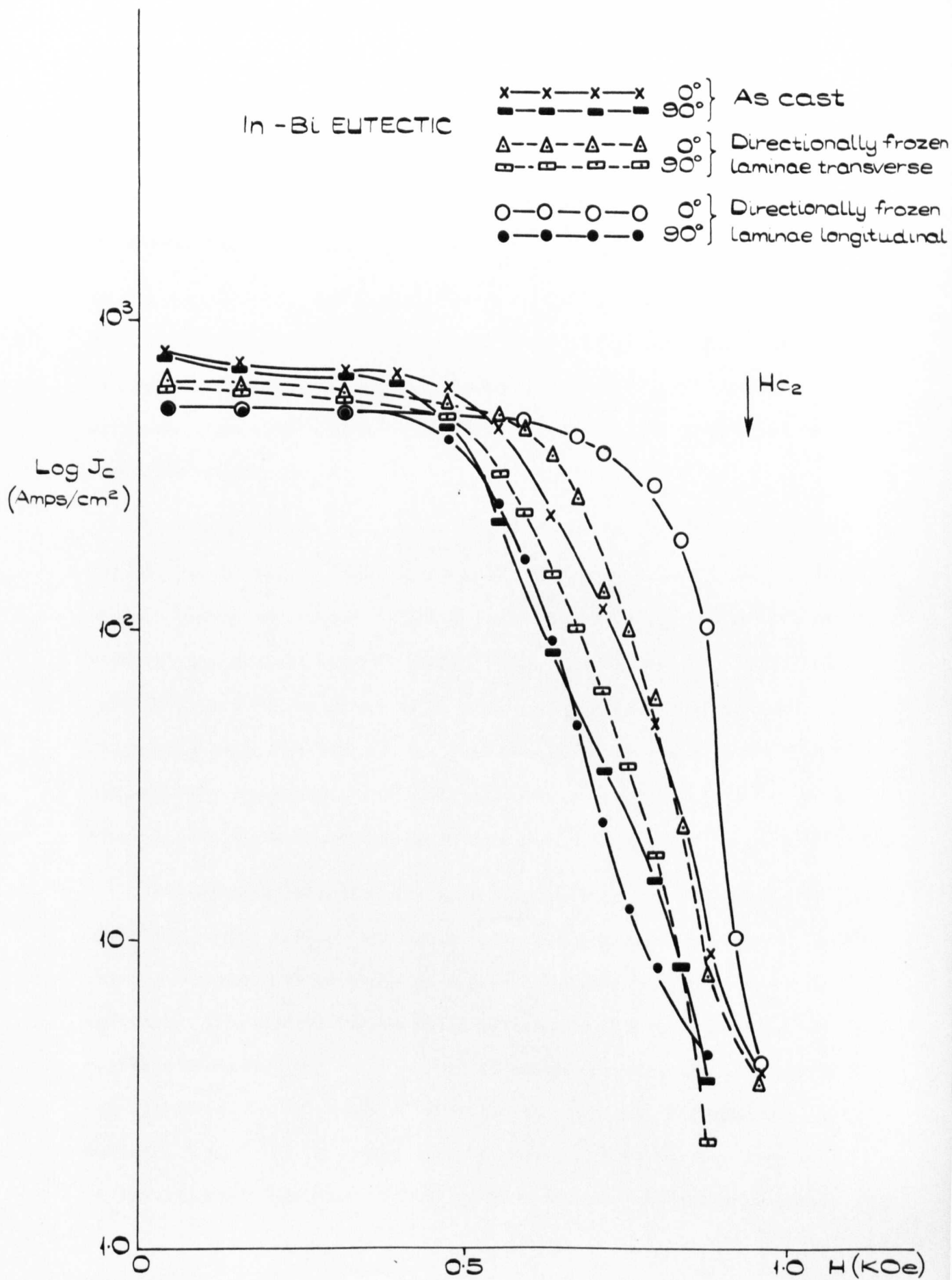
FIG. 46.

chemical polishing is also avoided. Only the surface geometry has been changed.

No conclusions can be made about the nature of these currents except that the results of this **experiment** indicate that the flux spot pinning mechanism does not operate, otherwise roughening should cause an increase in the critical current. The calculations of Park[52, 55] and Fink and Barnes[53] do not consider oblique incidence of the field. It is very possible that roughening the surface simply permits premature fluxoid nucleation because of local enhanced fields at the surface asperities due to demagnetising effects. Once nucleated little resistance will exist to prevent their inward movement.

When appreciable bulk pinning is present, as in the eutectics of fig.42, the 0° and 90° curves are both unaffected by roughening. This is simply because the transport current can be and is carried mainly in the bulk and the surface current contribution is small by comparison. Not only this, but fluxoids nucleated prematurely at the surface due to roughening would not be able to penetrate anyway because of the high pinning forces present. The similarity between the 0° and 90° curves below H_{c2} in these eutectics must also be due to these high pinning forces.

The higher k eutectics are more sensitive to the field orientation. Since roughening the surface again made no significant difference to the mixed state critical currents it may be concluded that they are bulk currents. The sensitivity to field orientation is very probably because of the reduced driving force on the fluxoids (as a result of the fluxoid configuration) in the parallel field case. Fig. 43, in which the Bi-Tl eutectic (47.5% Bi) is compared to the X-solid solution verifies this. In the magnetisation experiments on these alloys, the eutectic showed very

little more hysteresis than the X-solid solution because when a significant Lorentz force is present the precipitate surface offers little resistance to flux line penetration because the pinning force is so weak. This is further seen by comparing the eutectic and solid solution critical current curves in transverse field - they are very similar when the applied field is very **much** less than H_{c2}. However, when the Lorentz force is very small, as in the longitudinal field case, the small pinning effect of the precipitate interface is very significant and penetration is greatly delayed.

As H_{c2} is approached the eutectic is able to support more current even in transverse field than the solid solution. The orientation of the precipitate, however, seems to be unimportant except above and just below H_{c2} where the directionally frozen specimen carries a greater current. The role of precipitates in this region is discussed more fully in section 12.

The In-Bi eutectic, fig.46 and Bi-Tl eutectic (47.5% Bi), fig.43, curves show no discontinuities at the critical fields of In_2Bi (~ 430 Oe) and Bi_2Tl (~ 2000 Oe) respectively and so this result supports the hypothesis that a prominity effect is indeed occurring in these alloys. An increase in the pinning force would be expected[70] if the In_2Bi precipitate became normal, which would increase the critical currents. A decrease in critical current would be expected in the Bi-Tl case because Bi_2Tl is the matrix and rapid field penetration would be expected when it became normal. The absence of any discontinuity at these points indicates that the interface pinning strength is unaffected by whether one of the surfaces is superconducting in its own right or whether it is superconducting by means of a proximity effect.

In the In-Bi system the orientation relationship of the precipitate

with respect to the field direction is readily explainable in terms of pinning at the precipitate interface being stronger the greater the length of surface able to participate in the pinning process. The critical current is a maximum when the applied field is parallel to the greatest area of precipitate surface.

In longitudinal field, i.e. $\theta = 0^{\circ}$, the maximum current is clearly carried by the directionally frozen specimen. Despite the fact that the fluxoids are probably in a (distorted) helical formation, they are able to be pinned most effectively by roughly parallel surfaces because this formation, see micrograph (13), would pin them over the greatest possible length. Approaching H_{c2}, where the difference in current carrying capacity is greatest, two possibilities exist as to why this orientation of defects become even more effective. Just because there are more fluxoids in the sample its increased pinning capacity becomes more apparent. Alternatively it may be argued that the fluxoid lattice is becoming more rigid[23] anyway and effective pinning of sufficient fluxoids would prevent movement of the lattice as a whole. Thus any increase of pinning efficiency would be magnified.

In transverse field this sample carries the least current of the three measured. The specimen containing laminae orientated about an axis perpendicular to the specimen axis (see micrograph 2) has the greatest critical current. In this case the fluxoids are linear as in the magnet-isation experiments, and their relative orientation with respect to the precipitate gives maximum pinning.

Not surprisingly, the as-cast specimen, with randomly orientated laminae maintains an intermediate value of critical current for both configurations of the field.

There seems to be no correlation between critical transport currents and the area of the major loop in magnetisation experiments although nearly all those eutectic alloys exhibiting major loops of large area (and hence whose hysteretic behaviour is in part due to surface currents) show critical current curves very dependent on field orientation. This, however, is entirely due to the weaker pinning forces at the precipitate interfaces in these alloys being overcome by the Lorentz force more easily, thus allowing earlier field penetration. Surface currents do not appear to be involved. Pb-Sn eutectic is the exception but the pinning forces at the Pb-rich lamellae interfaces are strong and the critical current behaviour is similar to Pb-Cd and Pb-Sb eutectics.

The dumb-bell shape of the specimen may have a shielding effect on the specimen in longtudinal fields which may affect the results and this might be complicated by early penetration at the shoulders. However, once flux penetration had begun the specimen shape would not matter so much.

12. Resistance transitions in an external magnetic field.

12.1. Introduction

Since the discovery of type II superconductors, it has been recognised that any hypothesis of the resistance transition of type II superconductors must explain two principal phenomena - resistance below H_{c2} and resistance above it. With the discovery of Abrikosov flux lines came the realisation that they must be pinned in order that a lossless transport current may be carried in the mixed state. It is therefore assumed that the resistance below H_{c2} is due to the induction voltages arising from the movement of the flux lines - when the Lorentz is greater than the pinning force.

Above H_{c2}, superconductivity is thought to be due, not to filaments,

but to the St.James and DeGennes surface sheath. Much evidence supports this hypothesis. Bon Mardion et al[21] showed, by their measurements, that complete normality occurred at $H_{c3} = 1.69\ H_{c2}$, in agreement with St.James and DeGennes' predictions. Hempstead and Kim[78] determined H_{c3} in the same way and showed it to be a surface effect by plating Pb-In alloys with Cu and reducing H_{c3}. Tomasch and Joseph[79] employed magnetisation measurements to determine H_{c3} and they measured its orientation dependence. Gygax et al[80] found that the ratio of H_{c3} to H_{c2} was 1.69 and independent of the temperature. Cardona and Rosenblum[81], Hart and Swartz[32] and Strongin et al[83] showed the existence of H_{c3} in type I superconductors with k $>.419$.

The model for superconductivity above H_{c2} supposes that the sheath has a definite current carrying capacity at a given field, $i_s(H)$, which tends to zero as the field approaches H_{c3}. Any impressed transport current, i_t will be transmitted as $i_s(H)$ through the sheath and $\left[i_t - i_s(H) \right]$ through the normal bulk. The current through the normal region results in the observed voltage drop across the specimen. The relative value of i_t to $i_s(H)$ will decide the shape of the transition curve.

Druyvesteyn[84] measured resistance transitions of dilute Pb-In alloys that were nearly ideal type II superconductors and found a discontinuity at H_{c2} in the curve for certain values of i_t. He explained the discontinuity in terms of a change in the mechanism of voltage production in the mixed state and surface sheath.

12.2. Results.

In the following section the resistance transitions in an external magnetic field are investigated for eight of the eutectic alloy systems considered in section 10. The effects of the following parameters are investigated:

(i)   the magnitude of the measuring current,

(ii)   the orientation of the magnetic field with respect

to the specimen axis,

(iii)   the roughness of the specimen surface,

(iv)   the presence of a second phase,

(v)   the relative orientation of the second phase and the

external magnetic field.

Each alloy system has its own unique properties so they are considered separately.

12.2.1.   Pb-Cd system.

The resistance transitions in a longitudinal field for various values of current are shown in fig.47 for a Pb-Cd laminar eutectic directionally frozen at 3.8 cm/hr. and heat-treated at 118°C. These results are qualitatively similar to resistance transitions for other eutectics examined. As the current is increased, the transition occurs at lower values of the applied field. The field at which the specimen goes completely normal, H_N decreases slightly with increase in current.

With a constant current, the effect of varying the angle θ between the specimen axis and the direction of the external field is shown in fig.48. As θ increases, the transition occurs at a lower field and the sensitivity to field orientation is greatest at low angles. Similarly heat treated eutectic with the Cd-rich phase distributed as rods gave similar results in both the as-cast and directionally-frozen conditions.

A directionally frozen laminar eutectic heat treated at 118°C exhibits different behaviour (fig.49). A magnetoresistive effect is superimposed upon the transition for all values of $\theta \neq 0$. A similar specimen, aged at room temperature for about 17 months and thus a type I superconductor,[48]

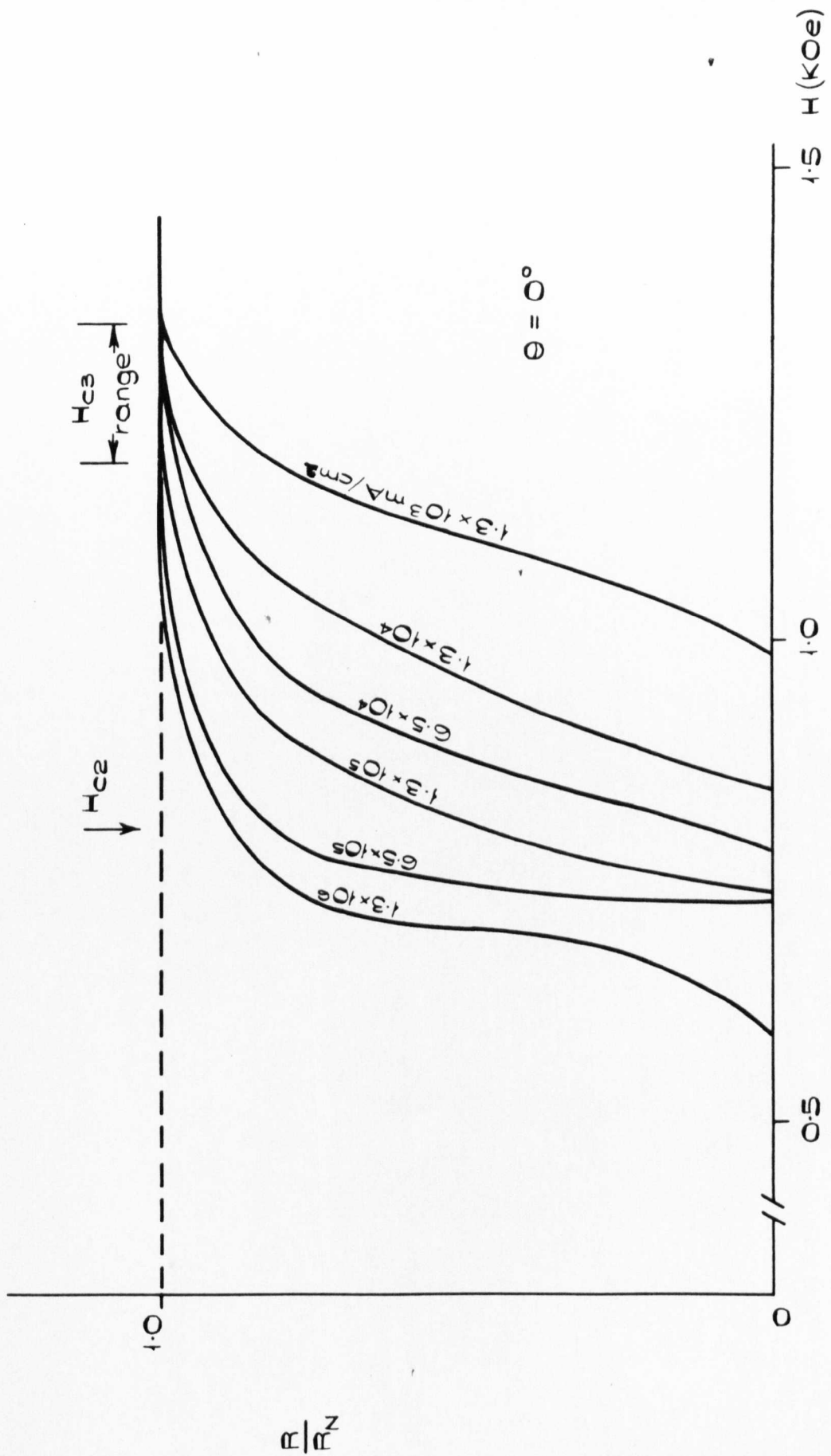FIG. 47. EFFECT OF THE MAGNITUDE OF THE TRANSPORT CURRENT ON THE RESISTANCE TRANSITION OF Pb-Cd EUTECTIC DIRECTIONALLY FROZEN AT 3·8 cm/hr.
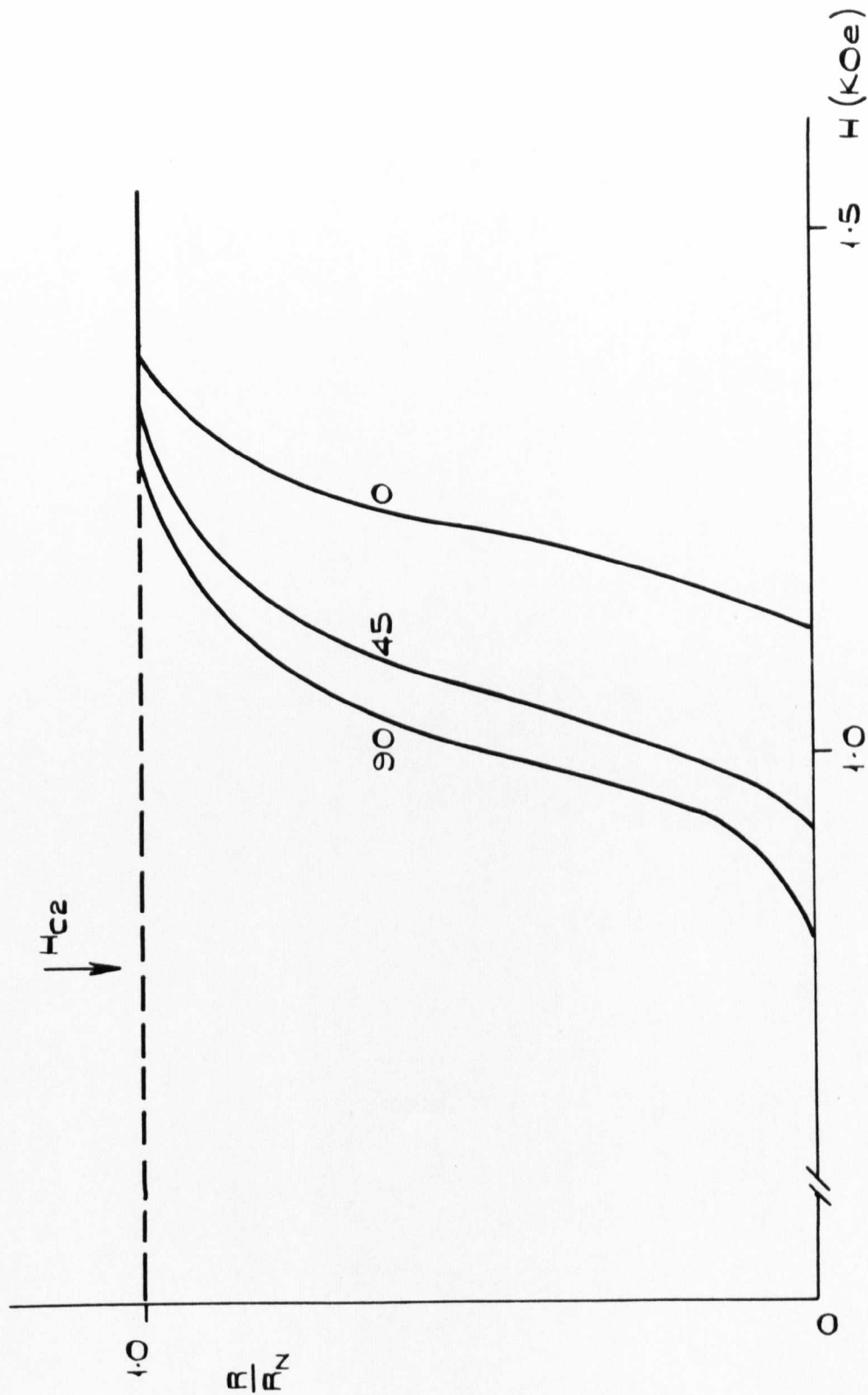
FIG. 48. RESISTANCE TRANSITION OF CAST LAMINAR Pb-Cd EUTECTIC HEAT TREATED AT 118°C. $J \approx 1.0 \times 10^3 \, mA/cm^2$
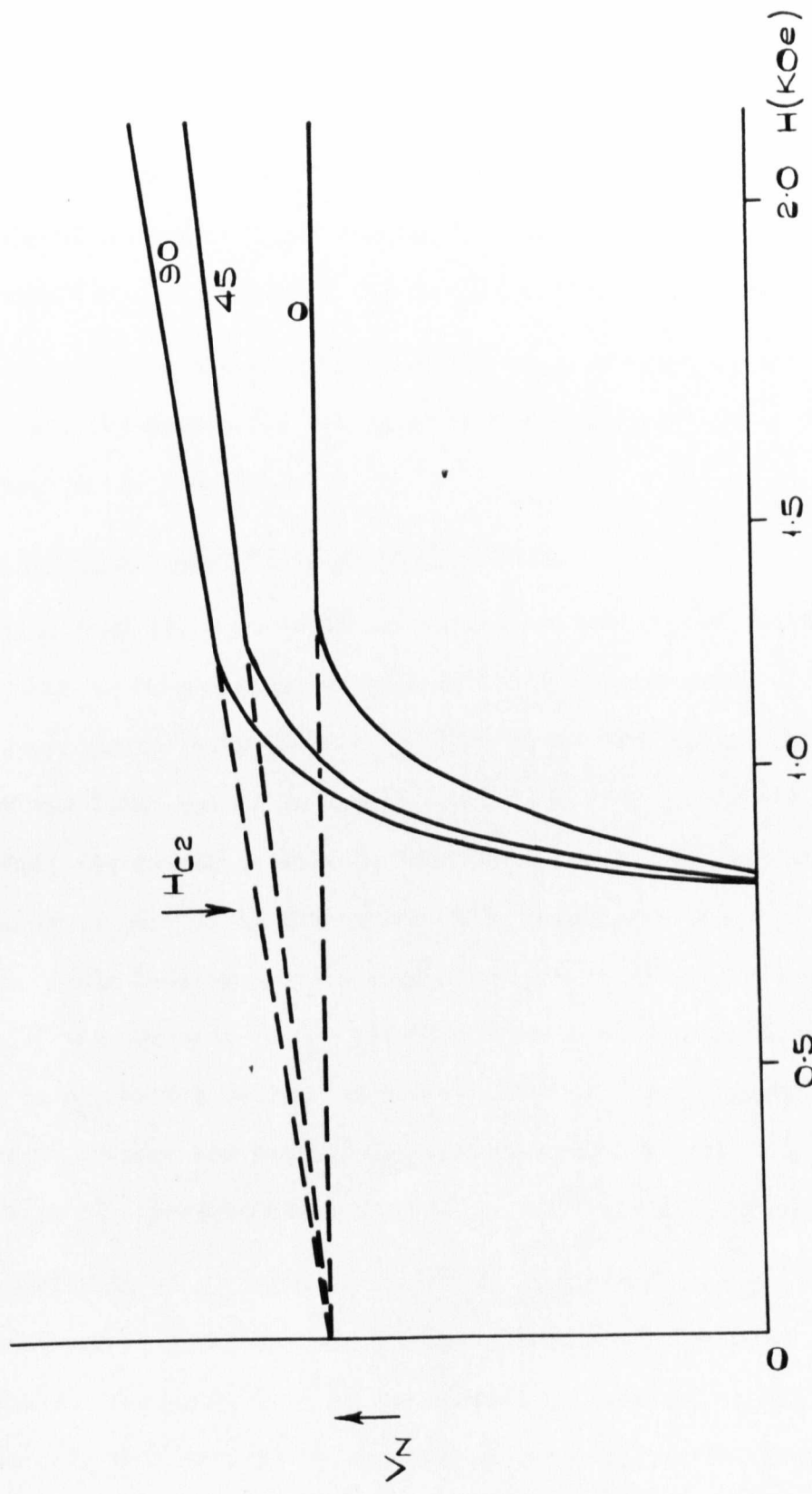
FIG. 49. RESISTANCE TRANSITION OF Pb-Cd EUTECTIC DIRECTIONALLY GROWN AT 3.8cm/hr AND HEAT TREATED AT 118°C $J \approx 1.3 \times 10^4$ mA/cm².

is shown in fig.50 and this also displays the magnetoresistive effect
in transverse fields.

The transition curves for the Pb-rich solid solution of the heat-
treated eutectic (Pb + .5% wt.Cd) can be seen in fig.51. Only the solid
solution showed a discontinuity or change in the slope in the region of
H_{c2} even when the sensitivity of the measurement was increased.

All the curves measured were identical in increasing and decreasing
field and were independent of the direction of the field and of the
current through the specimen.

12.2.2. Discussion of results of Pb-Cd system.

The effect of the transport current's magnitude on the position of
the transition is in qualitative agreement with the currently accepted
model of superconductivity above H_{c2}. When i_t is very small, the curve
approaches the ideal one of an abrupt transition at H_{c3}. As the current
is increased, the sheath is able to 'short-out' a smaller fraction and
the remainder is carried in the normal bulk, causing an ohmic voltage
to appear. Joule heating by this excess current in the bulk is probably
the cause of the decrease in H_N with increase in measuring current.
H_N tends to H_{c3} as the current is decreased and $H_N = H_{c3}$ probably when
these heating effects are negligible. Similar results have been obtained
in ideal type II superconductors by Gygax et al[80] and Druyvesteyn[84].

The variation of H_N with the angle θ would not be expected from
the calculations of St.James and DeGennes although the decrease in critical
current would. For $\theta \neq 0$, less of the surface is parallel to the field
and, since only that part of the surface parallel to the field can support
a superconducting sheath, the total current that can be shorted out by
the sheath will be decreased. Consequently, the result of changing θ
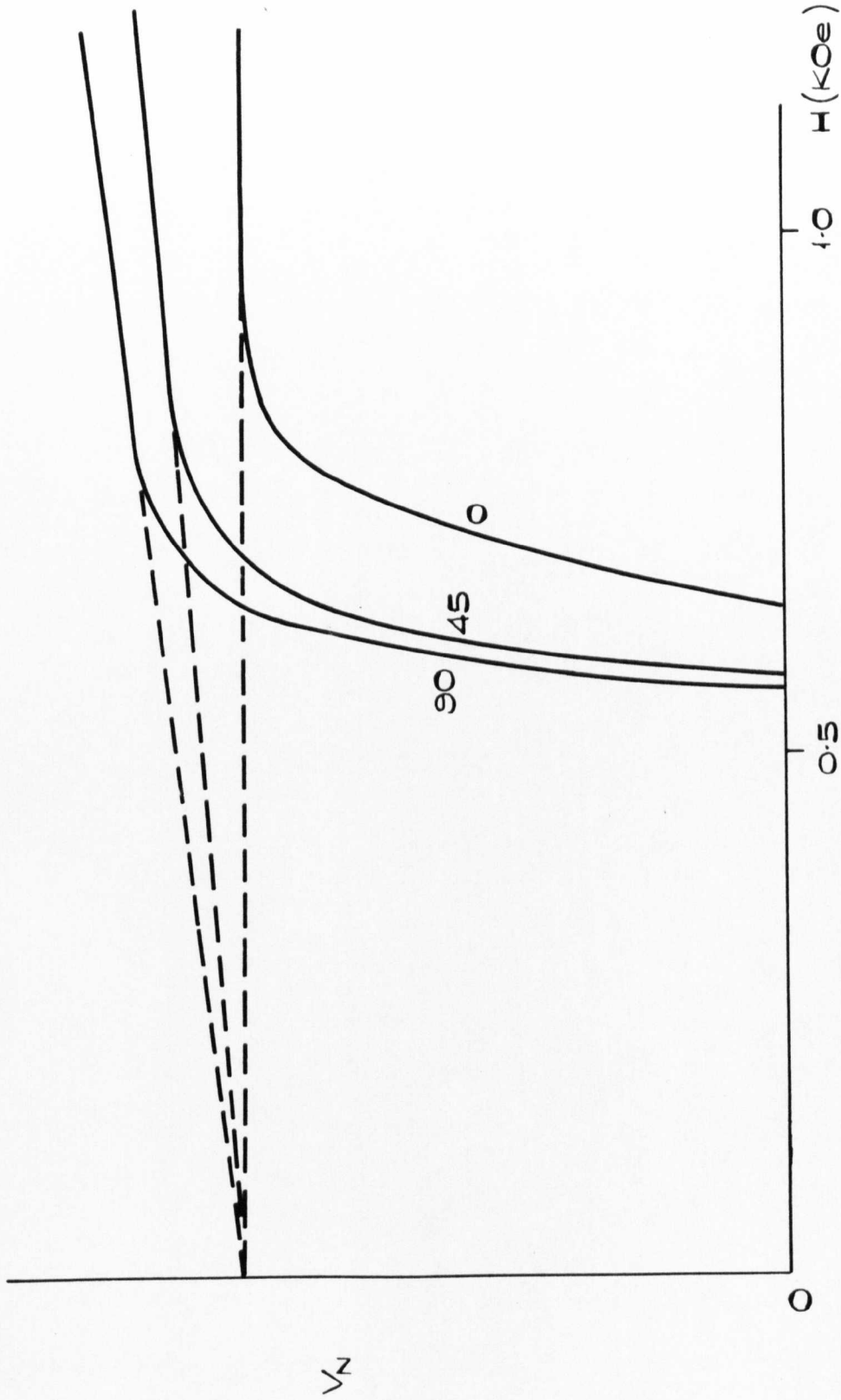
FIG. 50. RESISTANCE TRANSITION OF Pb-Cd EUTECTIC DIRECTIONALLY FROZEN AT 3·8 cm/hr AND AGED AT ROOM TEMPERATURE FOR 17 MONTHS. $J \approx 7.5 \times 10^4 \, mA/cm^2$.
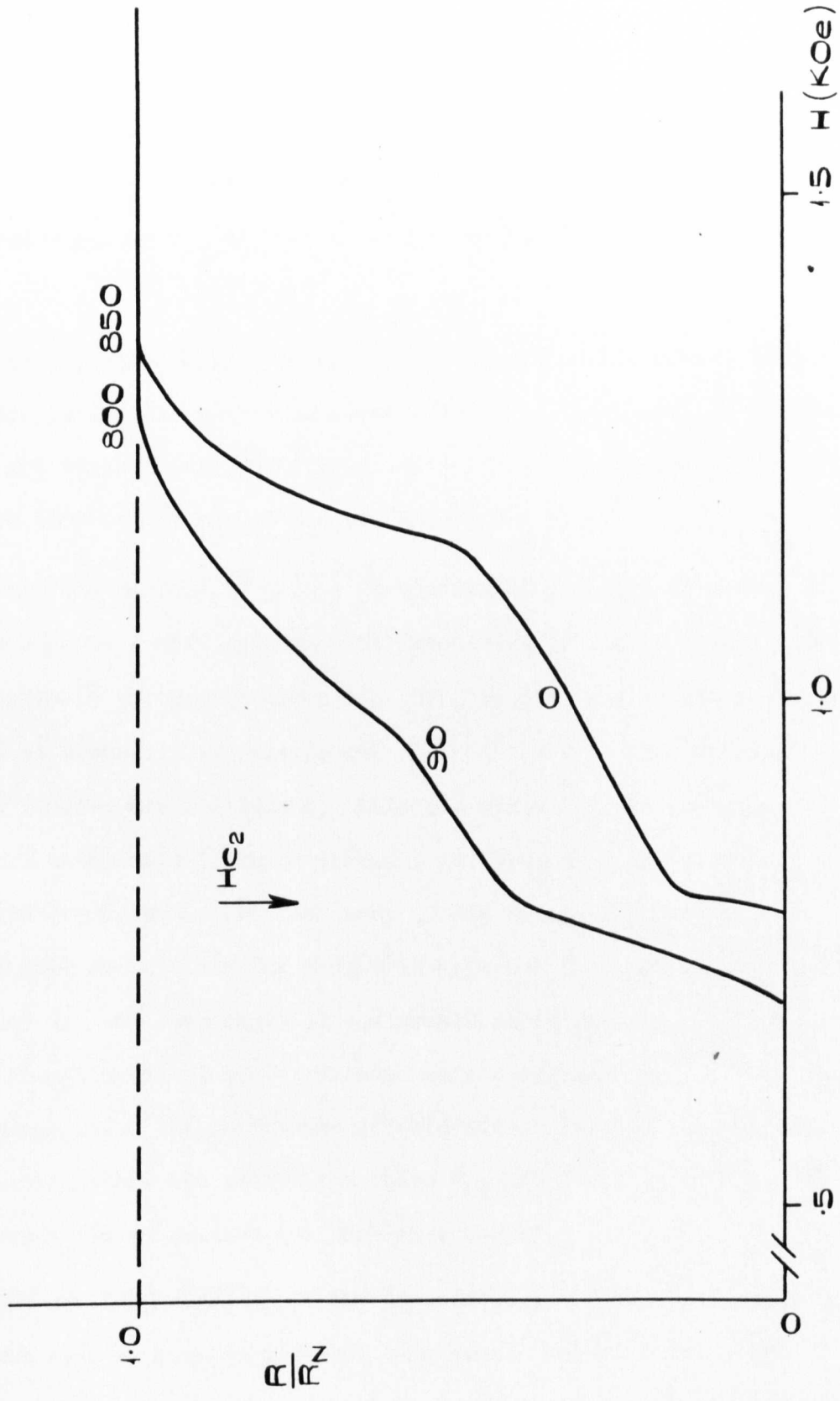
FIG. 51. RESISTANCE TRANSITION OF Pb + .5% Cd QUENCHED FROM 240°C

$J \approx 1.0 \times 10^3$ mA/cm².

is to change the normal bulk current at a given field and cause the transition
to be shifted to lower fields.

Increasing θ , therefore, has a similar effect to increasing the
magnitude of the transport current. The resultant increase in bulk current
will again increase resistive heating effects and decrease H_N .
The true value of H_{c3} is thus given for small transport currents when $\theta = 0$

The magnetoresistive effect of the directionally frozen laminar
eutectic is caused by current being carried in the normal Cd laminae
which **are** transversely magnetoresistive (this was checked by measuring
the low temperature resistance of Cd in a field).

When the current is passed perpendicularly to the direction of
growth e.g. in a wire specimen cut **from** a directionally frozen ingot
transverse to the growth direction (see fig.52), the magnetoresistive
effect is absent. For reasons not clear the effect is only manifested
if the laminae are continuous. This was proved when a specimen was
prepared with a small region (about 1 mm. length of the wire) not grown;
no magnetoresistive effect was seen . The reason why directionally
frozen rods do not show the effect is apparent from the microstructure -
the rods are not continuous in the growth direction for very long since
their formation is always associated with a cellular structure, (see
micrograph 16). The importance of this effect is that it demonstrates
conclusively that the resistance above H_{c2} has its origin in the normal
bulk since the Cd laminae are certainly normal.

The similar behaviour of the directionally frozen specimen which
had been aged at room temperature long enough for it to be a type I
superconductor is significant because it demonstrates that superconductivity
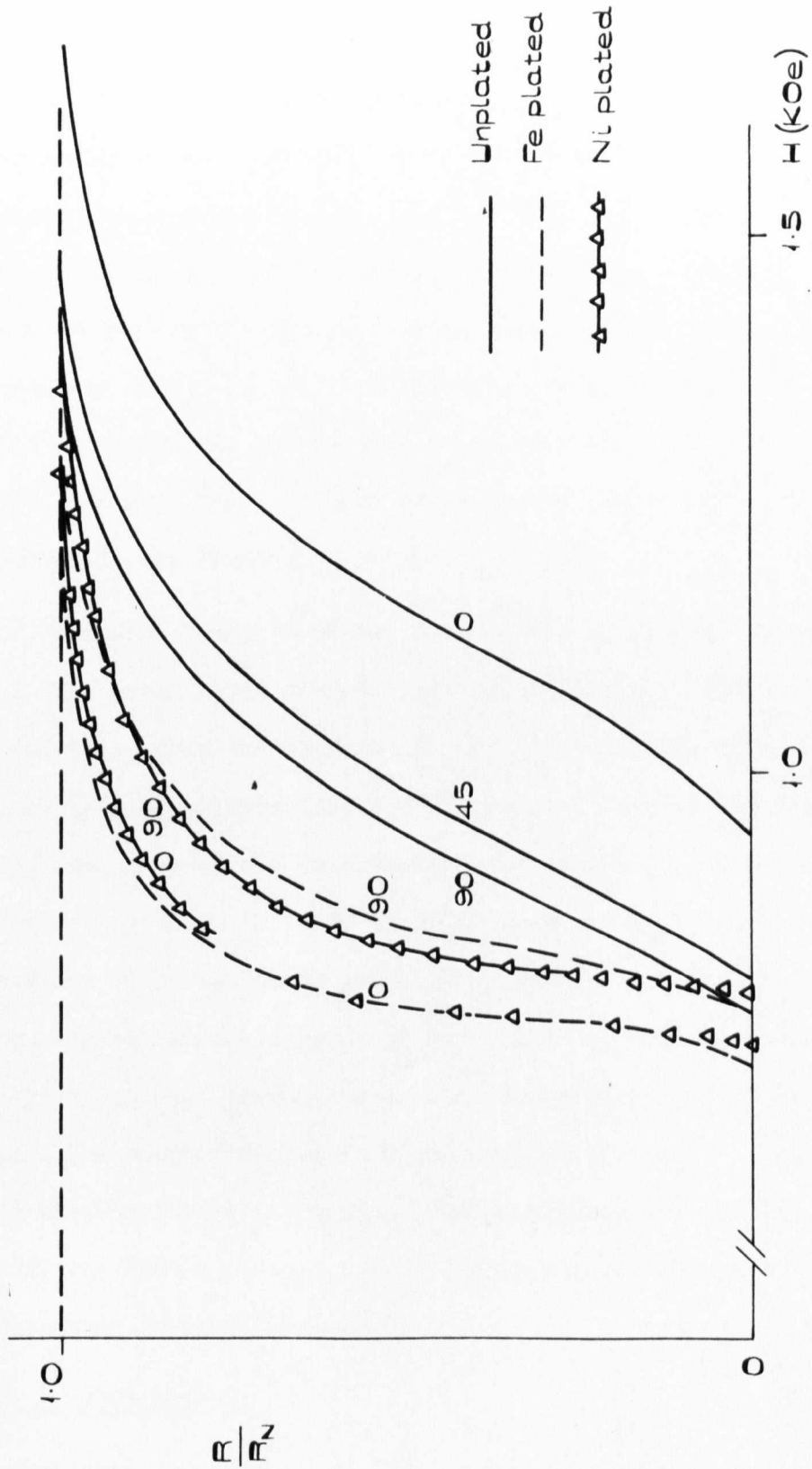
FIG. 52. EFFECT OF PLATING WITH A FERROMAGNETIC ON A Pb-Cd EUTECTIC DIRECTIONALLY-GROWN WITH DIRECTION OF GROWTH PERPENDICULAR TO SPECIMEN AXIS. $J \approx 5 \times 10^3 \, mA/cm^2$

above H_c for a type I superconductor is due to the same mechanism as is involved in a type II superconductor above H_{c2}.

This effect also has some metallurgical significance. It demonstrates that the laminae are continuous over macroscopic distances despite sub-grain boundaries which apparently shear them perpendicularly to their growth direction (see micrographs 12 and 13). It also shows that laminae in different grains are not connected. If they were, a magnetoresistance would be expected for the case of the laminae growth direction transverse to the specimen axis. In the directionally frozen rod-like eutectic the cell walls apparently do not contain Cd as they appear to under the microscope, since if they did they would behave similarly to widely spaced directionally frozen laminae.

A considerable fraction of the area of the surface of these alloys will be normal metal which cannot therefore maintain a sheath. It would be expected then, that the surface of any alloy containing normal inclusions would carry less superconducting surface current than an identically shaped specimen of entirely homogenous solid solution. Comparison of the curve obtained from the Pb + .5% Cd solid solution with the as-cast eutectic alloy heat treated at 118°C shows this not to be the case. In fact, the critical sheath current of the solid solution is less, despite an effectively reduced surface area of superconducting phase parallel to the field. The surface finish in both cases is the same, so it must be concluded that the normal inclusions have increased the current carrying capacity of the sheath in some way. This is a general result which applies to all the other systems measured.

12.2.3. Hg-Tl system.

As mentioned in section 10, this system is liquid at room temperature

and so enables the effect of surface roughness to be investigated without
kappa changes being introduced to the surface. In addition, the effect of
the presence of a second phase may be observed by comparing specimens of
α-solid solution and eutectic alloy with similar surface profiles.

A sample of Hg-Tl α-solid solution was introduced into a smooth nylon
tube with voltage and current leads attached and the transition curves
determined. Then the same sample was poured into a similar but roughened
tube. The results are given in fig.53. The smooth mold was then cleaned
and the eutectic alloy introduced. A comparison of the curves obtained
is given in fig.54.

The rough specimen carries less lossless current, H_{c3} is affected
slightly and the onset of resistance, H_R, occurs at a lower field.

An increase of H_R, the supercurrent carrying capacity i_s (H) and
H_{c3} is observed for the eutectic alloy.

12.2.4.   Discussion of results of Hg-Tl system.

The effect of surface roughness shown in fig.53 differs in part from
the results of Williamson and Furdyna[85], who studied resistance transitions
of wires and Lowell[74], who measured critical currents in a dilute Ta-Nb
alloy. Williamson and Furdyna[85] found H_R to be insensitive to the value
of the measuring current and the smoothness of the wire surfaces. They
suggested the anisotropy of H_R with θ may be due to nucleation of surface
superconductivity at interior grain boundaries. These results of fig.53
clearly show H_R to be dependent on surface conditions when H_R occurs
above H_{c2}. The results of varying the current in the Pb-Cd system show H_R
to be a function of current also.

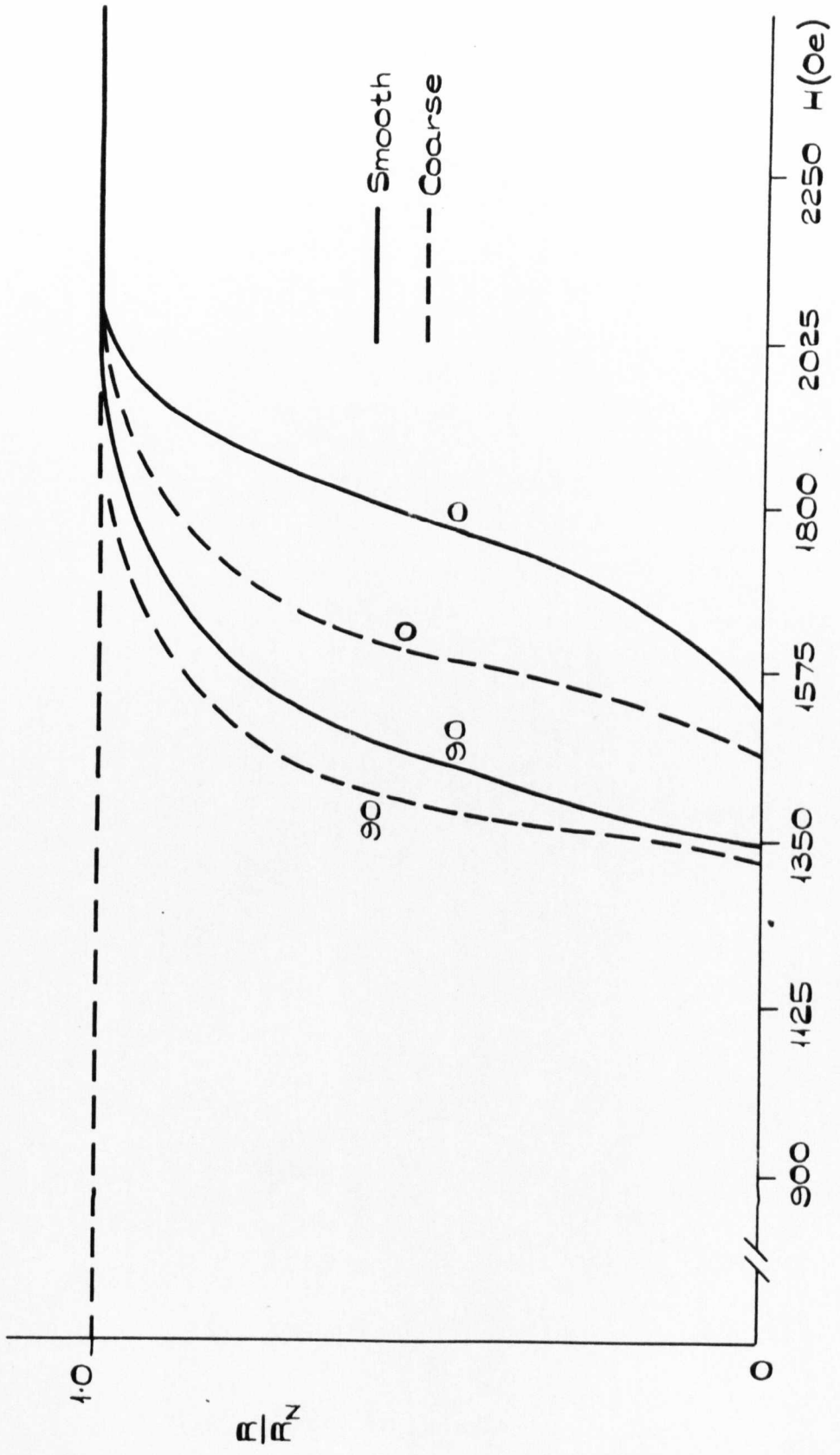Lowell[74] found that roughening the surface increased the sheath

FIG. 53. RESISTANCE TRANSITION OF Hg-Tl α-SOLID SOLUTION; EFFECT OF MOLD ROUGHNESS. $J \approx 7.5 \times 10^4$ mA/cm^2.
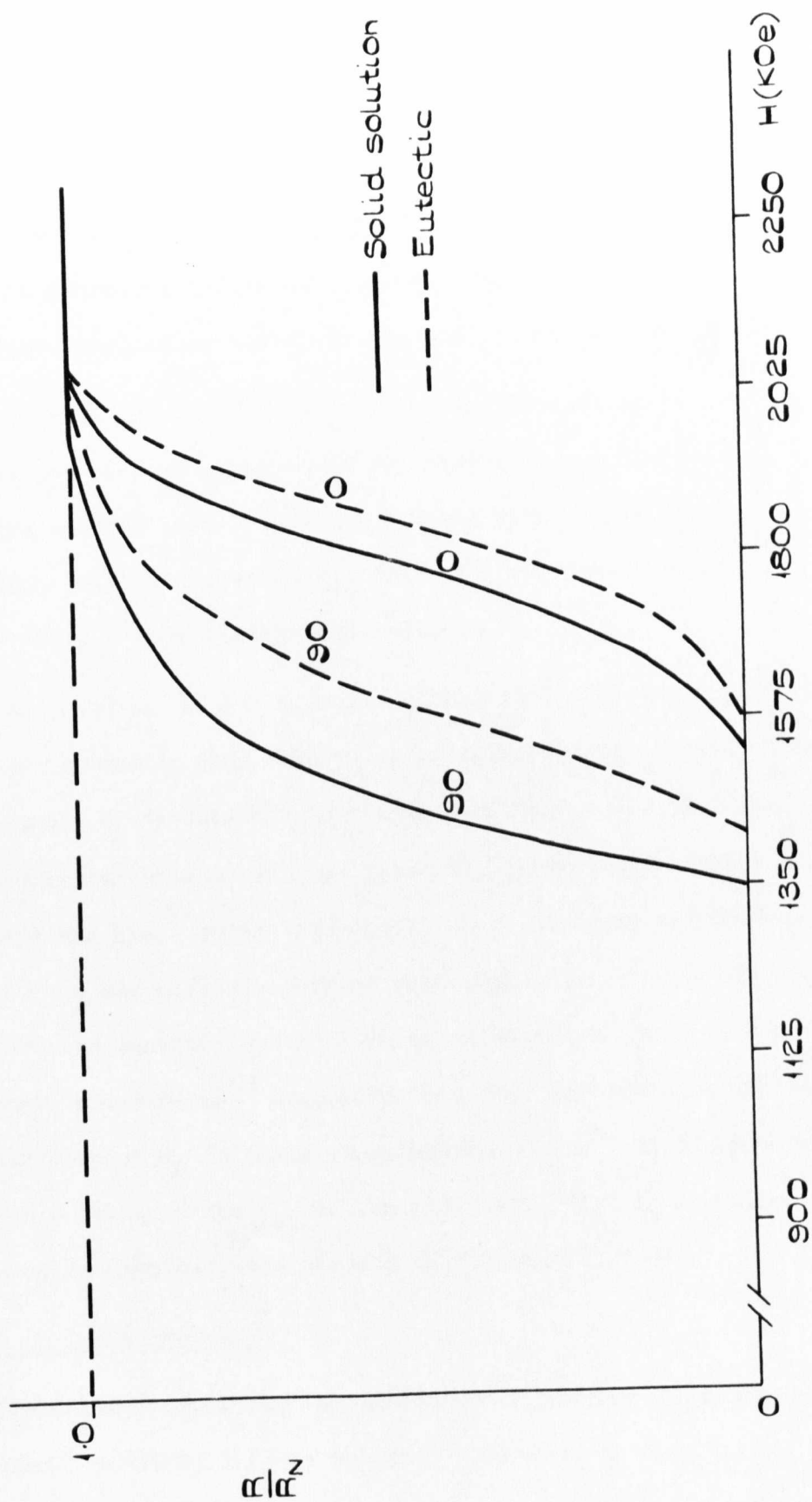
FIG. 54. RESISTANCE TRANSITION OF Hg-TL ALLOY (SMOOTH MOLDS).
$J \approx 7.5 \times 10^4 \text{ mA/cm}^2$

current - a result he attributed to a very thin zone of heavily deformed material near the surface having a higher value of k. In the present experiment, no change in k has taken place since the roughening has not been accomplished by abrasion. It may be concluded therefore that surface roughness decreases the sheath currents, most probably because the amount of surface parallel to the field has been decreased for all orientations.

Hempstead and Kim[78] noticed that the distinction between the parallel and perpendicular field orientations in a Nb-Ta sample became less when defects were introduced by cold work. They also noticed that generally, defects increased H_{c3} while H_{c2} remained the same. Schenck et al[86] made similar observations.

The behaviour of the eutectic alloy, which is essentially α-solid solution containing many defects is in agreement with these observations. Furthermore, H_R is slightly increased. Evidently, it is a function of defect concentration as well as measuring current and roughness. Hempstead and Kim[78] quote the suggestion of St.James and DeGennes that defects may nucleate surface superconductivity beyond H_{c2} to explain the decreased sensitivity to field orientation of their worked sample. Williamson and Furdyna[85] suggested this same mechanism to explain the insensitivity of H_R in their experiments. Ralls[87] also suggested that superconductivity above H_{c2} may be associated with internal surfaces. This idea is examined more closely in the next section.

12.2.5. In-Bi system.

Transition curves for two specimens of laminar In-Bi eutectic, one directionally frozen and one as-cast, are shown in figs.55 and 56. They were encapsulated and heat treated together at $60^\circ C$ in a water bath for two weeks. The transitions for various values of θ of the as-cast

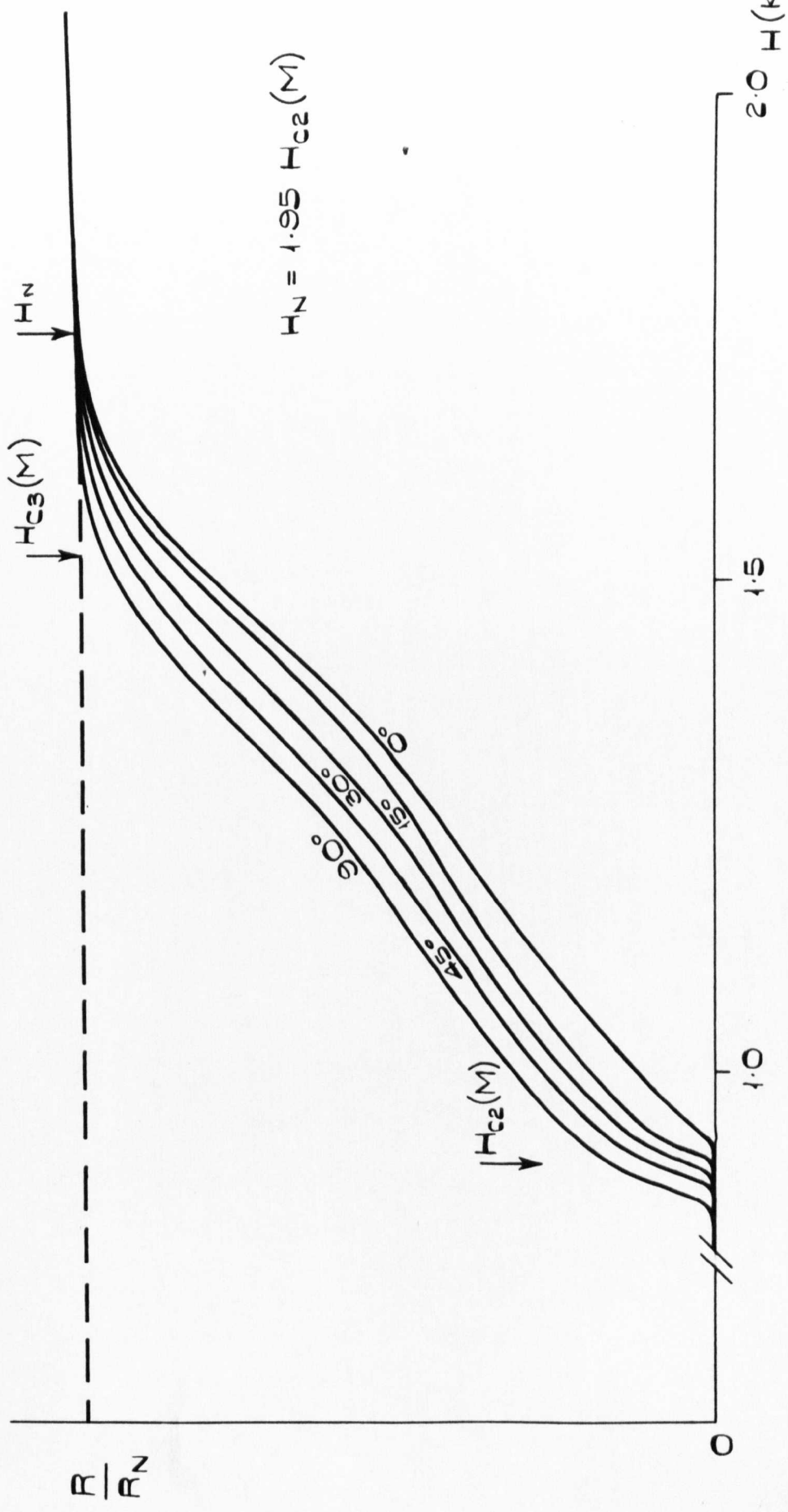FIG. 55. RESISTANCE TRANSITION OF In-Bi EUTECTIC, DIRECTIONALLY-GROWN AT 4.61 cm/hr. AND-TREATED AT 60°C. $J \approx 1.3 \times 10^4$ mA/cm².

$H_N = 1.95 \; H_{c2}(M)$
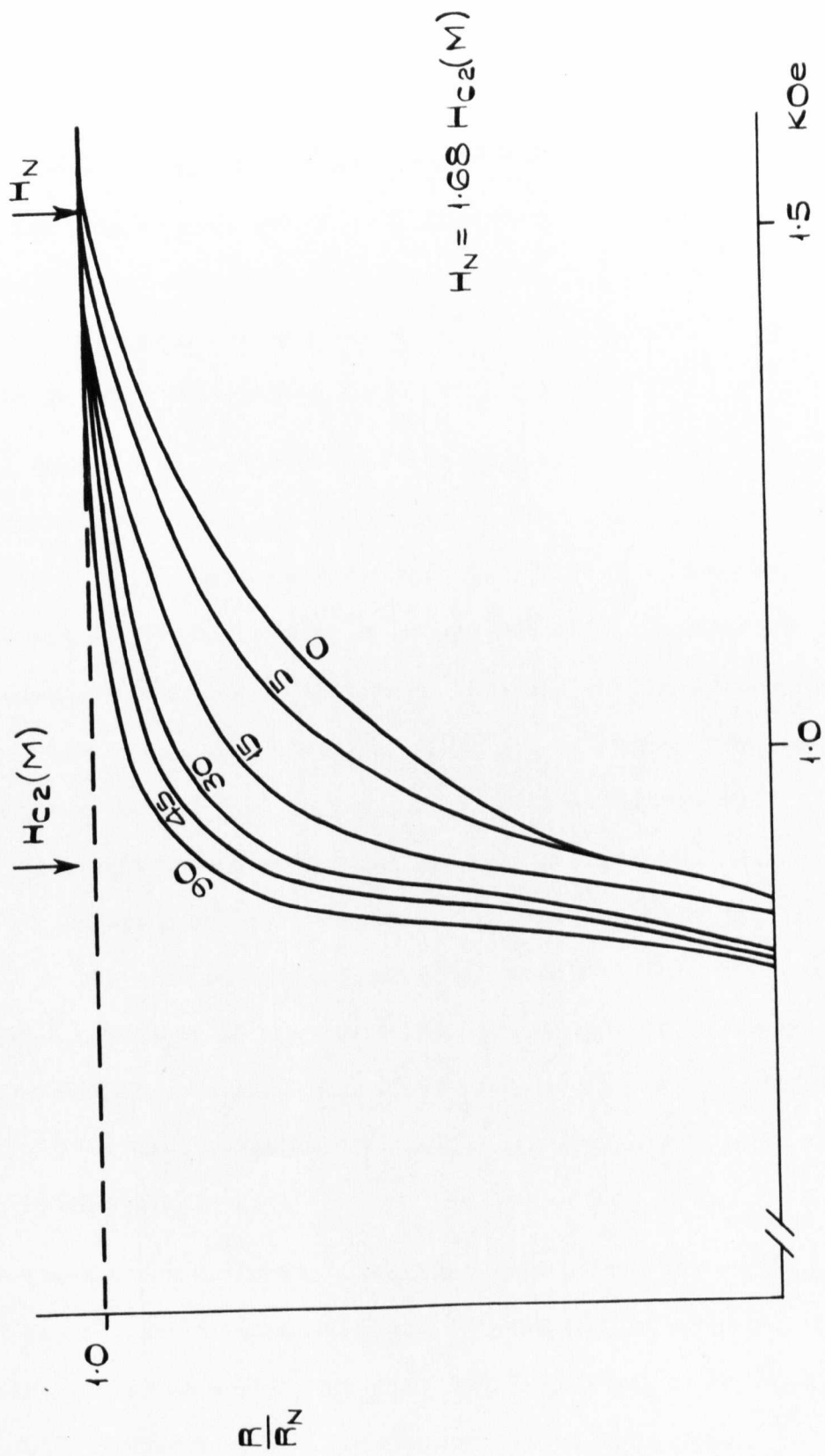
FIG. 56. RESISTANCE TRANSITANCE FOR In-Bi EUTECTIC AS CAST

$J \approx 1.3 \times 10^4$ mA/cm².

specimen start and finish at lower fields than the directionally frozen specimen and the curves are much more sensitive to the field orientation. No discontinuity is evident at H_{c2} in either case.

12.2.6. Discussion of results of In-Bi system.

H_R for both as-cast and directionally-frozen specimens occurs before H_{c2}. The critical current curves, shown in fig.45 show that just before H_{c2} the directionally frozen specimen has a higher critical current and therefore it is to be expected that the H_R will be higher.

The decrease in sensitivity of the directionally frozen specimen current to the field orientation and the greater supercurrent carrying capacity is thought to be due to surface superconductivity at the interfaces of the normal laminae. This is feasible for two reasons. St.James and DeGennes' theory makes no distinction between an internal and an external surface and so it may be expected that $|\psi|^2 \neq 0$ at H_{c2} (the condition for a sheath to exist, see section 3.5) in the region of these interfaces for parallel fields. Secondly, it is very possible that differential thermal contraction of the two phases results in deformation in the region of the interface. Lowell[74] in his work on surface currents, suggested that much more severe deformation may occur at a surface than can be induced in the bulk by any normal deformation process. An effect such as this might even be enhanced at internal surfaces where an orientation relationship also exists, thus causing an increase in k.

If these surfaces formed a continuous path the situation approaches that of Mendelssohn's filamentary model. However, since the internal superconductivity is a function of field orientation, a St.James type sheath would appear to be making the greatest contribution.

The results of figs. 55 and 56 can be explained with this model. Since

the planes of the laminae in different grains of the directionally frozen specimen are randomly orientated about the specimen axis (see micrographs 2, 11, 23) there is a strong possibility that the surfaces of many of them will be parallel to the field at any orientation and they will be able to support a sheath current. At $\theta = 0^0$, the number of laminae and the area of external free surface parallel to the field will be a maximum. As θ increases, both the external and internal surface sheath currents will decrease. However, the presence of some extended paths of internal surface superconductivity for all values of θ will result in the net resistanceless current being greater than in the as-cast specimen where the laminae are randomly disposed.

The high value of H_N (1.95 H_{c2}) obtained with the directionally frozen specimen is much greater than the theoretical maximum (1.69 H_{c2}). Several other authors have observed anomalously high value of H_N[69,80,81,88,89]. DeSorbo[89] suggested that impurities at the surface locally changed k and therefore the value of H_{c3}. Van Gurp[69] and DeSorbo[89] measured transitions on rolled strips of Nb and associated the anomalously high field with filamentary superconductivity along the elongated grain boundaries. The enhanced superconductivity here was assumed to be the cause of the increase in H_{c3}.

Tilley[90] considered this problem theoretically by extending a calculation of Boyd[91]. He suggested that the high value of H_N found by DeSorbo and Van Gurp was due to pairs of planar defects close together and parallel to the specimen surface. However, Tilley's calculation is concerned with defects smaller and closer together (by a factor 10) than the laminae in this eutectic alloy. The high value of H_N is thus most likely attributable to a small contribution from Mendelssohn - type filamentary superconductivity along thin high k paths associated with the internal surfaces because of their different thermal contraction from the

matrix. There is no reason why this could not occur together with surface sheath conductivity.

12.2.7.   Sb-Tl system.

The variation of the transition curves with θ for three values of transport current is shown in fig.57. This sample was directionally frozen and heat-treated at $91^{\circ}C$. $H_N = 1.69 H_{c2}$ but this decreases slightly at the high θ values for higher currents. The salient feature of the curves is that there is a reduction in their sensitivity to the field orientation as the current is increased. H_R varies with θ for a given transport current but as the current is increased this change in H_R with θ increases. There is no discontinuity in the curves at H_{c2} nor in the trends that these curves show as the current is increased.

12.2.8.   Discussion of results of Sb-Tl system.

Complete return to the normal state is achieved when the theoretical value of H_{c3} is reached. This is probably because the Sb precipitate is irregularly shaped and only continuous along the growth direction for short distances (see micrograph 25). Thus no significant effect due to parallel internal surfaces, as seen in the In-Bi system, for example, can be expected. No appreciable contribution from filamentary superconductivity seems to exist either.

H_R values for the two higher values of current are less than H_{c2} and are clearly θ and current dependent. The significance of these results is the lack of a discontinuity in the curves and the smooth continuation of their trend at H_{c2}. This strongly suggests that the mechanisms responsible for the resistance and for the transport of lossless current are the same before and after H_{c2}. (The field associated with the highest current is only 0.4 Oe, so its effect may be ignored). This infers that
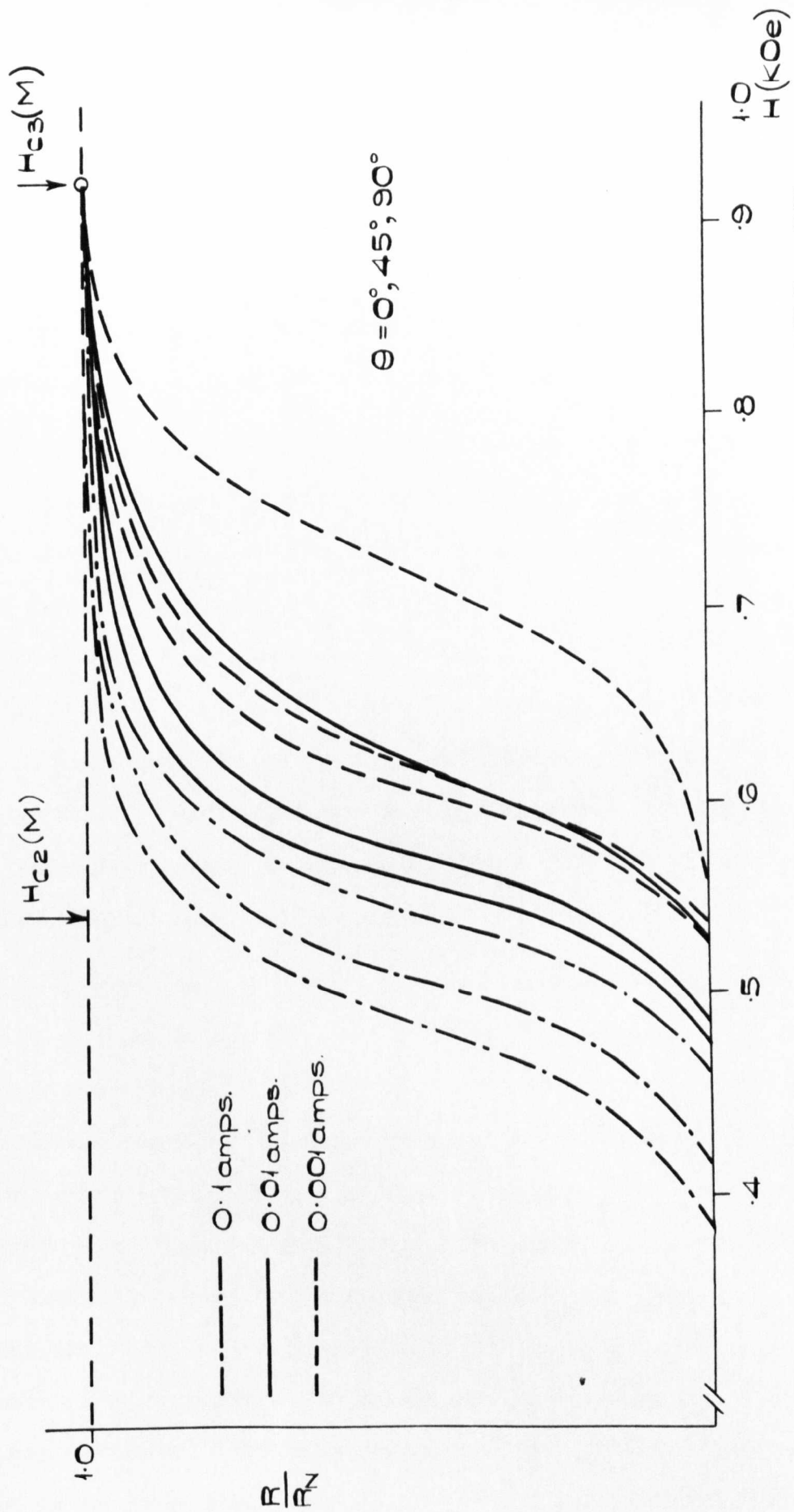
FIG. 57. EFFECT OF MEASURING CURRENT ON THE RESISTANCE TRANSITION OF Sb-Tl EUTECTIC.

a surface super-current exists below H_{c2} that decreases as the field increases and becomes equal in magnitude to the St.James and DeGennes sheath current at H_{c2}. Furthermore, its magnitude is a function of field orientation in exactly the same manner as is the St.James and DeGennes sheath. This also explains the absence of a discontinuity at H_{c2} where the mechanism of current transport is supposed to change.

However, there is the question of why should the transport current in the mixed state just before H_{c2} not be due to flux gradients and the resistance observed be caused by fluxoid motion under the influence of a driving force, as discussed in section 11.1. Anderson[21] suggested that his model of flux flow would break down near H_{c2}, since the flux lines would be forced so close together that the forces between them would no longer be long range, smooth electromagnetic forces on which he based his calculations. Instead, forces arising from vortex overlapping would predominate leading to different effects. This would mean that his bundle concept would fail completely.

More support for this idea is provided by all those magnetisation curves of superconductors having a sheath and a major loop[92]. Small minor hysteresis loops bounded by the major loop of Schweitzer et al[56] are continuous through H_{c2}. Since these loops are bounded by diamagnetic paths, a surface current must exist that is continuous through H_{c2}. These resistance transitions indicate that its magnitude depends on the field orientation with respect to the specimen surface, exactly as the St.James and DeGennes surface sheath and indeed, it is most likely a continuation of the sheath. The sheath clearly does not contribute all the surface current to the major loop nor all the critical transport current in the mixed state, otherwise the effect of roughening the surface of specimens in these experiments would have been more apparent.

Since a surface sheath exists below H_{c2} on the specimen surface, there is no reason why it should not exist on internal surfaces in the mixed state too. Whether this would contribute appreciably to the hysteresis is speculative. It could conceivably contribute to a small lossless transport current, however.

12.2.9. Pb-Sn system.

This eutectic consists of a superconducting laminar precipitate in a matrix that is normal at 4.2°K in isolation. Fig.58 shows the resistance transitions for a directionally-frozen and an as-cast specimen of Pb-Sn eutectic heat-treated at 118°C. The orientation of the field with respect to the specimen has little effect, the transitions for both specimens are separated by about 15 Oe for most of the curves. H_N for both is the same, equal to 1.7 H_{c2}. $H_R < H_{c2}$ for all values of θ and the curves merge at approximately H_{c2}.

12.2.10. Discussion of results of Pb-Sn system.

These results are direct evidence in support of the conclusion of Schiffman et al[98] that a proximity effect occurs in this alloy. They measured the specific heat and found no discontinuity at 3.7°K, the temperature they expected the Sn-rich phase to go normal. At 4.2°K only the Pb-rich laminae are superconducting in isolation and since, in the as-cast alloy, they do not form a continuous path (this statement is based on the microstructural examination and also by analogy to the Pb-Cd eutectic where the as-cast alloy has no magnetoresistive effect), a transport current must be conducted through Sn-rich regions. The Sn-rich phase must therefore be superconducting by a proximity effect.

The very small value of the sheath current may be related to the existence of the proximity effect. If the conclusions drawn on the Sb-Tl
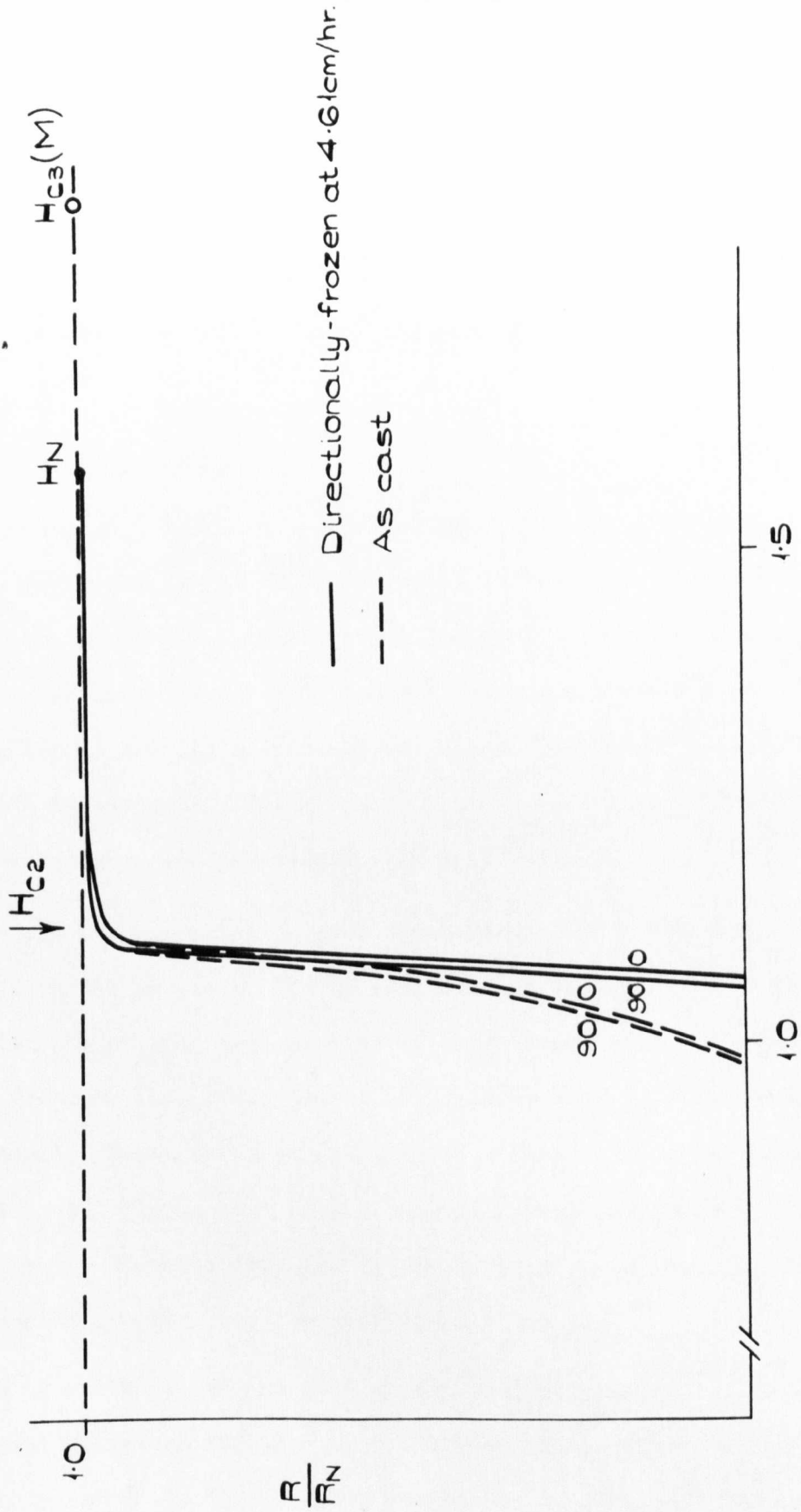
FIG. 58. RESISTANCE TRANSITION OF Pb-Sn EUTECTIC. $J \approx 1.3 \times 10^4$ mA/cm².

eutectic are applied, it seems likely that the surface currents involved below H_{c2} are very small too, since the orientation effect of the field is small. The higher current carried by the directionally grown specimen is probably due to more effective flux pinning resulting in a slightly higher critical current - a reflection of the magnetisation result of section 10.2.6.

12.2.11. Bi-Tl system.

Two eutectics exist in this alloy system both with essentially the same matrix Bi_2Tl but different precipitates. The eutectic at 76.5 weight per cent Bi has a 'herring-bone' distribution of normal Bi particles and the eutectic at 47.5 weight per cent Bi has a laminar precipitate of superconducting X-solid solution above about $75^{\circ}C$ and α-solid solution below this temperature. The effects of the presence and orientation of these precipitates are investigated in this section.

A small magnetoresistive effect was present with the 76.5 wt.% Bi alloy and so the curves of fig.59 have been normalised with respect to the resistance at H_N. Both samples of this eutectic have a value of H_N greater than the theoritical value of St.James and DeGennes and the directionally frozen specimen has slightly the greater value (2.02 H_{c2} c:f 1.96 H_{c2}). The as-cast sample carries approximately the same sheath current as the directionally frozen sample at $\theta = 90^{\circ}$ but in the parallel field case it carries less for all values of field.

The transitions for the 47.5 wt.% Bi eutectic alloy (as-cast and directionally-frozen) together with the X-solid solution are shown for three values of θ in fig.60. The curves are extrapolated from 10 kOe since this is the limit of the magnet. No accurate values of H_N can therefore be obtained.
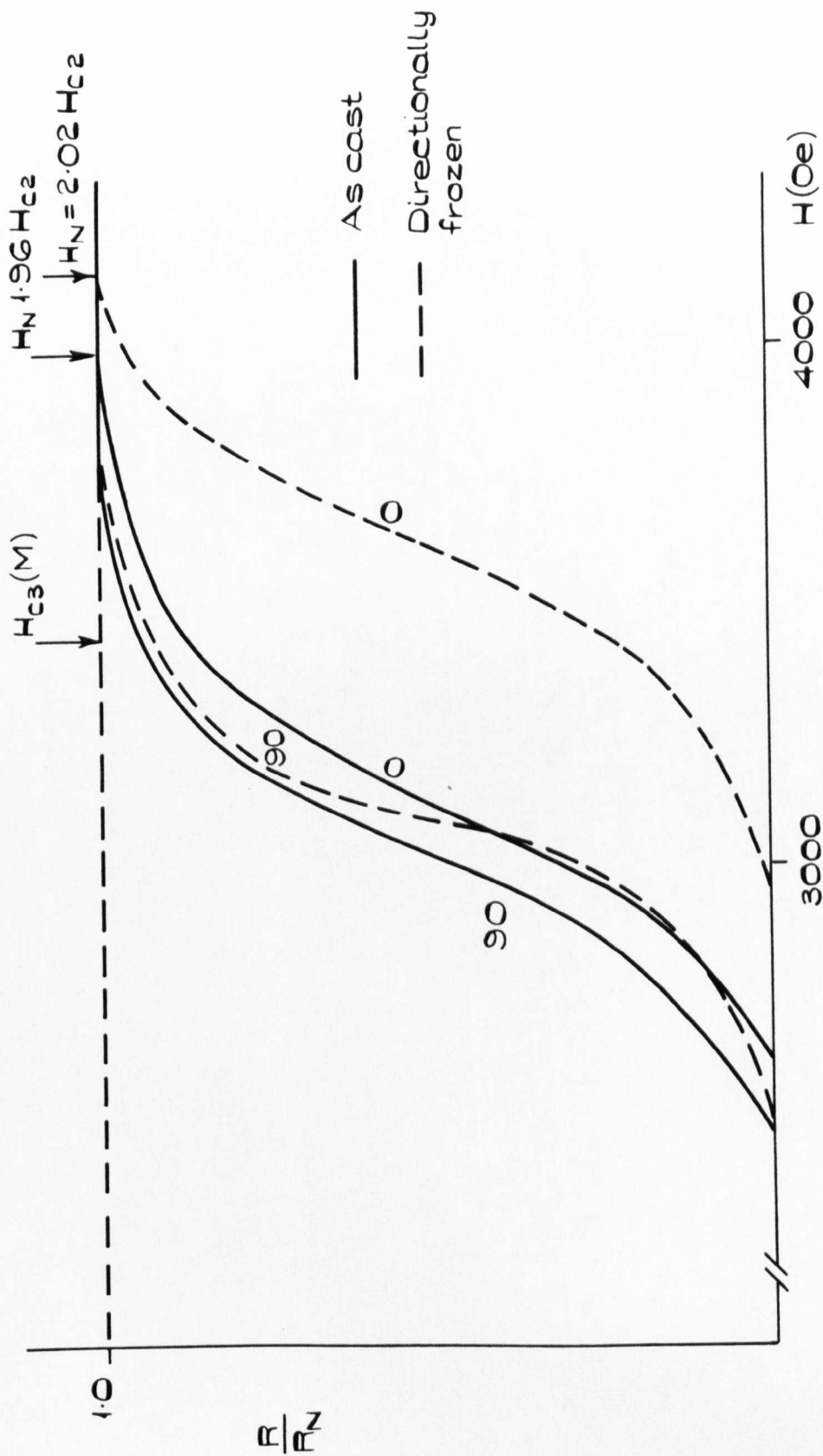
FIG. 59. RESISTANCE TRANSITIONS OF Bi-Tl EUTECTIC (76.5 wt% Bi) HEAT TREATED AT 91°C. $J = 1.3 \times 10^4 \, mA/cm^2$
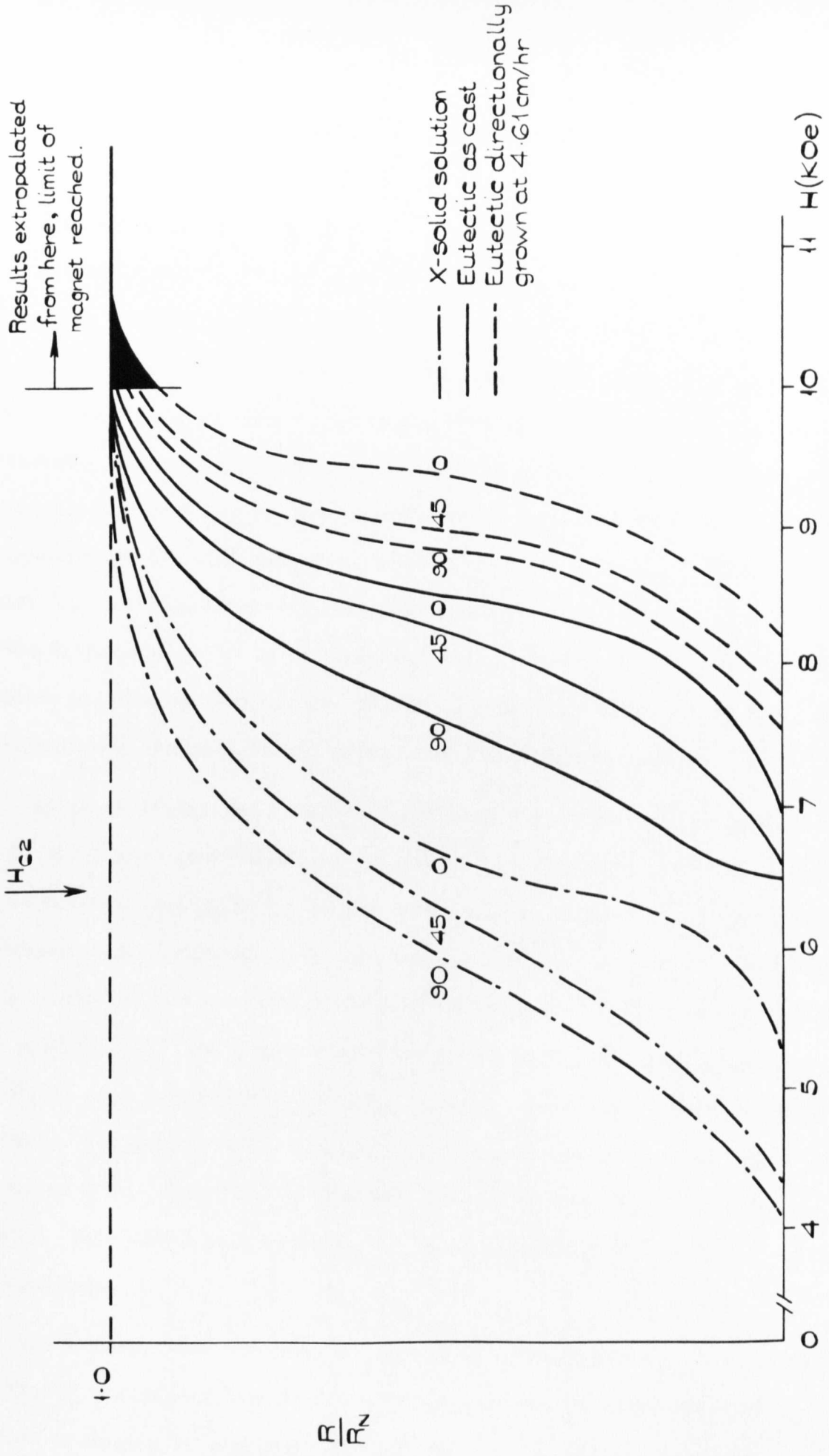
FIG. 60. RESISTANCE TRANSITIONS OF Bi-Tl (47·5 wt % Bi) EUTECTIC & Bi-Tl-x SOLID SOLUTION

$J \approx 1\cdot4 \times 10^3 \, mA/cm^2$

12.2.12.   Discussion of results of Bi-Tl system.

These results serve to corroborate the conclusions drawn so far.
Micrograph 9 shows that the laminae of the 'herring-bones' of Bi in the
directionally frozen 76.5 wt.% Bi alloy are orientated approximately
along the growth direction and in such a way as to give it the appearance
of a partially laminar eutectic. Consequently, the transition curve is
similar to that which would be expected from a partially grown laminar
eutectic. When the field is parallel to the specimen axis, it is also
approximately parallel to the precipitate surfaces and so internal sheath
superconductivity contributes to the St.James and DeGennes surface sheath.
Hence the total supercurrent carrying capacity is enhanced. When the
field is perpendicular to the specimen axis, however, the 90° curves are
similar because now not enough laminae lie parallel to the field to provide
a significant increase in the supercurrent carrying capacity.

Of great significance in the results of fig.60 is that the matrix of
Bi_2Tl would have gone normal in the region of 2000 Oe and yet the eutectic
is superconducting up to H_{c2} of the precipitate of X-solid solution and
maintains some sheath up to H_{c3} of the X-solid solution. Since the precipi-
tate laminae in the as-cast sample are not connected along the length of
the specimen, this must mean that the current must pass through regions
of Bi_2Tl. For it to remain lossless this must mean that, like the Pb-Sn
eutectic, a proximity effect exists, even though the dimensions over which
it occurs (the inter-lamellar spacing) is much greater than a coherence
length. This conclusion is supported by magnetisation and critical current
measurements.

The X-solid solution does not show a discontinuity at H_{c2} and since
the sheath current is orientation dependent, it may be concluded that a
surface mechanism is responsible, i.e. the sheath existing below H_{c2}.

Exactly why this eutectic supports a sheath current and Pb-Sn does not, is not clear. This eutectic also exhibits internal surface superconductivity. Fig. 60 clearly demonstrates that the directionally-frozen specimen carries more lossless current than the as-cast specimen and is also less field orientation sensitive.

Comparison of figs. 59 and 60 is a striking example of how the superconducting properties of essentially the same material (Bi_2Tl) can be drastically different because a different precipitate is present in each.

12.2.13. Pb-Zn system.

The transition of this eutectic alloy is very nearly the ideal for that of a superconductor with $k < 0.419$ and the critical field is almost that for pure Pb i.e. 540 Oe. No sheath is present, even for $\theta = 0^{\circ}$ (see fig.61).

12.2.14. Discussion of Pb-Zn system.

These curves are characteristic of 'soft' or type I superconductors without a sheath. The current is so small that its self field may be neglected and so the abrupt transition to the normal state for $\theta = 0^{\circ}$ occurs at H_c. For any other orientation the effect of the specimen shape on the magnetic field has to be considered. When the field is perpendicular to the specimen axis the result of the demagnetising effect is that the effective field at the specimen surface is $2H_c$ and so the specimen goes into the intermediate state at an applied field of $\frac{1}{2}H_c$. Demagnetising effects may be neglected for type II or type I superconductors with a sheath, since so little of the specimen volume resists flux penetration that the external field is hardly perturbed .

Many authors have observed a sheath current in pure Pb and since the addition of ever a small amount of Zn should enhance sheath nucleation (by increasing k) this result is surprising.
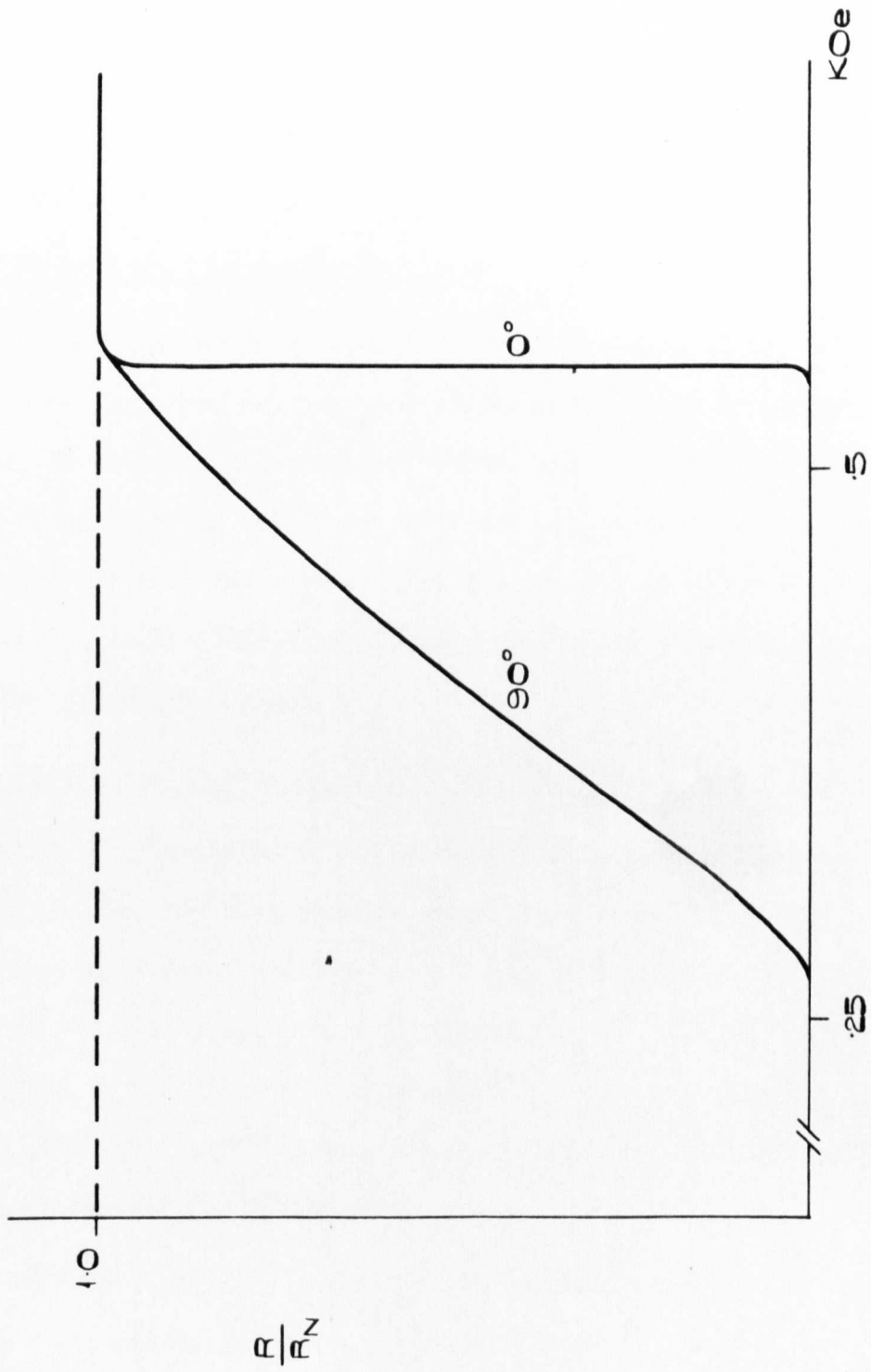
FIG. 61. RESISTANCE TRANSITION OF Pb-Zn EUTECTIC HEAT TREATED AT 110°C. $J \approx 1.5 \times 10^2$ mA/cm².

13. Resistance Transitions of Slab Specimens.

The use of slab specimens enables the relative orientations of measuring current, external magnetic field and precipitate orientation to be varied both with and without changing the area of the specimen parallel to the field.

13.1.1. Pb + .5 wt.% Cd solid solution.

The transitions are uncomplicated by the presence of defects and are shown in fig. 62. They are very sensitive to the field orientation (see fig. 63). An increase in measuring current causes the transition in parallel field to occur at lower values of field but the perpendicular transition remains substantially unchanged. When the current is 7.3×10^4 mA/cm^2 the transition in parallel field is the same as that in perpendicular fields for smaller values of current.

13.1.2. Discussion of results of Pb + .5wt.% Cd solid solution.

This field orientation behaviour is qualitatively similar to that of a wire except that the slab is more sensitive to the inclination of the field. This is because the slab has a large area parallel to the field when $\Theta = 0^o$ and consequently a large sheath current, but at $\Theta = 90^o$ the area parallel to the field is negligible for a thin slab and little or no sheath is present. A small change in the field's orientation will result in a large change in surface current.

The behaviour when the current is increased is the same as for wire specimens - the transition moves to lower fields, but when $i_t = 7.3 \times 10^4$ mA/cm^2
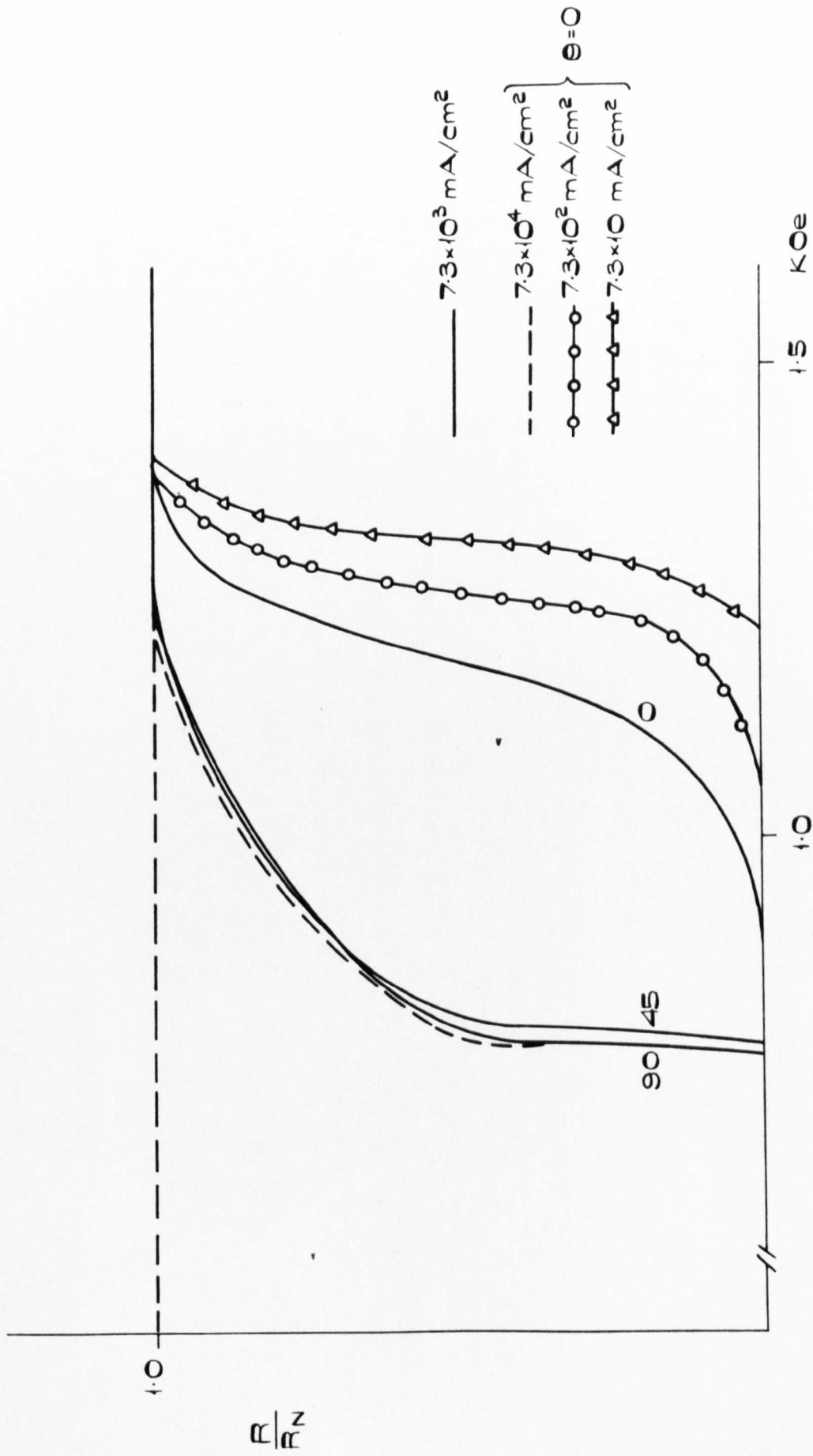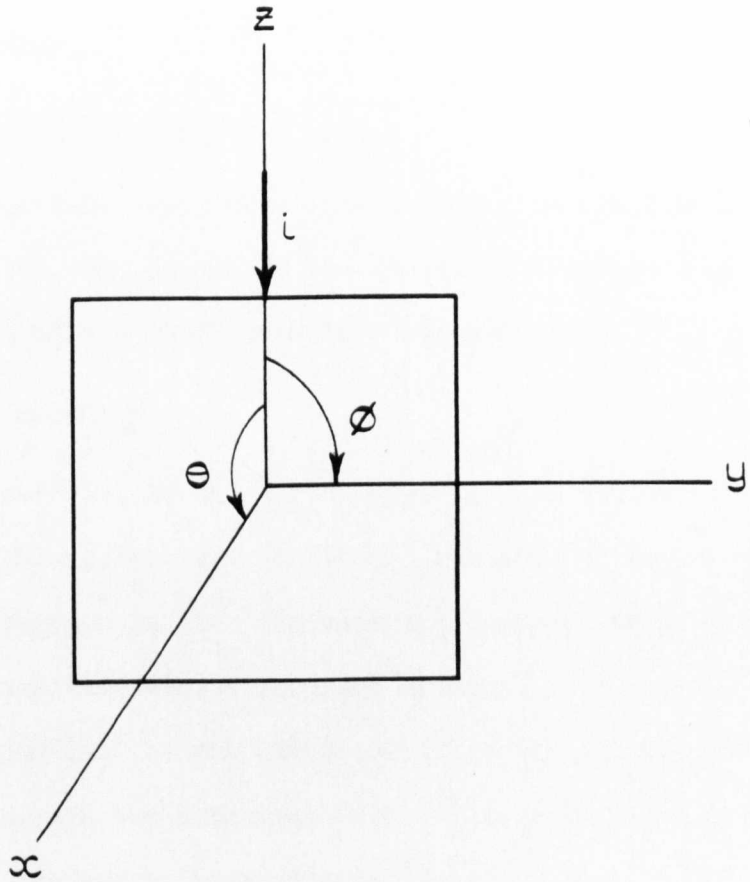
FIG. G2. RESISTANCE TRANSITIONS OF Pb + ·5% Cd SLAB.

FIG. 63. DEFINITION OF POLAR ANGLE Ø & AZIMUTHAL ANGLE θ.
THE SPECIMEN IS IN THE ZY PLANE PERPENDICULAR TO THE X AXIS.

the value of the sheath current is now relatively so small that only a fraction of the transport current is shorted out. Most of it will be carried in the normal bulk above H_{c2}, as in the case for $\theta = 90^{\circ}$. Joule heating in the bulk will only serve to enhance this effect by reducing the sheath current further.

13.2.1. Directionally frozen eutectics.

Transitions for four combinations of current and field orientation are shown in figs. 64, 65, 66 and 67 for directionally-frozen specimens of Pb-Cd, Pb-Sn, In-Bi and Sb-Tl eutectics respectively.

The combinations are :-

I.   Current parallel to the direction of growth and the field varied through the polar angle ϕ (see fig.63) in the plane of the specimen so that the external surface sheath current remains the same except for edge effects.

II. Current parallel to the direction of growth and the field varied through the azimuthal angle θ from parallel to the specimen surface to perpendicular to it.

III. Current transverse to the direction of growth with the field changed through the angle ϕ in the plane of the specimen.

IV. Current transverse to the direction of growth and the field changed through the azimuthal angle θ

In both cases, for Pb-Cd eutectic, when the current is passed along the direction of growth, magnetoresistance is present, but for transverse current the magnetoresistance effect is absent. For the same specimen, measurements II.and IV. are much more field orientation sensitive than I. and II. In measurement III. the $\phi = 90^{\circ}$ transition occurs at a higher

FIG. 64. RESISTANCE TRANSITIONS OF Pb-Cd EUTECTIC SLAB DIRECTIONALLY-FROZEN AT 6·8 cm/hr. $J \approx 2 \times 10^3 \, mA/cm^2$
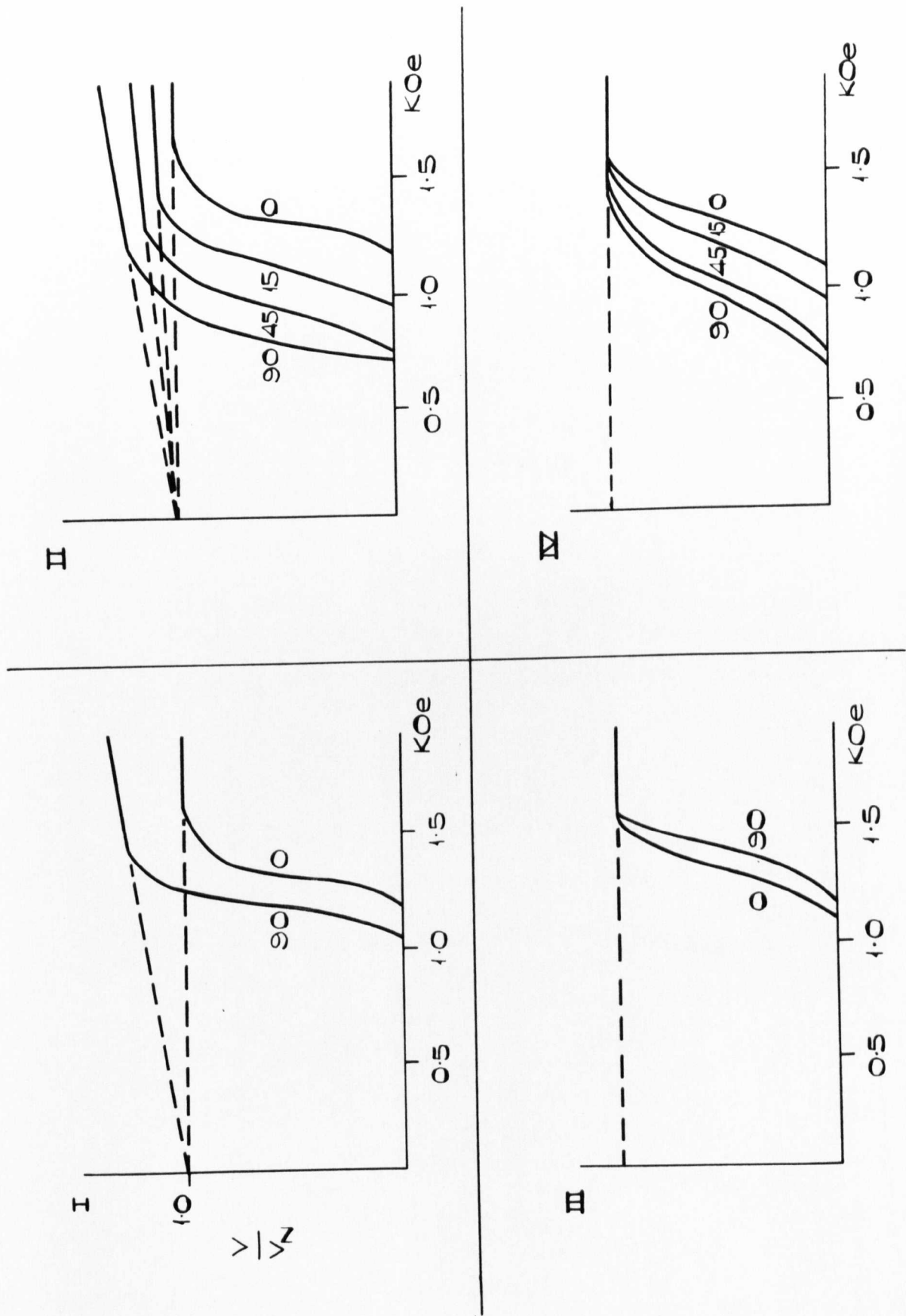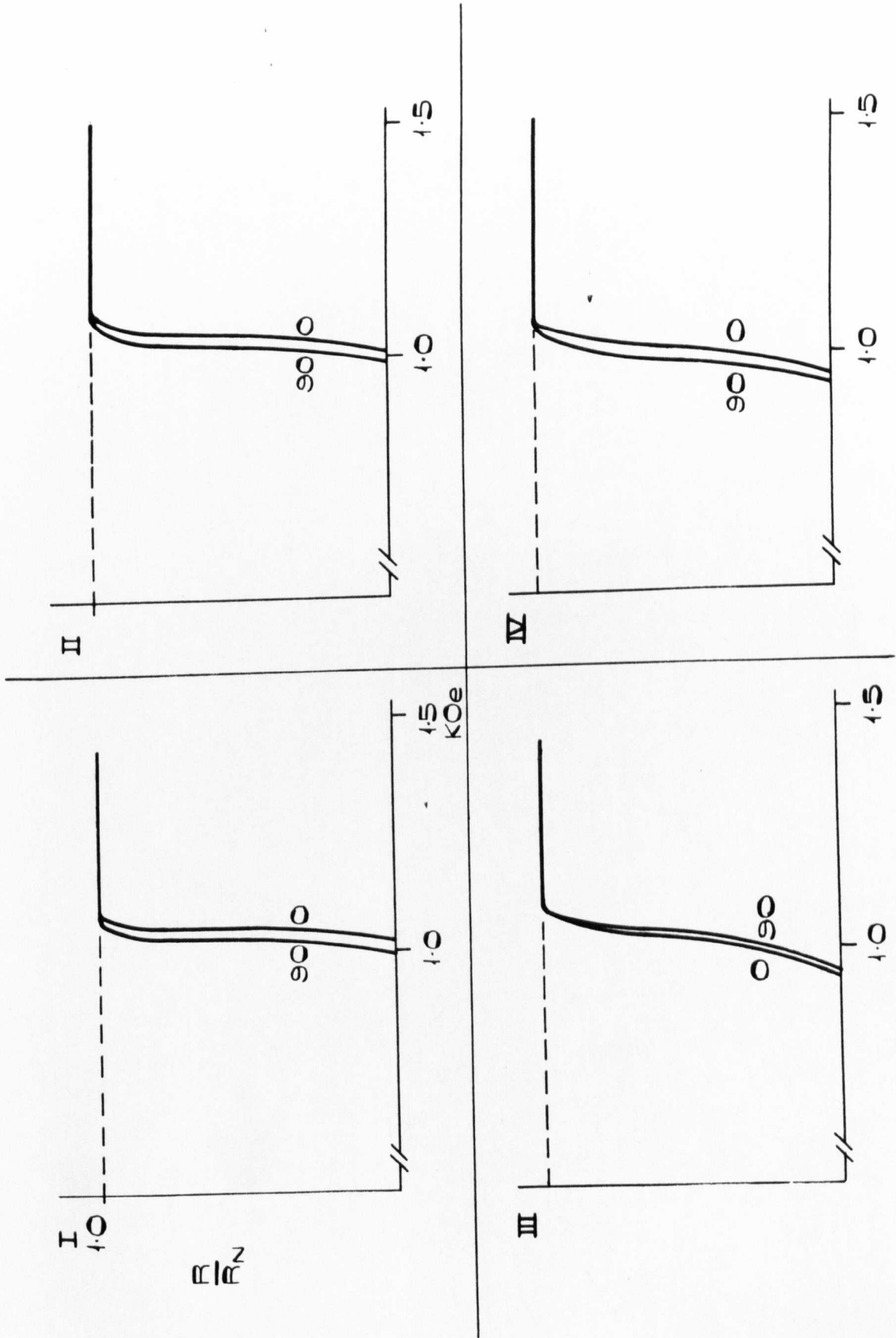
FIG.65. RESISTANCE TRANSITIONS OF A Pb-Sn EUTECTIC SLAB DIRECTIONALLY FROZEN AT 4·61 cm/hr. $J \approx 4·2 \times 10^3$ mA/cm^2
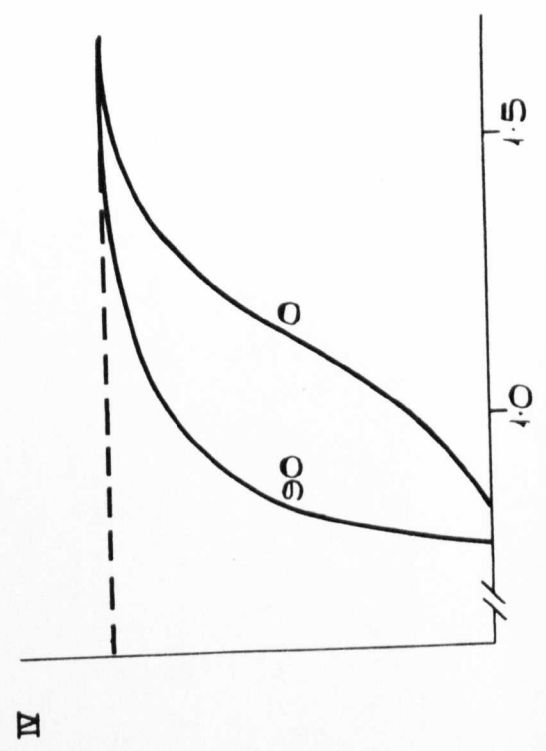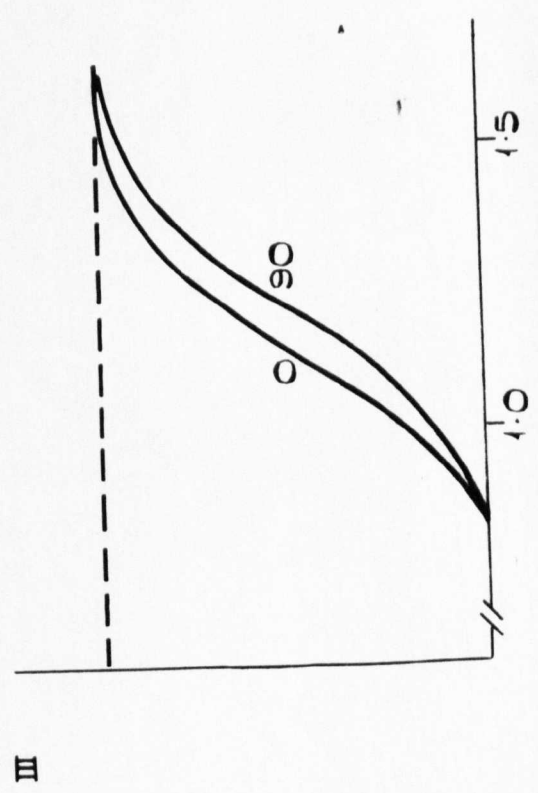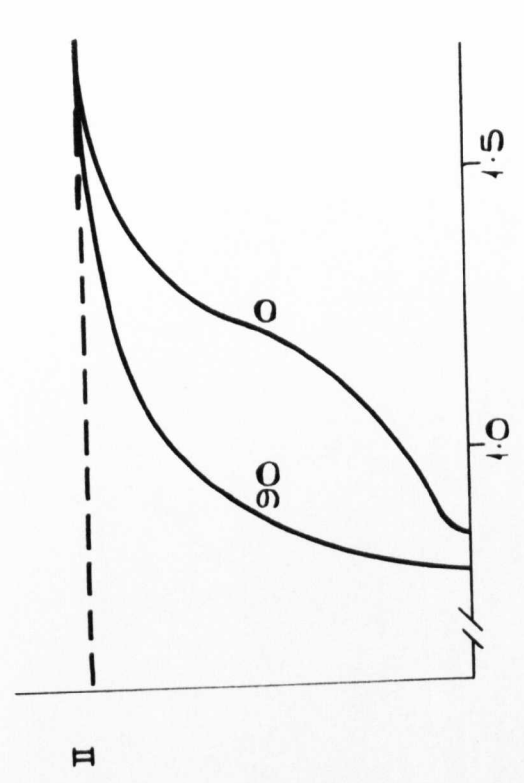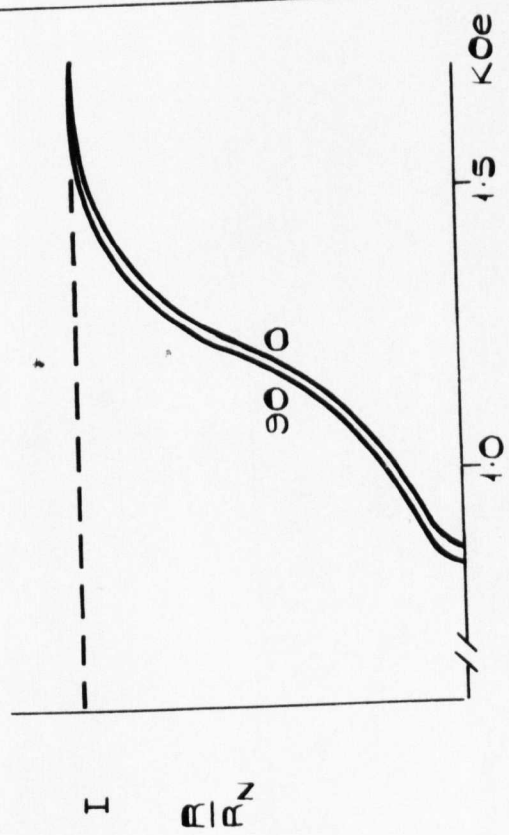
FIG. 66. RESISTANCE TRANSITIONS OF AN In-Bi EUTECTIC SLAB DIRECTIONALLY-FROZEN AT 3·8cm/hr
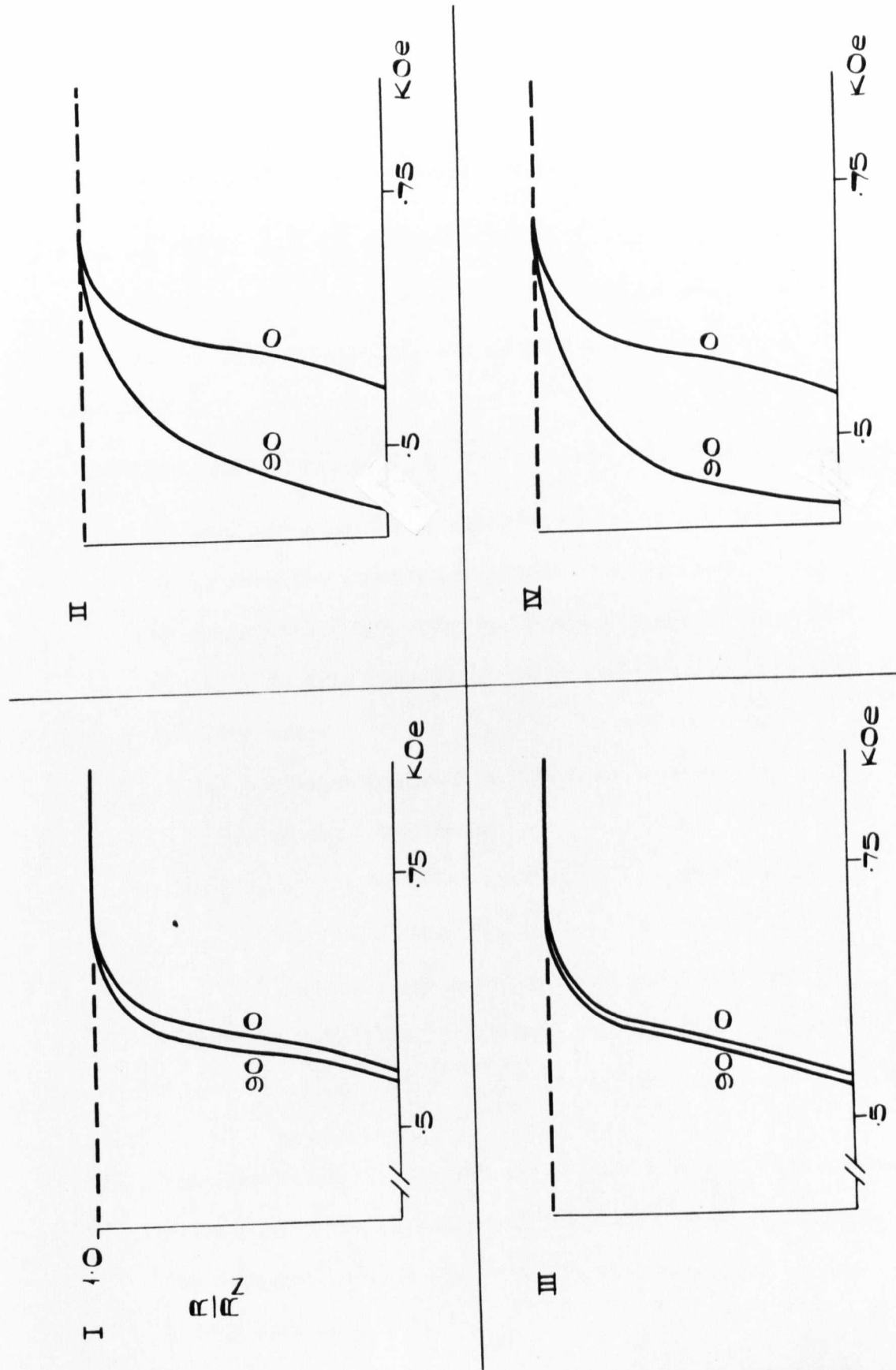
FIG. 67. RESISTANCE TRANSITIONS ON AN Sb-Tl EUTECTIC SLAB DIRECTIONALLY-FROZEN AT 3·81cm/hr $J \approx 10.5 \times 10^3 mA/cm^2$

field value than $\phi = 0^{\circ}$.

The other laminar eutectics exhibit qualitatively similar behaviour (except for the magnetoresistance) but Sb-Tl does not have an increased lossless current flowing for $\phi = 90^{\circ}$ in measurement III.

13.2.2. Discussion of results of directionally-frozen eutectics.

The presence of the magnetoresistive effect in Pb-Cd for current parallel to the laminae confirms the observations and conclusions of section 12.2.2.

Consider configurations I. to IV. separately for Pb-Cd eutectic:-

I. If this was a perfect, infinitely thin, ideal type II slab, then the transition curves would be expected to be coincident (neglecting the induced currents from the field). In this experiment there are three reasons why they are not:-

    (i)   a magnetoresistive effect is superimposed on the transition;

    (ii)   two longitudinal slab edges are parallel to the field when $\theta = 0^{\circ}$ are not when $\theta = 90^{\circ}$ (i.e. the specimen is not infinitely thin) ;

    (iii) a reduction in internal surface superconductivity occurs when $\theta = 90^{\circ}$ since few laminae are parallel to the field.

II. The increasing inclination of the field to the slab surface reduces both the St.James and DeGennes surface sheath and the internal surface superconductivity resulting in the curves obtained.

III. When $\phi = 0^{\circ}$, the external sheath current is a maximum

III. cont.

but internal surface superconductivity will be a minimum, since few laminae are parallel to the field. When $\phi = 90°$, the field is parallel to nearly all the Cd-rich laminae and so internal surface superconductivity will be at a maximum. A larger fraction of the transport current is now shorted out by superconducting paths over part of its length, resulting in less resistance for a given field. Thus the net resultant lossless current is greatest when $\phi = 90°$.

IV. In this case the only varying contribution to lossless current transport is the external surface which diminishes as θ increases (as in Pb + .5% wt. Cd solid solution).

The Pb-Sn eutectic shows much the same curves for situations I. and II. because little St.James and DeGennes sheath exists anyway. Measurement III. confirms the presence of a small amount of internal surface superconductivity, as it also does for In-Bi.

Sb-Tl behaves differently to the laminar eutectics in situation III. because the Sb precipitate is irregularly shaped and so the field can never be parallel to its surface over any significant area.

The critical current (defined when .3μV is measured) against field for configuration III. for In-Bi eutectic is shown in fig.68. Just below H_{c2} the influence of the internal sheath supercurrents are seen to be exceeded by the specimen surface and bulk supercurrents. An interesting comparison may be made between these curves and similar measurements made by Hart and Swartz[71] (see fig.69) on a thin film of ideal type II superconductor. The form of the curves is identical except the curvature above H_{c2}, yet

In-Bi EUTECTIC SLAB, DIRECTIONALLY FROZEN & HEAT TREATED AT 60°C.
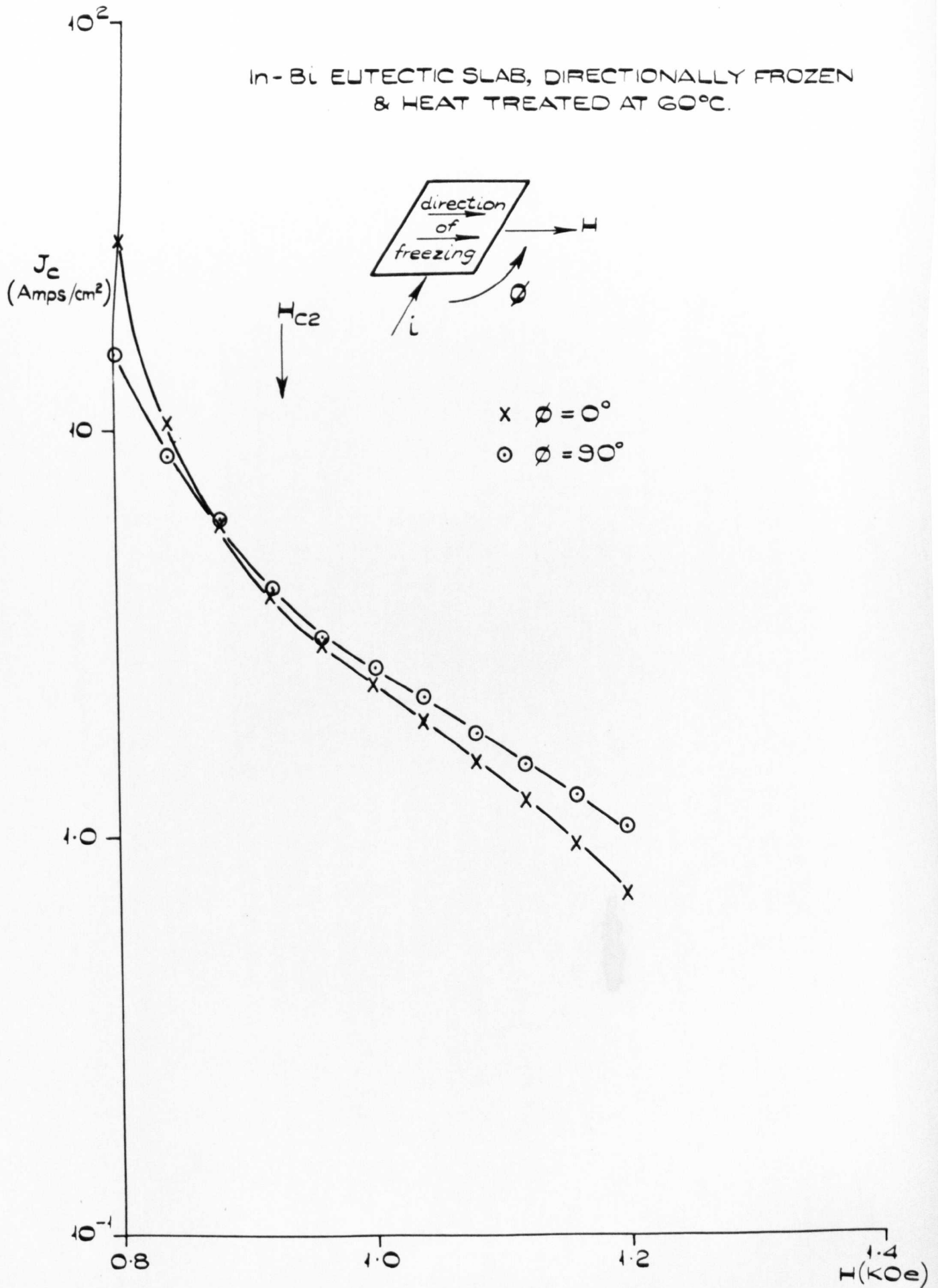
FIG. 68.
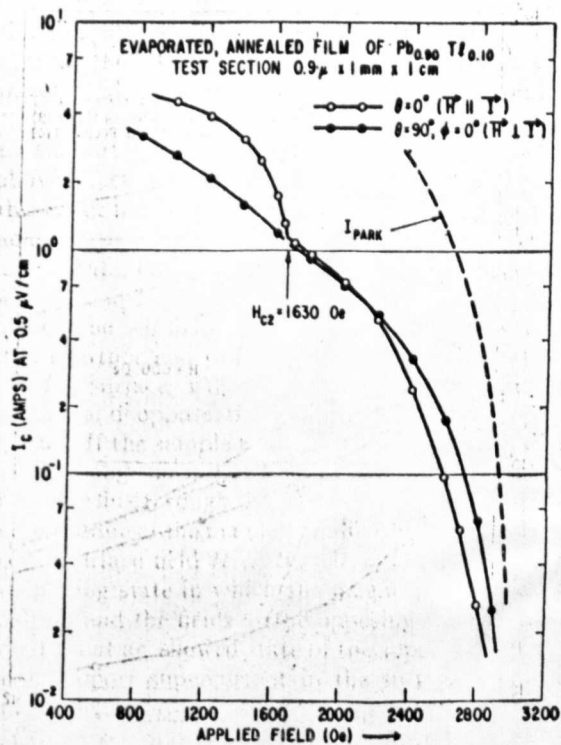
FIG. 4. The critical surface current at 4.2°K versus magnetic field for an evaporated and annealed film of $Pb_{0.90}Tl_{0.10}$. Below H_{c2} the critical current is larger when the field and current are parallel; above H_{c2}, when perpendicular. In both cases the critical surface current is much less than the calculated value (Ref. 12) (as shown).

Fig. 69. After H.R. Hart and P.S. Swartz [71]

(courtesy of Phys. Rev.)

their specimen had no orientated internal defects. It would be interesting
to have examined the texture of the substrate onto which their film was
evaporated. This effect was absent from the In-Bi when the current was
passed along the direction of growth (see fig.70).

14. The effect on the Resistance Transition of Plating with a Normal Metal.

14.1. Introduction.

Hempstead and Kim[78] were the first to show that plating a Nb-Ta alloy
reduced H_{c3} significantly and they established that the phenomenon of
superconductivity above H_{c2} was a surface effect. Fischer and Klein[93]
measured the decrease of H_{c3} as a function of the thickness of a Cu layer
deposited on Pb. The occurrence of superconductivity in their experiments
was observed by measuring the surface resistance at 9.5 GHz. Barnes and
Fink[55] observed that plating reduced the magnetic hysteresis of a Pb-Tl
alloy   and suggested that magnetic coatings were more effective
in destroying surface currents. In this section the effects on the
resistance by plating with Cu, Cd, Ni and Fe are investigated and compared.
Immediately prior to plating, each specimen was chemically polished and washed
in distilled water to obtain a good coating. The following plating baths
were used:-

(i)   Cu

KCN (91% KCN)	36.5	g/l
Na_2CO_3	6	"
CuCN	25	"
$NaHSO_3$	3	"
Anode:Cu		

In-Bi EUTECTIC SLAB, DIRECTIONALLY FROZEN & HEAT TREATED AT 60°C.
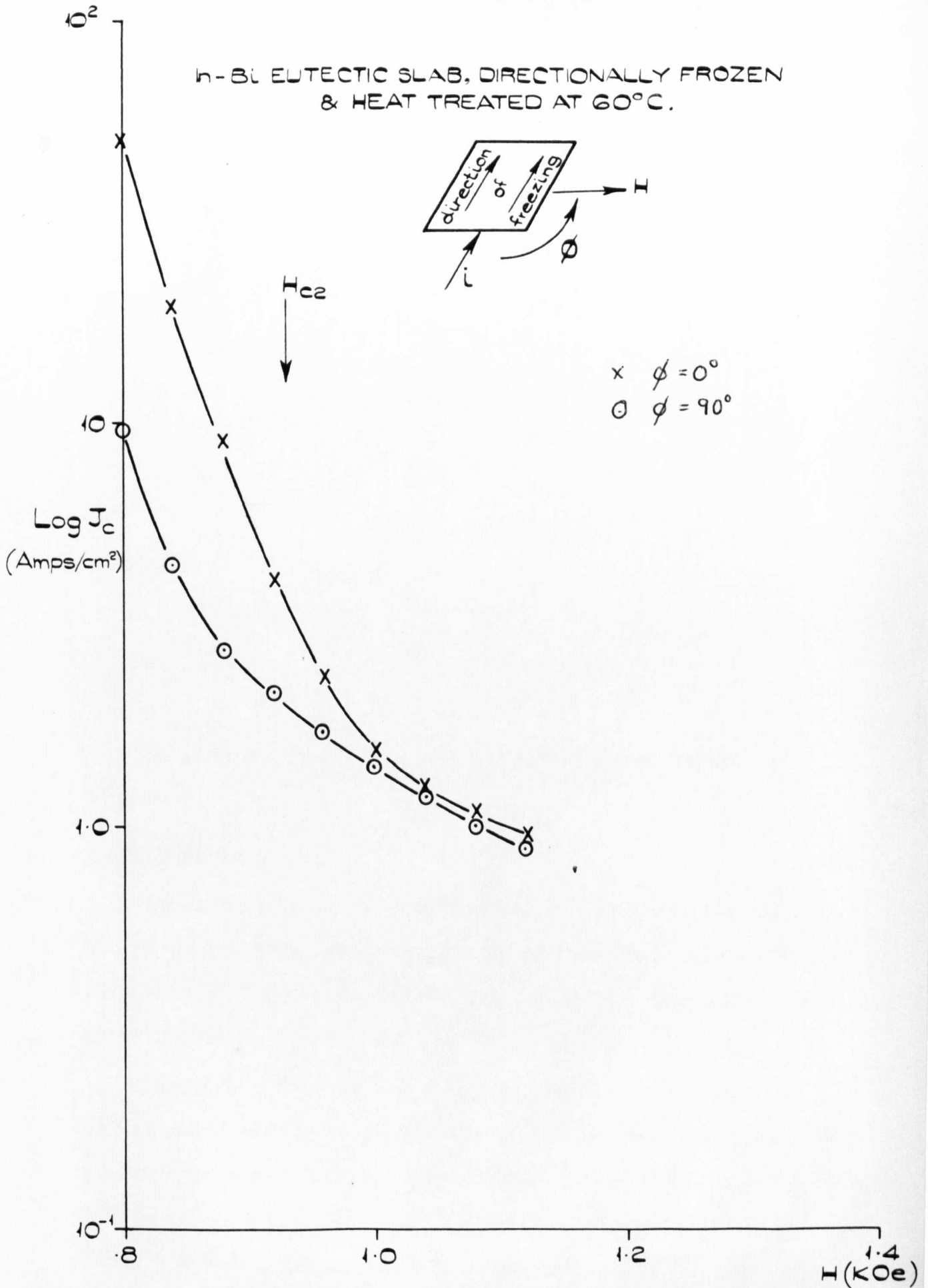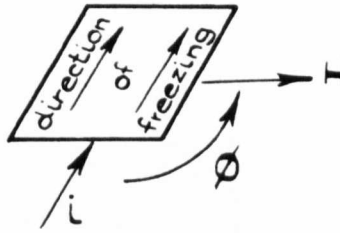
FIG. 70.

(ii) Cd

Na CN   88 g/l

CdO   33 "

Yellow dextrin   3   "

Anode: Cd.

(iii) Ni

$NiSO_4.7H_2O$ 250 g/l

$NiCl_2$ 37.5 "

H_3BO_2 25   "

NaF   12.5 "

Anode :Ni

(iv) Fe

$FeCl_2.4H_2O$ 600 g/l

$CaCl_2$ 670 "

Anode: Fe

The plating current was constant at .125 amps/cm^2 for all four
solutions.

14.2. Results.

The transitions of a wire specimen of Pb-Cd eutectic cut from a
directionally-frozen ingot such that the specimen axis was perpendicular to
the direction of freezing, unplated and then plated with Cu and Cd are
given in fig. 71. The plating time was 2 minutes.

The sheath current, H_R and H_N are all reduced for all angles of
both Cu and Cd coatings. Increase of the plating time (and hence plate
thickness) made no significant difference to these curves. A qualitatively
similar field orientation dependence exists before and after plating. On
removing the plated material, the 'unplated' curve
was obtained on remeasuring.
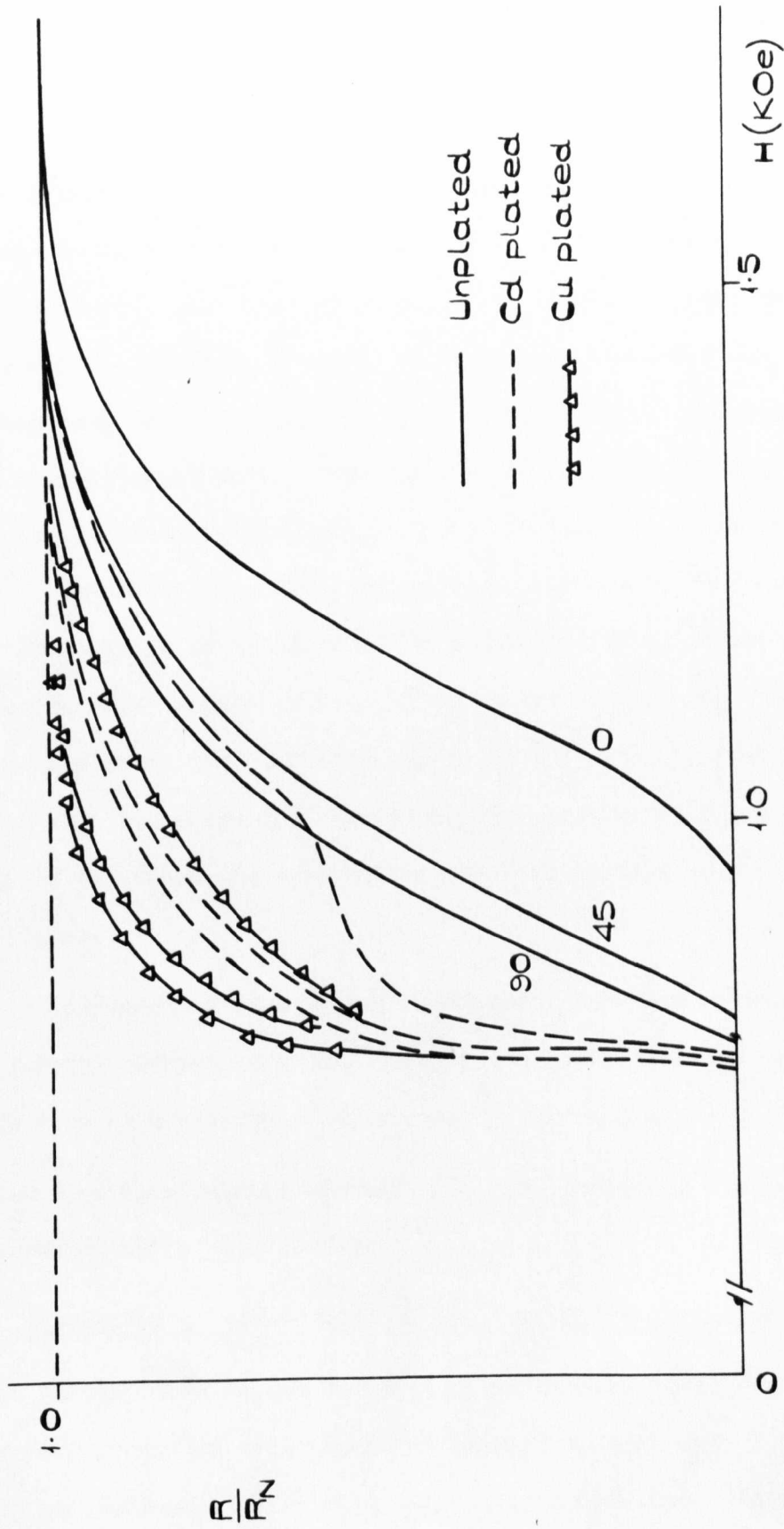
FIG. 71. EFFECT OF PLATING A Pb-Cd EUTECTIC DIRECTIONALLY-GROWN WITH THE DIRECTION OF GROWTH PERPENDICULAR TO SPECIMEN AXIS. $J \approx 5 \times 10^3 \, mA/cm^2$

Coating with the ferromagnetics Ni and Fe produced a very different result
for all transitions where $\theta \neq 0^\circ$, (fig.52). The transition curves where
the field is perpendicular to the specimen lie at the higher field, and the
onset of resistance in parallel field occurs at a slightly earlier field
than when plated with either Cu or Cd. The effect of the thickness of an
Fe coating is shown in figs. 72 and 73. The sheath current carrying
capacity and the field to which it is maintained both increase with the
plate thickness when the field is perpendicular to the specimen axis. The
$\theta = 0^\circ$ transition stays the same for all values of plate thickness.
Sensitivity to field orientation is shown in fig.74. It is greatest near
$\theta = 90^\circ$. The current carrying capacity of the sheath thus plated with
Fe as a function of θ is illustrated in fig.75. The current required to
generate the same voltage as i = .01 amps when $\theta = 0^\circ$ for the unplated
specimen is plotted for different values of the external field. It can be
seen that with the perpendicular orientation of the field the specimen can
carry up to ten times the current for the same voltage generated in the
parallel case.

When specimens of pure Pb and Pb-Zn eutectic (both of which display no
sheath current carrying capacity) were plated, the ferromagnetic's
presence made no appreciable difference to the curves.

Slab specimens behaved similarly to wire specimens when the field was
perpendicular to the slab surface.

14.3.   Discussion of the results of plating with a normal metal.

The plating with Cu and Cd reduces the surface sheath current because
the boundary condition of a superconducting/insulator interface which
St.James and DeGennes inserted into the Ginzburg-Landau equations does not
hold anymore. Instead of the order parameter ψ becoming zero at a field

FIG. 72.

"EFFECT OF PLATING AS-CAST Pb-Cd EUTECTIC WITH Fe

Unplated
t = 1 min
2 min
3 min
5 min
10 min
⎫ 90°

H (kOe)

R/Rₙ
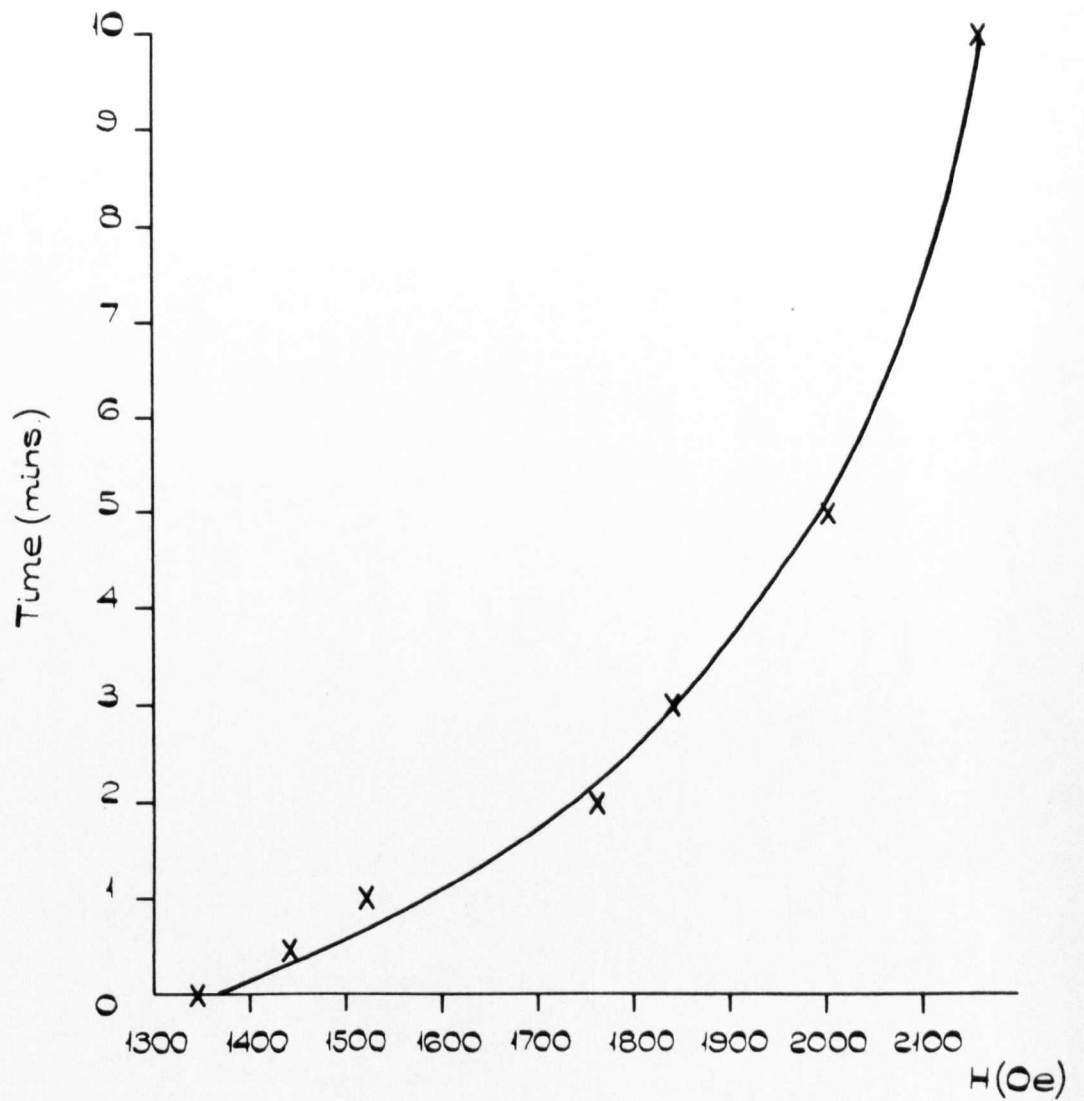
FIG. 73. FIELD AT WHICH SPECIMEN BECOMES NORMAL
WHEN PLATED WITH Fe; $\theta = 90°$.

(Plating current = 0·7 amps.)
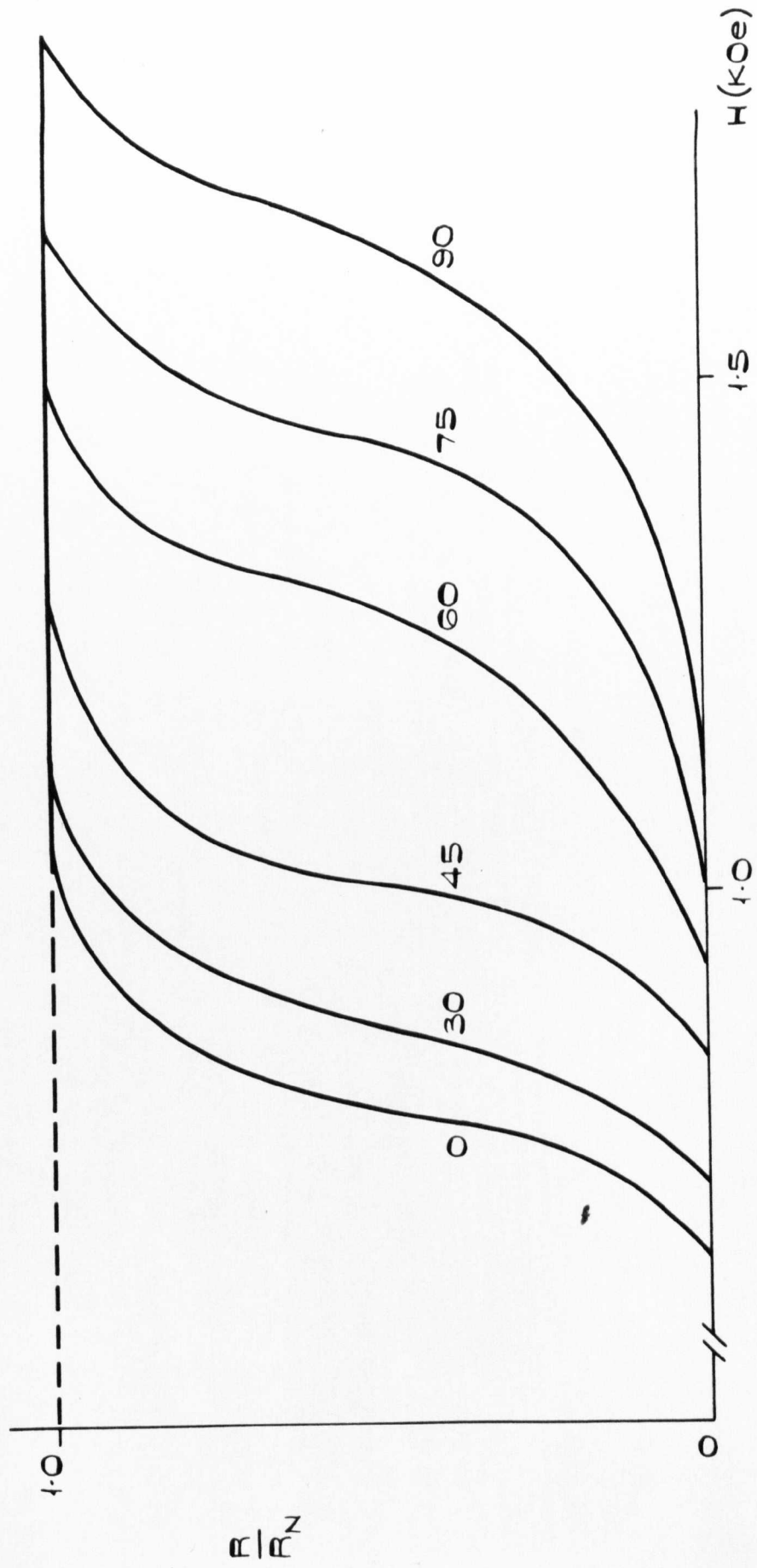
FIG. 74. EFFECT OF PLATING A Pb-Sb EUTECTIC SPECIMEN WITH Fe.
$J \approx 1.3 + 10^3 \text{mA/cm}^2$

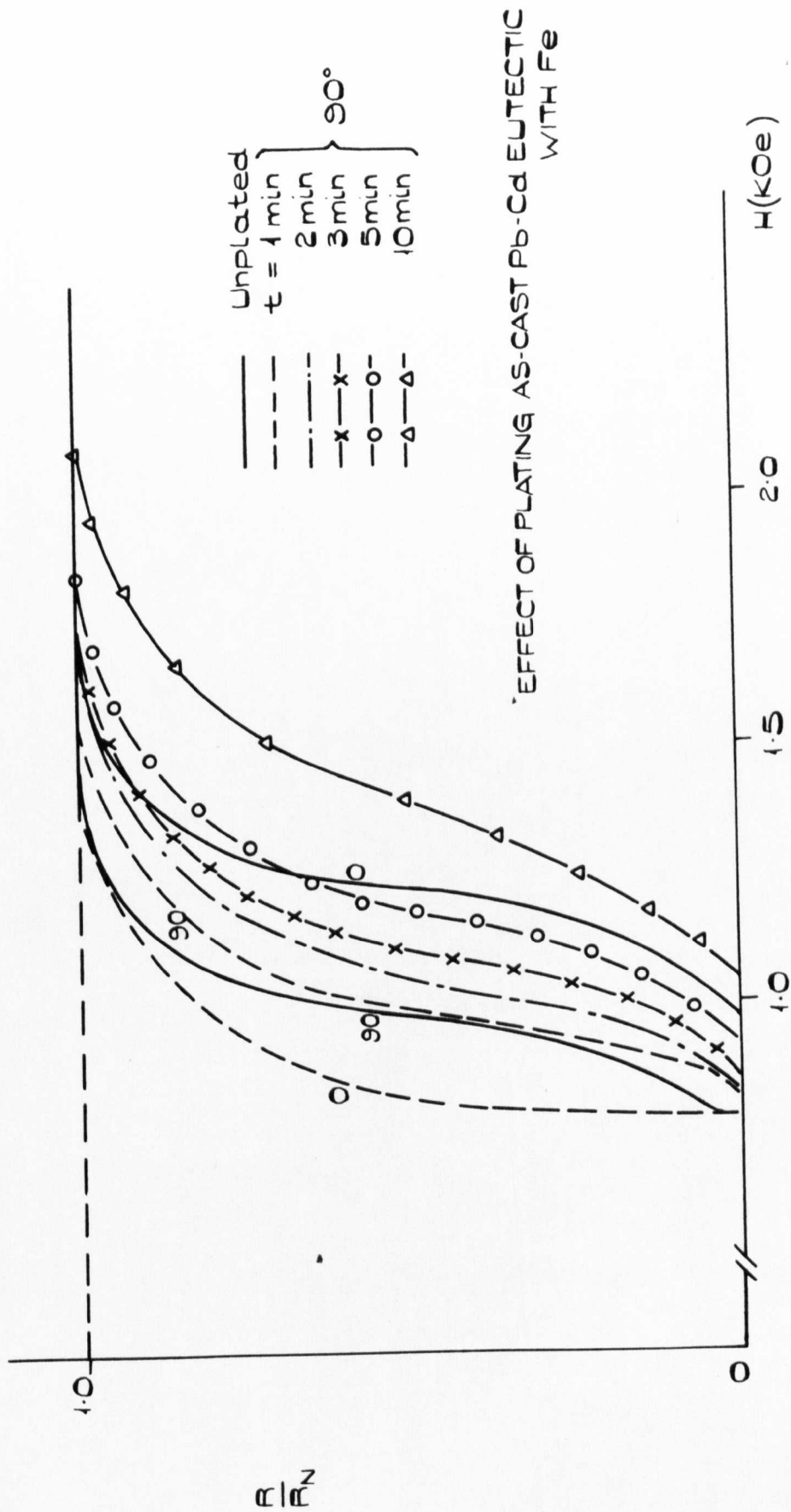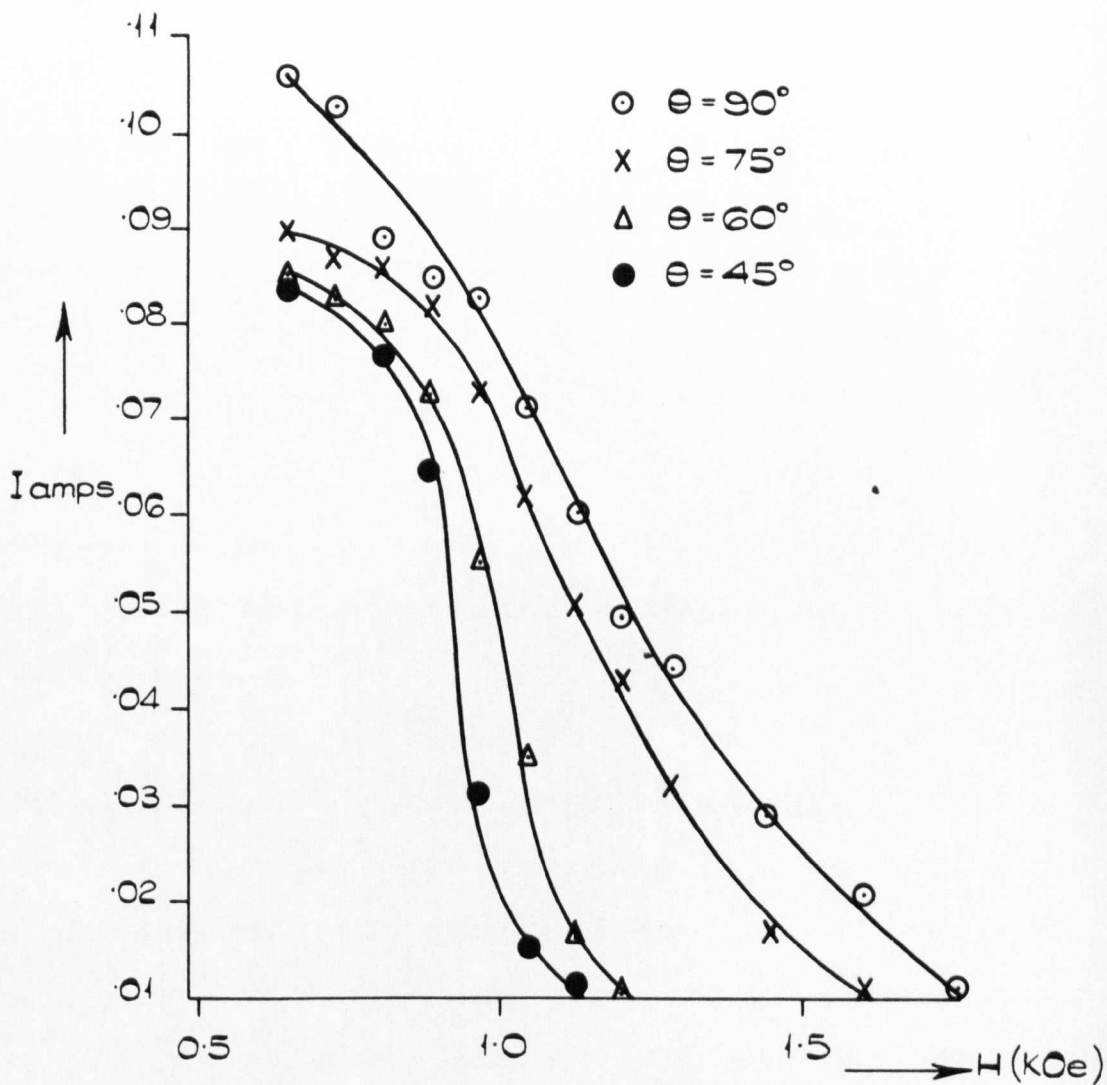FIG. 75. CURRENT REQUIRED TO GENERATE IN AN Fe-COATED
SPECIMEN THE SAME VOLTAGE AS i=0·01 amps
θ = 0° IN A NON-Fe PLATED SPECIMEN OF
Pb Sb EUTECTIC AT THE SAME FIELD.

$1.69 \, H_{c2}$, it becomes zero at some lower field. Since the orientation of the field with respect to the specimen surface is qualitatively the same before and after the coating, it is reasonable to assume that the super-conductivity above H_{c2} with a plating on is still due to the St.James and DeGennes sheath, though much reduced.

Fischer and Klein[93] reduced H_{c3} of their Pb specimen to H_c with a plate thickness of 545Å, whereas in this work the normal metal coatings were of the order of 1μ thick, probably above the value for a thickness effect to be seen. Gygax and Kropschot[94] also found that the thickness of a Cu film made no difference, probably for the same reason; their films were about ½μ thick.

These results raise the question of why internal surface super-conductivity should exist, except on an insulating surface, if a normal metal plating removes the sheath. Even when plated, however, a surface still carries some current and the cumulative effect of a large number of these surfaces (as is the case when a precipitate is present) will be significant. Also, Hurault[95] showed theoretically that the sheath will only be reduced by coating with a normal metal if the conductivity of the metal is greater than that of the superconductor in the normal state. No data is available on the conductivities of thin films of these precipitates, but it may well be that their conductivities are lower, especially in the region of the interface. Even more important perhaps is the effect of differential thermal contraction of the precipitates and matrix. If this does produce the effects discussed in section 12.2.6. and if this deformed region extends over a distance greater than the coherence length (and there is no reason why is should be related to this purely superconducting parameter) the plating effects of the precipitates themselves would be very much reduced.

The Fe and Ni coating effects are not simply magnetic shielding effects for the following reasons :-

(i)   no shielding occurs in the parallel field case whether the ends of the specimen are plated or not;

(ii) plating with a ferromagnetic has no effect on the perpendicular transitions of specimens with no sheath;

(iii) the displacement of the $\theta = 90^{\circ}$ transition curve depends on the sheath carrying capacity of the material; for example, the Pb-Sn eutectic when plated with Ni (five minutes in the bath at 1 amp/sq.cm.) has the curves separated by only about 15 Oe. See fig.76.

Why this behaviour occurs is not known: no one, to the author's knowledge, has considered the boundary conditions when a superconductor is plated with a ferromagnetic and the field is not parallel with the surface. Hauser[96] has measured the resistance transition of a Pb-In alloy coated with Ni, but only for the case of parallel field. His results were the same as in this work - superconductivity was suppressed.

These results, therefore, indicate that a coating of Cu is more effective in reducing surface superconductivity than a Cd coating despite the fact that a greater weight and also a thicker coating of Cd was deposited. (Each metal was plated for the same length of time at the same current density). Also, Fe is slightly better than Ni in showing the anomalous effect in perpendicular applied field. However, the condition of the interface between the superconductor and normal metal, which is certain to affect the results, is completely unknown.
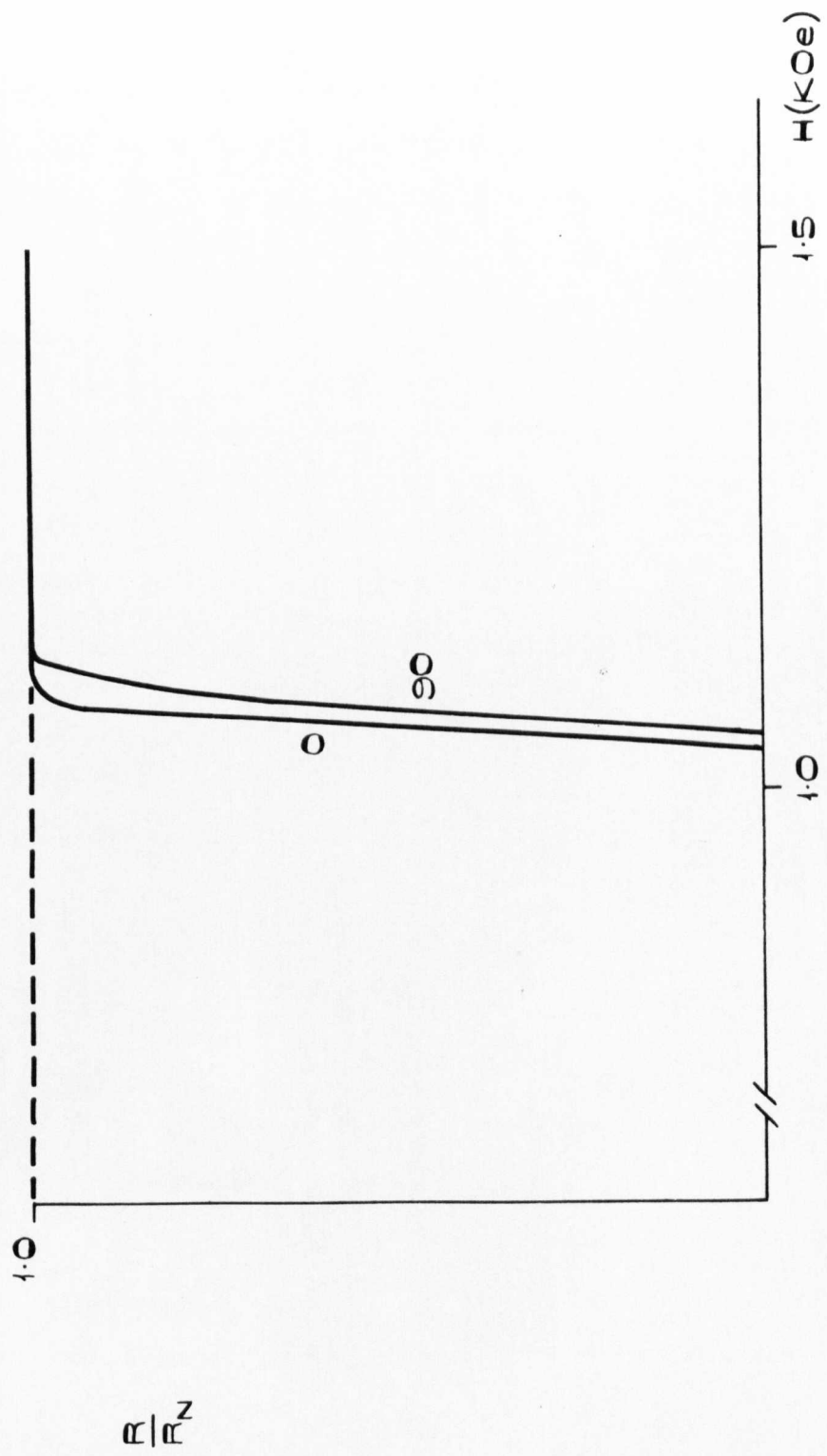
FIG. 76. Pb-Sn EUTECTIC, COATED WITH Fe $J \approx 1.3 \times 10^4\, mA/cm^2$

15. Conclusions

The magnetisation, critical current and resistive transition in a field were measured on ten eutectic alloy systems and on many of their component solid solutions in isolation. These eutectics are listed below and the following conclusions were drawn concerning the superconducting mechanisms prevailing and the effect of the presence of the precipitates.

System	Matrix	State	Precipitate	State	T^oK
Pb-Cd	Pb-rich solid solution	S	Cd	N	4.2
Pb-Zn	Pb	S	Zn	N	4.2
Pb-Sn	Sn-rich solid solution	S*	Pb-rich solid solution	S	4.2
Pb-Mg	Pb-rich solid solution	S	Mg_2Pb	N	4.2
Sb-Tl	Sb_2Tl_7	S	Sb	N	4.2
Pb-Sb	Pb-rich solid solution	S	Sb-rich solid solution	N	4.2
Bi-76.5%Tl	Bi_2Tl	S	Bi	N	4.2
Bi-47.5%Tl	Bi_2Tl	S	x - ⎫ α - ⎬ solid solution	S	4.2
In-Bi	In-rich solid solution	S	In_2Bi	S	4.2
Hg-Tl	α- solid solution	S	β - Tl	N(?)	2.2†

*N in isolation, $T_c \approx 3.7^oK$

†2.2°K was obtained by reducing the vapour pressure above the helium bath with standard laboratory equipment.

1.   All the eutectics, after the heat-treatment are type II, except Pb-Zn.
(Pb-Cd becomes type I on ageing at room temperature[48]).

2.   The presence of a second phase, whether superconducting or normal,
increases the magnetic hysteresis due to pinning. The pinning is most probably
caused by one or more of the following mechanisms:-

> (i)   if the precipitate is small, i.e. of the order of size of the
> coherence length, pinning is presumably accomplished by interaction
> of the precipitate with the normal core of the fluxoid;

> (ii)   if the precipitate is large, pinning occurs by interaction
> with the surface of the precipitate, either

>> (a)   because the presence of a surface locally decreases
>> the mean free path, thus providing high k, low energy
>> sites for preferential fluxoid repose;

> or   (b)   because of an image force mechanism, as suggested by
>> Campbell et al[59];

> (iii)   differential thermal contraction between the matrix and the
> precipitate by causing local regions of strain, i.e. regions
> of high k and hence low energy sites.

The experiment on Pb-Mg supersaturated solid solution indicates that
the change of pinning mechanism which must occur as the precipitate grows
is gradual and not accompanied by any discontinuity at a critical particle
size.

3.   Large normal particles are also able to interact with the boundaries
of the intermediate state of type I superconductors, whereas small particles
are not.

4.   The pinning effect of the precipitate can be eliminated by considering

very thin samples in which the effect of a flux gradient is negligible.
This was accomplished by coating the surface of a brass rod with the
eutectic and slitting it longitudinally to make it singly connected. A
size dependent magnetisation curve was obtained as predicted by the
Critical State model.

5.   The total surface area of precipitate present does not appear to be
as important as the surface area favourably orientated to invading flux
lines. This results in some magnetisation and critical current curves
being precipitate-orientation dependent.

6.   When the pinning effect of the precipitates is not too strong, the
current carrying capacity of the dumb-bell shaped specimens is greatest
when the applied field is parallel with the specimen axis. The decrease
in current when $\theta = 90^\circ$ is mainly due to a decreased Lorentz force
when $\theta = 0$ (as opposed to demagnetising effects). This is demonstrated
by the results on Bi-47.5 wt. per cent Tl. In this case the pinning is
very weak but it has a large effect in resisting the driving force in
longitudinal field. However, when the driving force is high (as in the
magnetisation experiment and critical current in transverse field
measurements) the effect of the precipitate is negligible and the results
approach those obtained on the defect-free solid solution specimens.

When the pinning forces are high, the critical current remains
fairly constant as the field is increased and then falls rapidly to zero
as H_{c2} is approached. In this case the longitudinal and transverse field
curves are very similar and are independent of precipitate orientation.

7.   The properties of eutectic mixtures are not necessarily the sum of
the properties of each phase in isolation. The Pb-Sn, Tl + 47.5 per cent
wt. Tl and In-Bi systems exhibit a proximity effect, i.e. a phase that

would be normal in isolation is rendered superconducting in the presence of
a second superconducting phase, despite the fact that the phase boundaries
are of dimensions greater than the coherence length. The proximity effect
can occur when either the precipitate (Pb-Sn, Tl-47.5 per cent wt.Bi) or
the matrix (In-Bi) are superconducting in isolation. A phase can be caused
to be superconducting both at temperatures above its usual transition
temperature (Pb-Sn) and/or above its usual upper critical field (Tl-47.5
per cent wt.Bi, In-Bi). The effect occurs above H_{c2} of the superconducting
phase in Tl-47.5 per cent wt.Bi but not very much in Pb-Sn.

8.   In the absence of any precipitates, the magnetic hysteresis is due
to surface currents which decrease when the surface is roughened and k
of the surface is kept constant. In the mixed state this is probably
due to easier nucleation of fluxoids at surface asperities due to de-
magnetising effects. The Swartz and Hart flux spot pinning mechanism does
not appear to operate - otherwise roughening the surface would increase
the hysteresis (and the critical transport current).

9.   Evidence concerning the role of the major loop has been presented and
discussed and it is suggested that the area of the major loop is a measure
of the relative effects of surface currents and bulk currents. The nature
of the surface currents involved are not known but they are in part defect
stabilised and in part St.James and DeGennes sheath currents. Thus the
loop starts with zero area for an ideal specimen, increases in area to a
maximum as the surface currents increase, then decreases to zero as bulk
pinning predominates. It is size dependent and can be made 'artificially'
either larger, by using a hollow cylinder, or reduced by slitting the
cylinder longitudinally.

10.   The effect of specimen edges was shown to allow earlier flux

penetration (c.f the hollow cylinder of Pb-Cd and the slit hollow cylinder)
and the presence of the end caps of a hollow ellipsoid revealed an unexpected
and ~~unpredictable~~ end effect which may possibly complicate results on solid
specimens.

11.   The model of St.James and DeGennes for superconductivity above H_{c2}
is confirmed. A resistanceless sheath current flows parallel to the normal
bulk current and the position of the resistance transition depends on the
value of the measuring current compared to the sheath current. The mag-
netoresistance effect in Pb-Cd confirms that the resistance is due to
current passing through normal bulk material. It also demonstrates that
this mechanism is the same for type I superconductors of $k > 0.419$ above
H_c.

12.   The field at which the specimen becomes completely normal, H_N, and the
sheath current at any field, $i_s(H)$, decrease as the field orientation
with respect to the specimen axis increases. When $\theta = 0$ the whole specimen
surface is parallel to the field and as θ increases the sheath is able to
'short out' less of the transport current. The excess is carried in the
bulk, resulting in an increase in Joule heating and consequently an increase
in the temperature of the specimen.

13.   The surface sheath appears to exist below H_{c2} in some specimens.
Consequently, the model of the resistance transition in which the mechanism
of the lossless current is supposed to change at H_{c2} does not apply. Above
and below H_{c2} the St.James and DeGennes sheath carries the current because:

(a)   no discontinuity exists at H_{c2} in the transition;

(b)   the angular dependence of the lossless current remains the
      same as the field is lowered through H_{c2}.

14.   Roughening the surface in Hg-Tl without affecting k shows that this

results in a decrease of the sheath current $i_s(H)$ above H_{c2}, together with
a decrease in H_N and H_R, the field at which resistance is first detected.
The roughening probably reduces the amount of surface parallel to the field
thus resulting in a lower total $i_s(H)$, but $i_s(H)$ per unit area parallel to
the field probably remains the same. The excess bulk current is thought
to cause the decrease in H_N by Joule heating.

15. Above H_{c2}, the presence of the precipitate has several effects:-

(i) it increases the current carrying capacity of the sheath,
despite the fact that the surface area of superconducting
phase has been reduced by its presence, at all fields and
orientations;

(ii) it reduces the sensitivity of the specimen to field
orientation;

(iii) it may increase the value of H_N to beyond $H_{c3} = 1.69H_{c2}$.

These results are believed to be caused by the nucleation of the
superconducting surface sheath at the internal surfaces between the
precipitate and matrix and this is confirmed by results obtained on slab
specimens. This internal surface superconductivity may exist because
St. James and DeGennes' theory applies equally well to internal and external
surfaces and it may be augmented by possible severe deformation occurring
in the region of the internal surface due to differential thermal contraction.
This would also lead to H_N being greater than H_{c3} in some cases.

16. Plating the specimen with normal metals Cu and Cd reduces the sheath
current and H_N for all field orientations. Cu is slightly the more
effective. Fe and Ni also reduce the sheath current in parallel fields but
increase it substantially at other orientations, the increase reaching a
maximum at $\Theta = 90^\circ$. The increase in sheath current (and H_N) increases
with plate thickness. The cause of this increase in $i_s(H)$ is not known but

it is not a ferromagnetic screening effect because it does not cause screening when no sheath is present and the magnitude of the effect depends on the current carrying capacity of the sheath.

17.   The results also gave some metallurgical information. They revealed that the laminae in a directionally-grown (Pb-Cd) eutectic are indeed continuous over macroscopic distances in the direction of freezing and are not connected physically to laminae in neighbouring grains, verifying the two-dimensional optical observations. They are continuous longitudinally in spite of apparent shears.

16.   Suggestions for future research and possible applications of this work.

Many questions remain unanswered concerning the role of precipitates in superconductors. The nature of the pinning process is still unknown; indeed, there is still disagreement as to the nature of the hysteresis in superconductors. The origin of the surface currents in the mixed state and the effect of precipitates near the surface upon them is completely unknown. The effect of precipitate nature, type, distribution and morphology is still not completely understood; we are still unable to predict exactly what effect a given distribution of a given precipitate will have on a particular superconducting parameter.

While our knowledge is thus imperfect, eutectic alloys (binary and ternary) will be useful in investigations which require a given precipitate's distribution and chemical composition to be manipulated over a limited range. They would also be useful in any investigation of precipitate-matrix orientation effects, since in a directionally frozen ingot the orientation relationship has been observed to change along the ingot length, reaching (presumably) the equilibrium relationship towards the end of the

ingot last to solidfy. Precipitate orientation and distribution effects on flux jumping may also be investigated by using these alloys.

The reason for the occurrence of the proximity effect in these alloys, especially over such large distances with respect to the coherence length, may be an important factor in our understanding of pinning effects.

Eutectic alloys of Nb and Ta could conceivably be attractive for use as conductors. They have several advantages:

(i)   a large volume of pinning defects may be introduced into the matrix;

(ii)   these defects may be superconducting, in which case they could pin fluxoids and still carry current themselves;

(iii) if a proximity effect occurred either in the precipitate or the matrix, then possibly a cheaper material (possibly occupying most of the volume of the alloy) than Nb or Ta may be induced with the properties of the latter.

It may be that a directionally frozen eutectic of Nb or Ta with the superconducting phase the precipitate will provide a method of producing a stabilized conductor. (Pb-Sb eutectic was investigated with this in mind, but the proximity effect caused the matrix of Sn to become superconducting).

In future investigations of these alloys (or any other multiphase alloys) specific heat measurements would be invaluable to ascertain which phases were superconducting at any given time.

Surface effects have been much investigated with respect to many parameters (in this laboratory particularly in relation to A.C. losses). Results are often difficult to interprete because the usual alloys considered (Nb-base and Pb-base) each present difficulties in the obtaining of (and the reproduction of) precise surface conditions. Study of Hg and its alloys in capsules of known surface profile would enable various reproducible surface finishes to be obtained on the same specimen without spurious k changes affecting the results.

17. References

1. H.Kammerlingh Onnes, Commum. Phys. Lab. Univ. Leiden, No.1196,(1911).

2. K.Mendelssohn, Rev. Mod. Phys., $\underline{36}$, 7, (1964).

3. G.B.Yntema, Phys. Rev., $\underline{98}$, 1197, (1955).

4. D.Schoenberg, Superconductivity, Cambridge Univ.Press, (1952).

   E.A.Lynton, Superconductivity, John Wiley & Sons Inc., (1962).

   J.D.Livingston & H.W.Schadler, Prog.Mat.Sc., Vol.$\underline{12}$, ■ (1964).

5. H.Kammerlingh Onnes, Commun. K.Onnes Lab. Leiden $\underline{13}$, Suppl.34b,
   (1913-14).

6. F.B.Silsbee, J.Wash. Acad. Sci., $\underline{6}$, 597,(1916).

7. W.Meissner & R.Ochsenfeld, Naturwiss, $\underline{21}$, 787, (1933).

8. F. & H. London, Superfluids, Dover Publications, New York, Vol. 1.

9. F.London, Physica, $\underline{3}$, 450, (1936).

10. A.B.Pippard, Proc. Roy. Soc., A 216, 547, (1953).

    Physica, $\underline{19}$, 765, (1953).

11. V.L.Ginzburg & L.D.Landau, J.E.T.P.,U.S.S.R., $\underline{20}$,1064,(1950).

12. A.A.Abrikosov, Phys. Chem.Sol., $\underline{2}$, 199, (1957).

    Sov. Phys. J.E.T.P., $\underline{5}$, 1174, (1957).

13. B.B.Goodman, Phys. Rev. Letts., $\underline{6}$, 597, (1961).

14. J.Matricon, Phys. Letts., $\underline{2}$, 289, (1964).

15. ᵀ Essman & H.Trauble, Phys, Letts., $\underline{24A}$, ■ 526, (1967).

16. L.P.Gor'kov, Sov. Phys., J.E.T.P., $\underline{9}$, 1364, (1959), $\underline{10}$, 908,(1960).

17. J.Bardeen, L.N.Cooper & J.R. Schrieffer, Phys.Rev., $\underline{108}$, 1175,(1957).

18. C.Caroli, P.G. DeGennes & J.Matricon, Phys, Kondens, Materie $\underline{1}$,
    176, (1963).

19. D.St.James & P.G.DeGennes, Phys. Letts., $\underline{7}$, 302, (1963).

20. M.Tinkham, Phys. Letts., $\underline{2}$, 217, (1964).

21. G.Bon Mardion, B.B.Goodman & A.Lacaze, Phys.Letts., $\underline{8}$, 15, (1964).

22. P.W. Anderson, Phys. Rev. Letts., 9, 309, (1962).

23. P.W. Anderson & Y.B. Kim, Rev. Mod. Phys., 36, 39, (1964).

24. J. Friedel & P.G. DeGennes & J. Matricon, App. Phys. Letts., 2, 119, (1963).

25. A.M. Campbell, Ph.D. Thesis, Cambridge, (1965).

26. C.P. Bean, Phys. Rev. Letts., 8, 250, (1962).

27. A.M. Campbell, J.E. Evetts & D. Dew-Hughes, Phil. Mag., 10, 333, (1964).

28. J.E. Evetts, Ph.D. Thesis, Cambridge, (1965).

29. Y.B. Kim, C.F. Hempstead, A.R. Strnad, Phys. Rev., 129, 528, (1963).

30. W.A. Fietz, M.R. Beasley, J. Silcox & W.W. Webb, Phys. Rev., 136, 335, (1964).

31. G.A. Chadwick, Prog. in Mat. Sc., Vol. 12, ▮, (1964).

32. R.W. Kraft & D.L. Albright, Trans. Met. Soc. A.I.M.E., 221, 95, (1961).

33. J.D. Hunt & J.P. Chilton, J.I.M., 91, 838, (1963).

34. J.D. Hunt & K.A. Jackson, Trans. Met. Soc. A.I.M.E., 236, 843, (1966).

35. W.A. Tiller, Liquid Metals & Solidification, American Soc. Metals, (1958).

36. H.W. Weart & J.D. Mack, Trans. Soc. A.I.M.E., 212, (1958).

37. J.P. Chilton & W.C. Wineguard, J.I.M., 89, 162, (1961).

38. G.A. Chadwick, J.I.M., 91, 298, (1963).

39. D. Munson & A. Hellawell, J.I.M., 92, 27, (1964).

40. D.J.S. Cooksey, D. Munson, M.P. Wilkinson & A. Hellawell, Phil.Mag., Vol. 10, ▮▮, 745, (1964).

41. M.G. Day & A. Hellawell, J. Aust. Int. Met., 9, 213, (1964).

42. M Hansen, 'Constitution of Binary Alloys,' 2nd. Ed., McGraw Hill, 1958

43. R.M.F. Linford, Ph.D. Thesis, Univ. Warwick, (1968).

44. R.J.A. Seebold, Min. Tech. Rep., No.4, Univ. Warwick, (1967).

45. W.W. Webb, Phys. Rev. Letts., 11, 191, (1963).

46. J.D.Livingston, Rev. Mod. Phys., 36, 54, (1964).

47. J.Friedel, P.G.DeGennes, J.Matricon, App.Phys.Letts., 2, 119, (1963).

48. J.D.Livingston, J.App. Phys., 34, 3028, (1963).

49. J.Sutton & C.Baker, Phys. Letts., 21, ▮ 601, (1966).

50. H.J.Fink, Phys. Rev. Letts., 14, 309, (1965).

51. H.J.Fink, Phys. Rev. Letts., 14, 853, (1965).

52. J.G.Park, Phys. Rev. Letts., 15, 352, (1965).

53. H.J.Fink & L.J.Barnes, Phys. Rev. Letts., 15, 792, (1965).

54. J.G.Park, Phys. Rev. Letts., 16, 1196, (1966).

55. L.J.Barnes & H.J.Fink, Phys.Letts., Vol.20, ▮ 583, (1966).

56. D.G.Schweitzer & B.Bertman, Phys. Letts., Vol.20, ▮ 263, (1966).

57. B.Bertman, D.G.Schweitzer & F.P.Lipschultz, Phys.Letts., Vol. 21, ▮ 260, (1966).

58. C.P.Bean & J.D.Livingston, Phys. Rev.Letts., 12, 14, (1964).

59. A.M.Campbell, J.E.Evetts & D.Dew-Hughes, Phil.Mag., Vol.18, ▮▮, 313. (1968).

60. K.Mendelssohn, Proc.Roy.Soc., (London), A152, 34, (1935).

61. K.Mendelssohn, Rev.Mod. Phys., 36, 50, (1964).

62. A.S.Joseph & W.J.Tomasch, Phys.Rev.Letts., 12, 219, (1964).

63. R.W.DeBlois & W.DeSorbo, Phys. Rev. Letts., 12, 499, (1964).

64. P.S.Swartz & H.R.Hart, Phys. Rev., 137, ▮, A818, (1965).

65. D.Kramer & C.G.Rhodes, J.I.M., 94, 261, (1966).

66. S.A.Levy, Y.B.Kim & R.W.Kraft, J.A.Phys., Vol.37, ▮, 3659,(1966).

67. J.E.Evetts, A.M.Campbell & D.Dew-hughes, Phil.Mag., 10, 339, (1964).

68. S.Foner, Rev.Sc.Inst., 30, 548, (1959).

69. J.E.Evetts, J.I.M., 93, 29, (1965).

70. J.D.Livingston, App.Phys. Letts., 118, 12, (1966).

71. H.R.Hart & P.S.Swartz, Phys. Rev., Vol.156, ▮ 403, (1967).

72. M.A.R.LeBlanc, Phys.Rev.Letts., $\underline{11}$, 149, (1963).

73. C.J.Bergeron Jnr., App.Phys. Letts., $\underline{3}$, 63, (1963).

74. J.Lowell, Phil. Mag., $\underline{16}$, 581, (1967).

75. W.C.H. Joiner & G.E.Kuhl, Phys.Rev., $\underline{168}$, 413, (1968).

76. K.Mendelssohn, Proc. Roy.Soc.(London), A153, 34, (1935).

77. G.Bon Mardion, B.B. Goodman & A.Lacaze, Phys.Letts., $\underline{8}$, 15,(1964).

78. C.F.Hempstead & Y.B.Kim, Phys. Rev. Letts., $\underline{12}$, 145, (1964).

79. W.J.Tomasch & A.S.Joseph, Phys.Rev.Letts., $\underline{12}$, 148, (1964).

80. S.Gygax, J.L.Olsen & R.H.Kropshot, Phys. Letts., $\underline{8}$, 228, (1964).

81. M.Cardona & B.Rosenblum, Phys. Letts., $\underline{8}$, 308, (1964).

82. H.R.Hart & P.S. Swartz, Phys. Letts., $\underline{10}$, 40, (1964).

83. M.Strongin, A.Paskin, D.G.Schweitzer, O.F.Kammerer & P.P.Craig,
    Phys. Rev. Letts., $\underline{12}$, 442, (1964).

84. W.F.Druyvestyn, Philips Res.Rept., $\underline{2}$, (1966).

85. S. J.Williamson & J.K.Furdyna, Phys.Letts., Vol. $\underline{21}$, 376, (1966).

86. J.F.Schenk, J.S.Willis & R.W.Shaw, Phys. Letts., $\underline{11}$, 285, (1964).

87. K.M.Ralls, Phys.Letts., Vo.$\underline{23}$, 29, (1966).

88. P.R.Doidge, Kwan Sik-Hung & D.R.Tilley, Phil. Mag., $\underline{13}$, 795, (1966).

89. W.DeSorbo, Phys. Rev., $\underline{134}$, 1119, (1964); ibid., $\underline{135}$, 1190.

90. D.R.Tilley, J.Phys.C. (Proc.Roy.Soc.) Phys., Vol.$\underline{1}$., 293, (1968).

91. R.G.Boyd, Phys.Rev., $\underline{153}$, 444, (1967).

92. J.P.McEvoy, D.P.Jones & J.G.Park, Sol. State Comm.,$\underline{5}$, 641,(1967).
    C.Chiou, R.A.Connell & D.P.Seraphim, Phys.Rev.,$\underline{129}$, 1070, (1963).

93. G.Fischer & R.Klein, Phys.Letts., Vol.$\underline{23}$, 311, (1966).

94. S.Gygax & R.H.Kropschot, Phys.Letts., $\underline{9}$, 91, (1964).

95. J.P.Hurault, Phys.Letts., $\underline{20}$, 587, (1966).

96. J.J.Hauser, Phys. Letts., Vol.$\underline{22}$, 378, (1966).

97. G.J.Van Gurp, Philips Res. Rep., $\underline{22}$, 10, (1967).

98. C.A.Schiffman, J.F.Cochran, M.Garber + William Gardner,
    Rev. Mod. Phys., $\underline{36}$, 127, (1964).